



Neidler, Sarah (2015) *Identification of tumour progression genes in a mouse model for non-small cell lung cancer*. PhD thesis.

<https://theses.gla.ac.uk/7111/>

Copyright and moral rights for this work are retained by the author

A copy can be downloaded for personal non-commercial research or study, without prior permission or charge

This work cannot be reproduced or quoted extensively from without first obtaining permission in writing from the author

The content must not be changed in any way or sold commercially in any format or medium without the formal permission of the author

When referring to this work, full bibliographic details including the author, title, awarding institution and date of the thesis must be given

Enlighten: Theses

<https://theses.gla.ac.uk/>
research-enlighten@glasgow.ac.uk

Identification of Tumour Progression Genes in a Mouse Model for Non-Small Cell Lung Cancer

Sarah Neidler

Submitted to the University of Glasgow in fulfilment of the requirements for the degree of Doctor of Philosophy in the Institute of Cancer Sciences, College of Medical, Veterinary, and Life Sciences

The Beatson Institute for Cancer Research

University of Glasgow

September 2015



BEATSON
INSTITUTE



University
of Glasgow

Abstract

The 5-year survival rate of lung cancer patients is only 16%. As most patients are diagnosed at an advanced stage, little is known about early stages and mechanisms underlying the progression to metastatic disease. There are few targeted therapies available and targeting KRas driven lung cancer is especially challenging. *KRAS* is one of the most frequently mutated oncogenes in lung adenocarcinomas at ~33% of cases and is notably associated with resistance to EGFR inhibitors.

In order to study tumour progression *in vivo* we chose a Cre/loxP inducible system in which Cre recombinase expressing Adenovirus is delivered to the lung by intranasal installation. In this model, Cre-mediated induction of a conditional *KRAS*^{G12D} allele gives rise to benign papillary adenomas (BPAs) that rarely progress to adenocarcinoma. Combined activation with conditional modest MYC overexpression however increases both the growth rate of the BPAs and their frequency of progression to adenocarcinoma. Deregulated MYC expression alone however gives rise to focal proliferation in the bronchioles but does not lead to tumours. Loss of functional *Tp53* does not increase MYC's tumour initiating potential in this model.

Importantly, the *KRAS*^{G12D}/*MYC* model faithfully recapitulates the morphology of a subset of the human disease. I used Erk phosphorylation status to distinguish between benign (p-Erk negative) and more advanced (p-Erk positive) tumour regions, and laser capture microdissection to harvest regions of interest. RNA was isolated from those regions and analyzed by RNA-Sequencing. GeneGo pathway analysis revealed that the ErbB and Wnt pathways are significantly upregulated in the p-Erk positive dataset. In order to validate the importance of these pathways, we treated cells derived from the same *KRAS*^{G12D}- and *MYC*-driven mouse tumours with the pan-ErbB-family inhibitor Neratinib and the WNT-inhibitor LGK974. Single treatment with either inhibitor suppressed cell propagation, migration and invasion into Matrigel, whereas combined treatment had a stronger effect on both characteristics. A panel of *KRAS* mutant human lung adenocarcinoma cell lines were similarly sensitive to at least one inhibitor or to the combination of both.

With KRas being downstream of ErbB family receptors and *EGFR*- and *KRAS*-mutations being mutually exclusive in NSCLC, the reliance on ErbB family signalling

in *KRas* mutant cells was not expected. These results suggest that broad-specificity inhibitors of these proteins may be effective against a broader spectrum of NSCLC than hitherto anticipated. These results moreover indicate significant cooperation between the Ras and Wnt pathways that likewise may be exploited for therapy.

Individual p-Erk associated genes that are also amplified or overexpressed in human NSCLC were selected for an *in vitro* siRNA screen. A significant number of these genes also correlate with decreased overall survival of NSCLC and in particular lung ADC patients. Screening of 3 *KRas* mutant human lung adenocarcinoma cell lines revealed that a considerable number of genes is important for cell viability of all tested cell lines. Also, knockdown of certain genes considerably suppressed cell migration in two efficiently migrating cell lines.

These results suggest, that I have identified a list of genes that play an important role in *KRas* mutant lung adenocarcinoma.

Table of Contents

Abstract	2
Table of Contents	4
List of Figures	7
List of Tables	9
Author's declaration	11
Acknowledgements	12
Abbreviations	14
1 Introduction	23
1.1 Lung Cancer	23
1.1.1 Mutations in Lung ADC.....	23
1.1.2 Current treatment options for NSCLC.....	24
1.1.3 KRas as a therapeutic target.....	26
1.1.4 CT screening for early detection.....	30
1.2 Ras and Myc proto-oncogenes	31
1.2.1 Ras.....	31
1.2.2 Myc.....	36
1.2.3 Myc/Ras cooperation	37
1.3 Mouse Models for Lung Cancer	39
1.3.1 Classification of proliferative lung tumour lesions.....	39
1.3.2 The need of mouse models to study lung tumour progression	40
1.3.3 Mouse Models for NSCLC.....	42
1.3.4 Mouse Models for KRas mutant lung cancer	46
1.3.5 Myc overexpression in NSCLC models	48
1.4 Thesis Aims	49
2 Materials and Methods	50
2.1 Animal work	50
2.1.1 Colony maintenance.....	50
2.1.2 Genotyping.....	51
2.1.3 Experimental Cohorts	51
2.1.4 Treatments.....	52
2.1.5 Tissue sample preparation.....	53
2.2 H&E staining	54
2.2.1 Preparation of sections for IHC or H&E staining	54
2.2.2 Hematoxylin and Eosin staining	54
2.3 IHC	54
2.3.1 Formalin fixed paraffin embedded tissue samples	54
2.3.2 TUNEL staining	57
2.3.3 Fresh frozen tissue samples	58
2.3.4 CV staining	59
2.4 PCR genotyping	59
2.4.1 Genomic DNA isolation.....	59
2.4.2 PCR.....	60
2.4.3 Agarose Gel electrophoresis	60
2.5 Cell culture techniques	61
2.5.1 Fibroblast Cell culture.....	61
2.5.2 Generation of primary lung cell lines	61
2.5.3 Passaging Cells in Culture.....	62
2.5.4 Freezing down cell lines.....	62
2.5.5 Thawing cells	62

2.6	Incucyte	62
2.6.1	Cell propagation analysis.....	62
2.6.2	Cell migration analysis.....	63
2.6.3	Cell invasion analysis.....	63
2.7	siRNA Screen	63
2.7.1	Viability Assay	64
2.7.2	Migration Assay	64
2.8	Adeno-Cre infection of MEFs	64
2.9	Analysis of Cell death with Annexin V/PI staining	64
2.10	RNA isolation and quantitative Real Time PCR	65
2.10.1	cDNA synthesis	65
2.10.2	Primer design	66
2.10.3	Real Time PCR.....	67
2.11	Protein extraction and Western Blot	67
2.11.1	Protein extraction.....	67
2.11.2	Preparation of Protein Samples.....	67
2.11.3	SDS-PAGE	67
2.11.4	Western Blot.....	68
2.12	RNA-sequencing	69
2.12.1	Standard protocol.....	69
2.12.2	Amplification protocol.....	73
2.12.3	Protocol for degraded RNA samples.....	81
2.12.4	Preparation of libraries for cluster generation and sequencing.....	86
2.12.5	Sequencing data analysis.....	86
2.13	Data analysis	87
2.13.1	Graphical presentation of the data	87
2.13.2	Survival analysis.....	87
3	The role of moderately deregulated MYC in lung tumour initiation and its potential cooperation with oncogenic KRas^{G12D} or loss of functional p53	88
3.1	Introduction	88
3.2	Results	90
3.2.1	MYC driven by the Rosa26 locus	90
3.2.2	Moderate levels of deregulated MYC do not give rise to tumours.....	94
3.2.3	Absence of functional p53 does not increase MYC's tumour initiating potential	95
3.2.4	Low levels of deregulated MYC accelerate KRas ^{G12D} driven tumourigenesis.....	97
3.3	Discussion	101
3.3.1	Future directions.....	103
4	RNA-sequencing from laser captured tissue material and identification of p-Erk associated genes	104
4.1	Introduction	104
4.2	Results	104
4.2.1	p-Erk as progression marker	104
4.2.2	Technical considerations: Fresh Frozen versus FFPE tissues	105
4.2.3	Amplification does not introduce bias	107
4.2.4	RNA-Sequencing from frozen material	109
4.2.5	RNA-Seq from FFPE material.....	113
4.2.6	Comparison of Gene expression between tumours from KRas ^{G12D} and R26 ^{DM.lsl-MYC/MYC} ;KRas ^{G12D} mice.....	116
4.3	Discussion	118
5	Validation of p-Erk associated genes	121
5.1	Introduction	121
5.1.1	ErbB signalling in cancer	121
5.1.2	The Wnt pathway in cancer	125
5.2	Results	129
5.2.1	<i>In vitro</i> pathway validation.....	129

5.2.2	<i>In vivo</i> pathway validation	137
5.2.3	<i>In vitro</i> siRNA screen	142
5.3	Discussion	155
6	Final discussion and future directions	161
6.1	The role of moderately deregulated MYC expression in the lung	161
6.2	Pharmacological inhibition of p-Erk associated pathways.....	162
6.3	Targeting the Wnt pathway.....	162
6.4	Targeting ErbB signalling	165
6.5	Validation of individual p-Erk associated genes	166
6.6	Serum markers for early disease detection	167
6.7	Future directions.....	169
	Bibliography	171

List of Figures

Figure 1-1 Synthetic lethality.....	28
Figure 1-2 Ras activation and downstream effectors.....	32
Figure 1-3 Cooperation between Myc and Ras.....	38
Figure 1-4 Tumour progression.....	41
Figure 1-5 Mouse models using tissue specific promoters.....	43
Figure 1-6 Classical knock-in and knock-out models.....	43
Figure 1-7 Bitransgenic conditional tetracycline inducible models.....	44
Figure 1-8 Conditional Cre inducible models.....	45
Figure 2-1 SPIA cDNA synthesis and amplification.....	76
Figure 2-2 SMARTer cDNA synthesis and library preparation.....	82
Figure 3-1 Schematic of mouse models.....	89
Figure 3-2 Characterization of Rosa-lsl-Myc MEFs.....	91
Figure 3-3 Rosa-lsl-Myc MEFs undergo MYC induced apoptosis.....	92
Figure 3-4 Activation of Rosa-lsl-Myc in the lung.....	93
Figure 3-5 Myc induced hyperplasia.....	94
Figure 3-6 Myc and p53 transcript detection in the bronchioles.....	97
Figure 3-7 Absence of functional p53 has no influence on the outcome of acute Myc activation.....	98
Figure 3-8 Myc accelerates growth of KRas ^{G12D} initiated lung tumours.....	99
Figure 3-9 R26 ^{RS.lsl-Myc} ;KRas ^{G12D} Histology.....	101
Figure 3-10 R26 ^{DM.lsl-MYC} ;KRas ^{G12D} Histology.....	102
Figure 4-1 p-Erk serves as a tumour progression marker in R26 ^{DM.lsl-MYC/MYC} ;KRas ^{G12D} lung tumours.....	105
Figure 4-2 RNA quality and p-Erk IHC in frozen and FFPE tissues.....	106
Figure 4-3 LCM of p-Erk negative and p-Erk positive tumour regions.....	107
Figure 4-4 The effect of transcript amplification on gene expression analysis.....	108
Figure 4-5 Workflow from tissue embedding to data analysis.....	109
Figure 4-6 Comparative gene expression analysis between p-Erk negative and positive tumour regions from R26 ^{DM.lsl-MYC/MYC} ;KRas ^{G12D} mice in frozen samples.....	110
Figure 4-7 Real Time PCR validation from frozen samples.....	113
Figure 4-8 Comparative gene expression analysis between p-Erk negative and positive tumour regions from R26 ^{DM.lsl-MYC/MYC} ;KRas ^{G12D} mice in FFPE samples.....	114
Figure 4-9 Sox9 correlates with p-Erk expression in lung tumours from R26 ^{DM.lsl-MYC/MYC} ;KRas ^{G12D} mice.....	115
Figure 4-10 Comparative gene expression analysis between R26 ^{DM.lsl-MYC/MYC} ;KRas ^{G12D} and KRas ^{G12D} lung tumours.....	117
Figure 5-1 ErbB signalling.....	123
Figure 5-2 Wnt signalling pathway.....	126
Figure 5-3 LGK974 Dilution series.....	130
Figure 5-4 Neratinib dilution series.....	131
Figure 5-5 Effect of LGK974 and Neratinib on Migration and Confluency of KRas mutant lung cancer cell lines – LGK974 sensitive cell lines.....	133
Figure 5-6 Effect of LGK974 and Neratinib on Migration and Confluency of KRas mutant lung cancer cell lines – Neratinib sensitive cell lines.....	134
Figure 5-7 Effect of LGK974 and Neratinib on Migration and Confluency of KRas mutant lung cancer cell lines – Dual sensitive cell lines.....	135
Figure 5-8 Effect of LGK974 and Neratinib on invasion, migration and propagation of KRas mutant mouse cell lines.....	136
Figure 5-9 Tumour burden after LGK974 and Neratinib treatment starting 4 weeks post allele induction.....	138

Figure 5-10 Proliferation and apoptosis after LGK974 and Neratinib treatment starting 4 weeks post allele induction.	139
Figure 5-11 Tumour progression after LGK974 and Neratinib treatment starting 4 weeks post allele induction.	140
Figure 5-12 Tumour burden after LGK974 and Neratinib treatment starting 2 weeks post allele induction	141
Figure 5-13 Viability screen human KRas mutant lung cancer cell lines.....	145
Figure 5-14 Summarized Viability of human KRas mutant lung cancer cell lines.	150
Figure 5-15 Migration screen human KRas mutant lung cancer cell lines.	152
Figure 5-16 Migration without Loss of Viabilty > 30%.	153
Figure 5-17 Combined migration graph.....	154
Figure 5-18 Model of how pan ErbB family ligands contribute to MAPK signalling.	156
Figure 6-1 In vivo shRNA screen.	169

List of Tables


Table 2-1 Transgenic mouse models used in this study.....	50
Table 2-2 Adenoviral calcium-phosphate mix.....	52
Table 2-3 IHC conditions.....	55
Table 2-4 Genotyping primers.....	60
Table 2-5 Genotyping PCR cycle.....	60
Table 2-6 Transfection conditions.....	63
Table 2-7 genomic DNA removal mix.....	65
Table 2-8 cDNA synthesis master mix.....	66
Table 2-9 Real Time PCR primers.....	66
Table 2-10 Real Time PCR master mix.....	66
Table 2-11 Real Time PCR cycle.....	66
Table 2-12 SDS gel composition.....	68
Table 2-13 1X SDS running buffer.....	68
Table 2-14 1X SDS transfer buffer.....	68
Table 2-15 10X Tris buffered saline with Tween20 (TBST).....	69
Table 2-16 Antibody conditions for Western Blot.....	69
Table 2-17 Poly (A)-RNA binding.....	70
Table 2-18 further poly (A)-RNA binding.....	70
Table 2-19 Elution master mix.....	70
Table 2-20 Poly (A)-RNA elution and fragmentation.....	70
Table 2-21 First strand cDNA synthesis master mix.....	70
Table 2-22 First strand cDNA synthesis program.....	71
Table 2-23 Second strand cDNA synthesis master mix.....	71
Table 2-24 Second strand cDNA synthesis program.....	71
Table 2-25 Ligation master mix.....	72
Table 2-26 PCR amplification master mix.....	72
Table 2-27 PCR amplification program.....	72
Table 2-28 Pico green standard curve concentrations for cDNA quantification.....	73
Table 2-29 Laser settings for LCM.....	74
Table 2-30 First strand cDNA synthesis master mix.....	77
Table 2-31 First strand cDNA synthesis program.....	77
Table 2-32 Second strand cDNA synthesis master mix.....	77
Table 2-33 Second strand cDNA synthesis program.....	77
Table 2-34 SPIA amplification master mix.....	78
Table 2-35 SPIA amplification program.....	78
Table 2-36 Sonication settings.....	78
Table 2-37 End repair master mix.....	79
Table 2-38 End repair program.....	79
Table 2-39 Ligation master mix.....	79
Table 2-40 Ligation program.....	79
Table 2-41 Final repair master mix.....	79
Table 2-42 Final repair program.....	79
Table 2-43 Standards for Real Time quantification.....	80
Table 2-44 Library quantification master mix.....	80
Table 2-45 Library quantification Real Time PCR program.....	81
Table 2-46 First strand master mix.....	85
Table 2-47 PCR amplification master mix.....	85
Table 2-48 PCR amplification program.....	85
Table 3-1 Numbers and genotypes of mice expressing human c-MYC from the Rosa26 locus harvested at the indicated times post allele induction.....	95

Table 3-2 Numbers and genotypes of mice expressing murine c-Myc from the Rosa26 locus harvested at the indicated times post allele induction.	96
Table 5-1 Genes that were included in the siRNA screen	144
Table 5-2 Viability data of the KRas mutant human lung Adenocarcinoma cell lines A549, H2009 and H460.	150

Author's declaration

I herewith declare that all presented data in this thesis are the result of my own work unless stated otherwise.

This work has not been submitted for any other degree at the University at Glasgow or at any other institution.

Signature: 

Printed name: Sarah Neidler

Acknowledgements

First of all I would like to thank my supervisor Daniel Murphy for having me as a PhD student in his lab and for giving me such an exciting project. Even though it was very challenging and frustrating at times, I did enjoy establishing the techniques that were needed to complete this project. In the end I have the impression to have achieved something meaningful. His enthusiasm can be very encouraging and helped me to stay the course. I am very glad that I joined him to move to the Beatson Institute. It was a good move into an inspiring environment. We also went through difficult times and I am very glad that everything had been resolved in the end.

Nathiya started her PhD with me in Würzburg and we moved together to Glasgow. I already enjoyed the time with her in Germany and it was great to also have her here in Glasgow as a good friend. I would like to thank her for reading this thesis. She is a great scientist with a very sharp mind and helped me to recognize weaknesses. She also has an amazing character and I am glad to have her as a friend.

It was not easy to leave so many people behind in Würzburg. I had a very good time there thanks to Eva, Maria, Anne, Francesca, Tina and Nadine. It was great to have Barbara in our lab. Besides being a great help she is a lovely person and fun talking to. It is a shame that she did not move to Glasgow with us.

The “M10” group is a great lab. We had a lot of fun during our coffee breaks and I will miss them. Special thanks to Tiziana for taking good care of everything while I was writing this thesis. I am very glad that Björn will continue this project. It will be in very good hands.

My life in Glasgow was enriched thanks to my good friends Elena, Christin, Linda, Nicola, Gabriel and Evangelos.

The biological and histological services at the Beatson Institute do a great job. Our *in vivo* work would not be possible without the BSU and histology team. Ann did a brilliant job analysing my countless sequencing data and Billy was very patient in dealing with my difficult samples. I enjoyed doing the screen together with Kay and Emma did a great job in analysing the data.

My parents always support me and I would not be where I am now without their encouragement.

To my boyfriend Niels for being there for me and for his mental support.

Abbreviations

Units

°C = degree Celsius

µg = microgram

µl = microlitre

µm = micrometre

µM = micromolar

ng = nanogram

nm = nanometre

mg = milligram

kg = kilogram

ml = millilitre

A

AAH = Atypical adenomatous hyperplasia

ABC = Avidin Biotin Complex

ADC = Adenocarcinoma

ADP = Adenosine Diphosphate

Afp = Alpha-fetoprotein

Alk = Anaplastic lymphoma kinase

AMP = Adenosine Monophosphate

Aox3 = Aldehyde oxidase

APC = Adenomatous Polyposis Coli

ARF = Alternative reading frame

Arid1a = AT rich interactive domain 1A

Arntl2 = Aryl hydrocarbon receptor nuclear translocator-like 2

ATP = Adenosine Triphosphate

Atp13a4 = ATPase type 13a4

Atp6v1g3 = ATPase, H⁺ transporting, lysosomal V1 subunit G3

B

Bad = Bcl2-associated death promoter

Basp1 = Brain abundant, membrane attached signal protein 1

Bcl2 = B-cell lymphoma 2

BET = Bromodomain and Extraterminal domain family

B4galt6 = UDP-Gal:betaGlcNAc beta 1,4-galactosyltransferase, polypeptide 6
bHLHZ = Basic helix loop helix leucine zipper motif
B2m = Beta 2 microtubulin
Bp = Base pair
BRaf = serine/threonine-protein kinase B-raf
Brd4 = Bromodomain-containing protein 4
BrdU = Bromodeoxyuridine
BSA = Bovine serum albumin

C

C9 = Complement component 9
CA-125 = Cancer antigen 125
Cacnb3 = Calcium channel, voltage-dependent, beta 3 subunit
Cbr2 = Carbonyl reductase 2
CC10 = Clara cell secretory protein
Cd24a = CD24a antigen
Cd38 = CD38 antigen
CDK = Cyclin-dependent kinase
Cdkn1a = Cyclin-dependent kinase inhibitor 1A (p21)
Cdkn2a = Cyclin-dependent kinase inhibitor 2A (p16-Ink4a)
Cdkn2b = Cyclin-dependent kinase inhibitor 2B (p15-Ink4b)
cDNA = Complementary DNA
CEA = Carcinoembryonic antigen
Ceacam1 = Carcinoembryonic antigen-related cell adhesion molecule 1
Cftr = Cystic fibrosis transmembrane conductance regulator
Cldn4 = Claudin 4
Cmas = Cytidine monophospho-N-acetylneuraminic acid synthetase
Cre = Recombinant enzyme derived from P1 bacteriophage
CMV = Cytomegalovirus
Creb = cAMP response element-binding protein
CT = Computerized tomography
CV = Cresyl violet

D

DAB = 3,3'-Diaminobenzidine
DcR2 = Decoy receptor 2

dH₂O = Distilled water
Dlk1 = Delta-like 1 homolog (Drosophila)
DMSO = Dimethyl sulfoxide
DNA = Deoxyribonucleic acid
dNTP = Deoxynucleotide triphosphate
Dsc2 = Desmocollin 2
Dvl = Dishevelled, dsh homolog (Drosophila)
DTT = Dithiothreitol

E

E1A = Adenoviral early region 1A protein
ECM = Extra cellular matrix
Ecm1 = Extracellular matrix protein 1
EDTA = Ethylenediaminetetraacetic acid
Egf = Epidermal growth factor
Egfr = Epidermal growth factor receptor
EH = Epithelial hyperplasia
Eml4 = Echinoderm microtubule associated protein like 4
EMT = Epithelial to Mesenchymal Transition
ErbB1 = Receptor tyrosine-protein kinase erbB1 (also EGFR, Her1)
ErbB2 = Receptor tyrosine-protein kinase erbB2 (also Her2)
ErbB3 = Receptor tyrosine-protein kinase erbB3 (also Her3)
ErbB4 = Receptor tyrosine-protein kinase erbB4 (also Her4)
Ereg = Epiregulin
Erk = Extracellular-signal-regulated kinase, also known as mitogen-activated protein kinase
E μ -Myc = Enhancer of immunoglobulin heavy chain μ linked to Myc transgene
ER = Estrogen receptor

F

Fabp5 = Fatty acid binding protein 5, epidermal
Fam3c = Family with sequence similarity 3, member C
FBS = Fetal bovine serum
FDG-PET = Fluorodeoxyglucose-positron-emission tomography
FFPE = Formalin fixed paraffin embedded
Fgfr = Fibroblast growth factor receptor

FLP = Flippase

Fmo1 = Flavin containing monooxygenase 1

Fmo2 = Flavin containing monooxygenase 2

FRT = Flippase recognition target

Fzd = Frizzled homolog (Drosophila)

G

Gapdh = Glyceraldehyde-3-phosphate dehydrogenase

GAPs = GTPase activating proteins

Gata2 = GATA binding protein 2

gDNA = Genomic DNA

GEF = Guanine nucleotide exchange factor

GDP = Guanosine diphosphate

GEMMs = Genetically engineered mouse models

GFP = Green fluorescent protein

GLUT1 = Glucose transporter protein type 1

Golm1 = Golgi membrane protein 1

Grb2 = Growth factor receptor bound protein 2

GSEA = Gene set enrichment analysis

Gsk 3- β = Glycogen synthase kinase 3 beta

GTP = Guanosine-5'-triphosphate

H

HA = Human influenza hemagglutinin

Hdc = Histidine decarboxylase

HEPES = 4-(2-hydroxyethyl)-1-piperazineethanesulfonic acid

H-3K27me3 = Histone 3 Lysine 27 trimethylation

Hp β = Haptoglobin β chain

HR = Hazard ratio

HRP = Horse radish peroxidase

H&E = Hematoxylin and Eosin staining

HRas = Harvey rat sarcoma virus oncogene

I

IHC = Immunohistochemistry

Ig = Immunoglobulin

Igfbp3 = Insulin-like growth factor binding protein 3

Igfbp5 = Insulin-like growth factor binding protein 5

IP injection = Intraperitoneal injection

Itga2 = Integrin alpha 2

Itgb4 = Integrin beta 4

IVCs = Individually ventilated cages

K

Keap1 = Kelch-like ECH-associated protein 1

Kif23 = Kinesin family member 23

Klkb1 = Plasma kallikrein

KRas = Kirsten rat sarcoma viral oncogene homolog

Krt8 = Keratin 8

Krt18 = Keratin 18

Krt19 = Keratin 19

L

Lad1 = Ladinin 1

Lamc2 = Laminin, gamma 2

Lars2 = Leucyl-tRNA synthetase

LCC = Large-cell carcinoma

LCM = Laser capture microscope

Lef = Lymphoid enhancer binding factor

Lgals3bp = Lectin, galactoside-binding, soluble, 3 binding protein

Lkb1 = Liver kinase B1

LoxP = Locus of x-over P1

LTR = Long terminal repeat

M

Malat = Metastasis associated lung adenocarcinoma transcript 1

MAPK = Mitogen-activated protein kinase

Max = Max protein

MEFs = Mouse embryonic fibroblasts

MEK = Mitogen-activated protein kinase kinase

Met = Met proto-oncogene

Mga = MAX gene associated

MMTV = Mouse mammary tumour virus
MNU = N-methyl-N-nitrosourea
mTOR = Mammalian target of Rapamycin
Myc = Myelocytomatosis oncogene
Myc-ER = Myc-oestrogen receptor fusion transgene
Myrf = Myelin regulatory factor

N

NdrG1 = N-myc downstream regulated gene 1
NGS = Normal goat serum
Nf1 = Neurofibromatosis 1
NLST = National lung screening trial
NRas = Neuroblastoma ras oncogene
NSCLC = Non-small cell lung cancer
NTC = Non-targeting control
Nt5e = 5' nucleotidase, ecto

O

4-OHT = 4-Hydroxy tamoxifen
OIS = Oncogene-induced senescence
OS = Overall survival

P

P130 = Retinoblastoma-related protein 2
p53 = Cellular tumour antigen p53
p63 = Transformation-related protein 63
PBS = Phosphate buffered saline
PCR = Polymerase chain reaction
PDGF = Platelet derived growth factor
Pdia4 = Protein disulfide isomerase associated 4
PFS = Progression free survival
Pgk1 = Phosphoglycerate kinase 1
PH domain = Pleckstrin homology domain
Phlda1 = Pleckstrin homology-like domain, family A, member 1
PI = Propidium iodide

Pi3kca = Phosphatidylinositol 4,5-bisphosphate 3-kinase catalytic subunit alpha isoform
PIP2 = Phosphatidylinositol (4,5)-bisphosphate
PIP3 = Phosphatidylinositol (3,4,5)-triphosphate
Plekha6 = Pleckstrin homology domain containing, family A member 6
PLL slides = Poly-L-Lysine coated slides
Porcn = Porcupine
PSA = Prostate-specific antigen
Pten = Phosphatase and tensin homolog
Ptges = Prostaglandin E synthase

R

Rabgap1l = RAB GTPase activating protein 1-like
Rap120 = Ras related protein 120
Ral = Ras related protein Ral
Rb1 = Retinoblastoma 1
Rbp7 = Retinol binding protein 7
Rbm10 = RNA binding motif protein 10
REF = Rat embryonic fibroblasts
RERTn = Cre-ERT2 recombinase under the control of the large subunit of RNA polymerase II locus
Ret = Ret proto-oncogene
Rgcc = Regulator of cell cycle
Rgs5 = Regulator of G-protein signalling
Rho = Rhodopsin
RKIP = Raf kinase inhibitor protein
Rock = Rho-associated coiled-coil containing protein kinase
RIN = RNA integrity number
RIPA = Radioimmunoprecipitation assay buffer
Rit1 = Ras-like without CAAX 1
RNA = Ribonucleic acid
RNAi = RNA interference
Ros1 = Ros1 proto-oncogene
rRNA = Ribosomal RNA
RT = Room temperature
Rtk = Receptor tyrosine kinase

rtTA = Reverse tetracycline-controlled transactivator

RWD = Relative wound density

S

S100a6 = S100 calcium binding protein A6 (calcyclin)

S100a11 = S100 calcium binding protein A11 (calcyclin)

S100a14 = S100 calcium binding protein A14 (calcyclin)

SA β -Gal = Senescence-associated beta-galactosidase

SCC = Squamous-cell carcinoma

SCLC = Small cell lung cancer

SDS = Sodium Dodecyl sulphate

Ser = Serine

Setd2 = SET domain containing 2

Sftpa1 = Surfactant associated protein A1

siRNA = Small interfering RNA

SH2 domain = Src homology 2 domain

SH3 domain = Src homology 3 domain

shRNA = Short hairpin RNA

Slc2a1 = Solute carrier family 2 (facilitated glucose transporter), member 1

Slc38a1 = Solute carrier family 38, member 1

Smarca4 = SWI/SNF related, matrix associated, actin dependent regulator of chromatin, subfamily a, member 4

Sox9 = SRY-box containing protein 9

Sp-C = Surfactant protein C

Spry = Sprouty homolog 2

Stk39 = Serine/threonine kinase 39

T

Tace = Tumour necrosis factor alpha converting enzyme

TAE = Tris-acetate-EDTA buffer

Tam = Tamoxifen

TBS = Tris-Buffered saline

TBS-T = Tris-Buffered saline and Tween20

Tcf = Transcription factor

TdT = Terminal nucleotidyl transferase enzyme

TGF- α = Transforming growth factor alpha

Tnfrsf12a = Tumor necrosis factor receptor superfamily, member 12a

Tnfrsf21 = Tumor necrosis factor receptor superfamily, member 21

Tp53 = p53 gene

TRE = Tetracycline-responsive promoter element

Tspan 8 = Tetraspanin 8

TTF-1 = Thyroid transcription factor 1

TUNEL = Terminal nucleotidyl transferase dUTP nick end labeling

Tyr = Tyrosine

U

U2af1 = U2 small nuclear ribonucleoprotein auxiliary factor 1

V

Vcam1 = Vascular cell adhesion molecule 1

VEGF = Vascular endothelial growth factor

VEGFR = Vascular endothelial growth factor receptor

W

Wnt = Wingless-related MMTV integration site

1 Introduction

1.1 Lung Cancer

Lung cancer is the leading cause of cancer death worldwide with a 5-year survival rate of 15.9% (Ettinger et al., 2013). Non-small-cell lung cancer (NSCLC) represents with 85% the major histopathological group of lung cancer and can be further subdivided into adenocarcinomas (ADC, ~50%), squamous-cell (SCC, ~40%) and large-cell carcinomas (LCC, ~10 %) (Chen et al., 2014). The remaining 15% of lung cancers have neuroendocrine origin; Small-cell lung cancer (SCLC) is the most common form in this group.

ADCs are located in the distal airways, whereas SCCs are more proximal. Histologically they can be distinguished by expression of biomarkers. Two useful biomarkers for this purpose are thyroid transcription factor 1 (Ttf-1) and p63. ADCs stain positive for Ttf-1 and are negative for transformation-related protein 63 (p63), whereas SCCs are Ttf-1 negative and stain positive for p63 (Rekhtman et al., 2011).

1.1.1 Mutations in Lung ADC

Recent molecular profiling of lung ADC revealed that kirsten rat sarcoma viral oncogene homolog (*KRAS*) is mutated in 33% of ADC (Cancer Genome Atlas Research, 2014), but is rarely mutated in SCC (Cancer Genome Atlas Research, 2012). Besides *KRAS* epidermal growth factor receptor (*EGFR*, 14%), liver kinase B1 (*LKB1*, 17%), kelch-like ECH-associated protein 1 (*KEAP1*, 17%) and cellular tumour antigen p53 (*Tp53*, 46%) are the most commonly mutated genes in lung ADC. Other mutations include serine/threonine-protein kinase B-Raf (*BRAF*, 10%), Phosphatidylinositol 4,5-bisphosphate 3-kinase catalytic subunit alpha isoform (*PI3KCA*, 7%), met proto-oncogene (*MET*, 7%), Ras-like without CAAX 1 (*RIT1*, 2%), neurofibromatosis 1 (*NF1*, 11%), retinoblastoma 1 (*RB1*, 4%), cyclin-dependent kinase inhibitor 2A (*CDKN2A*, 4%), SET domain containing 2 (*SETD2*, 9%), AT rich interactive domain 1A (*ARID1A*, 7%), SWI/SNF related, matrix associated, actin dependent regulator of chromatin, subfamily a, member 4 (*SMARCA4*, 6%), RNA binding motif protein 10 (*RBM10*, 8%), U2 small nuclear ribonucleoprotein auxiliary factor 1 (*U2AF1*, 3%) and MAX gene associated (*MGA*, 8%). *MGA* is a MAX interacting protein and mutations increase myelocytomatosis

oncogene (MYC) activity. Mutations in *MGA* are mutually exclusive with *MYC* amplification (Cancer Genome Atlas Research, 2014).

1.1.2 Current treatment options for NSCLC

Which treatment options is chosen mainly depends on the tumour stage and the overall health of the patient.

Treating stage 0

Stage 0 NSCLC is limited to a few layers of cells in the airways and has not grown deeper into the lung. It can be treated by surgery without the need of chemotherapy or radiation (www.cancer.org).

Treating stage I

In some cases stage I can be treated by surgery alone. Depending on the size and location of the tumour either the entire lobe (lobectomy) or a smaller piece of the lung (wedge resection) will be removed. Following adjuvant chemotherapy can be used to lower the risk of recurrence (Zarogoulidis et al., 2013). A platinum based drug such as cisplatin and carboplatin, is commonly used in combination with one other drug. Radiotherapy is used to kill cells that have been left behind during surgery (www.cancer.org).

Treating stage II

Stage II cancers are usually removed by surgery, along with local lymph nodes that are also likely to have cancer cells. Chemotherapy and radiotherapy can be used beforehand to shrink the tumour (www.cancer.org). Chemotherapy and radiation, either alone or in combination, help to kill cancer cells that may have left behind during surgery (Zarogoulidis et al., 2013).

Treating stage IIIA

Treatment of stage IIIA usually includes chemotherapy and radiotherapy, with or without surgery, depending on the health status of the patient. If the patient can tolerate it, treatment starts with chemotherapy, often in combination with radiotherapy. In a following surgery, remaining cancer can be removed. If the health

status does not allow surgery, radiation therapy, also in combination with chemotherapy is used (www.cancer.org).

Treating stage IIIB

Stage IIIB is defined as lung cancer that has spread to local lymph nodes and other parts of the chest. It therefore cannot be completely removed by surgery. If the patient is healthy enough, he can be treated with chemotherapy in combination with radiotherapy. Patients with a poor health status can be treated with either chemotherapy or radiotherapy alone (www.cancer.org).

Treating Stage IV

Stage IV cancer has spread to distant sites when it is diagnosed and is very difficult to cure. Treatments such as surgery, chemotherapy and radiotherapy can help to relieve symptoms and to increase survival (www.cancer.org). The tumours will also be tested for the presence of certain mutations. If certain markers are present, targeted therapy might be a good treatment option (Zarogoulidis et al., 2013).

1.1.2.1 Targeted therapies

Targeted treatment options improved recently for patients with *EGFR* mutant lung cancer and lung cancer with anaplastic lymphoma kinase (*ALK*), Ros1 proto-oncogene (*ROS1*) and ret proto-oncogene (*RET*) translocations.

EGFR mutations

The EGFR inhibitors Erlotinib and Gefitinib have been shown to increase progression free survival (PFS) compared to chemotherapy. Erlotinib has been shown to increase PFS to 10.4 months compared to chemotherapy (5.2 months) (Khozin et al., 2014) and Gefitinib improved survival to 10.8 months compared to chemotherapy (5.4 months) (Maemondo et al., 2010). However neither therapy provided a significant overall survival (OS) benefit.

EML4/ALK fusion genes

Echinoderm microtubule associated protein like 4 (*EML4*)/*ALK* fusion genes occur in 5% of NSCLC and these tumours are sensitive to the tyrosine kinase inhibitor Crizotinib (Shaw et al., 2013). Crizotinib has been shown to increase PFS to 7.7

months compared to 3 months with chemotherapy in patients with advanced *ALK* positive NSCLC, but it did not increase OS survival.

ROS1 rearrangements

ROS1 rearrangements occur in 1% of NSCLC. NSCLC patients with *ROS1* rearrangements that were treated with Crizotinib had similar response rates (72%) as patients with *ALK* fusion genes (61%) (Shaw et al., 2014). PFS was 19.2 months and overall survival rate at 12 months was 85%. The median overall survival could not be determined, as the median was not reached at the date of data-cutoff.

RET fusion genes

RET fusions occur in 1% of NSCLC. 3 patients were treated with Cabozantinib, a multi-tyrosine kinase inhibitor. At the time of data-cutoff, all 3 patients were still progression free. 2 patients had a partial response and the third patient had a prolonged stable disease of 8 months at the date of data-cutoff. A larger phase II clinical trial of Cabozantinib for *RET* fusion NSCLC is currently recruiting patients (Drilon et al., 2013).

Unfortunately, most tumours acquire resistance to tyrosine kinase inhibitors within 9-12 months of treatment (Chen et al., 2014; Katayama et al., 2012; Kobayashi et al., 2005). For this reason patients present with stage I to IIIA tumours with targetable driver mutations undergo surgery and receive combination chemotherapy as a standard of care (Chen et al., 2014; Pignon et al., 2008).

1.1.3 KRas as a therapeutic target

KRAS is with 33% the most frequently mutated oncogene in lung ADC and activating *KRAS* mutations are associated with poor prognosis (Cancer Genome Atlas Research, 2014; Slebos et al., 1990). *KRAS* withdrawal leads to tumour regression in *KRAS* mutant lung ADC mouse models and is thereby a promising target (Fisher et al., 2001).

1.1.3.1 Targeting KRas directly

KRAS has been proven difficult to be targeted directly. One approach is to use molecules that compete with GTP binding, which is essential for *KRAS* activation.

This has been impossible so far, as KRas has a very high GTP affinity in the picomolar range and GTP molecules are present in the cell in millimolar concentrations. Moreover, KRas does not possess deep hydrophobic pockets that would allow easy binding of small molecule inhibitors.

Another approach is to inhibit guanine exchange factors (GEFs). GEFs promote the dissociation of GDP from KRas, which then allows binding of GTP. Even though this strategy seems to be a good approach in theory, no inhibitors have been developed that would be potent enough to inhibit mutant KRas function *in vivo*.

Association of KRas with the plasma membrane is crucial for its function. This requires the addition of a C15 farnesyl isoprenoid lipid to the carboxyterminal end of KRas. Therefore, inhibiting farnesyl transferases might be a feasible approach to inhibit KRas (Berndt et al., 2011). Farnesyl inhibitors have made it to phase III clinical trials. They failed because they inhibited Harvey rat sarcoma virus oncogene (HRas), instead of KRas. Another caveat in the inhibition of farnesyl transferases is, that they are unspecific as many proteins in the cell are farnesylated. Moreover, KRas can become a target for a related prenyl transferase that leads to alternative prenylation of KRas that allows KRas' attachment to the membrane (Whyte et al., 1997).

1.1.3.2 Indirect targeting of KRas

Approaches to indirectly target *KRAS* mutant lung cancer include inhibiting downstream signalling and targeting proteins that are synthetic lethal with mutant *KRAS*.

Targeting the downstream MAPK pathway

Targeting the mitogen-activated protein kinase (MAPK) pathway with the mitogen-activated protein kinase kinase (MEK) inhibitor Selumetinib was shown to be effective in a subset of *KRAS* mutant lung cancers (Chen et al., 2012). A co-clinical trial involving mouse models with mutant *KRAS* and loss of *Lkb1*, as well as *KRAS* and *Tp53* mutations, revealed that *KRAS* and *Tp53* mutant but not *KRAS* and *Lkb1* mutant murine lung tumours were sensitive to Selumetinib in combination with the chemotherapeutic agent Docetaxel. The primary resistance of *KRAS/Lkb1* mutant tumours was associated with an increased metabolic activity of the tumours, which

was shown by fluorodeoxyglucose-positron-emission tomography (FDG-PET). Co-treatment of *KRAS* mutant lung cancer patients with Selumetinib and Docetaxel showed that *LKB1* mutation status and metabolic activity have prognostic value to Selumetinib response in human cancer as well.

Engelman et al. (Engelman et al., 2008) showed in a *KRas* mutant mouse model that Selumetinib in combination with a Pi3k and mammalian target of Rapamycin (mTor) inhibitor (Bez235) was more effective than Selumetinib on its own. A phase 2 study with patients with *KRAS* mutant advanced NSCLC showed that Selumetinib in combination with Docetaxel increased PFS (5.3 months) compared to Docetaxel alone (2.1 months) (Janne et al., 2013). Combination therapy however also increased toxicity with more grade 3-4 adverse events than with Docetaxel only.

Synthetic lethality approaches

Knockdown of genes that are synthetic lethal with *KRas* affects *KRas* mutant cells but not *KRas* wild-type cells (Figure 1-1). RNA interference (RNAi) screening led to the discovery of genes that are synthetic lethal in *KRas* mutant cancer.

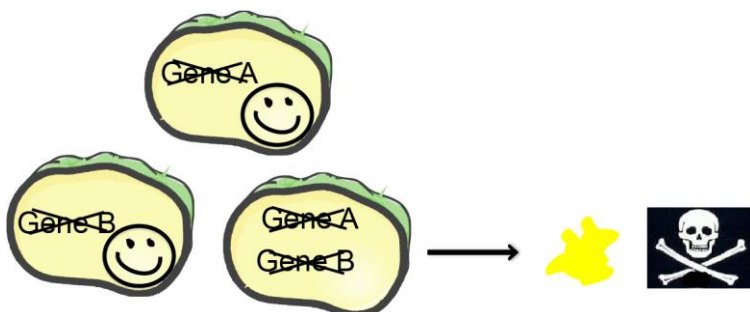


Figure 1-1 Synthetic lethality.

The principle of synthetic lethality: If either gene A or gene B is mutated, the cell is not affected. If gene A and gene B are mutated, the cell dies.

GATA2

One synthetic lethal gene that was discovered this way is the transcription factor GATA binding protein 2 (*GATA2*) (Kumar et al., 2012). Its synthetic lethal effect could be confirmed *in vivo* by inhibiting *GATA2* downstream pathways with the pharmacological inhibitors Bortezomib and Fasudil. This led to dramatic regression of established tumours in a *KRas* mutant lung cancer mouse model. Bortezomib is a proteasome inhibitor and Fasudil is a rhodopsin/Rho-associated coiled-coil containing protein kinase (RHO/ROCK) inhibitor and both have been approved for

use in human patients. A phase II trial of Bortezomib in patients with *KRAS* mutant NSCLC is currently on-going (<https://clinicaltrials.gov/show/NCT01833143>).

Cdk4

Loss of the interphase cyclin-dependent kinase 4 (*Cdk4*) has been shown to be synthetic lethal with mutant *KRas*. In a *KRas* mutant lung ADC model, ablation of *Cdk4* led to senescence in these tumours (Puyol et al., 2010). A clinical trial with the CDK4/6 inhibitor LY2835219 is currently on-going (<https://clinicaltrials.gov/show/NCT01394016>).

c-Raf

It was shown in a *KRas* mutant lung ADC mouse model that tumour initiation depends on the presence of *c-Raf* (Jackson et al., 2001). Surprisingly, *c-Raf* was not required for tissue homeostasis in adult mice. It still needs to be investigated if *c-Raf* abrogation has an effect on established tumours as well (Blasco et al., 2011).

Myc

Another synthetic lethal gene in *KRas* driven lung cancer is *Myc*. *Myc* is as a transcription factor difficult to target, but might be inhibited by targeting its interaction with other proteins. Omomyc, a dominant negative *Myc* interacting protein, binds *Myc* and thereby prevents *Myc* from binding to its binding partner max protein (Max), which is important for *Myc*'s transcriptional activity (Soucek et al., 2008). It was shown in a *KRas* driven mouse model that Omomyc is able to mediate rapid tumour regression and progressive eradication (Soucek et al., 2013).

Another approach of targeting *Myc* involves the use of bromodomain inhibitors. Monoacetylated lysine residues that are found on N-terminal tails of histones are bound by bromodomain containing proteins, which leads to chromatin remodelling and is required for transcriptional activation of certain genes. The bromodomain and extra terminal (BET) bromodomain inhibitor JQ1 has been shown to inhibit bromodomain-containing protein 4 (Brd4) and to downregulate *Myc* and its target genes (Ott et al., 2012). It has been shown In a *KRas*-mutant NSCLC model that JQ1 treatment leads to tumour regression (Shimamura et al., 2013).

1.1.4 CT screening for early detection

About 75% of lung cancer cases are diagnosed at advanced stage. Earlier detection could drastically improve survival rates. As part of a study that was designed in order to examine the diagnostic value of low-dose computerized tomography (CT), 31,567 asymptomatic persons were screened (International Early Lung Cancer Action Program et al., 2006). 85% of lung cancer that was detected in participants of this study was stage I and this group of patients had an estimated 10-year survival rate of 88%. Persons that were diagnosed with stage I lung cancer and underwent surgical resection within one month of diagnosis had an even better prognosis with an estimated 10 year survival rate of 92%.

Another trial, the National Lung Screening Trial (NLST), recruited 53,454 participants at high lung cancer risk and divided them randomly into 2 groups that were either screened using low-dose CT or chest radiography (National Lung Screening Trial Research et al., 2011). There was a 20% reduction of Lung Cancer deaths in the low-dose CT group compared to the chest radiography group.

These numbers demonstrate that early diagnosis is crucial in order to improve survival rates, as even with the improvement of targeted therapies treatment of late stage disease is very challenging. A big problem with low-dose CT however is the very high rate of false positives, which came to ~95% in the NLST (National Lung Screening Trial Research et al., 2011). These people then had to undergo further screening and biopsies, which was associated with unnecessary and potentially risky interventions, especially for old people with a poor health condition. Attempts to reduce the number of false positives include raising the threshold of the lesion size that are counted as positive and repeated imaging in order to detect a growing lesion (Henschke et al., 2013; Horeweg et al., 2013).

Nevertheless, additional methods that can complement or replace CT screening are needed. Ideal for this purpose would be biomarkers that are detectable in the blood or breath, as they could be tested in a non-invasive manner. Moreover, a simple reliable test such as a routine blood test could possibly be applied to a larger group of people than it is possible with CT screening. CT screening is considered for people at high lung cancer risk between 55 and 80 years of age, which means that

lung cancer cases that do not fall into this group will be missed (Humphrey et al., 2013).

Another approach to detect lung cancer is to look at gene expression profiles of cells in the airways, which can be sampled by brushes. A study compared gene expression profiles from smokers with and without lung cancer and identified 80 biomarkers that were associated with lung cancer (Spira et al., 2007). However, the prognostic value of this method still needs to be proven.

The difficulty of identifying suitable biomarkers for early disease detection goes back to the original problem, the fact that the vast majority of lung cancer cases are detected at an advanced stage. It would be possible to analyse biomarkers from late stage patients, but this would not tell anything about biomarkers that are increased in early disease, which are needed in order to detect the disease at an early stage. Genetically engineered mouse models (GEMMs) are able to close this gap. Tumour development is very reproducible in these models and they allow the study of early stage lung tumours. A better understanding of molecular changes during early disease would help to find reliable biomarkers that could allow early diagnosis and would thereby help to improve survival rates.

1.2 Ras and Myc proto-oncogenes

1.2.1 Ras

Ras proteins consist of 3 family members, HRas, NRas and KRas. KRas is essential during embryonic development, as *KRas* knockout is embryonic lethal (Koera et al., 1997), *HRas* and *NRas* knockout mice are however viable (Esteban et al., 2001; Umanoff et al., 1995). Ras proteins are GTPases that become activated through GTP binding and that hydrolyse GTP to GDP (McGrath et al., 1984). The activity of Ras proteins depends on extracellular stimuli (Figure 1-2).

One way of activating Ras proteins is through tyrosine protein kinase receptors, which are located in the plasma membrane and become activated through ligand binding, such as epidermal growth factor (EGF). Growth factor receptor bound protein 2 (GRB2) proteins function as adaptor proteins, which bind activated protein kinase receptors through an Src homology 2 (SH2) domain and Guanine exchange factors (GEFs) through 2 Src homology 3 (SH3) domains (Egan et al., 1993). GEFs

stimulate GDP release, which enables Ras to be bound and activated by a new GTP molecule (Wolfman and Macara, 1990). GTPase activating proteins (GAPs) on the other hand are able to inhibit Ras activity by stimulating GTP hydrolysis (Vogel et al., 1988).

Ras mutations that decrease the GTPase activity of the Ras protein and thereby increase its activity are often found in human cancer. The two most frequent mutations affect codons 12 and 61. Codon 12 of the Ras gene encodes for glycine, which is the only amino acid without a side chain. Replacement of glycine with a side chain containing amino acid results in a conformational change that affects the interaction with GAPs and thereby decreases the GTPase activity of Ras (Scheffzek et al., 1997). Codon 61 encodes for glutamine, which forms a hydrogen bond with Arg789 in Ras-related protein 120 (RAP120). A H₂O molecule can attack this hydrogen bond, which then leads to GTP hydrolysis (Scheffzek et al., 1997).

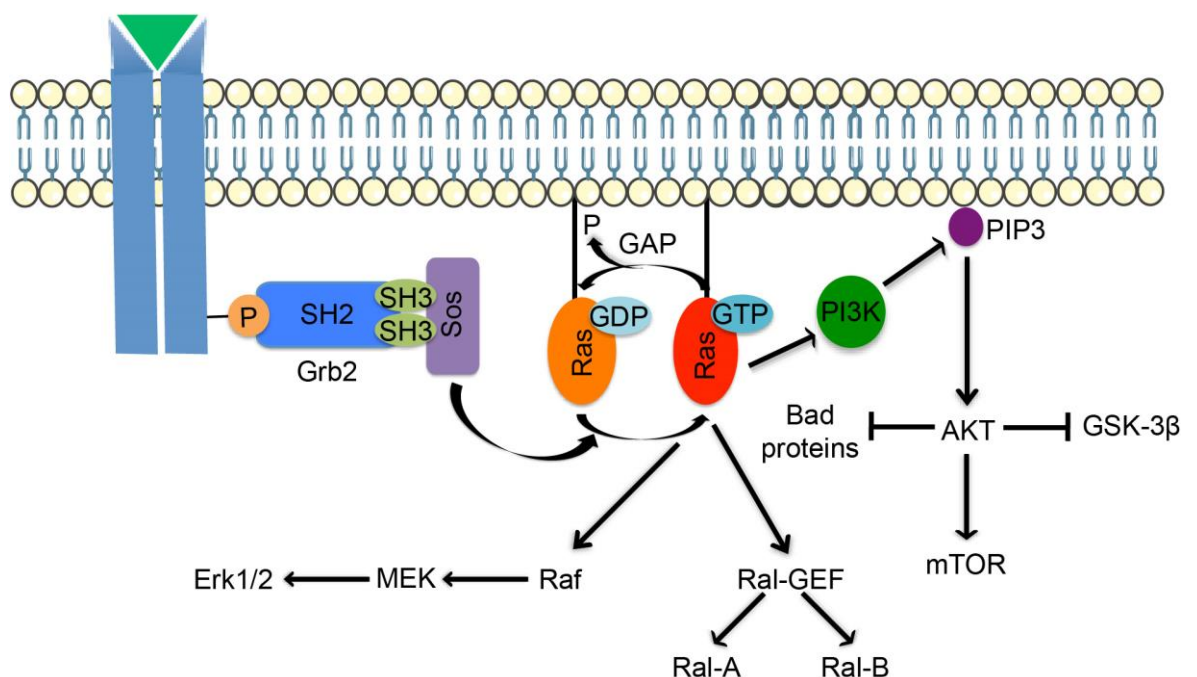


Figure 1-2 Ras activation and downstream effectors.

Ras is positively regulated by GEFs (Sos). Grb2 adaptor proteins bind phosphorylated receptors through their SH2 domain and Sos through their SH3 domains, which allows Sos to activate Ras. Ras is negatively regulated by GAPs. PI3K, Raf and Ral are three important Ras effectors.

These mutations make the Ras protein independent from activation through GEFs. The activated, GTP bound Ras protein can signal through various effector pathways. It can for instance interact with Raf, a serine/threonine kinase, which is part of the MAPK pathway (Vojtek et al., 1993; Zhang et al., 1993).

Another Ras effector is the catalytic subunit of phosphatidylinositol 3-phosphate (Pi3k) (Sjolander et al., 1991). Pi3k phosphorylates phosphatidylinositol (4,5)-bisphosphate (PIP₂), which then becomes phosphatidylinositol (3,4,5)-triphosphate (PIP₃). Pleckstrin homology (PH) domain containing proteins are able to bind PIP₃. One such PH domain containing protein is the serine/threonine kinase Akt, which gains kinase activity upon PIP₃ binding. Akt can then again activate multiple effector pathways such as mTor, which stimulates protein synthesis and thereby cell growth (Inoki et al., 2002). Akt can also inactivate glycogen synthase kinase 3 beta (Gsk-3 β) (Cross et al., 1995), which antagonises proteins involved in cell proliferation and pro-apoptotic Bcl-2-associated death promotor (Bad) proteins (Datta et al., 1997), thereby inhibiting apoptosis.

Another important Ras effector is Ras related protein Ral (Ral). Ral proteins are similar to Ras proteins and also become activated through GTP binding (Chardin and Tavitian, 1986). Ras activates Ral by activating Ral-GEFs (Hofer et al., 1994). Activated Ral proteins can again activate downstream effectors. There is some evidence that Ral proteins promote cell motility (Lim et al., 2006; Oxford et al., 2005).

1.2.1.1 Consequences of oncogenic Ras

Overexpression of oncogenic Ras leads after an initial wave of proliferation to growth arrest in primary rat embryonic fibroblasts (REFs) (Land et al., 1986). For transformation of primary cells, KRas needs a cooperating oncogene, such as Myc or the adenoviral early region 1A protein (E1A), or loss of tumour suppressor genes such as the alternate reading frame protein p19Arf or p53. KRas is however able to transform already immortalized cells, such as NIH-3T3 cells. These observations led to the discovery of oncogene-induced senescence (OIS), which is seen as a fail-safe mechanism to prevent tumourigenesis.

Until several years ago, OIS was seen as a cell culture artefact triggered by strong overexpression of oncogenes. In agreement with this Tuveson et al. showed that activation of endogenous Cre inducible mutant *KRas*^{G12D} in primary MEFs leads to immortalization instead to senescence (Tuveson et al., 2004). Interestingly, MAPK- and PI3K-pathway were not upregulated, but even suppressed in *KRas*^{G12D} MEFs compared to uninduced MEFs. In line with this, the MAPK pathway has been shown to trigger Ras induced senescence (Lin et al., 1998; Serrano et al., 1997). This

suggests that high but not low levels of oncogenic KRas are able to engage tumour suppressor pathways that then lead to senescence. Guerra et al. (Guerra et al., 2003) observed the same phenotype with endogenous mutant *KRas*^{G12V} in primary MEFs.

In vivo, the lung is susceptible to tumour formation upon *KRas* mutation (Johnson et al., 2001). Tuveson et al. confirmed in a Cre inducible *KRas*^{G12D} model, that mutant *KRas* gives rise to tumours in the lung (Tuveson et al., 2004). Epithelial hyperplasia could be detected 4 days after allele induction already, showing that no additional mutations are required. In agreement with the observations in MEFs, the hyperplastic lesions did not stain positive for p-Erk and no senescence or cell cycle arrest markers could be detected (p53, p16-Ink4a (Cdkn2a), p19Arf, p21).

Another study investigated the induction of p19Arf in a *KRas* mutant model (*KRas*^{La2}), in which mutant *KRas*^{G12D} is activated by spontaneous somatic recombination (Johnson et al., 2001), using a green fluorescent protein (*GFP*) allele that is knocked into the endogenous *p19Arf* locus. The mice are then null for *p19Arf* and on the same time activation of the *p19Arf* locus can be followed by GFP expression (Young and Jacks, 2010). The *KRas*^{La2}/*p19Arf*^{GFP} mice developed a tumour spectrum that was different from *KRas*^{La2} mice. Besides the lung tumours, thymic lymphomas and papillomas that were seen in the *KRas*^{La2} mice, *Kras*^{La2}/*p19Arf*^{GFP} mice developed also muscle-specific sarcomas and had enlarged spleens and kidneys with cells that displayed aberrant nuclei. Strikingly, lung tumours were negative for GFP, whereas sarcomas were positive, indicating that p19Arf suppressed sarcoma tumourigenesis in *KRas*^{La2} mice. This indicates, that not only expression levels of oncogenic KRas dictate whether the cells respond with proliferation or senescence, but also the cell type in which oncogenic KRas is expressed. Closer examination revealed that the *p19Arf* locus was silenced by Polycomb-group protein (PcG) mediated Histone 3 Lysine 27 trimethylation (H3-K27me3) in the lung tumours, which was not the case in sarcomas.

Two other independent studies confirmed that the p19Arf/p53 pathway is not engaged in early stage KRas driven lung tumours even though loss of *Tp53* has been shown to accelerate KRas driven tumourigenesis in the lung (Jackson et al., 2005). In a *KRas*^{G12D}/*Tp53*^{null} model, in which *Tp53* could be restored by Tamoxifen administration, it was shown that *Tp53* restoration had no effect on early stage lung

tumours, whereas in advanced stage tumours it led to p21 expression and tumour regression (Feldser et al., 2010). This was confirmed independently in a similar mouse model (Junttila et al., 2010). This shows that endogenous KRas is driving tumorigenesis in the lung without engaging tumour suppressive mechanisms, explaining why certain lung cells are susceptible to *KRas* mutations.

On the other hand in a *KRas*^{G12V} mutant mouse model in which endogenous *KRas* is replaced by *KRas*^{G12V} (Guerra et al., 2003), induction of *KRas*^{G12V} gave rise to tumours in the lung, but they were shown to initially express senescence markers (p16, p15-Ink4b (Cdkn2b), deleted in esophageal cancer 1 (Dec1), decoy receptor 2 (DcR2) and senescence-associated beta-galactosidase (SA β-Gal)), which were lost during progression to adenocarcinomas. The reason for the different phenotype in the two models is not clear. One difference is that induction of the allele was achieved in different ways: spontaneous somatic activation (Johnson et al., 2001) in the *KRas*^{La2} model, or Adeno-viral Cre induction in the *Isl-KRas*^{G12D} model, whereas the *Isl-KRas*^{G12V} allele was induced either by tamoxifen-inducible Cre (Cre-ER^{T2}) under the control of the large subunit of RNA polymerase II locus (*RERTn*), or by cytomegalovirus (*CMV*)-Cre. Therefore, induction in the *KRas*^{G12D} models was sporadic and limited to a relatively low number of cells, whereas the constitutively active promoters in the *KRas*^{G12V} model gave rise to Cre expression and allele induction in the whole animal. Besides this, the only variation is the amino acid substitution in the point mutation, but this should not make a difference as they are both activating the KRas protein by the same mechanism.

This is one example that shows that OIS is not a cell culture artefact, but indeed occurs *in vivo*. There are evidences that *in vivo* as well the decision if KRas induces proliferation or senescence is dose dependant. An elegant study using a dox inducible *KRas* allele under the mouse mammary tumour virus (*MMTV*) promoter showed that low levels of KRas induced proliferation leading to focal hyperplasias in the duct, whereas high level of KRas led initially to a high rate of proliferation that then soon decreased and resulted in inhibition of ductal elongation (Sarkisian et al., 2007). This demonstrated nicely that within the same model, the levels of KRas determine if KRas induces proliferation or senescence.

In summary, KRas levels crucially influence the fate of the cell by inducing either proliferation or senescence, but on the same time different cell types have variable

intrinsic properties that determine the cell's tumourigenic sensitivity to *KRas* mutations.

1.2.2 Myc

Myc (c-Myc) belongs to a family of genes consisting of c-Myc, N-Myc and L-Myc (Nau et al., 1985; Slamon et al., 1986; Vennstrom et al., 1982) and is a transcription factor that is involved in many physiological processes, such as cell proliferation and growth, differentiation, apoptosis, metabolism and DNA repair (Dang, 1999; Fernandez et al., 2003). As a basic helix-loop helix/leucine zipper (bHLHZ) protein, Myc binds together with its binding partner Max to specific DNA sequences, called E-boxes, to activate target genes (Blackwell et al., 1990; Blackwood and Eisenman, 1991). By binding to Miz-1 Myc is on the other hand also able to repress gene transcription (Peukert et al., 1997).

1.2.2.1 Consequences of oncogenic Myc

In vitro, Myc overexpression drives hyperproliferation, but also sensitizes cells to undergo apoptosis under low serum conditions (Evan et al., 1992). This is dose dependent, as clones expressing higher Myc levels showed higher levels of apoptosis.

In vivo, low levels of deregulated *MYC* expression driven by the *Rosa26* promoter drives proliferation in multiple tissues, but is on its own not sufficient for tumour initiation (Murphy et al., 2008). Colon is the only tissue with significant levels of apoptosis in this model, which is probably due to higher *MYC* expression. To confirm that high *MYC* levels can trigger apoptosis, the same study compared *MYC* levels in the pancreatic islets of *Rosa26-MYC-ER* mice with *MYC* levels in the *pnls-MYC-ER* model, in which the insulin promoter drives *MYC* expression. *pnls-MYC-ER* mice displayed ~15 times higher *MYC* mRNA levels than homozygous *Rosa26-MYC-ER* mice. In *Rosa-26MYC-ER* pancreatic islets, *MYC* activation by 4-OHT led to proliferation and hyperplasia, whereas it led to large amounts of apoptotic death in the *pnls-MYC-ER* mice, accompanied by islet involution. In the *Rosa26-MYC-ER* colonic epithelium, as well as *pnls-MYC-ER* pancreatic islets, the apoptotic phenotype went along with p19Arf expression. p19Arf was however absent in tissues, in which apoptosis was absent and *MYC* induction drove only proliferation. This suggests that oncogenic Myc levels that can induce p19Arf and thereby engage

tumour suppressive mechanisms (Zindy et al., 1998), require a certain threshold which is higher than the one needed for Myc induced proliferation.

In most mouse models *Myc* is strongly overexpressed by using very potent tissue specific promoters or enhancers. *Myc* fusion to the E μ immunoglobulin enhancer gives rise to B cell lymphomas within few months of age (Adams et al., 1985). Strong *Myc* overexpression proved to be potent cancer initiating event in this model.

However, in many tissues with epithelial cell origin *Myc* on its own does not seem to be a potent inducer of tumourigenesis. Mouse models in which *Myc* is fused to the long terminal repeat (LTR) of the MMTV promoter give rise to only few and sporadic tumours in the mammary glands and they were shown to have acquired *KRas* mutations (D'Cruz et al., 2001; Stewart et al., 1984). A similar phenomenon has been observed in the lung (Allen et al., 2011). *Myc*'s oncogenic potency is however accelerated by simultaneous activation of anti-apoptotic proteins such as Bcl-xL (Pelengaris et al., 2002), or deletion of tumour suppressor genes such as p19Arf or p53 (Elson et al., 1995; Zindy et al., 2003), confirming that oncogenic *Myc* levels engage tumour suppressive mechanisms, whose abrogation enable *Myc* to exert its full oncogenic potential.

1.2.3 Myc/Ras cooperation

The observation that *Myc* and *Ras* cooperate in transformation goes back to 1986 when Land et al. showed in primary rat fibroblasts that *Ras* on its own can drive initial colony formation, which stop growing after a while (Land et al., 1986). Cotransformation with *Myc* however helped to overcome this growth arrest.

Since then it has been established that *Myc* and *Ras* complement each other by interfering with each other's tumour suppressive functions (Figure 1-3). Oncogenic *Ras* leads to senescence in primary cells through p19Arf induction (Zindy et al., 1998) and co-overexpression of *Myc* overrides this senescent phenotype (Hydbring et al., 2010). *Ras* on the other hand can overcome *Myc* induced apoptosis, which is mediated through Pi3k/Akt signalling (Kauffmann-Zeh et al., 1997).

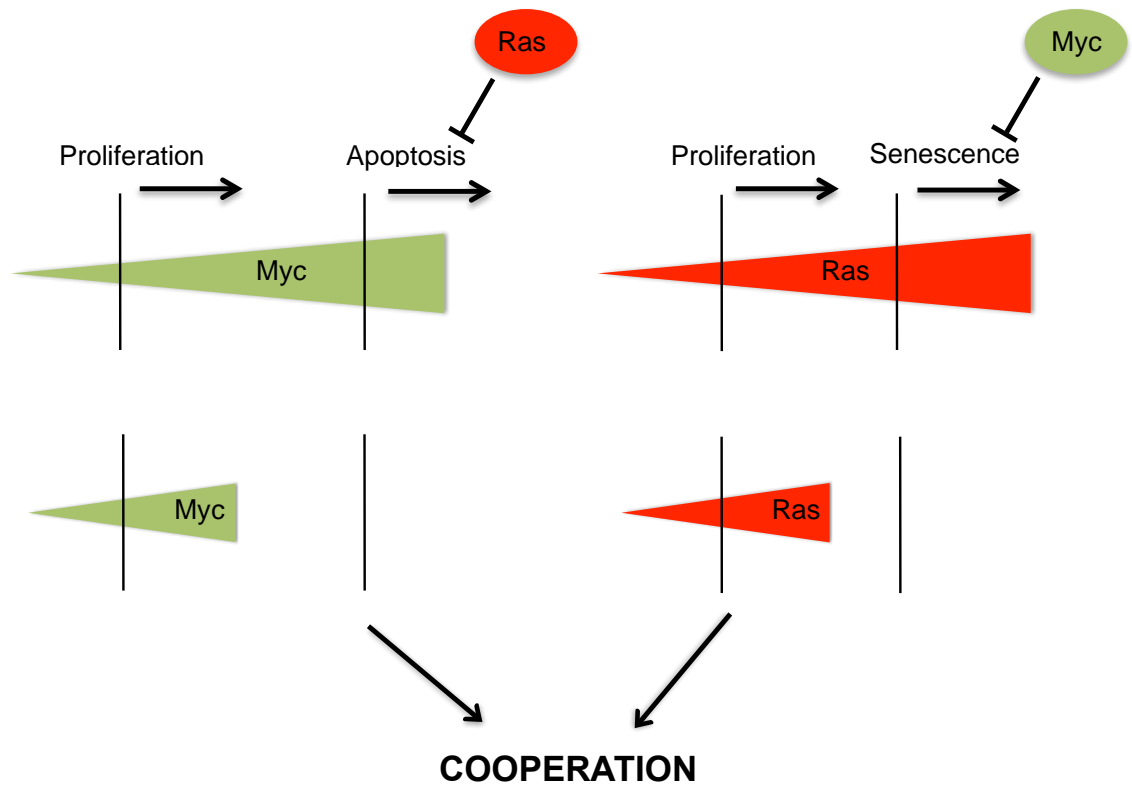


Figure 1-3 Cooperation between Myc and Ras.

The upper panel shows that Ras is inhibiting Myc induced apoptosis, caused by Myc levels above the threshold for Myc induced apoptosis. Myc on the other hand is able to inhibit Ras induced senescence. The lower panel illustrates that even below the tumour suppressive threshold levels, Myc and Ras are able to cooperate.

Mechanistically this cooperation seems to originate from the fact that Myc and Ras have opposing effects on the cell cycle clock. Ras induces cyclin D1 (Filmus et al., 1994), Myc can inhibit cyclin D1 (Philipp et al., 1994), but can on the other hand induce cyclin D2 (Bouchard et al., 2001). Moreover, Ras inhibits cyclin-dependent kinase 4 (Cdk4) expression (Lazarov et al., 2003), whereas Myc induces Cdk4 (Hermeking et al., 2000).

Also *in vivo*, Myc and Ras have been shown to cooperate. In a mammary model for instance, Myc dramatically increases Ras induced tumour incidence (Sinn et al., 1987). Both oncogenes were however expressed at high levels, driven by the MMTV promoter, and Ras was able to suppress Myc induced apoptosis in this model (Hundley et al., 1997).

The mechanism of Myc and Ras cooperation has always focussed on their ability to abrogate each other's tumour suppressive effects, which originates from a large amount of studies in which Myc and Ras were highly overexpressed. It is the case with both oncogenes that their tumour suppressive functions depend on their

expression level - Ras induced senescence is more pronounced when Ras is present at high levels and Myc induced apoptosis requires a threshold level, which is higher than the one for Myc induced proliferation. This work is the first *in vivo* attempt to carefully investigate the effect of weak *Myc* overexpression, which is still at physiological levels, on endogenous mutant *KRas* driven tumourigenesis. I show that Myc levels that drive proliferation but no apoptosis are able to accelerate *KRas* driven tumourigenesis (Figure 1-3). Abrogation of *KRas* induced senescence by Myc can be excluded as a mechanism of cooperation, as *KRas* does not lead to senescence in this model. This shows that there is an actual cooperation between Myc and Ras beyond mere abrogation of each other's tumour suppressive functions.

1.3 Mouse Models for Lung Cancer

1.3.1 Classification of proliferative lung tumour lesions

The following classification represents a summary of the recommendations of the Mouse Models of Human cancers consortium (Nikitin et al., 2004) with focus and references to how I classified lesions throughout my work.

Epithelial lesions can be divided into hyperplasias and tumours. Epithelial hyperplasia can be further divided depending if it arises from the airways or from alveoli. Airway hyperplasia describes the increase in number of respiratory epithelial cells in a diffuse or focal contribution, whereas alveolar hyperplasia describes foci in the distal to terminal bronchioles and is usually single layered. I do not distinguish between these two types of hyperplasia and refer to them in general as "hyperplasia".

Tumours are subdivided into benign, preinvasive lesions and malignant lesions. The term benign is used differently in human and mouse pathology. In human pathology benign tumours refer to tumours (papillomas and adenomas) that are likely to never progress to cancer. In the mouse benign adenoma lesions are seen as an intermediate stage before they progress to adenocarcinomas and are not distinguished from benign tumours that will never progress.

Benign tumours are represented by papillomas, which are defined by a papillary structure that is arising from the airways, and adenomas. Adenomas are usually

less than 5mm in diameter and retain the structure of nearby alveoli. They are further characterized by absence of vascular invasion and uniform nuclear morphology. Adenomas are further divided into solid, papillary or mixed depending on their structure. I refer to adenomas as tumours that consist of cells with regularly shaped nuclei and uniform organisation. I do not consider the size of the tumour, as from a tissue section it is not possible to determine the diameter of a 3-dimensional tumour. A small appearing tumour for instance could be a large tumour that was cut at its edge.

Preinvasive lesions can be grouped into squamous dysplasia displaying epithelial cells with squamous metaplasia, diffuse pulmonary neuroendocrine cell hyperplasia, which refers to accumulation of neuroendocrine cells in the bronchiolar regions and atypical adenomatous hyperplasia (AAH). AAH are lesions in the alveoli and terminal bronchioles that involve cellular and nuclear atypia.

Malignant tumours are more than 5mm in diameter and are characterized by invasion into airways and blood or lymphatic vessels. Moreover, cellular and nuclear atypia and a poor architecture are signs of malignancy. Malignant tumours can be grouped into squamous cell carcinomas, which are characterized by a broad keratinization, and adenocarcinomas.

Adenocarcinomas show a great cytological atypia and an increased mitotic rate and can be grouped into solid, papillary or acinar depending on their structure. As mentioned above, I do not consider the size of the tumour to distinguish adenocarcinomas from adenomas. I focus on the loss of organisation and structure and the presence of enlarged, pleomorphic nuclei sometimes with prominent nucleoli, as adenocarcinoma characteristics.

1.3.2 The need of mouse models to study lung tumour progression

An early, benign tumour starts as a hyperplastic lesion, which is defined by the occurrence of hyperproliferative cells. Over time, the tumour may undergo changes in gene expression, which might be due to epigenetic changes and/or due to the acquisition of additional mutations (Hanahan and Weinberg, 2011). These changes are likely to occur in only part of the tumour - the tumour is said to be heterogeneous - and are the first step towards tumour progression, which is defined by the potential

to invade the surrounding stroma and to metastasize eventually. As soon as the tumour has acquired invading abilities, it is called malignant.

In some cancer types such as colorectal cancer the process of tumour progression is very well understood (Kinzler and Vogelstein, 1996; Vogelstein et al., 1988). In colorectal cancer samples of different stage tumours, ranging from hyperplastic lesions to invasive carcinomas, are available, which makes it possible to study genetic alterations as the tumours progress. Lung cancer on the other hand is usually detected at an advanced stage. For this reason early stage material is very limited and extensive examination, including reasonable numbers, is only possible on advanced tumour material.

Genetically engineered mouse models, which enable tumour initiation at a chosen time point, allow the study of early tumours and their progression over time. In a mutant *KRas/Tp53^{null}* mouse model gene expression between the benign adenoma and more advanced adenocarcinoma stage was compared (Feldser et al., 2010). Genes involved in proliferation, Ras pathway, Myc, inflammation and immune responses, as well as chemokine regulation were found to be upregulated in adenocarcinomas. The transition from adenoma to adenocarcinoma is defined by a change in cell morphology (Figure 1-4). Cell nuclei become enlarged and pleomorphic and in some cells nucleoli become visible. Also, the cell arrangement becomes highly irregular as the cells transit to the adenocarcinoma stage.

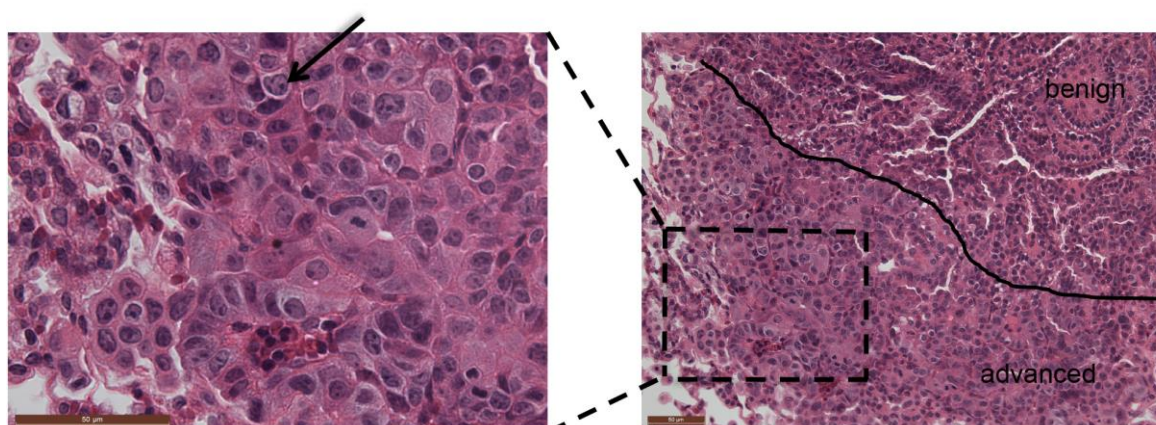


Figure 1-4 Tumour progression.

In benign tumour areas, cell nuclei are regularly shaped and arranged. Towards the transition to adenocarcinoma, nuclei become enlarged and pleomorphic and nucleoli become visible. The arrow points to a nucleolus.

The MAPK pathway, which is downstream of KRas is highly active in many cancers (Dhillon et al., 2007). Erk 1 and 2 (42 and 44 MAPK) are part of this pathway and Erk phosphorylation was only detected in adenocarcinomas, whereas adenomas were p-Erk negative in this model. In this thesis changes in cell morphology were used to distinguish between adenomas and adenocarcinomas and in the used *R26^{DM.lsl-MYC/MYC};KRas^{G12D}* model this morphological change correlates with Erk phosphorylation, which was used as an progression marker.

1.3.3 Mouse Models for NSCLC

KRas mutant mouse models are widely used, either on its own or in combination with mutation or loss of tumour suppressor genes, such as *Tp53* (Jackson et al., 2005), *Lkb1* (Ji et al., 2007), *p16-Ink4a* or *Ink4a/Arf/Ink* (Fisher et al., 2001), *Rb*, retinoblastoma-related protein 2 (*p130*) (Ho et al., 2009) and phosphatase and tensin homolog (*Pten*) (Iwanaga et al., 2008), which accelerates *KRas* driven tumourigenesis. Most *KRas* mutant models give rise to ADC; *KRas* in combination with *Lkb1* is one exception, which leads to ADC but also SCC, mixed ADC/SCC histology and LCC (Ji et al., 2007). There are only few Mouse Models for SCC, another one uses combinatorial inactivation of *Lkb1* and *Pten*, which leads only to SCC (Xu et al., 2014).

Other mutated oncogenes that are used in NSCLC models are *Egfr* (Li et al., 2007), *BRaf* (Dankort et al., 2007), receptor tyrosine-protein kinase *ErbB2* (Perera et al., 2009), *EML4-ALK* fusion gene (Soda et al., 2008) and *Pik3ca* (PI3K p110- α subunit) (Engelman et al., 2008). Most of these genetic alterations give rise to adenocarcinoma spectrum, *ErbB2* activation leads to adenosquamous tumours.

1.3.3.1 Gene overexpression by tissue specific promoters

Transgenic mouse models for human lung cancer improved over the years. Early mouse models used tissue specific promoters to overexpress genes that are amplified in human lung cancer. The surfactant protein C (Sp-C) promoter (Glasser et al., 1991) that is active in alveolar type II cells and the Clara Cell secretory protein (CC10) promoter (Stripp et al., 1992) that is active in Clara cells were commonly used and are still used today (Figure 1-5). As adenocarcinomas of the lung are Sp-C positive, alveolar type II cells were seen as likely cells of origin (Linnoila et al., 1992). However, as transgenes driven by both promoters can give rise to

bronchioalveolar hyperplasias that develop into adenocarcinomas, both cell types represented potential cells of origins (DeMayo et al., 1991; Wikenheiser et al., 1992). Nowadays, dual positive bronchio-alveolar stem cells are considered as likely cells of origin for ADC (Giangreco et al., 2002; Kim et al., 2005).

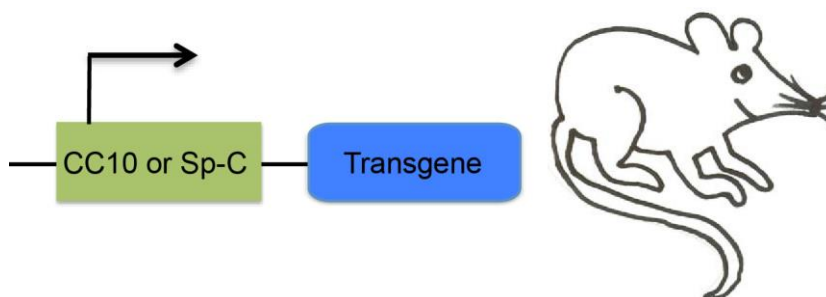


Figure 1-5 Mouse models using tissue specific promoters.

The transgene is driven, and thereby overexpressed, by tissue specific promoters. In NSCLC models, CC10 and Sp-C are commonly used promoters.

1.3.3.2 Classical Knock-out and knock-in models

Knock-out or knock-in models are used to delete tumour suppressor genes or to bring in oncogenic versions of proto-oncogenes (Figure 1-6). In knock-out models intervening sequences interrupt the coding sequence. This cannot be done for gene knock-outs that are embryonic lethal, such as *Rb* (Jacks et al., 1992). Other tumour suppressor knock-outs that are not embryonic lethal, such as *Tp53* can be used, but they are likely to give rise to tumours in multiple organs possibly even before they do so in the lung (Donehower et al., 1992).

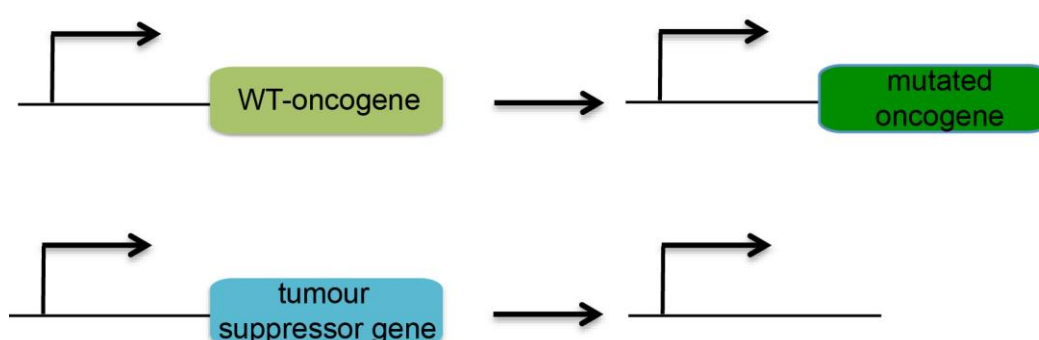


Figure 1-6 Classical knock-in and knock-out models.

In the knock-in model, a proto-oncogene is replaced by a mutated version, within the endogenous locus. In the knock-out model, a tumour suppressor gene is deleted.

In the knock-in version an oncogene is replaced by a mutated version. Advantage of this system over tissue specific promoters is that the mutated oncogene is driven by its endogenous gene locus at physiological levels. For instance, endogenous *KRas* is replaced by *KRas^{G12D}* and gets activated by spontaneous somatic

recombination. This allele gives rise to ADCs, but leads also to tumour formation in other organs (Johnson et al., 2001).

1.3.3.3 Conditional bitransgenic Mouse Models

Conditional bitransgenic tetracycline-inducible mouse models allow the control of conditional alleles by addition and withdrawal of tetracycline derivatives, such as Doxycycline (Furth et al., 1994). The reverse tetracycline-controlled transactivator (rtTA) is under the control of a chosen (in most cases a tissue specific) promoter. At the same time the transgene that is to be overexpressed is cloned into a tetracycline-responsive promoter element (TRE). The rtTA then binds together with Doxycycline to the TRE to induce transgene expression in the cells in which the promoter by which rtTA is driven is active (Figure 1-7). Advantage of this system is that expression of the transgene can be induced at any time point by doxycycline and that it is also possible to stop the transgene expression by withdrawal of doxycycline. This way not only tumour initiation can be studied, but also the effect of transgene removal on established tumours (Fisher et al., 2001).

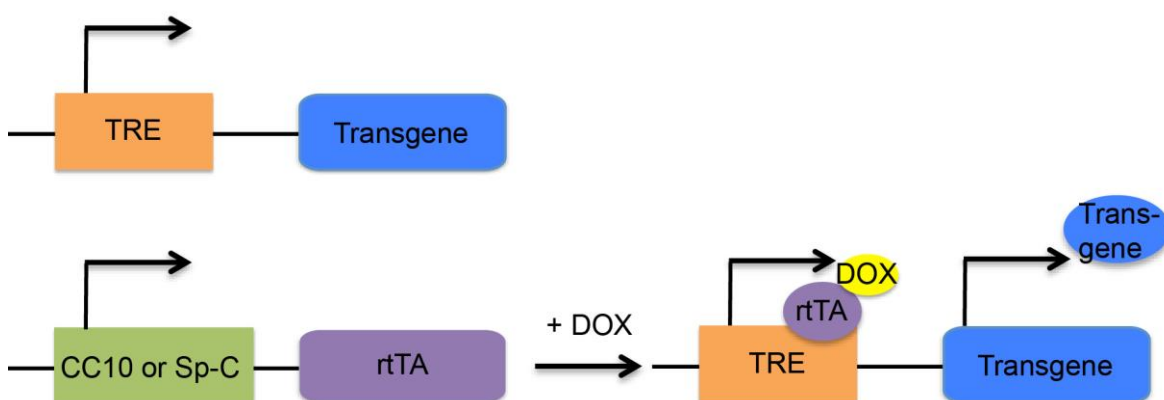


Figure 1-7 Bitransgenice conditional tetracycline inducible models.

The transgene is under the control of a TRE promoter and rtTA is under the control of a tissue specific promoter. TRE requires rtTA and a tetracycline derivate (doxycycline) for transcriptional activity. Transgene expression can be controlled by addition or withdrawal of doxycycline (DOX).

1.3.3.4 Conditional mouse models using the Cre/loxP system

This system can be used to knock-out tumour suppressor genes or to induce conditional transgenes (Guerra et al., 2003; Jackson et al., 2005; Jackson et al., 2001) (Figure 1-8). In the case of knock-out the targeted gene is flanked by locus of x-over P1 (loxP) sites (or alternatively by flippase recognition target (FRT) sites), which are recognised and recombined by Cre recombinase (or flippase (Flp) recombinase), which leads to deletion of the sequence that lies between the loxP

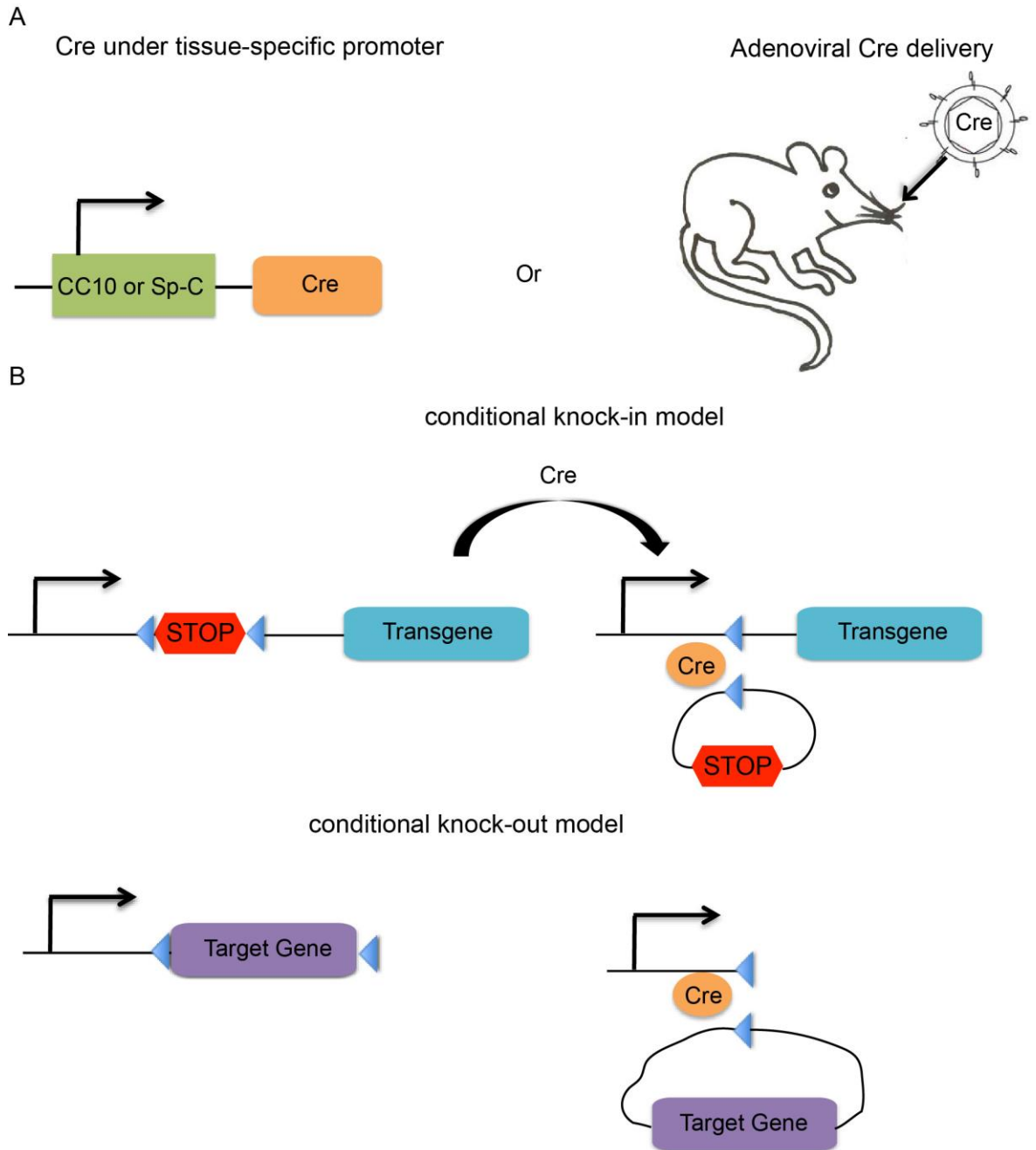


Figure 1-8 Conditional Cre inducible models.

A) Cre can be either under the control of a tissue-specific promoter or can be delivered to the lung by nasal installation of Cre expressing adenovirus. B) In the conditional knock-in model, the inducible transgene is preceded by a loxP flanked Stop cassette, which prevents transcription. Cre recombinase mediates recombination of the loxP sites, which leads to excision of the Stop cassette. In the conditional knock-out model, the transgene is flanked by loxP sites. Cre recombinase again mediates recombination of the loxP sites, which in this case leads to excision of the transgene.

(or FRT) sites (DuPage et al., 2009; Lee et al., 2012). In the case of knock-in, the conditional alleles are kept silent by a STOP cassette, which is flanked by loxP (or FRT) sites. Upon Cre (or Flp) recombination the STOP cassette gets excised and the allele can be transcribed. Cre (or Flp) can be either driven by a tissue specific promoter or, a method that is very commonly used to induce conditional alleles in

the lung, can be delivered to the lung by Cre (or Flp) expressing Adeno- or Lentivirus, via intranasal delivery (DuPage et al., 2009).

Cre that is under the control of tissue specific promoters can be delivered this way as well (Sutherland et al., 2011). The loxp/Cre and FRT/Flp systems can be combined in order to allow induction of different alleles at different time points.

This system allows induction of the alleles at a chosen time point, which makes the tumour phenotypes very reproducible. Another advantage of this system is that only the cells that are infected by the virus and recombine the alleles give rise to tumours, which are surrounded by nontransformed cells. This closely recapitulates the scenario of human lung tumour initiation where one mutated cell gives rise to a tumour. This approach also bypasses the problem of the cell of origin, as only cells that are naturally sensitive to the genetic alteration will give rise to tumours. Moreover, this system allows control over the number of tumours by varying the viral dose. Disadvantage of this system is that the infection rate relies on the breathing rate of the mouse, which leads to a high variation in terms of achieved tumour number and burden. Therefore, the qualitative characteristics of tumourigenesis are very reproducible in this system but the tumour quantity underlies fluctuations.

1.3.4 Mouse Models for KRas mutant lung cancer

1.3.4.1 KRas induction by spontaneous somatic recombination

Mutations at codon 12 in *KRas* replace glycine with either aspartic acid (G12D) or valine (G12V). Both mutations, which lead to decreased GTPase activity of *KRas* and thereby make *KRas* constitutively active, are common in human lung cancer. *KRas^{G12D}* and *KRas^{G12V}* are both used in *KRas* mutant Mouse models for lung cancer (Guerra et al., 2003; Jackson et al., 2001). Two mouse models in which mutant *KRas* is expressed in the whole animal demonstrate that the lung is especially sensitive to *KRas* mutations compared to other tissues. The first one uses the latent *KRas^{LA2}* allele, which gets induced by spontaneous somatic recombination. The recombination activated mutant *KRas^{G12D}* allele gives primarily rise to lung tumours (Jackson et al., 2001). At two weeks of age 100% of the mice present lung ADC, more than 50% thymic lymphoma and less than 20% papilloma tumours. This suggests that lung cells are prone to tumourigenesis upon *KRas* mutation and that other organs are less prone. However, it cannot be excluded that

recombination rate varies across different organs, which might contribute to an increased rate of tumourigenesis in the lung.

Another mouse model using *KRas*^{G12V} however confirms this phenotype (Guerra et al., 2003). In this model *KRas*^{G12V} is kept silent by a loxP flanked STOP cassette, which has to be excised by Cre recombinase for allele induction. For this purpose, mice were crossed with either CMV-Cre^{+T} mice that express Cre under the constitutively active CMV promoter or with *RERTn* mice that express inducible Cre-ER^{T2} under control of the locus encoding the large subunit of RNA polymerase II. All *KRas*^{G12V};CMV-Cre^{+T} mice develop breathing difficulties after seven to eight months of age. A subset of mice also develops sarcomas and papillomas. Similar phenotypes were obtained in *KRas*^{G12V};RERTn mice. The mice also express β-geo upon recombination of the conditional *KRas*^{G12V} allele, which allows to follow recombined cells and to examine which ones give rise to tumour formation. Interestingly, many cells in the bronchio-alveolar lung epithelia were β-geo positive, but were morphologically normal. Also in other tissues in which tumours or hyperplastic growth was absent, β-geo positive cells were found. Other cell types possibly respond with senescence, cell cycle arrest or apoptosis to mutant *KRas* expression and give therefore not rise to tumours. This confirms that mutant *KRas* makes the lung susceptible to tumourigenesis and that other organs are less susceptible.

1.3.4.2 Conditional Cre inducible mutant *KRas*

In order to induce mutant *KRas* only in the lung the conditional Cre-inducible *Isl-KRas*^{G12D} or *Isl-KRas*^{G12V} alleles are used. The alleles can be either induced by tissue specific Cre under the Sp-C or CC10 promoter or by intranasal delivery of Cre expressing Adeno- or Lentivirus (DuPage et al., 2009). *KRas*^{G12D} that is recombined by Cre-ER under the Sp-C promoter gives rise to alveolar hyperplasia that progresses to adenoma and adenocarcinoma (Xu et al., 2012). Recombination of *KRas*^{G12D} by Cre-ER under the CC10 promoter gave rise to hyperplasias in the bronchio-alveolar duct region that did not progress to adenoma or adenocarcinoma.

Isl-KRas^{G12D} induction by intranasal delivery of Cre expressing adenovirus gives rise to bronchiolar hyperplasia 2 weeks post induction. 6 weeks post induction hyperplasia can still be found, but hyperplastic regions are larger than after 2 weeks

and some lesions had progressed to papillary adenomas at this time point. 12 weeks post infection few regions of bronchiolar hyperplasia were still present among a large number of adenomas, in which a subset started to show signs of malignancy, such as nuclear hyperchromatism and increased proliferation. 16 weeks post infection larger adenomas and also adenocarcinomas were observed (Jackson et al., 2001).

1.3.5 *Myc* overexpression in NSCLC models

Mouse Models that are modelling *Myc* overexpression in the lung use either tissue specific SP-C or CC10 promoters, or a Cre inducible *Myc* allele under the ubiquitously active Rosa26 promoter (Murphy et al., 2008).

Myc under the CC10 promoter gives rise to Clara Cell hyperplasia (Geick et al., 2001). Several founder mice for *SP-C/Myc* were generated, some of them developed hyperplasias in the alveolar epithelium, others developed bronchiolo-alveolar adenomas and adenocarcinomas (Ehrhardt et al., 2001). The reason for the difference in phenotypes could not be explained as they had comparable copy numbers of the transgene. The mouse model that uses the Cre inducible allele works after the similar principle as the Cre inducible *KRas* mutant mouse models with the difference that *MYC-ER* is driven by the ubiquitously active Rosa26 promoter instead from its endogenous promoter and has to be activated by 4-OHT. *MYC* activation in this model leads to proliferation of cells in the bronchioles after 3 days and to hyperplasia after 6 weeks without giving rise to tumours in the lung (Murphy et al., 2008).

In human lung ADC *MYC* is amplified or mutated in about 8% of cases and co-occur in 2-3% with *KRAS* mutations (Cancer Genome Atlas Research, 2014; Gao et al., 2013). Moreover, 2-3% of *KRAS* mutant lung ADCs carry *MGA* inactivating mutations, which are mutually exclusive with *MYC* amplification. *MGA* is a MAX binding transcription factor and inhibits *MYC*'s transcriptional activity.

In the mouse *MYC* overexpression driven by the Rosa26 promoter has been shown to accelerate *KRas*^{G12D} driven tumourigenesis (Murphy et al., 2008). In a dox-inducible system in which *Myc* was driven by either the Sp-C or CC10 promoter, *Myc* overexpression gave rise to adenomas and adenocarcinomas. However, all

tested tumours carried an activation *KRas* mutation, suggesting that *Myc* on its own is not able to drive tumourigenesis in the lung (Allen et al., 2011). Interestingly, when *KRas* mutagenesis was induced by the DNA-alkylating agent N-methyl-N-nitrosourea (MNU) *Myc* overexpression interfered with *KRas* driven tumourigenesis, as dox-induced mice developed a lower number of tumours than uninduced mice. The tissue specific promoters Sp-C and CC10 are presumably stronger than the Rosa26 promoter. This suggests that low levels of *Myc* are able to cooperate with *KRas* initiated tumourigenesis, whereas higher *Myc* levels play an interfering role. This might be due to the fact that low levels of *Myc* drive proliferation and that higher *Myc* levels can engage the apoptotic machinery of the cell (Murphy et al., 2008).

1.4 Thesis Aims

Lung cancer is usually detected at an advanced stage, which is the reason why only little is known about disease progression. Aim of the thesis is to better understand the mechanism of lung ADC progression. For this purpose a mutant *KRas* driven mouse model was chosen. It was found that low levels of deregulated *Myc* expression are able to accelerate *KRas* driven tumourigenesis, which facilitates the study of tumour progression in a timely manner.

Chapter 3 focuses on the outcome of low level deregulated *Myc* expression in the lung. The phenotypic characterization of *Myc* overexpression on its own, in combination with loss of functional *Tp53* and in combination with *KRas*^{G12D} is described in this chapter.

In order to study gene expression changes from the adenoma to the adenocarcinoma stage, RNA was isolated from the respective tumour regions. This process required the establishment of a protocol that allows RNA isolation from very limited amounts of tissue material. The development of this process, which finally resulted in a gene list with candidate tumour progression genes, is described in chapter 4.

Chapter 5 concentrates on the validation of these candidate target genes and also explores their potential as targets for therapeutic intervention.

2 Materials and Methods

2.1 Animal work

Transgenic mice were obtained from different laboratories (outlined in Table 2-1). The mice were kept on a 12h light cycle, and fed and watered ad libitum. The mouse procedures were performed according to protocol numbers 55.2-2531.01-30/11 (University of Würzburg, Germany) and Home Office licence numbers 60/4183 and 70/7950 (CRUK BICR, UK).

Transgene and Source	Tissue expression
<i>Lsl-KRas^{G12D}</i> (Jackson et al., 2001)	Endogenous <i>KRas</i> is replaced by mutant <i>KRas^{G12D}</i> , bearing a loxP flanked STOP cassette in the 5'UTR
<i>R26^{DM.lsl-MYC/MYC}</i> (Neidler et al. submitted)	Human <i>MYC</i> is knocked into the Rosa26 locus, including an upstream loxP flanked STOP cassette
<i>R26^{RS.lsl-Myc/Myc}</i> (Wang et al., 2011)	Murine <i>Myc</i> is knocked into the Rosa26 locus, including an upstream loxP flanked STOP cassette
<i>Tp53^{R172H}</i> (Jackson et al., 2005)	Endogenous <i>Tp53</i> is replaced by mutant <i>Tp53^{R172H/R172H}</i> , including a loxP flanked STOP cassette
<i>Tp53^{F1/F1}</i> (Jonkers et al., 2001)	Endogenous <i>Tp53</i> is flanked by loxP sites

Table 2-1 Transgenic mouse models used in this study.

2.1.1 Colony maintenance

Animals were bred to maintain the colony and to generate experimental mice. Matings were set up with one male and one or two females. At approximately 4 weeks of age, pups were weaned and ear notched for genotyping. All mice were maintained in positively pressured individually ventilated cages (IVCs). In order to avoid contamination, cages were opened only in a laminar flow changing station. After genotyping, mice that were chosen for experiments were transferred to non-barrier cages. The mice received an irradiated standard diet (CRM (E) expanded diet from Special Diet Services; Cat: 801730) and sterilized water ad libitum.

2.1.2 Genotyping

At approximately weeks of age mice were ear notched and the piece of tissue was genotyped by Transnetyx (Cordova, TN, USA), using a combination of quantitative PCR and DNA hybridization to determine the presence of transgenic alleles.

2.1.3 Experimental Cohorts

2.1.3.1 Conditional Genetically-Engineered Mouse Models for human NSCLC

All used alleles are conditional alleles that are induced by Cre recombinase. Cre recombinase recognizes LoxP sites, and excises region in between, which is flanked by these sites, leading to expression or deletion of the transgenes. The alleles were induced in the lung through intranasal delivery of Cre expressing Adenovirus, a method which has been described by DuPage et al. (DuPage et al., 2009). The phenotype of Adeno-Cre induced *KRas*^{G12D} in the lung has been first described by Jackson et al. (Jackson et al., 2001).

By interbreeding the appropriate colonies, *Isl-KRas*^{G12D}, *R26*^{DM.Isl-MYC/WT}, *R26*^{DM.Isl-MYC/MYC}, *R26*^{DM.Isl-MYC/WT;KRas}G12D, *R26*^{DM.Isl-MYC/MYC;KRas}G12D, *R26*^{DM.Isl-MYC/WT;p53}R172H/WT, *R26*^{DM.Isl-MYC/WT;Tp53}R172H/R172H, *R26*^{DM.Isl-MYC/MYC;Tp53}R172H/WT, *R26*^{DM.Isl-MYC/MYC;Tp53}R172H/R172H, *R26*^{RS.Isl-Myc/WT}, *R26*^{RS.Isl-Myc/Myc}, *R26*^{RS.Isl-Myc/WT;KRas}G12D, *R26*^{RS.Isl-Myc/Myc;KRas}G12D, *R26*^{RS.Isl-Myc/WT;Tp53}R172H/WT, *R26*^{RS.Isl-Myc/WT;Tp53}R172H/R172H, *R26*^{RS.Isl-Myc/Myc;Tp53}R172H/WT, *R26*^{RS.Isl-Myc/Myc;Tp53}R172H/R172H, *R26*^{RS.Isl-Myc/WT;Tp53}FI/WT, *R26*^{RS.Isl-Myc/Myc;Tp53}FI/WT and *R26*^{RS.Isl-Myc/Myc;Tp53}FI/WT cohorts were generated. Tissues were sampled at defined time points unless the animal had to be culled for health issues, which was especially the case for *Tp53*^{R172H/R172H} cohorts, as these animals are null for *Tp53* and express mutant *Tp53*^{R172H} only upon Cre recombination.

For survival analysis, animals were taken at defined end points described below.

2.1.3.2 End points

Experimental animals were monitored at least 3 times weekly and culled when any of the following symptoms were observed: weight loss of > 10%, hunching, impaired breathing/panting, decreased mobility.

The mice were sacrificed by schedule 1 methods. Mice were euthanized by rising concentrations of CO₂, followed by cervical dislocation.

2.1.3.3 Allele induction

For allele induction by nasal installation of Adenovirus, mice were anaesthetised using a mix of 5% Domitor/10% Ketamine in 0.9% NaCl, which was injected via intraperitoneal (IP) injection. The mice were weighed and received 200µl per 30g body weight.

Adenoviral-Calcium-Phosphate precipitate

EMEM (Invitrogen) was dissolved in H₂O and titrated with NaOH to a pH of 7.86. Adeno-Cre was thawed and kept on ice until needed. The appropriate volume of virus (Table 2-2) was mixed with EMEM. CaCl₂ was then added drop-wise and mixed by inverting the tube. The mix was incubated at room temperature for 40-50 min to allow the precipitate to form. Mice received either 1*10⁷ PFU or 5*10⁷ PFU Adeno-Cre as indicated in the figure legends.

Reagent	Volume (µl) for 10 mice
Adeno-Cre	PFU per mouse *10 / virus titre
EMEM	441 – virus volume
0.2M CaCl ₂	9
Total	450

Table 2-2 Adenoviral calcium-phosphate mix.

Once the mice were sleeping and breathing slowly and evenly, 45µl of the precipitate was pipetted slowly on the nasal septum of the mouse, which was then inhaled. The mice were then kept warm and monitored until they recovered, which usually took about 6 hours.

2.1.4 Treatments

Neratinib

Neratinib (LC Laboratories, N-6404) was dissolved in 0.5% methocellulose-0.4% Tween-80 and given daily by oral gavage at a dose of 40mg/kg/day.

LGK974

LGK974 (Novartis) was dissolved in 0.5% methocellulose-0.4% Tween-80 and given twice daily by oral gavage for a total dose of 10mg/kg/day.

2.1.5 Tissue sample preparation

Animals were sacrificed by schedule 1 method and dissected immediately. To prepare the mouse for post-mortem, the abdomen was sprayed with 70% EtOH. The abdominal cavity was first opened by cutting through the skin and then through the smooth muscle layer. A small incision into the diaphragm was made carefully without touching the lung, before opening the ribcage. In order to clean the organs from blood, a heart perfusion with PBS was performed. For this, an incision was made into the right atrium, to create an outlet. Then, the needle of a syringe containing 10ml PBS was inserted into the left ventricle and slowly emptied by applying constant pressure. After this the heart was removed. The skin above the thymus was then carefully removed until the underlying trachea became visible. An incision was made into the trachea and using a blunt needle, Zinc-buffered formalin (for FFPE samples) or OCT (1:1 diluted in 0.9% NaCl, for fresh frozen samples) was injected to inflate the lung. The lung was then removed and either fixed in Zinc-buffered formalin at 4°C overnight or embedded and frozen in OCT on dry ice and then stored at -80°C.

2.1.5.1 Tissue processing

Formalin-fixed paraffin-embedded (FFPE) tissues

After fixation, all tissues were dehydrated with increasing an alcohol gradient (30%, 50%, 70%, 95%, 100%) for 30 min each. The tissues were then further processed by the BICR histology team, using an automated processor (Thermo scientific Excelsior ES). Tissues were then finally embedded in paraffin wax and left to cool down and harden.

2.1.5.2 Sectioning of fixed tissues

Paraffin embedded tissues were cut to 4µm sections using a microtome and were placed on poly-L-Lysine (PLL) coated slides, then baked at 65°C over night. The sections were then dewaxed and dehydrated either for Haematoxylin and Eosin

(H&E) staining or immunohistochemistry (IHC) (see section 2.2.1). The sectioning and part of the IHCs were done by the BICR histology team.

2.2 H&E staining

2.2.1 Preparation of sections for IHC or H&E staining

Paraffin embedded tissue sections were first de-waxed by incubation in xylene for 3 x 5 min in a series of xylene containers. The sections were then rehydrated in decreasing gradients of EtOH (100%, 100%, 95%, 95%, 70%, 70%) for 2 min each and then left in deionised water (dH₂O).

2.2.2 Hematoxylin and Eosin staining

In order to visualize the cell morphology, tissue sections were stained with haematoxylin and eosin to stain the nuclei and cytoplasm of cells. Tissue sections were de-waxed and rehydrated as described in section 2.2.1 and were then stained by placing the sections in Gli1Haematoxylin (Sigma) for 3 min. This was followed by a wash in running tap water for 5 min and 20 dips in differentiation solution (Sigma). Sections were then washed again in running tap water for 30 sec and then dipped 20 times in scotts tap water substitute (MgSo⁴⁺ sodium bicarbonate). Finally, slides were washed in running tap water for 30 sec and stained with an aqueous solution of 1% Eosin for 5 min, followed by 2 washes in tap water.

2.2.2.1 Slide mounting

The sections were then dehydrated through an increasing alcohol gradient (2x 70% ethanol, 2x 95% ethanol, 2 100% ethanol, 2 min each) and then placed in xylene for 2x 5 min. Slides were then mounted in DPX mounting medium (VWR), coverslipped and left to air-dry over night in a fume hood.

2.3 IHC

2.3.1 Formalin fixed paraffin embedded tissue samples

IHC was used to visualize the specific cellular proteins in the tissue. A general outline of the protocol is described in this section and individual protocols are listed in Table 2-3.

Primary antibody	Antigen Retrieval	Primary Antibody conditions	Secondary Antibody
Ki67 Fisher scientific- RM-9106	Sodium citrate, microwave (10 min)	1:200, 1% BSA O/N at 4°C or 2h at 37°C	Vectastain, ABC-kit-rabbit, biotinylated 1:1000, 1h
BrdU abD Serotec OBT0030C	Sodium citrate, microwave (10 min)	1:250, 3% BSA O/N at 4°C or 2h at 37°C	HRP-conjugated anti-rat GE Healthcare NA935, 1:250, 1h
CC10 Millipore 07-623	Not needed	1:2000, 3% NGS O/N at 4°C or 2h at 37°C	Vectastain, ABC-kit-rabbit, biotinylated 1:1000, 1h
Sp-C Millipore AB3786	Not needed	1:2000, 3% NGS O/N at 4°C or 2h at 37°C	Vectastain, ABC-kit-rabbit, biotinylated 1:1000, 1h
p-Erk p-P44/42 MAPK (Thr202/Tyr204) Cell signaling cs4370	Sodium citrate, microwave (10 min)	1:500, 5% NGS O/N at 4°C or 2h at 37°C	Vectastain, ABC-kit-rabbit, biotinylated 1:1000, 1h
Myc Abcam ab32072	Sodium citrate, waterbath (40 min)	1:100, 5% NGS/1 % BSA 72h at 4°C	Vectastain, ABC-kit-rabbit, biotinylated 1:1000, 1h
Sox9 Millipore AB5535	Sodium citrate, microwave (10 min)	1:500, 10% NGS O/N at 4°C or 2h at 37°C	Signal boost rabbit (sigma), 30min

Table 2-3 IHC conditions.

2.3.1.1 Preparation of Sections for IHC

Formalin fixed, paraffin embedded tissues were sectioned onto PLL coated slides as described in section 2.1.5.2 and then further processed as described in section 2.2.1.

2.3.1.2 Blocking of Endogenous Peroxidase

Bound antibodies were visualized by an enzymatic reaction of 3,3'-diaminobenzidine (DAB), which is catalyzed by horseradish peroxidase (HRP). In order to quench the endogenous form of peroxidase, slides were incubated in 3% hydrogen peroxide (in dH₂O) for 15 min. This irreversibly blocks endogenous peroxidase, prevents false positive signals and reduces background detection. This was followed by a wash in dH₂O.

2.3.1.3 Antigen Retrieval

Fixation leads to the formation of methylene bridges that crosslink proteins. These bridges mask the antigen and can prevent the antibody from binding. Therefore, formalin fixed, paraffin embedded tissues undergo antigen retrieval in order to unmask the antibody epitopes. This is often mediated by heat antigen retrieval. The tissue sections are boiled in an unmasking solution in a microwave for 10 min and then left to cool at room temperature for 30 min.

2.3.1.4 Blocking of non-specific antibody binding

Although antibodies have a high affinity for specific epitopes, antibodies may weakly bind to nonspecific proteins sites, causing background staining. In order to reduce the background staining, the samples were incubated in a solution that blocks unspecific binding sites. For this purpose, either BSA or normal goat serum were used. Tissue sections were first encircled using a hydrophobic barrier pen, PAP pen (Dako) and then incubated with blocking solution. The blocking solution was diluted in PBS in a concentration that blocks unspecific binding. The blocking solution was aspirated and the tissue sections were then incubated with primary antibody.

2.3.1.5 Primary Antibody incubation

Tissue sections were then incubated with a primary antibody at a concentration outlined in Table 2-3. Antibodies were incubated in a humidified chamber either overnight at 4°C, or at 37°C for 2 hours. After incubation the slides were washed 3x in PBS to remove unbound antibodies.

2.3.1.6 Secondary Antibody incubation

Tissue sections were then incubated in secondary antibody solution. Secondary antibodies recognize the primary antibody because they are raised against antibodies from the animal in which the primary antibody was raised. They thereby bind only primary antibodies that bind to the antigen of interest. The sections were incubated with secondary antibody for 1 h in a humidified chamber, and then washed 3x in PBS. The secondary antibody was either HRP conjugated, or biotinylated. Biotinylated antibodies require an additional signal amplification step, to link HRP to the secondary antibody.

2.3.1.7 Signal Amplification

The amplification step involved the formation of a complex between the Biotin, which was bound to the secondary antibody and Avidin, which was bound to HRP (Vectastain Avidin-Biotin Complex (ABC) kit, Vector labs). The so called ABC reagent was prepared in 0.3M NaCl and incubated for 30 min at room temperature. The tissue sections were then incubated with ABC reagent for 30 min and washed 3x in PBS.

2.3.1.8 Visualization of the signal

A chromogenic detection method was used to visualize the respective protein. This method requires the HRP enzyme, which converts its substrate, DAB (Invitrogen), into a brown coloured product. Tissue sections were incubated with DAB reagent until the signal had the desired strength. Excess DAB was removed and quenched in dH₂O water.

2.3.1.9 Counterstaining and slide mounting

To stain the nuclei, the slides were dipped 3x in hematoxylin and then washed in tap water until water became clear. This step was followed by 20 dips in differentiation solution. The slides were again rinsed in running tap water for 15 sec, which was followed by 20 dips in Scotts tap water substitute. After washing in running tap water for 2 min, slides were dehydrated in an EtOH series and mounted as described in section 2.2.2.1.

2.3.2 TUNEL staining

TUNEL staining was performed with the ApopTag peroxidase labelling kit (Millipore; S7100). The principle of the staining is based on DNA fragmentation, a hallmark event of apoptosis. Digoxigenin conjugated nucleotides were added to free 3'OH ends of single or double stranded DNA by an enzyme called terminal deoxynucleotidyl transferase (TdT). The digoxigenin containing, incorporated nucleotides were then detected by an HRP conjugated antibody against digoxigenin. Signal was detected with DAB as described in section 2.3.1.8. The protocol according to the manufacturer's instructions was followed and an additional blocking step (1% BSA for 1h at room temperature) was incorporated prior to the

incubation with HRP conjugated anti-digoxigenin. The tissue sections were then counterstained as described in section 2.3.1.9.

2.3.3 Fresh frozen tissue samples

2.3.3.1 Sectioning of frozen tissue samples

Cryo-sections were made using a Leica cryostat. 10 µm sections were sectioned on PLL coated slides. The slides were placed into fresh 50ml tubes and stored at -80°C until needed.

2.3.3.2 Fixation

The slides were removed from -80°C, air-dried for ~3 min and then fixed for 10 min in 1% formaldehyde in PBS. Slides were then washed 3x in PBS and fixed further for 10 min in ice-cold methanol on ice. Slides were again washed 3x in PBS.

2.3.3.3 Blocking of endogenous peroxidase

To block endogenous peroxidase slides were incubated for 20 min in 3% H₂O₂ in dH₂O and then washed 3x in PBS.

2.3.3.4 Cell membrane permeabilization

Slides were incubated for 10 min in 1% Triton X-100 in PBS and then washed 3x in PBS. Then slides were incubated for 5 min in 1% SDS in PBS and again washed 3x in PBS.

2.3.3.5 Blocking of non-specific antibody binding

The sections were blocked with 5% normal goat serum (NGS) for 1h at RT.

2.3.3.6 Primary antibody incubation

Sections were incubated with phospho-Erk1/Erk2 (T202/T204) antibody (Cell signaling, 4370), 1:500 in 5% NGS ON at 4°C. The next morning slides were washed 3x in PBS.

2.3.3.7 Secondary antibody incubation

Sections were incubated with secondary HRP-conjugated signal boost anti rabbit (cell signaling) for 30 min at RT and then washed 3x in PBS.

2.3.3.8 Visualization of the signal

See section 2.3.1.8 for details.

2.3.3.9 Slide mounting

Slides were cover-slipped with fluorescence mounting media (Dako, S3023), containing Hoechst for nuclear staining. Slides were then dried for at least 2 nights at RT in the dark before microscopic inspection.

2.3.4 CV staining

The sections were removed from -80°C and air-dried for ~10 min. The slides were then incubated in 70% and 50% EtOH for 2 min each to remove the OCT followed by incubation in 1% CV in 50% EtOH for 45 sec. Sections were then rinsed under running tap water until clear. The slides were then incubated in an increasing EtOH series (50%, 70%, 95%, 100%, 100%) for 2 min each, followed by 2 xylene incubations for 5 min each. Slides were mounted in DPX mounting medium, cover-slipped and left to air-dry under the fume hood.

2.4 PCR genotyping

2.4.1 Genomic DNA isolation

Genomic DNA was isolated from mouse tail tissue. The tissue sample was stored at 4°C prior to extraction. The tissue was first incubated overnight at 55°C in 500µl tail lysis buffer (10mM Tris [pH 8], 100mM NaCl, 10mM EDTA [pH 8], 10% SDS) containing 10µg/ml of Proteinase K (Sigma), to digest the tissue. Protein was precipitated by addition of 250µl 6M NaCl, the solution was mixed by inversion and incubated on ice for 10 min. Any insoluble debris was pelleted by centrifugation at 2000 rpm for 10 min at 4°C. The supernatant was removed and 500µl of isopropanol was added to precipitate the DNA. The tube was inverted to mix and incubated at RT for 15 min, then centrifuged at 14,000 rpm for 10 min. The supernatant was

discarded and the pellet was left to air dry. The DNA pellet was then resuspended in 50µl of PCR grade water.

2.4.2 PCR

The DNA was used to detect the transgenic allele by polymerase chain reaction (PCR). The PCR reaction contains 1x Phusion high fidelity GC buffer (Thermo scientific), Phusion DNA polymerase, 0.5µM gene specific primers, 200µM dNTPs, and template DNA. The primers used are outlined in Table 2-4 and PCR conditions used are outlined in Table 2-5.

Primer	Sequence
Rosa forward	cccaaagtcgctctgagttg
Rosa reverse	ggagcgggagaaatggatatga
Rosa modified reverse	gcgaagagttgtcctcaacc

Table 2-4 Genotyping primers.

2.4.3 Agarose Gel electrophoresis

The PCR products were visualized using agarose-gel electrophoresis. 2% agarose gels were made by adding 2% (w/v) of agarose (sigma) in 1X Tris Acetate-EDTA buffer [TAE: 40mM Tris-acetate, 1mM EDTA (pH8.3)], and heated in a microwave until boiling and left to cool down at room temperature for a few min. 5µl of ethidium bromide (Sigma) was added per 100ml of agarose solution. The agarose solution was then poured into a mould (BioRad) and the combs were placed inside to create wells. After gels were solidified, they were placed into a TAE buffer containing gel electrophoresis tank.

Temperature°C	Duration
1. 94°C	30 sec
2. 94°C	30 sec
3. 66°C	20 sec
4. 72°C	80 sec
go to step 2. 35x	

Table 2-5 Genotyping PCR cycle.

PCR products were mixed with 4µl of 6x loading dye (NEB). The PCR samples were then loaded to the well (20µl) and a 100bp molecular weight DNA ladder (NEB) was loaded to one of the wells in order to be able to assess the size of the PCR product.

The gel was run at 120V until the ladder was well separated and the products were visualized with a GelDoc Transilluminator.

2.5 Cell culture techniques

2.5.1 Fibroblast Cell culture

Primary mouse embryonic fibroblasts (MEFs) were isolated on day 13.5. Embryos were removed from the pregnant female and placed into a dish containing sterile PBS. The uterine wall was removed with sterile forceps and each embryo was placed in a separate 6 cm culture dish. "Red" tissue was removed with a spatula. The head was then removed and a part of the head tissue was genotyped by Transnetyx (USA). The rest of the embryo was homogenized with a scalpel, resuspended and collected in 1ml of PBS and transferred to a 15ml tube. 1ml of 1x trypsin was added and the homogenized embryo was incubated for 15 min at room temperature. The trypsin was then quenched with 8ml of complete medium the suspension was transferred to a 10cm tissue culture dish. After 24h, cells were washed and fresh medium was added. To avoid contamination, all steps were carried out in a sterile laminar air-flow hood and the forceps were rinsed in-between with 70% ethanol and dH₂O. The cells were cultured in DMEM containing 10% FBS, 1% glutamine, Penicillin (50,000units) and Streptomycin (50,000µg), and were grown at 37°C at 5% carbon dioxide (CO₂). The MEFs were cultured using the standard 3T3 protocol. They were passaged (see section 2.5.3) once in 3 days 1.3x10⁶ cells were seeded into a 10cm tissue culture dish. Primary MEFs were kept in culture for a maximum of 5 passages.

2.5.2 Generation of primary lung cell lines

Mice displaying signs of tumour burden were euthanized using a schedule 1 method. The lung was washed in PBS, the lobes were separated and placed into separate 6 cm dishes. A scalpel was used to breakup the tumour containing tissue, which was then collected in full media supplemented with 10% FBS and cultured in 12 well plates. Cells were maintained at 37°C in a 5% CO₂ incubator. Medium was changed every 2 days. Once cells started to grow, which took several weeks up to months in some cases, cells were moved to larger plates and finally maintained in 10 cm culture dishes in 10ml culture medium and passaged as required.

2.5.3 Passaging Cells in Culture

Once the cells were confluent, they were split to prevent them from overgrowing. The medium was aspirated and the cells were washed with PBS. 1ml of 10% trypsin was added and incubated for 5-10 min in the incubator to break peptide crosslinking. Cells were then washed off the plastic surface by resuspension in cell culture medium and split into new dishes.

2.5.4 Freezing down cell lines

Cells were seeded into a 15 cm plate and grown until confluent. Medium was aspirated and the cells were washed using 5ml PBS. Cells were trypsinized using 1.5ml of 10% trypsin and incubated for 5-10 at 37°C. Cells were then suspended in 6.5ml freezing media (90% FBS: 10% DMSO). 5 1.5ml aliquots were transferred to 1.8 ml cryovials and placed in a freezing container (Mr.Frosty™), which allows a cooling rate at -1°C/min in a -80°C freezer. The next day, cells were transferred to liquid nitrogen for long-term cold storage.

2.5.5 Thawing cells

Frozen cells were taken from liquid nitrogen and defrosted in a 37°C water bath. Cells were then gently resuspended in 10ml culture medium and plated into a 10 cm culture dish. The cell culture medium was changed 24 h later.

2.6 Incucyte

2.6.1 Cell propagation analysis

Cells were seeded in the evening into 96-well plates at ~30% confluency. 10mM LGK974 stock and 100µM Neratinib stock were diluted in DMSO so that further 1:1000 dilution in cell culture media resulted in the desired final concentration. The next morning LGK974 and Neratinib stocks were diluted 1:1000 in cell culture media and 100µl was added to each well. Cell propagation over time was monitored using long term Incucyte (ESSEN BioScience) video microscopy.

2.6.2 Cell migration analysis

Cells were seeded in the evening into 96-well plates at 100% confluency. The next morning a scratch was made using a woundmaker (ESSEN BioScience). The woundmaker is a device that makes a scratch through the cell layer, in every single well of a 96-well plate. The wells were washed once with PBS. LGK974 10mM stock and Neratinib 100 μ M stock were diluted 1:1000 in cell culture media and 100 μ l was added to each well. The plates were then transferred to a long term Incucyte video microscopy incubator. The Incucyte takes pictures of the scratch at a set interval and calculates the wound width relative to the initial wound width (relative wound density).

2.6.3 Cell invasion analysis

Cells were seeded as described in 2.6.2. The same evening, Matrigel (BD Biosciences, 225) was removed from -20°C and thawed over night on ice at 4°C. The next morning the scratch was made as in section 2.6.2 and layered with cold diluted Matrigel (1:1 in PBS). Plates were then incubated at 37°C for 1 h, treated and placed into the Incucyte as described in section 2.6.2.

2.7 siRNA Screen

The siRNA library, containing 4 individual siRNAs against 51 selected genes was purchased from Qiagen. In each 96-well, 5 μ l of 25nM siRNA was mixed with 15 μ l transfection reagent (diluted in serum-free media) and left on the shaker for 30 min. Transfection and cell seeding occurred at the same time and 80 μ l cell suspension was added to the transfection mix. The plates were placed in a for the screen designated incubator, at 37°C and 5% CO₂. Transfection conditions and cell seeding numbers are summarized in Table 2-6.

Cell line	Assay	Cells/well	Transfection reagent	Dilution
A549	viability	3 500	Lipofectamine 2000	120
A549	migration	15 000	Lipofectamine 2000	60
H2009	viability	5 000	RNAi Max	120
H2009	migration	22 000	Lipofectamine 2000	85.71
H460	viability	5 000	RNAi Max	120

Table 2-6 Transfection conditions.

2.7.1 Viability Assay

For the viability assay, cells were seeded at a density that resulted in ~70% confluency after 72 h for cells that were transfected with a non-targeting control (NTC). After 72 h, cells were washed with PBS, fixed with 4% PFA for 20 min, again washed with PBS and then stained with DAPI. Pictures were taken and Nuclei counted with Operetta. Cell number relative to NTC was determined to calculate “loss of viability”.

2.7.2 Migration Assay

For the migration assay, cells were seeded at a density that resulted in 100% confluency after 48 h for cells that were transfected with NTC. After 48 h, a scratch was made, using a woundmaker. After the scratch was made, the plates were washed with media and transferred to a long term Incucyte video microscopy incubator. The Incucyte takes pictures of the scratch at a set interval and calculates the wound width relative to the initial wound width (relative wound density).

2.8 Adeno-Cre infection of MEFs

MEFs were seeded for Adeno-Cre infection (500 000/10 cm plate) and infected with Adeno-Cre the next morning. For infection, 3 ml of full media was mixed with polybrene (1:1000) and the virus at a multiplicity of infection (MOI) of 300 of added. The virus/polybrene mix was added to the cells and cells were incubated at 37°C and 5% CO₂. 3 h later, another 7 ml of media was added to the plate. The next morning, cells were seeded for experiment.

2.9 Analysis of Cell death with Annexin V/PI staining

Annexin V/PI staining was used to measure apoptosis *in vitro*. The morning after Adeno-Cre infection, MEFs were seeded in 6-well plate (70,000 cells/well). 24 h later, the medium was changed to low serum medium (0.2% FBS). Cells were prepared for Annexin V/PI staining 30 h later. Cells were prepared for flow cytometry as follows; the culture medium of cells was collected in a 15ml centrifuge tube and kept on ice, then cells were trypsinized using 10% trypsin, 1% BSA was added to quench the trypsin and cells were collected in the same tube as the medium. Cells were centrifuged at 300g for 5 min. Supernatant was aspirated, 300µl of Annexin V

binding buffer (10mM HEPES [pH7.4], 140mM NaCl, 2.5mM CaCl₂) and 2µl of Annexin V (conjugated with OG488 or APC, Biolegend) was added to the pellet and incubated in the dark for 15 min. Propidium iodide (1µg/ml) was added prior to the analysis.

2.10 RNA isolation and quantitative Real Time PCR

The morning after Adeno-Cre infection, MEFs were seeded at a concentration of 1x10⁵ cells per well in a 6-well plate. After 24 h, the cells were collected using 1ml of Trizol (Ambion) in a 1.5ml centrifuge tube and 200µL of chloroform (sigma) was added. Solutions were then mixed by gently inverting the tubes for 15 sec and incubated at room temperature for 2 to 3 min. The mixture was then centrifuged at 14,000 g for 15 min at 4°C. After centrifugation, the aqueous, upper phase was carefully removed and collected in a fresh autoclaved 1.5ml centrifuge tube. 500µl of isopropanol was added, mixed by inverting the tube and incubated on ice for 5-10 min. Next the tubes were centrifuged at 14,000 g for 10 min at 4°C. The supernatant was carefully removed and the pellet was washed twice with 1ml of 70% Ethanol at 12,000 g for 10 min. The pellet was air dried until it was translucent and dissolved in an appropriate volume of sterile water (usually 30µl). Finally, the sample was heated at 56°C for 10 min and stored at -80°C until further use.

2.10.1 cDNA synthesis

RNA quantity was measured using Nanodrop (Thermo scientific). 1 µg of RNA was used to synthesize cDNA using QuantiTect Reverse transcriptase kit (Qiagen). In this method genomic DNA contamination was eliminated first by incubation with gDNA wipe out buffer at 42°C for 2 min (Table 2-7). RNA was incubated with reverse-transcription reaction components (Table 2-8) and incubated at 42°C for 15 min followed by 95°C for 3 min. The generated cDNA was later used for SYBR green based Real Time PCR analysis. The RT-Primer mix includes both oligo-dT and random primers that enable cDNA synthesis from all regions of RNA transcripts.

gDNA wipeout buffer (7x)	2µl
1µg template RNA	variable
<u>RNase free water</u>	<u>variable</u>
Total	14µl

Table 2-7 genomic DNA removal mix.

Reverse Transcriptase	1µl
RT buffer	4µl
RT primer mix	1µl
<u>Genomic DNA elimination reaction</u>	<u>14µl</u>
Total	20µl

Table 2-8 cDNA synthesis master mix.

2.10.2 Primer design

SYBR green quantitative Real Time PCR was employed. Intron spanning primers were designed using Universal Probe Library Assay Design Centre, a publically available website run by Roche. Primers are listed in Table 2-9.

Gene	Primer sequence
B2M forward	AGCCGAACATACTGAACTGCTACG
B2M reverse	CGGCCATACTGTCATGCTTAACTC
TP53 forward	ATGCCCATGCTACAGAGGAG
TP53 reverse	AGACTGGCCCTTCTTGGTCT
Murine Myc forward	CGCGTCCGAGTGCATTGA
Murine Myc reverse	AGCAGCGAGTCCGAGGAA
Human MYC forward	GCCCCTGGTGCTCCATGA
Human MYC reverse	CAACATCGATTTCTTCCTCATCTTCT
Total Myc forward	GAAAAGGCCCCCAAGGTAGT
Total Myc reverse	CAACTGTTCTCGTCGTTTCC

Table 2-9 Real Time PCR primers.

SYBR green Buffer (2x)	5µl
Forward primer (20µM)	0.2µl
Reverse primer (20µM)	0.2µl
<u>Water</u>	<u>4.6µl</u>
Total	9µl

Table 2-10 Real Time PCR master mix.

Temperature (°C)	Duration
1. 95	5 min
2. 95	30 sec
3. 60	20 sec
Go to step 2. 35 x	
4. 72	10 min
5. 65	10 sec
6. 95	30 sec

Table 2-11 Real Time PCR cycle.

2.10.3 Real Time PCR

SYBR Green mix from Quanta Biosciences (QUNT95072-012) was used. A master PCR mix was prepared and 9 μ l of this mix was added to 1 μ l cDNA (Table 2-10). The following PCR cycling protocol is outlined in Table 2-11.

2.11 Protein extraction and Western Blot

2.11.1 Protein extraction

The morning after Adeno-Cre infection, cells were seeded for protein extraction at a density of 800,000 cells/10 cm plate. 24 h later the plate was removed from the incubator and placed on ice. The medium was aspirated and cells were washed 1X with PBS. Cells were then scraped in 600 μ L PBS and centrifuged for 5 min at 5,000 rpm. Cytoplasmic and nuclear fractions were prepared by resuspending the pellet in Tris/Triton buffer (50mM Tris/HCl [pH 7.2], 1% [w/v] Triton X-100), followed by incubation on ice for 10 min. The samples were centrifuged for 10 min at full speed and the supernatant (cytoplasmic fraction) was transferred to a fresh tube. The nuclear pellet was resuspended in RIPA buffer (150mM NaCl, 50mM Tris [pH7.5], 1% NP-40, 0.5% sodium deoxycholate, 0.1% SDS) plus complete protease inhibitor cocktail [Roche, 4693124001].

2.11.2 Preparation of Protein Samples

Protein samples were stored at -80°C, and then thawed on ice. 5X Laemmli Buffer (300mM Tris [pH 6.8], 50% Glycerol, 10% SDS, 4% β -Mercaptoethanol, 0.5% Bromophenol blue) was added to the samples to denature the proteins and then heated at 95°C for 5 min.

2.11.3 SDS-PAGE

Proteins were separated by SDS-PAGE. Polyacrylamide gels were prepared with the mini-protean (Biorad) gel apparatus. First, the separating gel was poured and allowed to solidify (Table 2-12). A layer of isopropanol prevented the desiccation of the gel and ensured that the gel surface was flat. The isopropanol was then removed and 4% stacking gel was poured on top of the separating gel. The gel comb (10 well) was inserted to allow the formation of wells. Once the stacking gel was

solidified, the entire gel was transferred into a 1xSDS-PAGE running buffer containing gel tank (Table 2-13). The comb was then carefully removed and 5µl of protein molecular weight marker (GE healthcare Life sciences) was added to one of the wells. The protein samples were loaded to the remaining wells. Each gel was run at 100V until an appropriate separation was achieved.

Components	Separating gel (10%)	Stacking gel (4%)
Acrylamide	5.1ml	650µl
1M Tris pH 8.9	5.6ml	-
1M Tris pH 6.8	-	600µl
H ₂ O	4.2ml	3.6ml
SDS (10%)	150µl	150µl
APS (20%)	75µl	25µl
TEMED	15µl	5µl

Table 2-12 SDS gel composition.

SDS: Sodium dodecyl sulphate, APS: Ammonium persulfate, TEMED: Tetramethylethylenediamine

10% SDS
250mM Tris
1.92M Glycine

Table 2-13 1X SDS running buffer.

2.11.4 Western Blot

Following protein separation by SDS-PAGE, a Hoefer transfer module (TE22) was used to transfer the proteins from the gel to a nitrocellulose membrane (Protran) following the manufacturer's instructions. The gel, the membrane and the sponges were placed inside the cassettes and then placed into a Mini-transfer tank and locked in place. 1x transfer buffer was then filled into the tank (Table 2-14). The transfer was performed at 230mA for 2h at 4°C. To determine if the transfer was successful, the membrane was incubated briefly in Ponceau S solution (0.1% Ponceau S in 5% acetic acid), washed in TBS-T and incubated in 5% milk (Marvel milk powder) in TBS-T (Table 2-15) for 1h to block the membrane. The membrane was then incubated overnight in primary antibody in 5% milk (and 0.1% sodium azide) at 4°C (Table 2-16).

0.1% SDS
25mM Tris
0.192M Glycine
20% Methanol

Table 2-14 1X SDS transfer buffer.

200mM Tris
 1.37M Sodium Chloride
 1% Tween20

Table 2-15 10X Tris buffered saline with Tween20 (TBST).
 pH was adjusted to 7.5

Primary antibody	Primary antibody conditions	Secondary antibody	Secondary antibody conditions
Myc Abcam ab32072	1:2000, 5% BSA	Anti-rabbit IRDYe 800CW, Licor 926-32213	1:10,000, 5% milk
H2B Abcam ab1790	1:1000, 5% BSA	Anti-rabbit IRDYe 800CW, Licor 926-32213	1:10,000, 5% milk

Table 2-16 Antibody conditions for Western Blot.

The following day the membrane was washed 3x 5 min in TBS-T, and then incubated with fluorescent secondary antibody (LI-COR) in 5% milk solution for 1h at room temperature. The membrane was then washed again 3x in TBST and fluorescent signal was detected with Odyssey imager from LI-COR.

2.12 RNA-sequencing

2.12.1 Standard protocol

The standard protocol was used for RNA that had been isolated from cell cultured cells. The TruSeq kit from Illumina (RS-930-20 01) was used.

2.12.1.1 Principle of the protocol

mRNA is isolated with the help of oligo(dt) magnetic beads. cDNA is then synthesized with random primers. Individual adaptors are then ligated to the cDNA fragments and the libraries are amplified by PCR.

2.12.1.2 mRNA isolation and purification

4 µg of total RNA were adjusted to 50µl volume with H₂O. The samples were mixed with 50µl magnetic oligo (dt) beads and placed into a thermocycler to allow poly(A)-RNA to bind to the beads. The program outlined in Table 2-17 was started. The beads were then washed twice with 200µl wash buffer. 50µl buffer was added to the beads and the samples were placed into a thermocycler. The program outlined in

Table 2-18 was started. 50µl RNA binding buffer was added to each sample and mixed. The beads were then washed twice with 200µl wash buffer and once with 200µl elution buffer. In order to elute the RNA from the beads, 15µl of elution master mix was added to each sample (Table 2-19) and placed into a thermocycler. The program outlined in Table 2-20 was started.

2.12.1.3 First strand synthesis

The supernatant was transferred to a fresh tube and mixed with 10µl first strand synthesis master mix (Table 2-21). The tubes were placed into a thermocycler and the program outlined in Table 2-22 was started.

Temperature (°C)	Duration
65	5 min
4	1 min
25	5 min

Table 2-17 Poly (A)-RNA binding.

Temperature (°C)	Duration
80	2 min
25	3 min

Table 2-18 further poly (A)-RNA binding.

6µl	First strand buffer
1.5µl	Random primers
<u>7.5µl</u>	<u>H₂O</u>
15µl	Total

Table 2-19 Elution master mix.

Temperature (°C)	Duration
95	15 min
25	3 min

Table 2-20 Poly (A)-RNA elution and fragmentation.

0.5µl	RNase inhibitor
1µl	Reverse transcriptase
<u>8.5µl</u>	<u>H₂O</u>
10µl	Total

Table 2-21 First strand cDNA synthesis master mix.

2.12.1.4 Second strand synthesis

60µl second strand master mix (Table 2-23) was added to each sample, mixed and placed into a thermocycler. The program outlined in Table 2-24 was started.

Temperature (°C)	Duration
25	10 min
42	50 min
70	15 min
4	hold

Table 2-22 First strand cDNA synthesis program.

2.12.1.5 cDNA purification

The cDNA was purified with Qiaquick PCR purification kit (QIAGEN). 400µl PB buffer was added to each sample, transferred to the column and centrifuged for 1 min at full speed. The column was washed with 750µl PE buffer and centrifuged for 1 min at full speed. The cDNA was eluted by adding 63µl of resuspension buffer and centrifugation for 1 min at full speed.

48µl	H ₂ O
8µl	Second strand buffer
4µl	<u>Second strand enzyme</u>
60	Total

Table 2-23 Second strand cDNA synthesis master mix.

Temperature (°C)	Duration
16	150 min
25	3 min

Table 2-24 Second strand cDNA synthesis program.

2.12.1.6 End repair

40µl of end repair buffer was added to each sample and incubated at 30°C for 30 min. Samples were purified with QIAGEN MinElute Reaction Cleanup kit. 300µl ERC buffer was mixed with the sample, transferred to a MinElute spin column and centrifuged for 1 min at maximum speed. 750µl PE buffer was added and centrifuged for 1 min at maximum speed. The cDNA was eluted in 18.5µl TE buffer by centrifugation for 1 min at maximum speed.

2.12.1.7 Adenylation of 3'Ends and adapter ligation

12.5µl of A-tailing buffer was added to each sample, mixed and incubated at 37°C for 30 min. 2.5µl of individual adaptors were added to each sample and mixed. 5µl ligation mix (Table 2-25) was then added to each sample, mixed and incubated at 30°C for 10 min. 5µl Stop buffer was added to each sample. Samples were purified with Qiaquick PCR purification kit as described in section 2.12.1.5. The samples

were eluted in 52µl resuspension buffer. The samples were then further purified with magnetic beads. 50µl magnetic beads were added to the sample and incubated for 10 min at room temperature. The tubes were transferred to a magnetic plate and the beads were washed twice with 200µl 70% EtOH. The samples were eluted in 33µl resuspension buffer.

2.5µl	DNA ligase
<u>2.5µl</u>	<u>Buffer</u>
5µl	Total

Table 2-25 Ligation master mix.

2.12.1.8 PCR amplification

30µl PCR master mix (Table 2-26) was added to each sample and placed into a thermocycler. The program outlined in Table 2-27 was started.

5µl	PCR primers
<u>25µl</u>	<u>PCR buffer</u>
30µl	Total

Table 2-26 PCR amplification master mix.

Temperature (°C)	Duration
1. 98	30 sec
2. 98	10 sec
3. 60	30 sec
4. 72	30 sec
Go to step 2. 12 x	
5. 72	5 min
6. 4	hold

Table 2-27 PCR amplification program.

2.12.1.9 Library purification and quantification

The samples were purified with magnetic beads. 50µl magnetic beads were added to the sample and incubated for 10 min at room temperature. The tubes were transferred to a magnetic plate and the beads were washed twice with 200µl 70% EtOH. The samples were eluted in 33µl resuspension buffer. Libraries were quantified using Quant-iT Pico green kit from Invitrogen. The pico green reagent is a fluorescent nucleic acid stain that binds double stranded DNA. The pico green excitation wavelength is 480 nm and its emission wavelength 520 nm. In order to measure DNA concentration a standard curve was prepared and the concentration of each sample was calculated based on standard. The protocol for the standard

curve is outlined in Table 2-28. After determination of the sample concentration in ng/μl, the average fragment length had to be determined for each sample in order to calculate the nM concentration. The fragment length was determined using the Agilent bioanalyzer with a DNA High Sens chip. The average length was estimated from the electropherogram and was ~300 bp. Libraries were mixed with a final concentration of 10nM for each library.

2.12.2 Amplification protocol

The amplification protocol was used for RNA that was isolated from laser captured frozen sections.

TE (μl)	50 ng/ml DNA stock (μl)	Diluted (1:200) Pico Green reagent	Final DNA concentration
0	1,000	1,000	25 ng/ml
900	100	1,000	2.5 ng/ml
990	10	1,000	250 pg/ml
999	1	1,000	25 pg/ml
1,000	0	1,000	blank

Table 2-28 Pico green standard curve concentrations for cDNA quantification.

2.12.2.1 Tissue sample preparation

Mouse dissection was performed as described in section 2.1.5.

2.12.2.2 Preparation of sections

Cryo-sections were made using a Leica cryostat. The cryostat was cleaned with RNase Zap and the UV light was switched on for 15 min. A new blade was used. 10 μm sections were sectioned on framed membrane slides. The slides were placed into fresh 50ml tubes and stored at -80°C until needed. Adjacent sections were sectioned on PLL coated slides and stained for p-Erk as described in section 2.3.3.

2.12.2.3 Selection of p-Erk positive and p-Erk negative regions for LCM

Overview pictures were taken of p-Erk stained sections and p-Erk positive and negative regions were marked on the printouts. The p-Erk stained sections thus served as a template for the adjacent CV stained sections that were used for LCM.

2.12.2.4 Cresyl Violet staining

Before LCM, the framed membrane slides were stained with CV. The staining was started immediately after taking the slides out of -80°C, only 1 slide was stained at a time. The overall time for CV staining and LCM did not exceed 20 min.

Fresh EtOH solutions using Ethanol p.a. and DEPC water were mixed in fresh 50ml tubes. RNase Inhibitor 500x concentrate (Sigma R7397) was added to the EtOH solutions following Cresyl Violet (RNase inhibitor interferes with the staining) and EtOH solutions were kept on ice. 1% Cresyl Violet was diluted in 50% EtOH, filtered through a 0.45µm filter and was also kept on ice. The sections were first placed into 70% and 50% EtOH for 30 sec each to remove the OCT. Incubation in 1% CV was done for 45 sec, followed by a few dips into 2 H₂O containing tubes to wash the slides. Then the slides were incubated in an increasing EtOH series (50%, 70%, 95%, 100%, 100%) for 30 sec each.

2.12.2.5 Microdissection

Before LCM with a Leica DM 6000B Laser Microdissection Microscope the accessible parts of the microscope and the surrounding area were cleaned with RNase Zap. The Laser control settings are outlined in Table 2-29. 20µl RLT lysis buffer (part of the RNeasy micro kit) was placed into the lid of a 200µl PCR tube. LCM was done immediately after the CV staining.

Laser characteristic	Setting
Power	50
Aperture	56
Speed	1
Specimen balance	0

Table 2-29 Laser settings for LCM.

After LCM another 30µl RLT buffer (+ 1% β-mercaptoethanol) was added, and the sample was pulled 3-4 times through a 26 G needle. The sample was immediately frozen on dry ice and then stored at -80°C until RNA was isolated. In total for each sample at least 1mm² area was captured. Usually samples from several slides had to be pooled for RNA isolation.

2.12.2.6 RNA isolation

Samples were thawed at 37°C for 2 min. Samples were pooled for RNA isolation and the volume was adjusted to 350µl with RLT buffer. 350µl of 70% EtOH was added to the sample and transferred to an RNeasy MinElute spin column and centrifuged at 8,000 g for 15 sec to bind RNA. 350 µl RW1 buffer was added and the column was centrifuged at 8,000 g for 15 sec. 10µl DNase stock solution + 70µl RDD buffer was added to the column and incubated for 15 min at RT. Another 350µl RW1 buffer was added and centrifuged at 8,000 g for 15 sec. The column was then first washed with 500 µl RPE buffer by centrifugation at 8,000 g for 15 sec and then with 500µl 80% EtOH by centrifugation at 8,000 g for 2 min. RNA was eluted in 14µl H₂O by centrifugation at full speed for 1 min.

2.12.2.7 Measurement of RNA integrity

The RNA integrity and quantity was analysed with an Agilent Bioanalyzer, using an RNA pico chip. The Bioanalyser is a machine that runs a small agarose gel on a chip and determines the RNA integrity number (RIN) by measuring the ratio between 18S rRNA, 28S rRNA and the rest. 10 is the highest possible RIN for intact RNA.

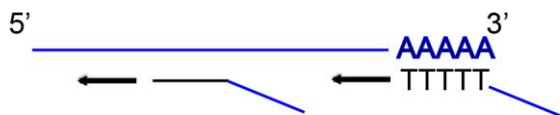
2.12.2.8 Principle of cDNA synthesis

The Ovation RNA-Seq System V2 kit from Nugen (7102) was used for cDNA synthesis and amplification. For first strand synthesis, oligo (dt) primers and also random primers are used. Therefore, intact RNA is needed for this protocol. First strand primers that consist of an RNA and DNA part bind to the RNA and the 3'DNA ends of each primer are extended. The mRNA within the cDNA/mRNA hybrid molecule is then fragmented. The fragments create binding sites for second strand synthesis. For amplification, the RNA portion of the DNA/RNA chimeric primers is digested with RNase H. This creates a binding site for a SPIA DNA/RNA chimeric primer. DNA polymerase extends the 3'end of the primer and thereby displaces the already existing forward strand. The RNA portion of the SPIA primer is also removed by RNase H, which creates a new binding site for the next SPIA primer. This cycle of RNA removal by RNase H, SPIA primer binding and strand displacement leads to very rapid cDNA amplification (Figure 2-1).

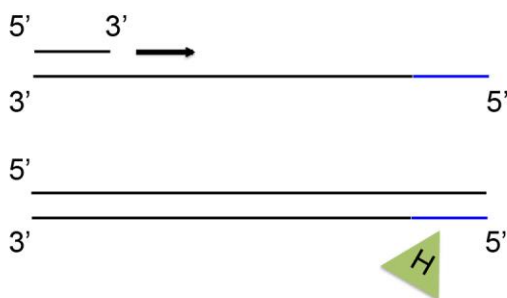
2.12.2.9 First strand cDNA synthesis

At least 3 ng RNA were used at input. 5µl RNA were mixed with 2µl first strand primers and incubated for 5 min at 65°C to allow the primers to anneal. 3µl of first strand master mix (Table 2-30) was then added to the sample, mixed and placed in a thermocycler. The program outlined in Table 2-31 was started.

First strand synthesis



Second strand synthesis



Amplification

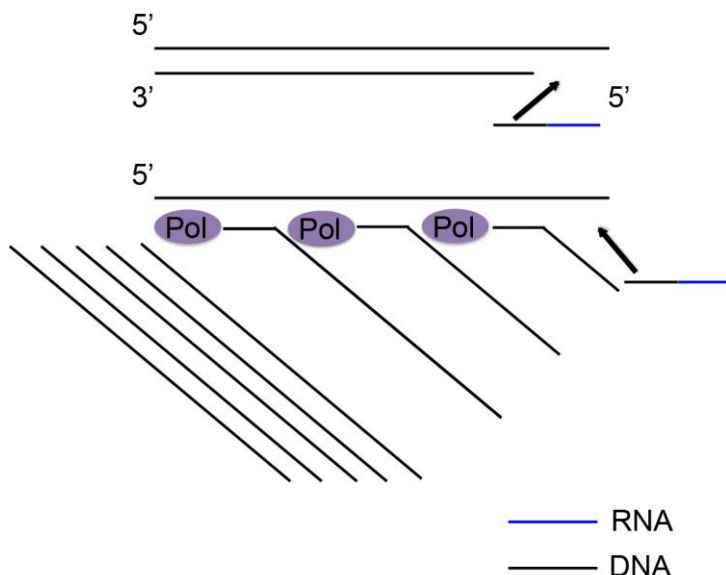


Figure 2-1 SPIA cDNA synthesis and amplification.

First strand synthesis primers either bind the 5' poly(A) portion of the RNA or bind randomly across the transcript. For amplification, the RNA portion of the DNA/RNA chimeric primers is digested with RNase H, which creates a binding site for another DNA/RNA chimeric primer.

2.5µl First strand buffer
 0.5µl First strand enzyme
 3µl Total

Table 2-30 First strand cDNA synthesis master mix.

Temperature (°C)	Duration
4	1 min
25	10 min
42	10 min
70	15 min
4	hold

Table 2-31 First strand cDNA synthesis program.

2.12.2.10 Second strand cDNA synthesis

10µl of second strand master mix (Table 2-32) was added to the sample, mixed and placed in a thermocycler. The program outlined in Table 2-33 was started.

9.7µl Second strand buffer
 0.3µl Second strand enzyme
 10µl Total

Table 2-32 Second strand cDNA synthesis master mix.

Temperature (°C)	Duration
4	1 min
25	10 min
50	30 min
80	20 min
4	hold

Table 2-33 Second strand cDNA synthesis program.

2.12.2.11 cDNA purification

Before the cDNA can be amplified, it has to be purified with the help of magnetic beads. 32µl of bead suspension was added to each sample, mixed and incubated at room temperature for 10 min. The tubes were transferred to a magnetic plate, the supernatant was removed and the samples were washed 3 times with 70% EtOH.

2.12.2.12 SPIA amplification

40µl master mix (Table 2-34) was added to the dried beads and mixed by resuspension. Samples were then placed into a thermocycler and the program outlined in Table 2-35 was started.

20µl SPIA buffer
 10µl SPIA primers
10µl SPIA enzyme
 40µl Total

Table 2-34 SPIA amplification master mix.

Temperature (°C)	Duration
4	1 min
47	60 min
80	20 min
4	hold

Table 2-35 SPIA amplification program.

2.12.2.13 cDNA purification

Final cDNA purification was done with the QIAGEN MinElute Reaction Cleanup kit as described in section 2.12.1.6. The cDNA was eluted in 22µl TE buffer by centrifugation for 1 min at maximum speed.

cDNA was quantified by Nanodrop. The yield was ~200ng/µl.

2.12.2.14 Shearing of cDNA

cDNA had to be sheared to a size ~200bp. This was done with a sonicator (Covaris). 9µl cDNA were mixed with 41µl TE buffer. The sonication settings are outlined in Table 2-36. The fragment size was determined with the Agilent bioanalyzer using a DNA 1000 chip. The fragment size was ~200bp.

Characteristic	Setting
Power (W)	175
Duty factor	10 %
Cycles per boost	200
Treatment time	120 sec

Table 2-36 Sonication settings.

The cDNA was concentrated using the MinElute Reaction Cleanup kit as described in section 2.12.1.6. The samples were eluted in 10µl TE buffer.

2.12.2.15 End repair

For library preparation, the Ovation rapid DR multiplex system from Nugen (0320-32) was used. 7µl master mix (Table 2-37) was added to 8µl sample, mixed and placed into a thermocycler. The program outlined in Table 2-38 was started.

3.0µl End repair buffer
 2.5µl H₂O
 0.5µl End repair enzyme
 1.0µl End repair enhancer
 7µl Total

Table 2-37 End repair master mix.

Temperature (°C)	Duration
25	30 min
70	10 min
4	hold

Table 2-38 End repair program.

2.12.2.16 Adaptor ligation

3µl of the appropriate adaptor was added to each sample. Then, 12µl of ligation master mix (Table 2-39) was added to each sample, mixed and placed into a thermocycler. The program outlined in Table 2-40 was started.

4.5µl H₂O
 6.0µl Ligation buffer
 1.5µl Ligation enzyme
 12µl Total

Table 2-39 Ligation master mix.

Temperature (°C)	Duration
25	10 min
65	10 min
4	hold

Table 2-40 Ligation program.

2.12.2.17 Final repair

20µl final repair master mix (Table 2-41) was added to each sample, mixed and placed into a thermocycler. The program outlined in Table 2-42 was started.

19µl Final repair buffer
 1µl Final repair enzyme
 20µl Total

Table 2-41 Final repair master mix.

Temperature (°C)	Duration
72	2 min
25	hold

Table 2-42 Final repair program.

2.12.2.18 Library purification

50µl magnetic bead suspension was added to each sample, mixed and incubated at room temperature for 10 min. The tubes were transferred to a magnetic plate and washed twice with 200µl 70% EtOH. The libraries were eluted in 11µl TE buffer.

2.12.2.19 Library quantification

In order to verify that only cDNA fragments with ligated adaptors are measured, the library was quantified by Real Time PCR, using a library quantification kit (KAPA Biosystems, KK4824). The Real Time primers can bind all adaptors and only cDNA fragments with ligated adaptors become amplified. 3 dilutions for each library and for 6 standards with known concentration (Table 2-43) were prepared. 4µl sample dilution was added to 16µl master mix (Table 2-44). All samples and dilutions were measured in triplicates. The PCR program is outlined in Table 2-45. The most concentrated library dilution that fell into the dynamic range of the DNA standards was used to calculate the library concentration. The Real Time products were run on a 2% agarose gel and the average fragment size was estimated. The DNA standards have a fragment size of 452bp and in order to take the library fragment size into account, the concentration in pM was calculated with the following formula:

$$c = \text{dilution} \times \frac{452}{\text{fragment length}} \times \text{concentration calculated by qPCR}$$

Standard	Concentration (pM)
1	20
2	2
3	0.2
4	0.02
5	0.002
6	0.0002

Table 2-43 Standards for Real Time quantification.

12µl	KAPA SYBR master mix
4µl	H ₂ O
16µl	Total

Table 2-44 Library quantification master mix.

2.12.3 Protocol for degraded RNA samples

This protocol was used for RNA that had been isolated from laser captured FFPE sections.

Temperature (°C)	Duration
1. 95	5 min
2. 95	30 sec
3. 60	45 sec
Go to step 2. 35 x	
4. 72	10 min
5. 65	10 sec
6. 95	30 sec

Table 2-45 Library quantification Real Time PCR program.

2.12.3.1 Mouse dissection

The mouse dissection protocol described in section 2.1.5 was followed and the tissue was fixed and processed as described in section 2.1.5.1.

2.12.3.2 Preparation of sections

The microtome was carefully cleaned with RNase Zap, and DEPC treated water was filled into the waterbath tank. A fresh blade was used. 10 µm sections were sectioned on framed membrane slides, adjacent sections were sectioned on normal PLL coated slides. After sectioning the slides were left to dry at 65°C for a few hours. The framed membrane slides were stored in the fridge in cardboard boxes until needed, up to few days. In the meantime, the adjacent sections were stained for p-Erk (section 2.3).

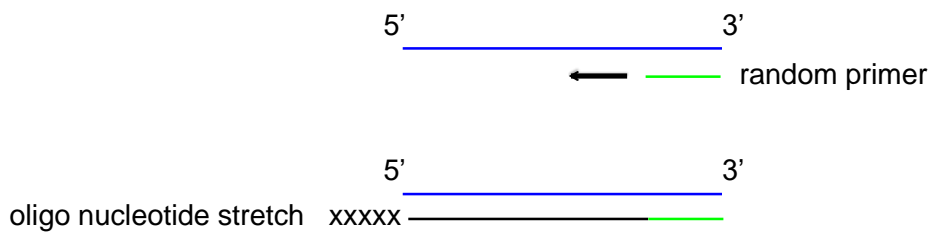
2.12.3.3 Selection of p-Erk positive and p-Erk negative regions for LCM

See section 2.12.2.3 for details.

2.12.3.4 Cresyl Violet staining

Before LCM, the framed membrane slides were stained with CV. The sections were taken out of the fridge ~30 min before starting and left to air-dry at room temperature. I only stained 1 slide at a time and overall time for CV staining and LCM did not exceed 20 min.

First strand cDNA synthesis



Second strand cDNA synthesis and adaptor ligation

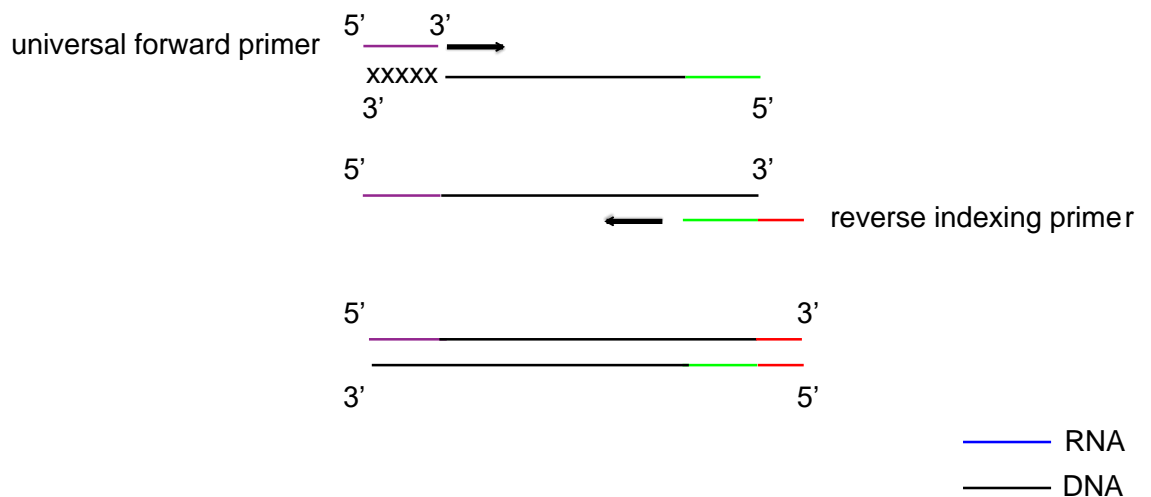


Figure 2-2 SMARTer cDNA synthesis and library preparation.

Random primers are used for first strand cDNA synthesis. Second strand synthesis is performed with universal primers, followed by adapter ligation and PCR amplification.

The staining containers and slide holders were cleaned with Rnase Zap. Fresh Xylene was used and fresh EtOH solutions using Ethanol p.a. and DEPC water were mixed in fresh 50ml tubes. RNase Inhibitor 500x concentrate (Sigma R7397) was added to the EtOH solutions following Cresyl Violet (RNase inhibitor interferes with the staining) and EtOH solutions were kept on ice. 1% Cresyl Violet was diluted in 50% EtOH, filtered through a 0.45µm filter and was also kept on ice. The sections were then first deparaffinised in xylene, using 3 separate containers and sections were incubated for 30 sec in each one. This was followed by incubations in decreasing EtOH solutions (100%, 100%, 95%, 95%, 70%, 70%), for 30 sec each. Incubation in 1% CV was done for 30 sec, followed by a few dips into 2 H₂O containing tubes to wash the slides. Then the slides were incubated in an increasing EtOH series (50%, 70%, 95%, 100%) for 30 sec each.

2.12.3.5 Microdissection

LCM was performed as described in section 2.12.2.5 with the modification that PKD buffer was used instead of RLT buffer.

RNA isolation

RNA was isolated with Qiagen RNeasy FFPE Kit. Samples were removed from -80°C, thawed and pooled. The volume was adjusted to 150µl with PKD buffer. If pooling resulted in a larger volume, all other volumes were adjusted accordingly. 10µl proteinase K was added, mixed and then incubated at 56°C for 15min, followed by 80°C for 15min. The sample was then incubated on ice for 3 min and centrifuged for 15min at 20 000 g. The supernatant was transferred to a fresh 1.5ml Eppendorf tube, 16µl DNase booster buffer and 10µl DNase I stock solution was added and incubated for 15min at RT. 320µl RBC buffer and 720µl 100% EtOH was added, mixed and transferred to a RNeasy MinElute spin column. For RNA binding to the column, the samples were centrifuged at 8 000 g for 15 sec. The columns were then washed by adding 500µl RPE buffer and centrifuging for 2 min at 8 000g. The samples were eluted in 18µl H₂O by centrifuging for 1 min at full speed. The samples were either stored at -80°C or RNA integrity was measured immediately.

2.12.3.6 Measurement of RNA integrity

See section 2.12.2.7 for details.

2.12.3.7 Principle of cDNA synthesis

This protocol allows cDNA synthesis from degraded RNA. In contrast to most cDNA synthesis protocols that use Oligo (dT) primers for first strand synthesis, the SMARTER Stranded RNA-seq kit from Takara/Clontech (634836) uses random primers instead. For this reason the RNA has to be depleted from rRNA before cDNA synthesis. This is done with the help of magnetic beads that bind rRNA.

For first strand synthesis, random primers bind to the RNA and are extended by reverse transcriptase. When the reverse transcriptase reaches the 5'end of the mRNA, an additional oligo nucleotide stretch is attached to the 3'end. This oligo nucleotide stretch is complementary to a universal forward primer and serves as a template. The forward primer can then be used for the second strand synthesis. If

high quality, undegraded was used, the cDNA has to be sheared to a size of ~200bp. As RNA from FFPE samples is highly degraded, the synthesized cDNA is relatively short and hence does not need to be sheared. During library preparation, Illumina indexing primer sets are used and attached to both ends of the cDNA, involving a Real Time quantification step (Figure 2-2).

2.12.3.8 Ribosomal RNA depletion

The SMARTER Stranded RNA-Seq kit recommends at least 100pg ribosomal RNA-depleted RNA input, I used at least 80ng total RNA. Ribosomal RNA was depleted using the Ribo-Zero magnetic kit from Epicentre (MRZH116), followed by cleanup with NucleoSpin RNA XS kit from Machery-Nagel (740902.10). Magnetic beads had to be washed with H₂O, using a magnetic plate. The beads were then resuspended in magnetic bead resuspension solution and for each reaction, 35µl of the washed magnetic beads was aliquoted to a fresh 1.5ml eppendorf tube. 0.5µl RNase inhibitor was added to each reaction.

2µl Ribo-Zero reaction buffer and 1µl Ribo-Zero rRNA removal solution was added to 17µl RNA and incubated first at 68°C for 10 min and then at RT for 5 min. The RNA sample was then added to the magnetic beads and mixed and first incubated at RT for 5 min and then at 50°C for 5 min. The incubations allow binding of rRNA to the magnetic beads. The samples are then placed into a magnetic plate and the supernatant, containing rRNA-depleted RNA is transferred to a fresh 1.5ml eppendorf tube.

In order to clean up the sample, 50µl H₂O and 100µl lysis buffer premix (25µl lysis buffer + 75µl 100% EtOH) were added, mixed and transferred to a NucleoSpin RNA XS column. The RNA was bound to the column by centrifuging first for 30 sec at 2,000 g and then for 30 sec at 11,000 g. The column was washed by adding 400µl wash buffer and centrifugation for 30 sec at 11,000 g, which was repeated with 200µl wash buffer and centrifugation for 2 min at 11,000 g. RNA was eluted in 11µl H₂O by centrifugation for 30 sec at 11,000 g.

2.12.3.9 First strand synthesis

8µl rRNA depleted RNA were mixed with 1µl SMART N6 primer. The samples were then incubated at 72°C for 3 min and placed on ice afterwards. For first strand

synthesis a master mix was prepared (Table 2-46). 11µl master mix was added to each sample and the samples were incubated at 42°C for 90 min. The reaction was terminated by increasing the temperature to 70°C for 10 min and then cooled down to 4°C.

4µl	5x first strand buffer
0.5µl	DTT
0.5µl	RNase inhibitor
2µl	dNTP mix
2µl	Stranded oligo
<u>2µl</u>	<u>reverse transcriptase</u>
11µl	Total volume per reaction

Table 2-46 First strand master mix.

2.12.3.10 First strand purification

The first strand cDNA reaction was purified using SPRI magnetic beads. cDNA binds to the beads and can then be washed with the help of a magnetic plate. 20µl SPRI magnetic beads were added to each sample and incubate for 8 min at RT to allow the cDNA to bind to the beads. The tubes were then placed into a magnetic plate and the supernatant was removed. While still on the magnetic plate, the beads were washed twice with 200µl 70% EtOH and left to dry for 3-5 min.

25µl	2x SeqAmp PCR buffer
1µl	Universal forward PCR primer
1µl	Indexed reverse PCR primer
1µl	DNA polymerase
<u>22µl</u>	<u>H₂O</u>
50µl	Total volume per reaction

Table 2-47 PCR amplification master mix.

Temperature (°C)	Duration
1. 94	1 min
2. 98	15 sec
3. 55	15 sec
4. 68	30 sec
Go to step 2. 16x	
5. 4	hold

Table 2-48 PCR amplification program.

2.12.3.11 Second strand synthesis and PCR amplification

The beads were resuspended in 50µl PCR master mix (Table 2-47) and placed in a PCR cycler with the cycling program outlined in Table 2-48. During PCR, the second

strand is synthesized (universal forward primer) and the double stranded cDNA is amplified. The reverse primer contains an individually indexed sequence that is needed for sample identification after sequencing. After the PCR another 50µl of SPRI AMPure magnetic beads was added to each sample. The beads were allowed to bind to the cDNA libraries, placed into the magnetic plate and washed twice with 200µl 70% EtOH. The beads were left to dry for 3-5 min and resuspended in 20µl elution buffer.

2.12.3.12 Library quantification

Libraries were quantified using Quant-iT Pico green kit from Invitrogen as outlined in section 2.12.1.9.

2.12.3.13 Determination of library length

After determination of the sample concentration in ng/µl, the average fragment length had to be determined for each sample in order to calculate the nM concentration. The fragment length was determined using the Agilent bioanalyzer with a DNA 1000 chip. The average length was estimated from the electropherogram and was ~300 bp. Libraries were mixed with a final concentration of 10nM for each library.

2.12.4 Preparation of libraries for cluster generation and sequencing

10nM libraries were denatured with 0.1N NaOH (1:1 dilution). Denatured libraries were diluted by addition of 980µl HT1 buffer, for a final library concentration of 10pM. Clusters were generated and libraries were sequenced with a paired-end run on the Illumina GA11x sequencer.

2.12.5 Sequencing data analysis

The raw RNA-Sequencing data files underwent quality checks using FastQC software. RNA-Sequencing reads were aligned to the GRCm38 version of the mouse genome using Tophat2. Expression levels were determined and statistically analysed by a combination of HTSeq and the R 3.0.2 environment, utilizing packages from the Bioconductor data analysis suite and differential gene

expression analysis based on the negative binomial distribution using the EdgeR package.

2.13 Data analysis

2.13.1 Graphical presentation of the data

Raw data obtained from quantitative Real Time PCR, FACS, and Incucyte assays were copied into Excel (Microsoft) spreadsheets. All means, standard deviation, standard error of mean were calculated using the calculator function. Graphical representation of all data was also produced in Excel (Microsoft)

2.13.2 Survival analysis

Survival data were analysed using SPSS software. Kaplan-Meier plots were used to present the data, and significance was measured using Log-Rank test.

3 The role of moderately deregulated MYC in lung tumour initiation and its potential cooperation with oncogenic KRas^{G12D} or loss of functional p53

3.1 Introduction

Myc's tumour promoting potential has been shown in multiple mouse models (Morton and Sansom, 2013). Myc-driven tumour formation however usually requires additional genetic modifications such as coexpression of antiapoptotic proteins (Jager et al., 1997; Strasser et al., 1990).

Low levels of Myc drive proliferation, whereas high levels of Myc are able to engage the apoptotic machinery and therefore high levels of Myc are unlikely to be a tumour initiating event in epithelial cell derived cancer (Jager et al., 1997; Muthalagu et al., 2014; Pelengaris et al., 2002). It is more likely that Myc levels are initially only slightly elevated, e.g as the result of deregulation of upstream pathways such as the PI3K- and MAPK-pathway (Sears et al., 2000). By accumulation of Myc upregulating events over time, Myc levels rise gradually and as the tumour further progresses and acquires mutations that abrogate tumour suppressive mechanisms, high Myc levels can exert their full oncogenic potential.

In most mouse models however, Myc is expressed at high levels through the use of strong tissue specific promoters, such as MMTV promoter in mammary tissue (Stewart et al., 1984) and SP-C or CC10 promoters in the lung (Ehrhardt et al., 2001; Geick et al., 2001). In the lung it has been shown that strong Myc expression can even interfere with KRas induced tumourigenesis (Allen et al., 2011). In this study, the DNA-alkylating agent N-methyl-N-nitrosourea (MNU) was used to induce KRas mutations. MNU treatment led to KRas mutant lung tumours and simultaneous induction of Myc driven by the Sp-C promoter reduced tumour number compared to uninduced mice.

The consequences of low levels of deregulated MYC expression in the lung has been well described in a mouse model in which MYC was driven by the Rosa promoter (Murphy et al., 2008). A 4-hydroxytamoxifen (4-OHT)-dependent MYC protein that was fused to Estrogen Receptor (MYC-ER^{T2}) was used. In this model,

short term MYC activation by 4-OHT led to acute ectopic proliferation in the bronchiolar epithelium, which was detected by BrdU incorporation after 3 days of MYC induction. 6 weeks of MYC induction gave rise to mild epithelial hyperplasia, however MYC was not able to give rise to frank tumours within this time frame. The study also showed that low, deregulated MYC expression is able to accelerate $KRas^{G12D}$ driven tumourigenesis in the lung. Combination of $KRas^{G12D}$ with *Rosa-MYC-ER* increased the size of the lesions and also led to sporadic progression to adenocarcinoma, which was not observed in $KRas^{G12D}$ mice within this time frame.

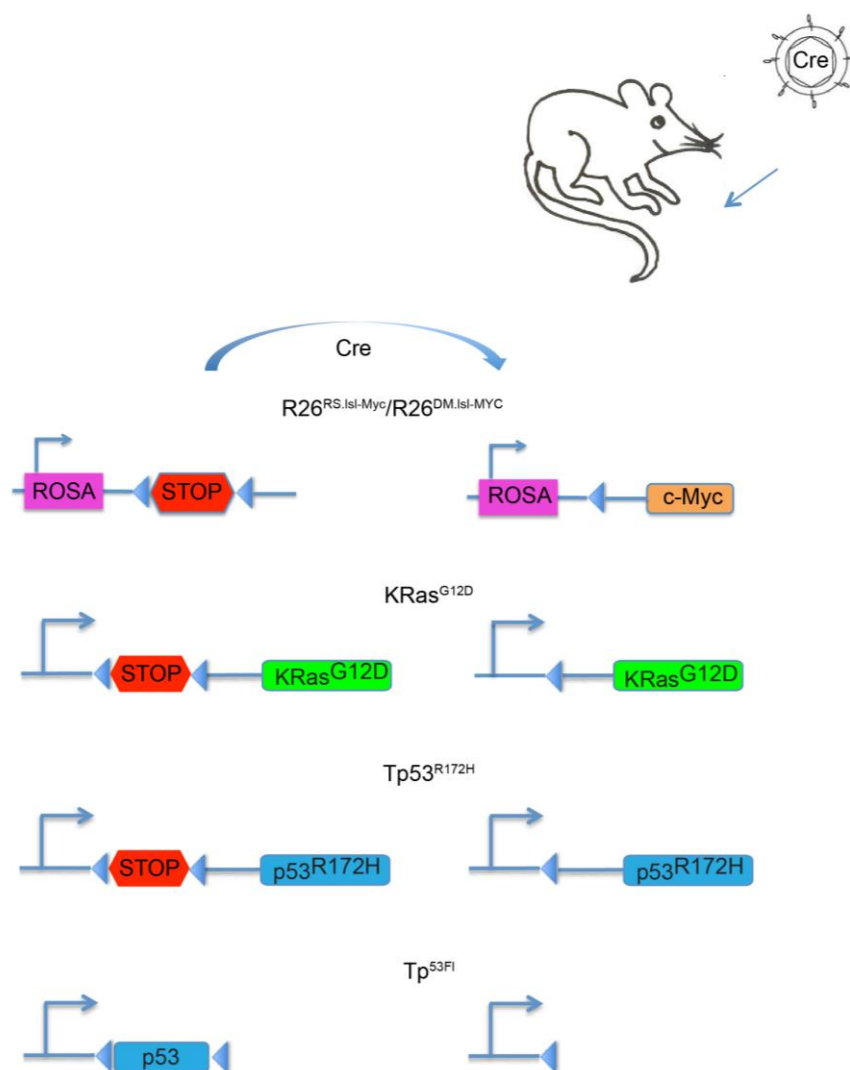


Figure 3-1 Schematic of mouse models.

All alleles are Cre inducible alleles and induced by intranasal inhalation of Cre expressing Adenovirus. Murine *Myc* ($R26^{RS, Isl-Myc}$) or human *MYC* ($R26^{DM, Isl-MYC}$) are both knocked into the Rosa26 locus. $KRas^{G12D}$: Endogenous *KRas* is replaced by $KRas^{G12D}$. $Tp53^{R172H}$: Endogenous *Tp53* is replaced by mutant $Tp53^{R172H}$. $Tp53^{Fl}$: The floxed endogenous *Tp53* allele is flanked by loxP sites.

One disadvantage of this model is that daily tamoxifen administration cannot be tolerated by the mouse for more than 6 weeks, making long-term studies impossible.

To overcome this problem, we decided to use a Myc model, in which human influenza hemagglutinin (HA)-tagged murine c-Myc is knocked into the Rosa26 locus, preceded by a floxed transcription Stop sequence ($R26^{RS.Isl-Myc}$) (Wang et al., 2011). Additionally, we generated our own version of this allele, using human c-MYC (without HA-tag) instead of murine c-Myc ($R26^{DM.Isl-MYC}$). This chapter focuses on the characterization of these 2 mouse models, exploring the tumour initiating potential of low level deregulated MYC expression in the lung and the potential cooperation with oncogenic KRas^{G12D} and loss or mutation of p53. The MYC models were crossed with a well described KRas^{G12D} model (Jackson et al., 2001) or with floxed *Tp53* (Jonkers et al., 2001), or conditional mutant *Tp53*^{Isl-R172H} (Jackson et al., 2005). All used alleles are conditional alleles that are induced in the lung by intranasal delivery of recombinant Adenovirus expressing Cre recombinase.

As $R26^{DM.Isl-MYC}$ proved more potent in collaborating with KRas^{G12D} than $R26^{RS.Isl-Myc}$, we eventually focused on the former, which is why the $R26^{DM.Isl-MYC}$ model is described in more detail.

3.2 Results

3.2.1 MYC driven by the Rosa26 locus

To confirm the presence of the transgenic MYC allele, genomic DNA was extracted from tails from $R26^{DM.Isl-MYC}$ mice and genotyping PCR was carried out. Figure 3-2 A shows the correct size for the R26 wild type locus (600bp) and R26 locus containing the MYC transgene (300bp).

In order to determine Myc transcript levels in $R26^{DM.Isl-MYC}$ and $R26^{RS.Isl-Myc}$ mouse embryonic fibroblasts (MEFs), Real Time polymerase chain reaction (PCR) was performed after infection with Cre expressing Adenovirus, using primers that specifically detect mouse Myc, human MYC or both. Figure 3-2 B shows Myc mRNA levels in $R26^{RS.Isl-Myc}$ (left) and $R26^{DM.Isl-MYC}$ (right) MEFs. $R26^{RS.Isl-Myc}$ MEFs do not contain human MYC, hence it could not be detected. $R26^{RS.Isl-Myc}$ MEFs that contain the transgene have higher murine Myc and total Myc levels than wild-type MEFs in a dose dependent manner, $R26^{RS.Isl-Myc/Myc}$ murine and total Myc transcript levels are approximately 2 times higher than in wild-MEFs. $R26^{DM.Isl-MYC}$ MEFs express human MYC and total MYC levels are comparable to those in $R26^{RS.Isl-Myc}$ MEFs. In $R26^{DM.Isl-$

MYC/MYC MEFs, endogenous, murine Myc levels go down to less than 50% compared to wild-type MEFs after Cre mediated activation of the

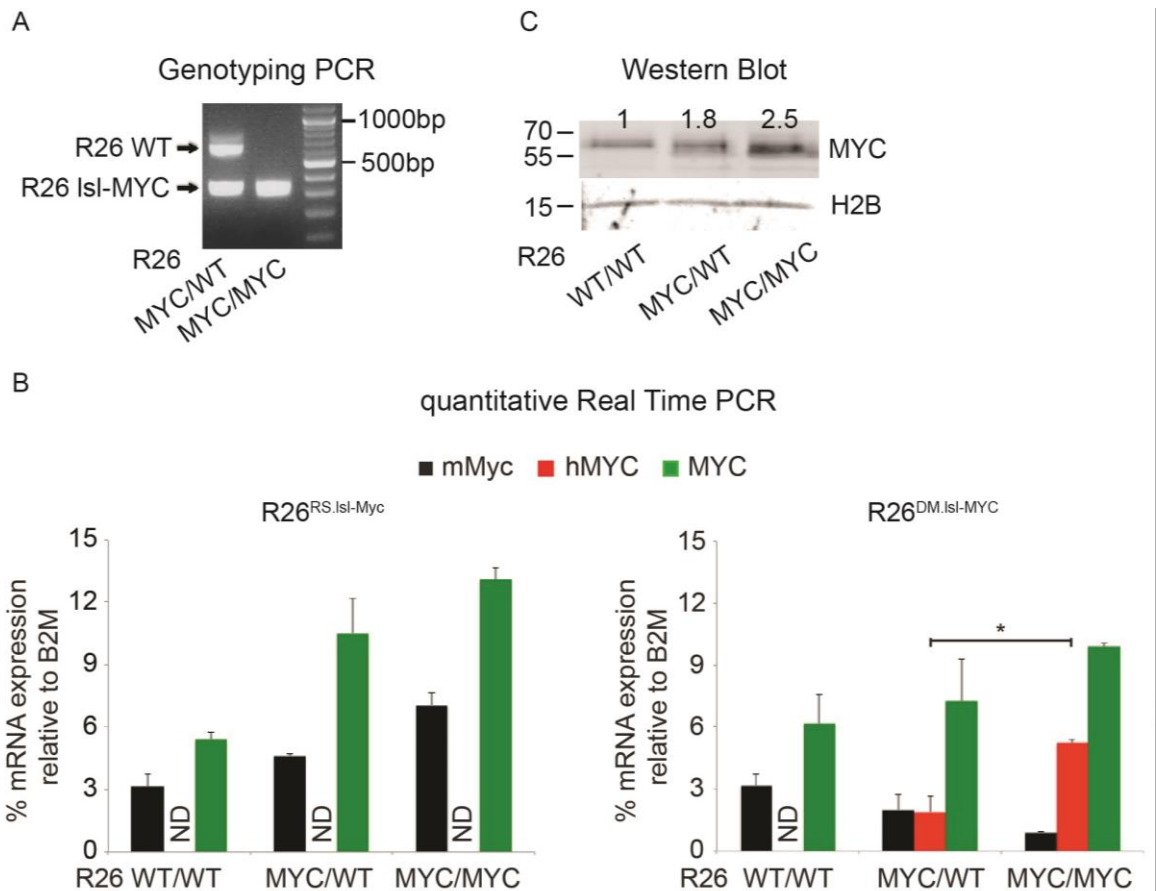


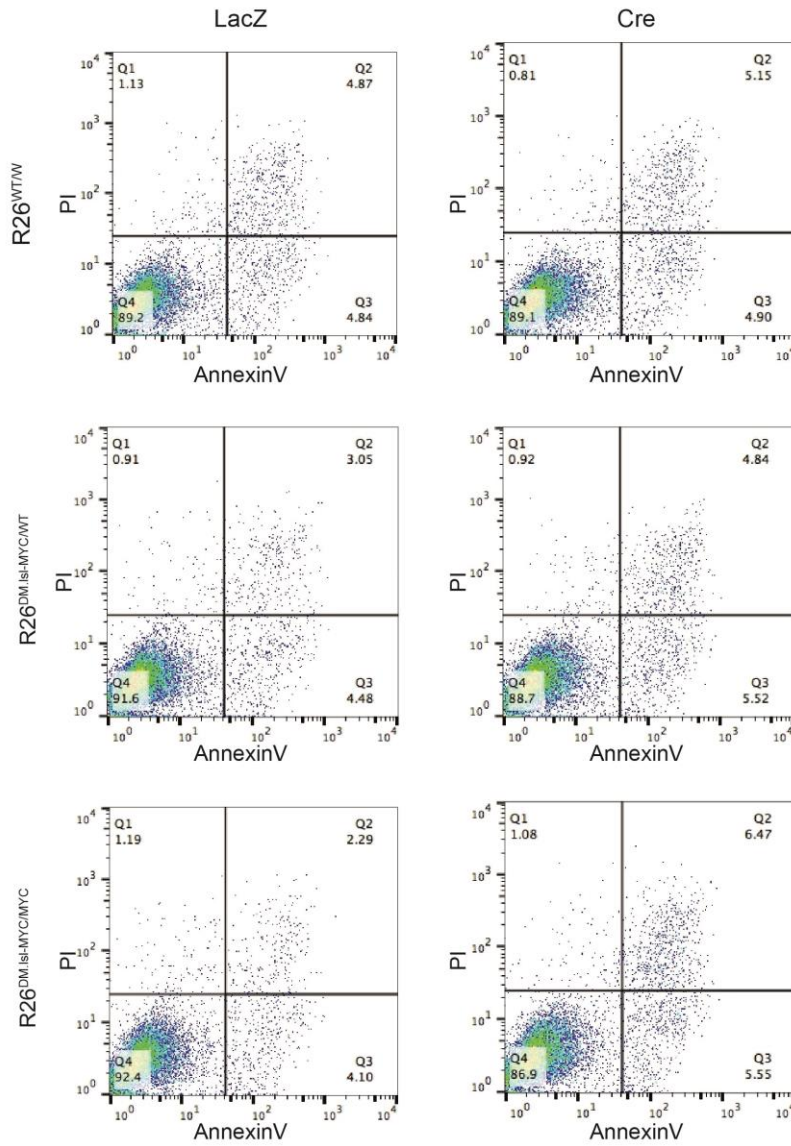
Figure 3-2 Characterization of Rosa-Isi-Myc MEFs.

A) Genotyping of *R26^{DM.Isi-MYC/WT}* and *R26^{DM.Isi-MYC/MYC}* mice for the Rosa26 locus. WT band = 600bp, MYC band = 300bp. B) Quantitative real time PCR on mRNA from *R26^{WT/WT}*, *R26^{RS.Isi-Myc/WT}* and *R26^{RS.Isi-Myc/Myc}* (left) and *R26^{WT/WT}*, *R26^{DM.Isi-MYC/WT}* and *R26^{DM.Isi-MYC/MYC}* (right) MEFs after Adeno-Cre infection with primers specific for murine Myc, human MYC and primers that recognize both transcripts. Numbers represent % expression of Beta 2 microglobulin mRNA. Myc transgene levels increase in heterozygous and homozygous transgenic animals in a dose-dependent manner. Mean \pm SEM from biological triplicates is shown. Asterisk indicates statistical significance ($p < 0.05$), ANOVA, followed by post Hoc Tukey test. C) c-Myc immunoblot from *R26^{DM.Isi-MYC}* MEFs after AdCre infection. Myc levels increase in a dose-dependent manner. Numbers indicate the fold change of total MYC expression.

transgenic MYC allele. This is likely due to negative autoregulation of Myc that has been described before (Cleveland et al., 1988; Penn et al., 1990). *R26^{DM.Isi-MYC/MYC}* MEFs also have about 2.5 times higher MYC protein levels than WT MEFs, which was detected with Y69 antibody that recognises murine and human MYC (Figure 3-2 C). It has been reported that Myc overexpressing cells are sensitized to undergo apoptosis under low serum conditions (Evan et al., 1992; Murphy et al., 2008). To verify this I carried out AnnexinV/PI FACS analysis. *R26^{DM.Isi-MYC}* MEFs were infected with Cre or LacZ expressing Adenovirus and apoptosis was measured after

A

AnnexinV/PI FACS



B

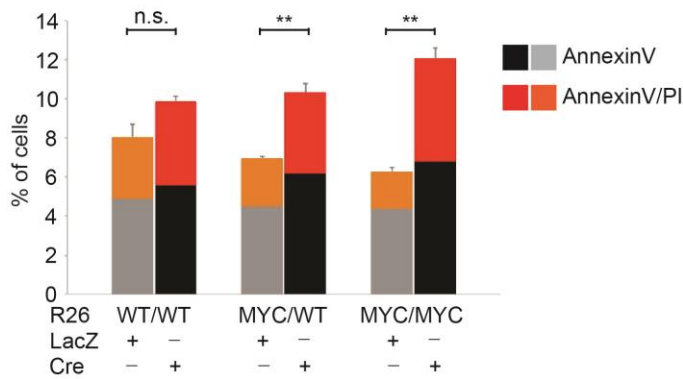


Figure 3-3 Rosa-IsI-Myc MEFs undergo MYC induced apoptosis.

A) Measurement of MYC induced apoptosis in MEFs by AnnexinV/PI FACS: Early passage (< 4) R26^{DM,IsI-MYC} MEFs were infected with AdCre or AdLacZ and cultured for 30h under low (0.2%) serum conditions. B) The lower grey/black bar shows the percentage of cells stained positive AnnexinV, the upper orange/red bar shows cells positive for both, AnnexinV and PI (Propidium iodide). AdCre infected R26^{DM,IsI-MYC/WT} and R26^{DM,IsI-MYC/MYC} MEFs undergo MYC induced apoptosis. Mean \pm SEM from biological triplicates is shown. Asterisks indicate statistical significance ($p < 0.01$), student's t-Test.

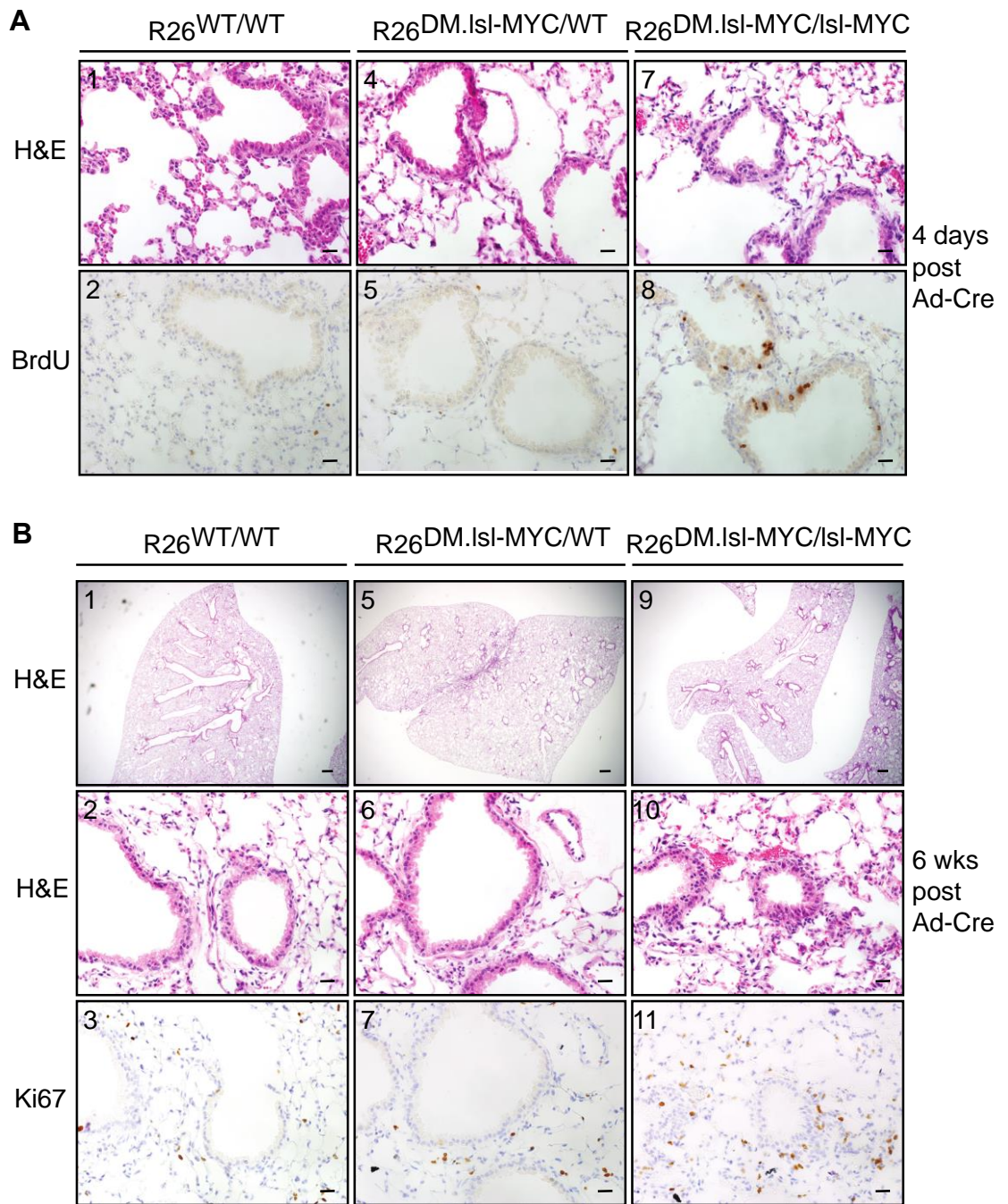


Figure 3-4 Activation of Rosa-Isi-Myc in the lung.

Lungs from R26^{WT/WT}, R26^{DM.Isi-MYC/WT} and R26^{DM.Isi-MYC/MYC} mice (A) 4 days and (B) 6 weeks after AdCre infection (5×10^7 PFU). BrdU was injected the day before harvest and again 2h before harvest. 4 days post allele induction, clusters of BrdU positive cells could be detected in R26^{DM.Isi-MYC/MYC} mice. 6 weeks post allele induction hyperplastic lesions that stain positive for Ki67 could be detected in the bronchiolar epithelium. Pictures are representative for at least 4 mice for each genotype and time point. Scale bars: A: 20 μ m, B 1,5,9: 300 μ m, rest: 20 μ m

culturing the cells for 30h under low (0.2%) serum conditions. As shown in Figure 3-3 , Cre infection resulted in a modest but statistically significant amount of apoptosis in R26^{DM.Isi-MYC} MEFs compared to wild-type cells. Also, apoptosis induced by MYC is dose dependent, as R26^{DM.Isi-MYC/MYC} MEFs exerted higher levels of apoptosis than R26^{DM.Isi-MYC/WT} MEFs (Figure 3-2 D).

3.2.2 Moderate levels of deregulated MYC do not give rise to tumours

It is known that acute MYC expression drives proliferation in the lung (Murphy et al., 2008). However, previously a 4-OHT inducible version of MYC was used (MYC-ER) and I could confirm this phenotype without the use of 4-OHT (Figure 3-4 A). In $R26^{DM.lsl-MYC/MYC}$ mice, clusters of Bromodeoxyuridine (BrdU) positive cells in the bronchioles were reliably detectable 4 days post allele induction, whereas these clusters could not be detected in heterozygous $R26^{DM.lsl-MYC/WT}$ mice or wild-type mice.

$R26^{DM.lsl-MYC/MYC}$ bronchioles 6 weeks post Ad-Cre

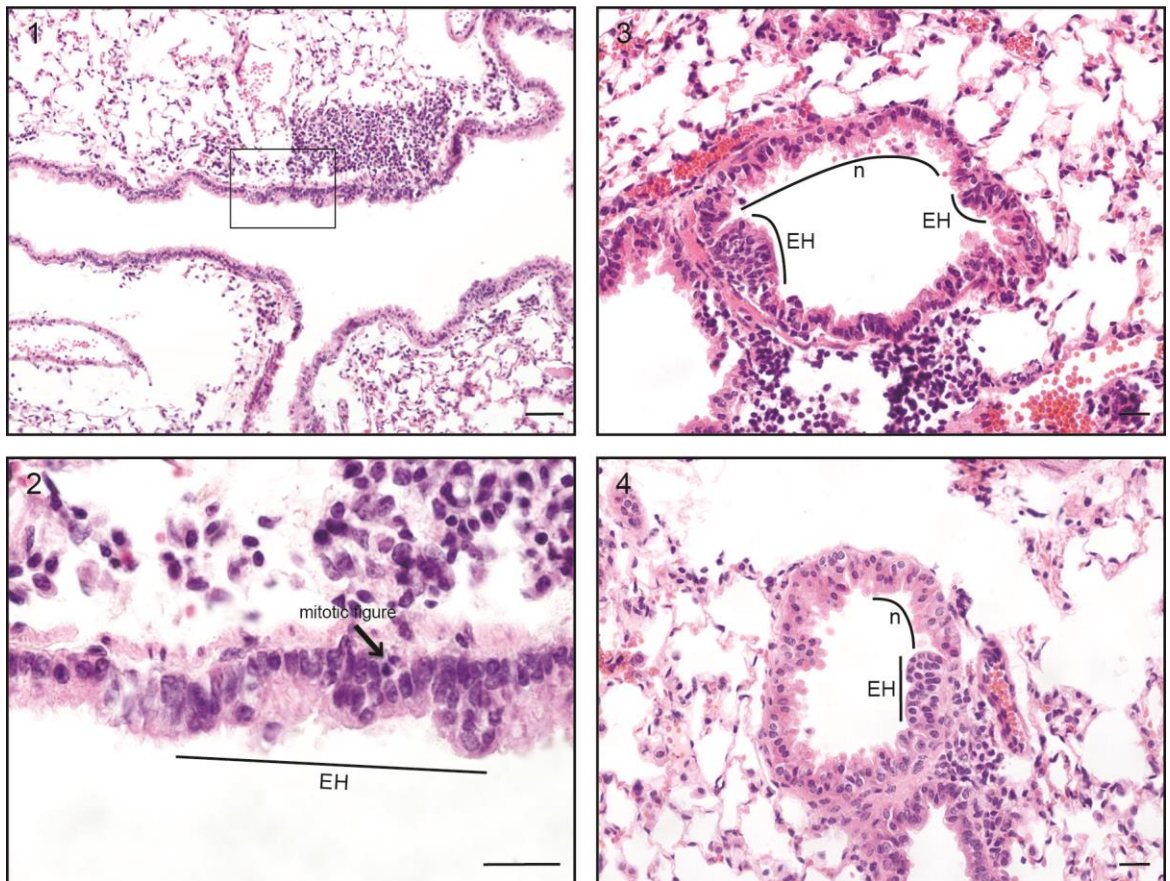


Figure 3-5 Myc induced hyperplasia.

High magnification bronchioles from $R26^{DM.lsl-MYC/MYC}$ mice 6 weeks after AdCre infection (5×10^7 PFU) to illustrate epithelial hyperplasia. EH: epithelial hyperplasia, n: normal bronchiolar epithelium. The arrow is pointing to a mitotic figure. Scale bars: 1: $50\mu\text{m}$, 2: $10\mu\text{m}$, 3,4: $20\mu\text{m}$.

Even 6 weeks post induction tumours could not be detected (Figure 3-4 B), which again confirms the observation of the 4-OHT inducible MYC-ER model (Murphy et al., 2008). MYC is however able to drive local proliferation, which can be seen in the small hyperplastic lesions, that stain positive for Ki67. In the higher magnification

(Figure 3-5) examples of epithelial hyperplasia (EH) next to normal bronchiolar epithelium can be seen. Epithelial cells in the bronchioles usually form a single row of columnar cells, however as they become hyperplastic, multiple layers can accumulate. The cells also undergo a morphological change, the nuclei are displaced and stain differently for haematoxylin. In Figure 3-5 panel 2, the arrow indicates a mitotic figure, an event that is usually not seen in untransformed bronchioles, confirming that deregulated MYC expression drives proliferation.

Even though MYC is able to drive proliferation in the bronchioles, it does not give rise to tumours, even after a long time. Lungs from $R26^{DM.lsl-MYC/MYC}$ mice were examined 4 months post induction and did not show any sign of tumour formation (Table 3-1). This shows that Myc on its own is not sufficient to initiate tumourigenesis in the lung.

	3 days	6 weeks	4 months
$R26^{DM.lsl-Myc/WT}$	7	4	7
$R26^{DM.lsl-Myc/lsl-Myc}$	12	4	4
$R26^{DM.lsl-Myc/WT}$ $TP53^{R172H/WT}$	nd	11	nd
$R26^{DM.lsl-Myc/WT}$ $TP53^{R172H/R172H}$	1	1	nd
$R26^{DM.lsl-Myc/lsl-Myc}$ $TP53^{R172H/WT}$	nd	8	6
$R26^{DM.lsl-Myc/lsl-Myc}$ $TP53^{R172H/R172H}$	6	2	nd

Table 3-1 Numbers and genotypes of mice expressing human c-MYC from the Rosa26 locus harvested at the indicated times post allele induction.

nd: not done

3.2.3 Absence of functional p53 does not increase MYC's tumour initiating potential

As Myc on its own was unable to drive tumourigenesis, I reasoned that p53 might restrain tumour development in our model. Loss of p53 is known to accelerate MYC's oncogenic potential in lymphomas (Schmitt et al., 1999). We therefore crossed the structural mutant $TP53^{R172H}$ or floxed $TP53$ allele into $R26^{RS.lsl-Myc}$ mice and mutant $TP53^{R172H}$ into $R26^{DM.lsl-MYC}$ mice (see table 1&2 for all allele combinations and harvest timepoints) to see if deregulated MYC is able to drive tumourigenesis in the absence of functional p53.

R26^{DM}.Isl-MYC/MYC;Tp53^{R172H/WT} mice had not developed any tumours 4 months post induction and *R26^{RS}.Isl-Myc/Myc;Tp53^{FL/WT}* and *R26^{RS}.Isl-Myc/Myc;Tp53^{FL/FL}* did not have tumours 12 and 6 months post induction, respectively. It should be noted that *Tp53^{R172H/R172H}* mice are constitutively null for p53 before allele induction and therefore develop lymphomas, limiting the duration of the experiment.

	3 days	6 weeks	9 weeks	3 months	6 months	12 months
<i>R26^{RS}-Isl-Myc/WT</i>	2	4	nd	nd	nd	nd
<i>R26^{RS}-Isl-Myc/Isl-Myc</i>	1	2	nd	nd	nd	nd
<i>R26^{RS}-Isl-Myc/WT Tp53^{R172H/WT}</i>	nd	2	nd	nd	nd	nd
<i>R26^{RS}-Isl-Myc/WT Tp53^{R172H/R172H}</i>	nd	4	nd	nd	nd	nd
<i>R26^{RS}-Isl-Myc/Isl-Myc Tp53^{R172H/WT}</i>	nd	8	nd	nd	nd	nd
<i>R26^{RS}-Isl-Myc/Isl-Myc Tp53^{R172H/R172H}</i>	nd	2	nd	nd	nd	nd
<i>R26^{RS}-Isl-Myc/WT Tp53^{Fl/Fl}</i>	nd	2	nd	nd	nd	nd
<i>R26^{RS}-Isl-Myc/Isl-Myc Tp53^{Fl/WT}</i>	nd	nd	nd	nd	nd	3
<i>R26^{RS}-Isl-Myc/Isl-Myc Tp53^{Fl/Fl}</i>	nd	13	7	8	6	nd

Table 3-2 Numbers and genotypes of mice expressing murine c-Myc from the Rosa26 locus harvested at the indicated times post allele induction.

nd: not done

In order to control for transgene expression, bronchioles from *R26^{DM}.Isl-MYC/MYC;Tp53^{R172H/R172H}* mice were laser captured 4 days after allele induction (uninduced mice served as control), RNA was isolated and Real Time PCR for p53 and MYC mRNA was carried out. P53 and human MYC transcripts could be detected after induction, confirming that both alleles are expressed upon exposure to Cre (Figure 3-6).

Looking at the effects of acute MYC expression 4 days post allele induction, MYC drives proliferation in the bronchioles in the presence or absence of mutant P53^{R172H}, as detected by BrdU staining (Figure 3-7 A), and p53 had no effect on the number of BrdU positive bronchioles or on the number of BrdU positive cells within a bronchiole (Figure 3-7 B). MYC expression did not lead to apoptosis, neither in the presence (*R26^{DM}.Isl-MYC/MYC*) nor absence of functional p53 (*R26^{DM}.Isl-MYC/MYC;Tp53^{R172H/R172H}*). In *R26^{DM}.Isl-MYC/MYC* lungs, MYC is not detectable by

immunohistochemistry (IHC), using Y69 antibody, that recognizes murine and human MYC. KRas^{G12D} on its own, or in combination with MYC (*R26^{DM.Isi-MYC/MYC};KRas^{G12D}*) drives proliferation in the bronchioles. In *R26^{DM.Isi-MYC/MYC};KRas^{G12D}* mice MYC is detectable in the bronchiolar regions where clusters of BrdU positive cells are found (Figure 3-7 A). Loss of functional p53 however, (*R26^{DM.Isi-MYC/MYC};P53^{R172H/R172H}*) did not improve MYC detection by IHC. This suggest that KRas^{G12D}, but not mutant p53 is able to stabilize MYC protein (Sears et al., 2000).

quantitative Real Time PCR of *R26^{DM.Isi-MYC/MYC};Tp53^{R172H/R172H}* bronchioles

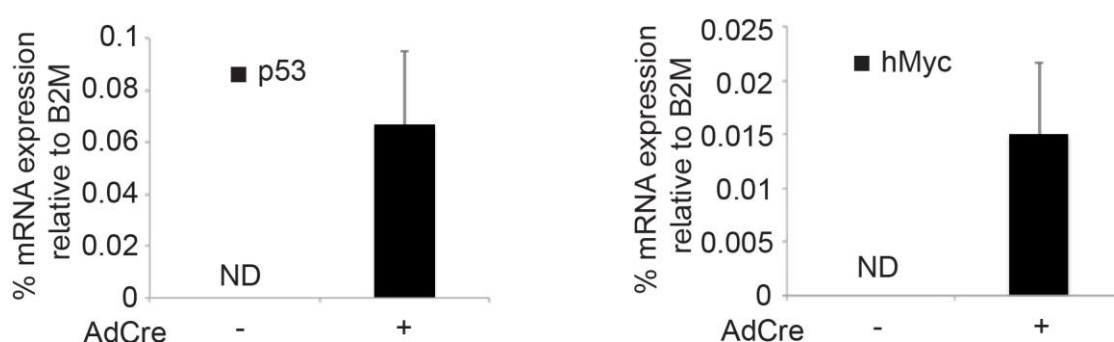


Figure 3-6 Myc and p53 transcript detection in the bronchioles.

Quantitative real Time PCR on mRNA from *R26^{DM.Isi-MYC/MYC};Tp53^{R172H/R172H}* bronchioles with (n=3) and without (n=2) AdCre infection (5×10^7 PFU). Tp53 and hMyc transcripts could only be detected in AdCre infected animals. Mean \pm SEM is shown.

The fact that there was no apoptosis detected in *R26^{DM.Isi-MYC/MYC}* lungs and that simultaneous mutant p53^{R172H} expression did not increase the proliferation rate in the bronchioles, suggests that Myc levels were not high enough to induce p53. Our data suggest that Myc is not a driver oncogene in the lung and has a lower oncogenic potential than KRas. Low levels of Myc may not be strong enough to engage p53 expression and hence presence or absence of p53 does not make any difference.

3.2.4 Low levels of deregulated MYC accelerate KRas^{G12D} driven tumourigenesis

It has been shown before that MYC-ER is able to accelerate KRas^{G12D} driven tumourigenesis (Murphy et al., 2008). In this model, MYC-ER had to be activated daily by 4-OHT administration, which might have influenced tumourigenesis.

Therefore, we decided to explore the long term effect of MYC and Ras combination in the lung without 4-OHT influence and we examined lungs from heterozygous and

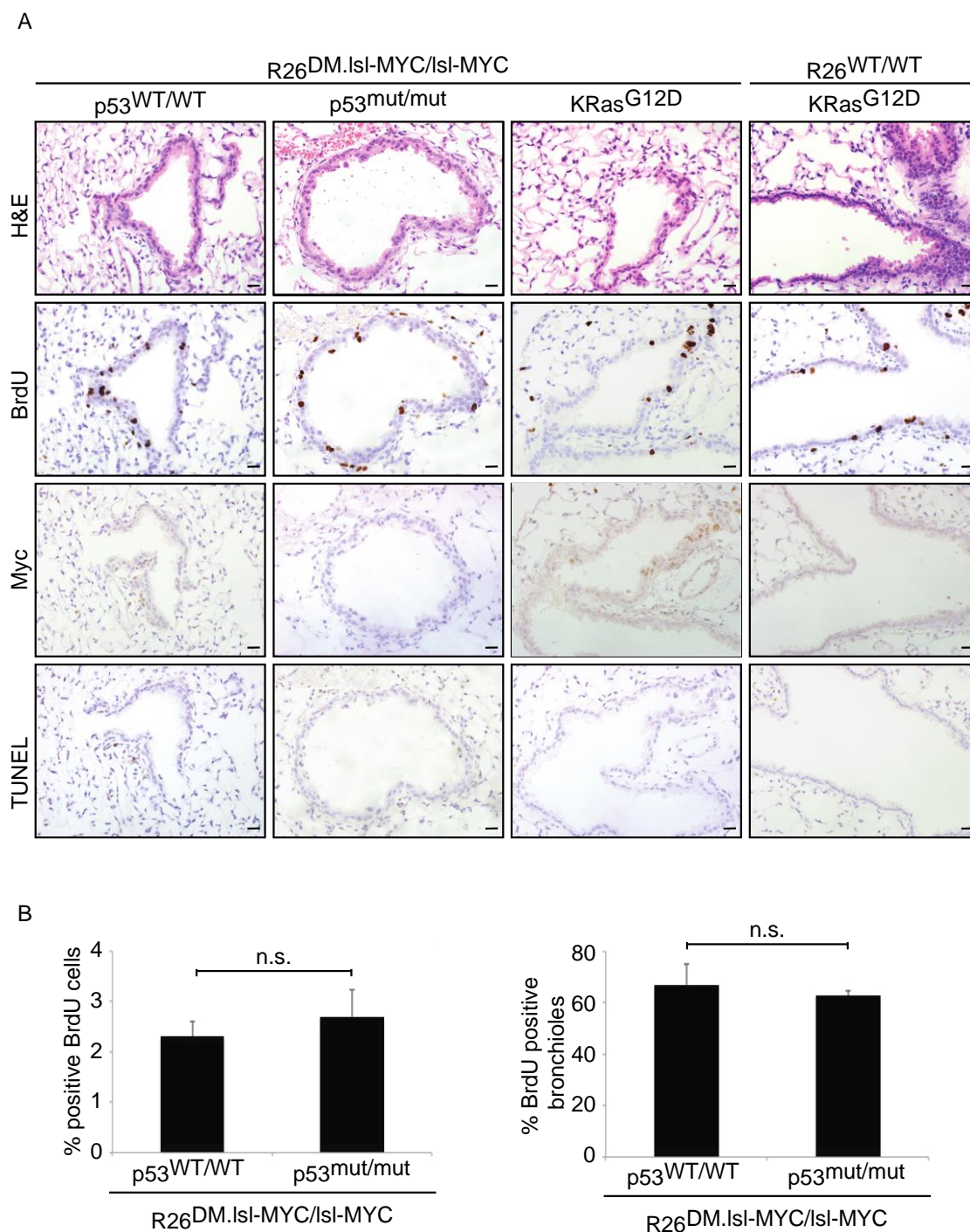


Figure 3-7 Absence of functional p53 has no influence on the outcome of acute Myc activation.

A) H&E, BrdU, Myc and TUNEL staining of R26^{DM}.Isl-MYC/MYC;p53^{WT/WT} (n=10), R26^{DM}.Isl-MYC/MYC;p53^{R172H/R172H} (n=4), R26^{DM}.Isl-MYC/MYC;KRas^{G12D} (n=4) and KRas^{G12D} (n=3) bronchioles 4 days after AdCre infection (5*10⁷ PFU). In R26^{DM}.Isl-MYC/MYC bronchioles clusters of BrdU positive cells could be detected irrespective of p53 status. Myc protein could only be detected in R26^{DM}.Isl-MYC/MYC;KRas^{G12D} bronchioles. TUNEL positive cells could be detected in neither genotype. B) Quantification of the number of bronchioles/tissue section showing ectopic proliferation and % BrdU positivity of induced bronchioles in mice of the indicated genotypes.

homozygous $R26^{DM.Isl-MYC};KRas^{G12D}$ and $R26^{RS.Isl-Myc};KRas^{G12D}$ mice 6 weeks post allele induction. Figure 3-8 A shows that $KRas^{G12D}$ on its own leads to hyperplasia and small benign tumours 6 weeks post induction, which has been shown before (Jackson et al., 2001). One copy of MYC ($R26^{DM.Isl-MYC/WT};KRas^{G12D}$ and $R26^{RS.Isl-Myc/WT};KRas^{G12D}$) can already accelerate this phenotype, which leads to bigger, and in $R26^{DM.Isl-MYC/WT};KRas$ lungs, to more tumours. This is particularly interesting, as the same Myc levels that can accelerate the $KRas^{G12D}$ phenotype do not induce proliferation in the bronchiolar epithelium (Figure 3-4). Two copies of MYC accelerate this phenotype even further, resulting in increase in tumour size compared to the heterozygous counterpart (Figure 3-8 A). The effect of both on tumour burden was quantified and can be seen in Figure 3-8 B, demonstrating that with two copies of MYC the tumour burden is about 6 times higher in $R26^{RS.Isl-Myc/Myc};KRas^{G12D}$ mice and more than 20 times higher in $R26^{DM.Isl-MYC/MYC};KRas^{G12D}$ mice than in $KRas^{G12D}$ mice.

The increased tumour burden also results in shorter survival of the mice with a median survival of about 10 weeks for $R26^{DM.Isl-MYC/WT};KRas^{G12D}$ mice and less than 8 weeks for $R26^{DM.Isl-MYC/MYC};KRas^{G12D}$ mice (Figure 3-8 C), whereas $KRas^{G12D}$ mice have been reported to live for approximately 28 weeks (Xue et al., 2011).

Interestingly, human Myc ($R26^{DM.Isl-MYC}$) accelerates the $KRas^{G12D}$ phenotype much further than murine Myc ($R26^{RS.Isl-Myc}$). From MYC transcript analysis in MEFs we know that MYC levels are comparable (Figure 3-2 B), therefore this phenotype cannot be explained by differences in transcript levels. This suggests that murine and human MYC are differently regulated on protein level or that human MYC does not interact with murine proteins in the same way as murine Myc does.

Closer examination of the lungs revealed that the vast majority of the tumours express the alveolar type II pneumocyte marker SP-C, and that bronchioles are CC10 positive (Mason et al., 2000) (Figure 3-9 and Figure 3-10). A small fraction of tumours show small regions that are CC10 positive. These tumours were morphologically indistinguishable from SP-C positive tumours (not shown). All tumours are Ki67 positive, with a tendency for more Ki67 positive cells towards the edge of the tumour, and each tumour has few terminal nucleotidyl transferase dUTP nick end labeling (TUNEL) positive cells.

In a very small fraction of tumours, a subpopulation is emerging, that shows a change in cell morphology, which again confirms the *KRas^{G12D}/Rosa-MYC-ER* phenotype (Murphy et al., 2008). In these small regions that are part of otherwise benign appearing tumours, nuclei become enlarged and pleomorphic, a feature of tumour progression. Examples of this can be seen in Figure 8 panel 2 and Figure 9 panel 2 and 10. Feldser et al. showed in a *KRas^{G12D};Tp53^{null}* model that these regions, that are different in morphology and represent a more advanced stage, stain positive for p-Erk (Feldser et al., 2010). In the *R26^{RS.Isi-Myc};KRas^{G12D}* and *R26^{DM.Isi-MYC};KRas^{G12D}* model this is the case as well. The next two chapters will focus on the study of gene expression changes that occur during the transition from the benign to the more progressed tumour regions.

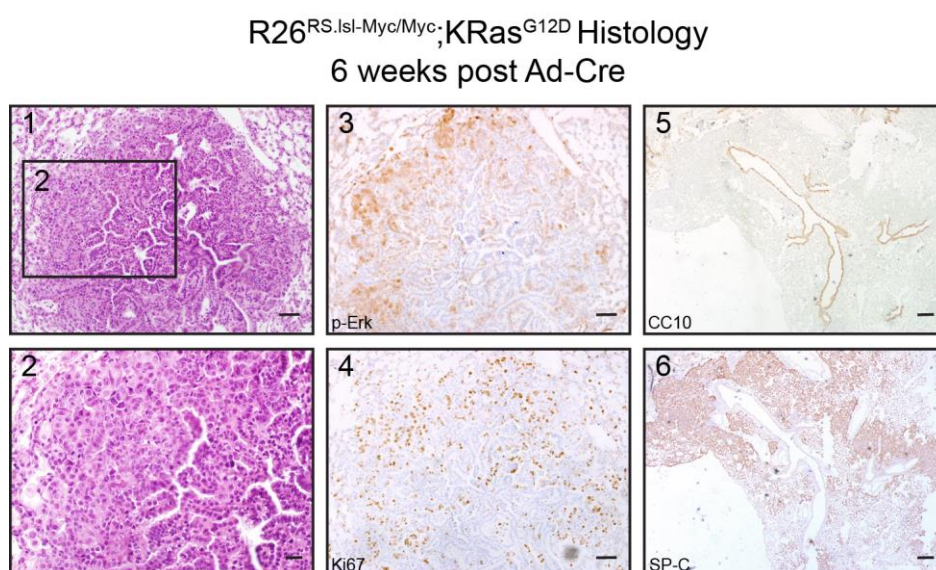


Figure 3-9 R26^{RS.Isi-Myc};KRas^{G12D} Histology.

Lung tumours from R26^{RS.Isi-Myc/Myc};KRas^{G12D} (n=4) mice 6 weeks after AdCre infection (5*10⁷ PFU). 3: p-Erk, 4: Ki67, 5: CC10, 6: SP-C. A small fraction of tumours has a p-Erk positive subpopulation. All tumours are Ki67 positive, bronchioles stain positive for Clara Cell marker CC10 and tumours stain positive for alveolar cell marker Sp-C. Scale bars: 1, 3, 4: 50µm, 2, 10: 20µm, 5, 6: 200µm.

3.3 Discussion

Deregulated Myc expression in the adult lung is alone able to drive proliferation, which is detectable shortly after Myc induction and still detectable after 6 weeks. Surprisingly, this proliferation wave does not lead to tumours, which raises the question about the fate of these cells. It has been shown before (Murphy et al., 2008), that low levels of deregulated MYC as achieved by being driven by the weak Rosa promoter do not engage apoptosis in the lung, which we could confirm in our model. I therefore hypothesise that as the threshold to engage apoptosis is not

reached, p53 is also not engaged, explaining why loss of functional p53 had no effect on the consequences of acute MYC activation and could not facilitate tumourigenesis, even in the longer term. Possibly, a different tumour suppressive mechanism that engaged at a lower threshold of Myc deregulation forces the proliferating cells to undergo cell cycle arrest.

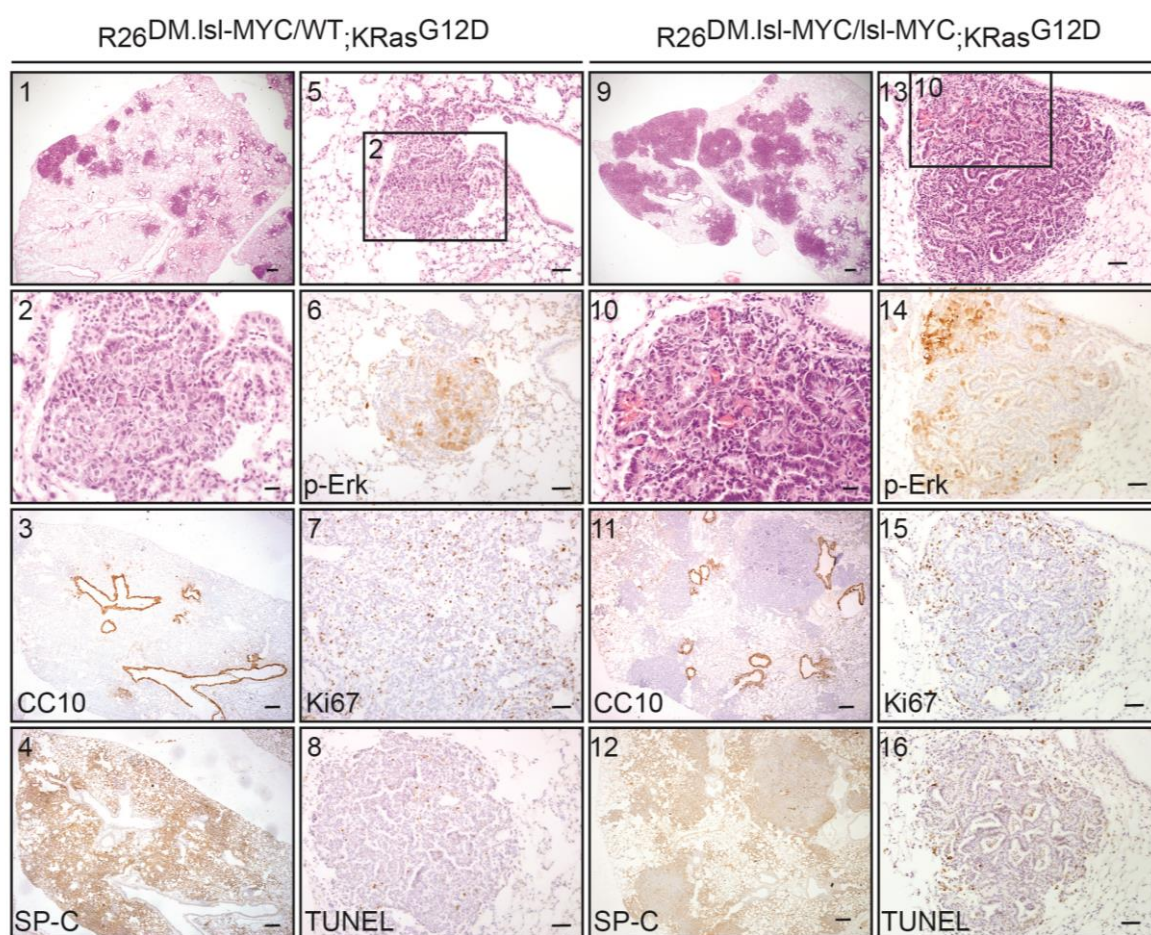


Figure 3-10 R26^{DM.Isl-MYC};KRas^{G12D} Histology.

Lungs from R26^{DM.Isl-MYC};WT;KRas^{G12D} (n=13) and R26^{DM.Isl-MYC/Isl-MYC};KRas^{G12D} (n=12) mice 6 weeks after AdCre infection (5×10^7 PFU). 6 and 14: p-Erk staining, 7 and 15: Ki67 staining, 8 and 16: TUNEL staining, 3 and 11: CC10 staining, 4 and 12: Sp-C staining. A small fraction of tumours has a p-Erk positive subpopulation. All tumours are Ki67 positive, and display a few TUNEL positive cells. Bronchioles stain positive for Clara Cell marker CC10 and tumours stain positive for alveolar cell marker Sp-C. Scale bars: 1, 9: 300 μ m, 3, 4, 11, 12: 200 μ m, 5, 6, 7, 8, 13, 14, 15, 16: 50 μ m, 2, 10: 20 μ m.

Interestingly, I showed that the same Myc levels that do not drive tumourigenesis on its own, on the other hand accelerate KRas driven tumourigenesis. In human lung tumours, Myc is amplified or mutated in 2-3% of KRas mutant lung adenocarcinomas (Cancer Genome Atlas Research, 2014; Gao et al., 2013). A reporter assay showed that MGA loss-of-function mutations increase Myc activity (Hurlin et al., 1999). MGA is a Max binding transcription factor and is able to inhibit transcriptional activation by Myc. MGA loss-of-function mutations happen to occur

in 2-3% of KRas mutant human lung adenocarcinomas and are mutually exclusive with MYC mutations (Cancer Genome Atlas Research, 2014). Moreover, the KRas independent Wnt pathway, which is known to induce Myc (Sansom et al., 2007) is found to be upregulated in KRas mutant lung cancer. Several canonical Wnt ligands are amplified in human KRas mutant lung adenocarcinoma (Gao et al., 2013). Furthermore, the importance of Wnt signalling was shown recently in a BRaf driven mouse model (Juan et al., 2014). This suggests that Myc levels limit KRas driven tumorigenesis and that tumours find multiple ways to functionally increase MYC. KRas downstream signalling, such as MAPK and PI3K pathway lead to MYC protein stabilization by Ser62 phosphorylation (Sears et al., 2000). The more abundant the Myc protein, either through amplification or increased Myc transcription, the more proteins can be stabilized by KRas signalling.

3.3.1 Future directions

I observed that human MYC is able to accelerate KRas^{G12D} driven tumorigenesis much further than murine Myc. As transcript levels are comparable, human and murine Myc proteins might be differentially regulated in the mouse. Determining MYC protein levels in MEFS would answer this question, ideally with and without KRas^{G12D}, in order to see if KRas dependent signalling has different effects on murine and mouse MYC. Furthermore, I showed by IHC that loss of p53 function does not stabilize MYC, at least not to a detectable level, whereas presence of KRas^{G12D} does. A possibility to confirm this result would be to determine MYC protein levels in *R26^{DM}.Isl-MYC;P53^{R172H}* and *R26^{DM}.Isl-MYC;KRas^{G12D}* MEFs. For a deeper understanding of Myc and KRas cooperation, it would help to do transcriptome analysis of *R26^{DM}.Isl-MYC* MEFs, with and without *KRas^{G12D}*, to see which pathways are engaged. This work is currently on-going.

4 RNA-sequencing from laser captured tissue material and identification of p-Erk associated genes

4.1 Introduction

Lung cancer is usually detected at an advanced stage. For this reason only little is known about tumour progression in the lung. Genetically engineered mouse models of cancer that allow allele induction at a specific time point are useful to study tumour progression, as they allow examination of the tumours at an early stage. The gene expression changes during tumour progression have been examined previously in a *KRas^{G12D}/Tp53^{null}* model of NSCLC (Feldser et al., 2010). In this paper, gene expression between adenomas and adenocarcinomas was compared and it was found that pathways associated with cell cycle processes were enriched in the adenocarcinoma samples. Moreover they found a Ras oncogenic signature and Myc target genes upregulated in adenocarcinomas. They also found that adenocarcinomas, but not adenomas, stain positively for phospho-Erk (p-Erk), which I used as a progression marker in the *R26^{DM.lsl-MYC/MYC/KRas^{G12D}}* model.

As shown in chapter 3, *R26^{DM.lsl-MYC/MYC/KRas^{G12D}}* tumours give rise to sporadic tumour progression to adenocarcinoma, which stains positively for p-Erk. Tumour progression is a relatively infrequent, but reliably detectable event in this model, and the progressed tumour regions are clearly distinguishable from the benign adenomas, which makes it a good model to study early tumour progression.

4.2 Results

4.2.1 p-Erk as progression marker

I showed in Chapter 3 that cells undergo a morphological change as tumours progress from adenoma to adenocarcinoma. Nuclei become enlarged and pleomorphic with prominent nucleoli. This process is accompanied by increased Erk phosphorylation, which is only detectable in adenocarcinomas. P-Erk as well as Ki67 and high levels of Myc detection tend to occur at the edge of the tumours. I therefore investigated if besides p-Erk, Ki67 or Myc positivity correlates with tumour progression. Figure 4-1 shows that irrespective of p-Erk signal, Ki67 and Myc staining increases towards the edge of the tumour. There is no difference in staining

intensity or number of Ki67 and Myc positive cells in p-Erk positive compared to p-Erk negative tumours. This suggests that this co-localization is a coincidence rather than a functional correlation. Tumours have a higher proliferation rate towards the edge of the tumour, but this alone does not result in tumour progression, as the vast majority of tumours are p-Erk negative. Therefore, p-Erk, but not Ki67 or Myc, correlates with the morphological changes associated with tumour progression.

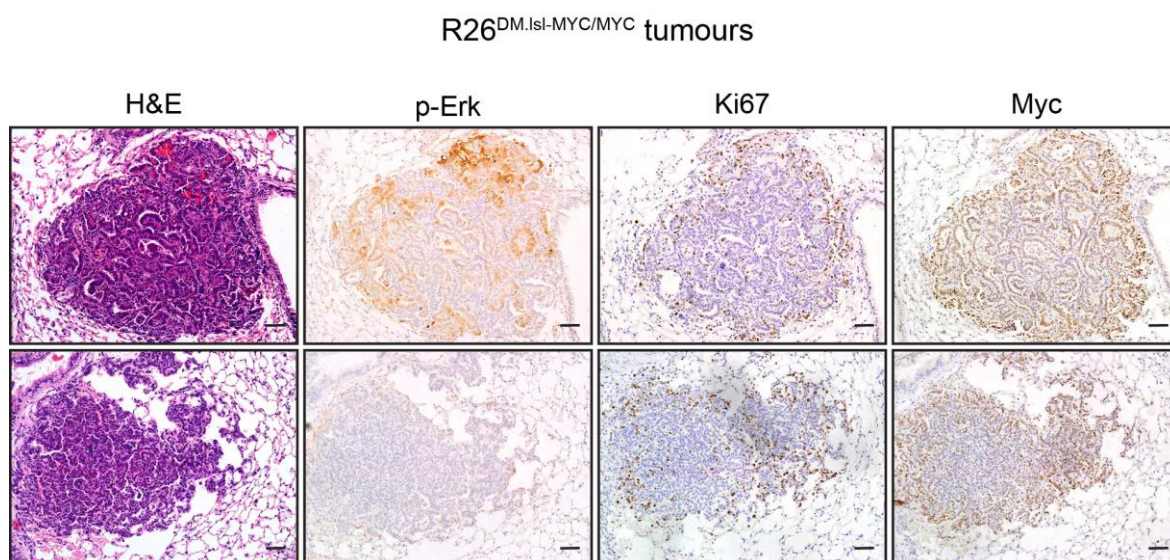


Figure 4-1 p-Erk serves as a tumour progression marker in *R26^{DM.IsI-MYC/MYC};KRas^{G12D}* lung tumours.

Adjacent H&E, p-Erk, Ki67 and Myc stainings from *R26^{DM.IsI-MYC/MYC};KRas^{G12D}* lung tumours 6 weeks after allele induction. P-Erk signal, but not Ki67 or Myc, correlates with tumour progression. Scale bar: 50 μ m.

4.2.2 Technical considerations: Fresh Frozen versus FFPE tissues

I had to decide whether to use fresh frozen or formalin fixed paraffin embedded (FFPE) material for gene expression analysis. In order to maintain RNA integrity it is advisable to freeze the samples as quickly as possible, to minimize time during which RNA degradation can occur. Formalin fixation however crosslinks RNA which can lead to RNA degradation. Therefore, for RNA analysis, freshly frozen samples are usually the better choice.

With these considerations in mind, I compared the quality of RNA recovered from frozen tissue with that recovered from FFPE tissue. RNA quality was determined using a Bioanalyzer, which determines the integrity of RNA based on the ratio between 18S ribosomal RNA (rRNA), 28 rRNA and remaining RNA. The resulting RNA integrity number (RIN) represents the ratio of 18S rRNA, 28S rRNA and the

rest, with 10 being the highest score in case of completely intact RNA. From frozen tissue I was able to recover high quality RNA, with a RIN number ~9. From FFPE tissue I was only able to achieve a RIN of ~2 (Figure 4-2).

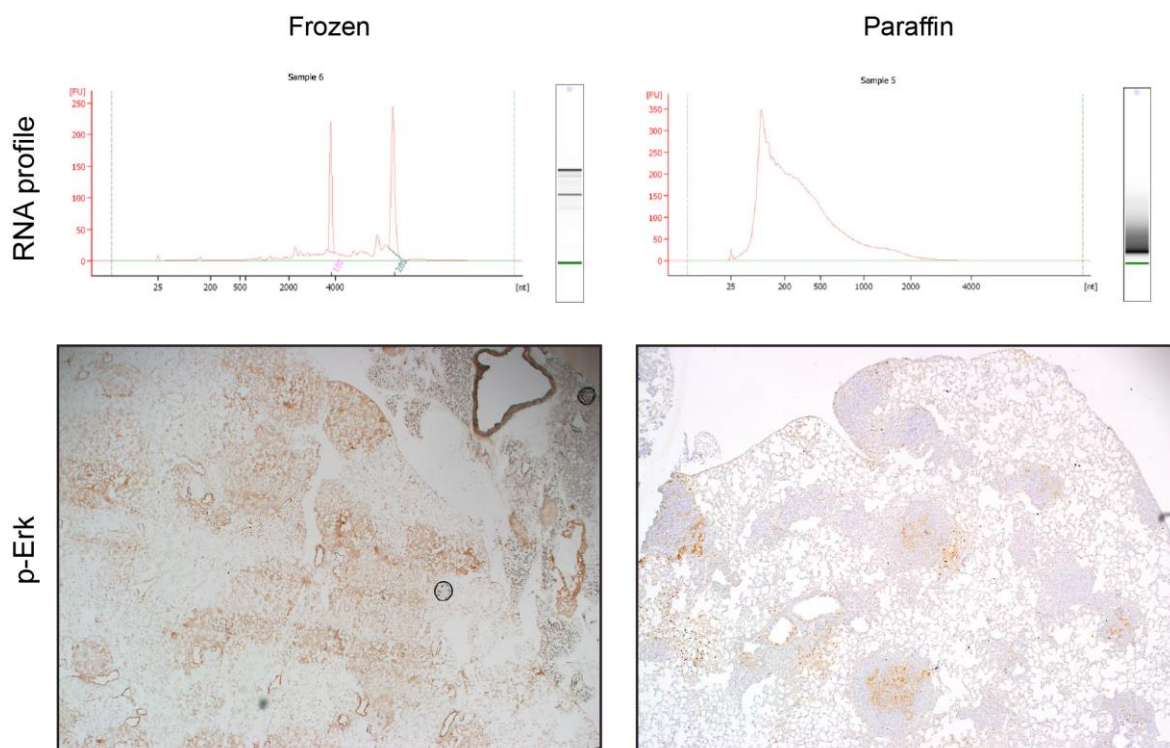


Figure 4-2 RNA quality and p-Erk IHC in frozen and FFPE tissues.

Upper part: RNA was isolated from frozen and FFPE LCM samples and analysed with agilent bioanalyzer. High quality RNA was isolated from frozen samples as 18S and 28S rRNA peaks are clearly visible. RNA isolated from FFPE samples were largely degraded. Lower part: p-Erk IHC on frozen and FFPE R26^{DM,Isi-MYC/MYC;KRas^{G12D}} lungs 6 weeks after allele induction. The staining is very clean on FFPE sections, on frozen sections it gives a lot of background signal.

FFPE material on the other hand has the advantage that the histology is very well preserved, making it easy to study morphological changes in a sample. In frozen tissues, cell morphology is much less well preserved and I was morphologically not able to reliably distinguish between adenocarcinoma and adenoma regions. As the success of the project relied on the ability to reliably distinguish between adenoma and adenocarcinoma regions, FFPE samples seemed to be more suitable in this regard. However, after having identified p-Erk as a suitable progression marker, distinguishing adenoma and adenocarcinoma regions in frozen tissue samples seemed feasible.

Unfortunately, p-Erk staining on frozen material is not as clean and clear as it is on FFPE material (Figure 4-2). There are tumour regions that stain more strongly for p-Erk than other regions, but there is a high background signal on the entire tissue. By staining several adjacent sections with p-Erk I was however able to follow the

signal through the sections and was confident that I was able to distinguish between p-Erk-positive and –negative tumour regions. Therefore, I chose to isolate RNA from frozen material.

Laser capture microscopy based on p-Erk signal

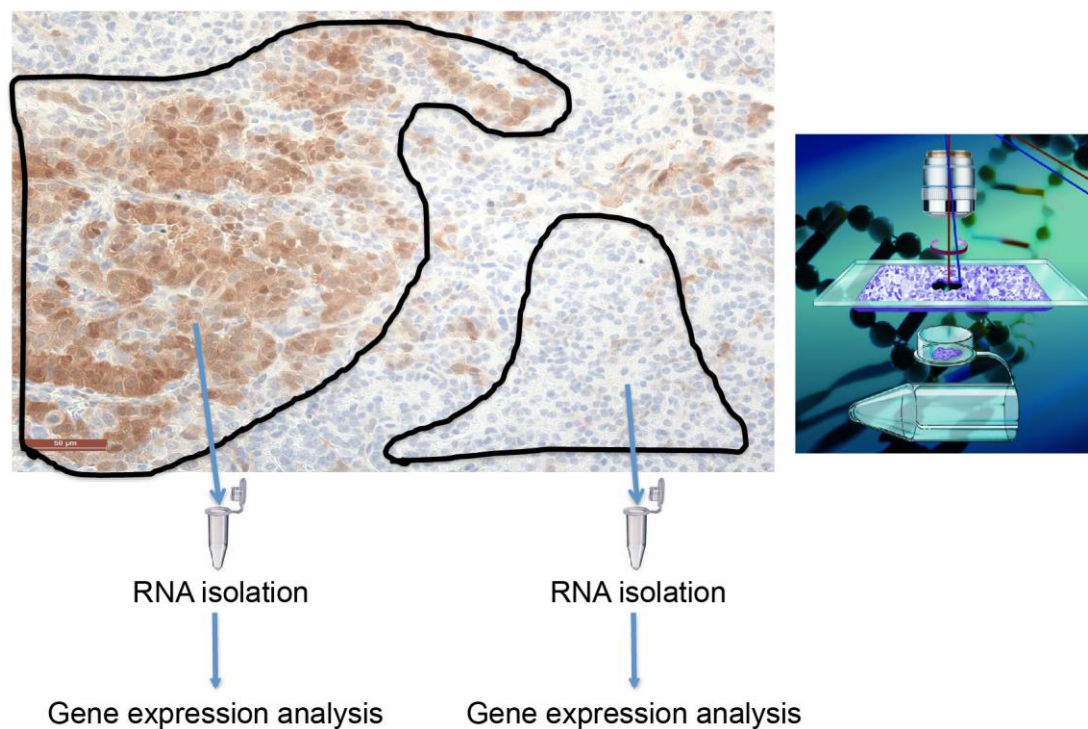


Figure 4-3 LCM of p-Erk negative and p-Erk positive tumour regions.

Schematic of the process of Laser Capture Microscopy to capture p-Erk negative and positive samples for gene expression analysis. Note, that LCM was done on adjacent, CV stained sections.

4.2.3 Amplification does not introduce bias

In order to isolate RNA from different tumour regions, tissues were cut into 10 μ M sections and stained and regions of interest were then captured with a Laser Capture Microscope (LCM) (Figure 4-3). The amount of tissue that can be recovered during this procedure is very small, resulting in only few nanograms of total RNA. As the protocol for library preparation requires larger amounts of complementary DNA (cDNA), RNA had to be amplified during the process of reverse transcription to cDNA (see materials and methods section 2.12.2). This step results in a strong amplification, yielding in several micrograms of cDNA. To test whether the amplification step introduces a bias, a test experiment using cell culture cells was carried out. It is possible that during the amplification process some transcripts would be more strongly amplified than others and the number of reads for each

gene would not represent the real abundance of the individual transcripts in the sample.

To address this issue, a *KRas^{G12D};Tp53^{null}* murine lung cancer cell line was transfected with MYC-ER construct and treated for 6 hours with 4-OHT or vehicle control. RNA was isolated and libraries were either prepared using either a) the standard protocol or b) small amounts of RNA were amplified using the amplification protocol needed for Laser Capture samples (Figure 4-4).

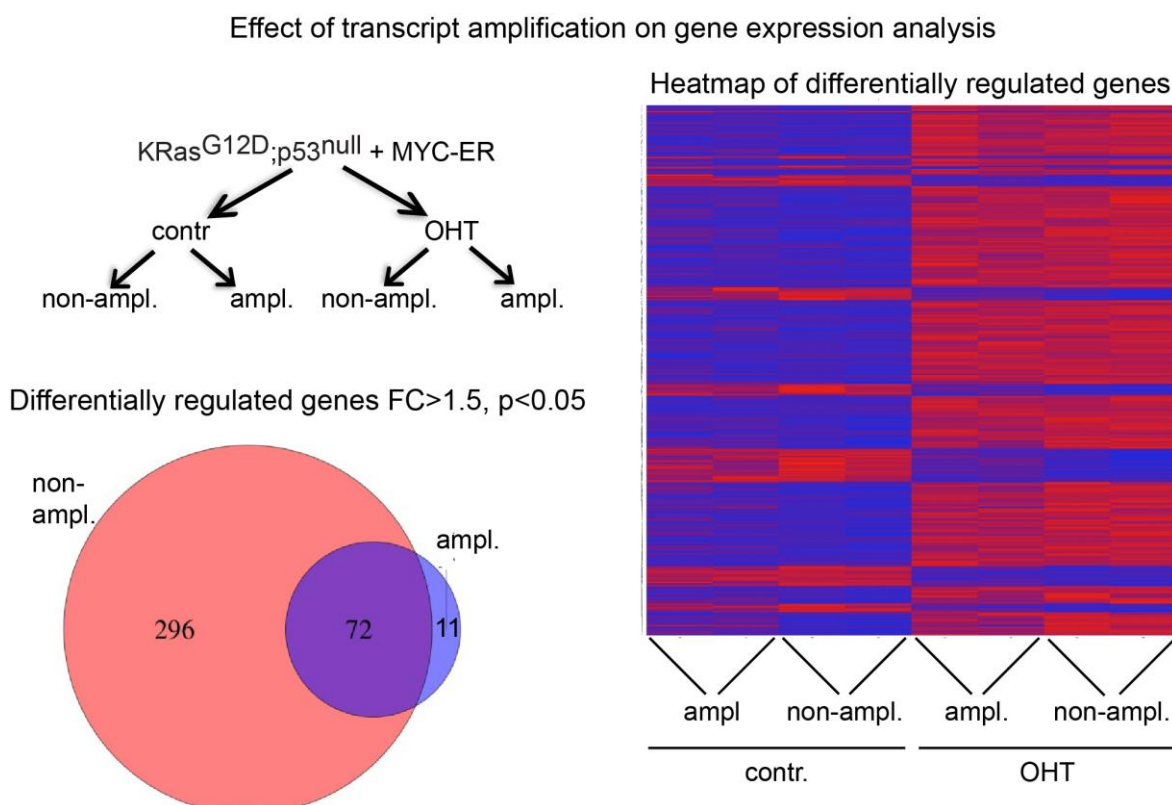


Figure 4-4 The effect of transcript amplification on gene expression analysis.

KRas^{G12D};p53^{null} cells were transfected with MYC-ER and treated with OHT or EtOH. 2 sample sets were prepared using standard library preparation or amplification protocol. N=2. The VENN diagram shows that there is a high overlap in the differentially regulated genes determined with both protocols, showing that the amplification protocol generates reliable data. The heatmap shows that the gene expression data generated with the standard and the amplification protocol are very similar.

Gene set enrichment analysis (GSEA) revealed that in both sample sets, Myc activation by 4-OHT led to upregulation of pathways involved in RNA processing, ribosome biogenesis, rRNA metabolic processes and regulation of apoptosis. With the standard protocol, 368 differentially regulated genes with a fold change (FC)>1.5, p<0.05 could be identified, whereas with the amplification protocol only 83 differentially regulated genes were identified. 72 of the 83 genes overlapped with the genes from the standard protocol. The 11 genes that did not overlap with the

standard protocol, went however in the same direction, but did not reach statistical significance in the standard protocol. The heatmap shows as well that the gene expression changes in the samples that were prepared with the amplification or standard protocol are very similar. This means that the data obtained from the amplification protocol are highly reliable. There are less statistically significantly regulated genes in the data from the amplification protocol, however, those that are significantly regulated were also found to be regulated using the standard protocol.

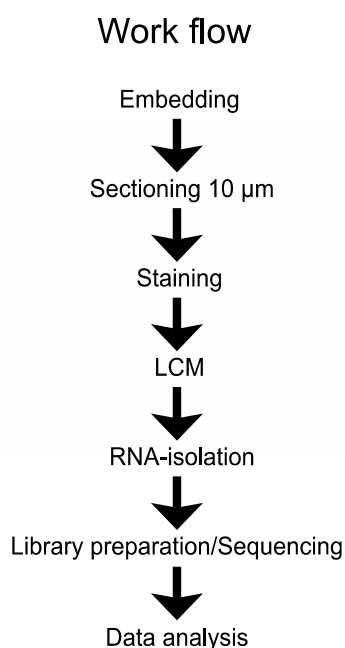


Figure 4-5 Workflow from tissue embedding to data analysis. Individual steps from tissue embedding to data analysis are shown.

4.2.4 RNA-Sequencing from frozen material

The workflow for gene expression analysis starts with freezing the tissue, followed by sectioning, staining, laser capturing the regions of interest, isolating RNA, preparing libraries for sequencing and data analysis (Figure 4-5). All steps before RNA isolation had to be performed as fast and cold as possible to avoid RNA degradation. For this reason, the sections that were used for laser capture were stained with Cresyl Violet (CV), following a protocol that was completed within a few minutes. Adjacent sections were stained for p-Erk and coverslipped. Regions were captured based on the p-Erk staining in the adjacent sections, assuming that the p-Erk distribution is almost the same from one section to the next. After RNA isolation, libraries were prepared using the amplification protocol. Initially, a sample set consisting of 6 samples from 3 mice (1 p-Erk negative and a p-Erk positive sample

Most significantly regulated genes between p-Erk negative and positive tumour regions - frozen tissues

Symbol	FC	FDR
Hc	1.21	3.36E-93
Lars2	2.25	1.33E-33
Scgb1a1	-2.77	2.63E-10
Sftpa1	1.46	7.18E-05
Fmo2	2.12	9.64E-04
Gpr141	-3.49	1.24E-03
4930461G14Rik	-12.10	5.31E-03
Cd74	1.22	8.04E-03
Melk	-2.30	9.12E-03
Cd300lg	2.92	1.38E-02
Cxcl13	-7.50	2.09E-02
Malat1	1.40	2.09E-02
Lgals4	2.52	2.35E-02
Ckap2	-2.52	5.69E-02
Dpep3	3.78	5.80E-02
Tmem221	2.79	5.80E-02
Slc17a2	2.51	5.81E-02
Tcirg1	1.83	5.81E-02
Appl2	1.75	5.81E-02
Sv2a	2.54	5.81E-02
Pdia2	4.17	5.81E-02
Sulf1	2.10	5.96E-02
Dock4	1.68	5.96E-02
Wisp3	-9.88	7.68E-02
COX1	1.33	8.92E-02
Uba7	1.79	9.05E-02
Rapsn	3.45	9.14E-02
9130213A22Rik	4.60	9.32E-02

MetaCore pathway analysis FC>1.5, p<0.5

Enrichment analysis report							
Enrichment by Pathway Maps					7 frozen samples		
#	Maps	Total	pValue	Min FDR	p-value	FDR	In Data
1	Development Adiponectin signaling	45	9.790E-06	2.036E-03	9.790E-06	2.036E-03	4
2	Cell adhesion Chemokines and adhesion	100	2.293E-04	2.385E-02	2.293E-04	2.385E-02	4
3	Protein folding Membrane trafficking and signal transduction	19	1.507E-03	1.045E-01	1.507E-03	1.045E-01	2
4	HIV-1 signaling via CCR5 in macrophages and T lymphocytes	39	6.287E-03	1.692E-01	6.287E-03	1.692E-01	2
5	Development ACM2 and ACM4 activation of ERK	43	7.604E-03	1.692E-01	7.604E-03	1.692E-01	2
6	Immune response Substance P-stimulated expression of p	43	7.604E-03	1.692E-01	7.604E-03	1.692E-01	2
7	Role of platelets in the initiation of in-stent restenosis	43	7.604E-03	1.692E-01	7.604E-03	1.692E-01	2
8	Development G-Proteins mediated regulation MAPK-ERK	46	8.666E-03	1.692E-01	8.666E-03	1.692E-01	2
9	Immune response C3a signaling	48	9.409E-03	1.692E-01	9.409E-03	1.692E-01	2
10	PDE4 regulation of cyto/chemokine expression in arthritis	49	9.791E-03	1.692E-01	9.791E-03	1.692E-01	2

Figure 4-6 Comparative gene expression analysis between p-Erk negative and positive tumour regions from R26^{DM,ISI-MYC/MYC};KRas^{G12D} mice in frozen samples.

7 p-Erk negative and 7 p-Erk positive samples from 7 mice were prepared for RNA-seq following the amplification protocol. FC for p-Erk positive/p-Erk negative was calculated individually for samples from each mouse and statistical analysis was done with data from all 14 samples. The upper part shows the most significantly regulated genes. The lower part shows MetaCore pathway analysis that was done for genes upregulated in p-Erk positive samples, with FC>1.5 and p<0.5.

per mouse) was prepared and sequenced. As the statistics were not good, another sample set consisting of an additional 8 samples from 4 mice had to be prepared.

When designing an experiment it is important to do power analysis in order to determine the sample size that is needed to obtain a certain statistically significant effect. If the chosen sample size is too small the experiment is wasted and has to be repeated in the worst case scenario. This leads to a waste of time and money and when working with animals to unnecessary suffering. If the sample size is higher than actually needed, resources will be wasted as well.

The first thing that has to be done is to determine the effect size that is expected. The smaller the effect size, the higher the required sample size in order to achieve statistical significance. When working with biological samples the variation among the replicates has also to be considered. The dispersion among biological replicates is much higher than among technical replicates and requires a bigger sample size. Within biological samples paired and unpaired sample analysis is possible. Paired sample analysis describes two different states within one biological specimen. In the present experiment, p-Erk-negative and -positive samples from the same mouse were compared, it falls therefore in the category of a paired experiment. Paired experiments require a smaller sample size than unpaired experiments because the expected dispersion is smaller (Ching et al., 2014).

In the case of a paired RNA-seq experiment, the effect size corresponds to the log fold change (LFC) between the two sample groups and the p-value, the statistical significance of the LFC. In gene expression analysis, a LFC ≥ 1.5 and a p-value ≤ 0.05 are usually set as a threshold. In RNA-seq experiments it is also important to consider how the samples will be prepared and what kind of transcripts will be present in the sample. If a polyA enrichment method is used, the sample will contain mainly mRNA transcripts. If a ribosomal RNA depletion method is used, lincRNA will be present as well. lincRNAs are expressed at a lower level than mRNAs. Also, the number of different transcripts is higher when lincRNAs are present, which has influence on the statistics (Ching et al., 2014). Therefore, a higher sample size is needed to achieve significant statistical power. In the present experiment an mRNA enrichment method was used.

In the present experiment, because nobody has worked with this mouse model or has done this kind of experiment before, the LFC of differentially expressed genes was very difficult to estimate. A sample number of 3 is however the bare minimum in an experiment with biological samples and given the high degree of uncertainty in this kind of experiment a higher sample number of 4 or 5 sample pairs should have been chosen and the requirement to repeat the experiment would have been avoided.

Including the new sample set, the fold changes from each p-Erk negative to p-Erk positive sample from the same mouse was calculated individually and samples from all 7 mice were included in the statistical analysis. Data analysis performed by Ann Hedley revealed that only 11 genes were significantly regulated between p-Erk-negative and -positive regions, with a $FC > 2$ and $p < 0.05$. By choosing a less stringent p-value of $p < 0.1$, the list could be extended to 27 regulated genes (Figure 4-6). For pathway enrichment analysis, I set the $FC > 1.5$ and relaxed the p-value further to $p < 0.5$, in order to have a reasonable number of genes. 3 pathways that are associated with increased Erk signalling were among the top 10 upregulated pathways: development ACM activation of Erk, expression of proinflammatory cytokines via MAPKs and G protein mediated regulation MAPK ERK signalling. Interestingly, a cell adhesion pathway was also enriched.

The fact that only a small number of genes were differently regulated between the two sample sets suggest that the distinction of the p-Erk positive regions from the p-Erk negative regions was not as clear as desired. P-Erk staining on frozen tissues does not seem to be reliable and as multiple regions had to be pooled for each sample, it is possible that some regions that went into the respective sample were of the wrong type, diluting the distinction of the regions that were categorized correctly and thereby reducing the significance.

I confirmed some of the most upregulated genes from the p-Erk negative to p-Erk positive transition by Real Time analysis, using the same cDNA that was used for library preparation (Figure 4-7). All tested genes went in the same direction as the sequencing data: leucyl-tRNA synthetase (*Lars2*, $FC=2.25$), sprouty homolog 2 (*Spry2*, $FC=1.8$), histidine decarboxylase (*Hdc*, $FC=2.0$), surfactant associated protein A1 (*Sftpa1*, $FC=1.46$), metastasis associated lung adenocarcinoma transcript 1 (*Malat1*, $FC=1.4$), carbonyl reductase 2 (*Cbr2*, $FC=1.56$), aldehyde

oxidase 3 (*Aox3*, FC=1.89), insulin-like growth factor binding protein 3 (*Igfbp3*, FC=1.85), regulator of cell cycle (*Rgcc*, FC=1.62), flavin containing monooxygenase 2 (*Fmo2*, FC=2.12), regulator of G-protein signalling 5 (*Rgs5*, FC=1.36) and retinol binding protein 7 (*Rbp7*, FC=1.92). This confirms that the gene expression changes detected by RNA-sequencing are reproducible.

In the meantime, technology had advanced and new kits were on the market that allowed sample preparation for RNA-Seq even from heavily degraded RNA (see Materials and Methods section 2.12.3). We therefore decided to prepare a separate sample set from FFPE material.

Sequencing data validation by quantitative Real Time PCR

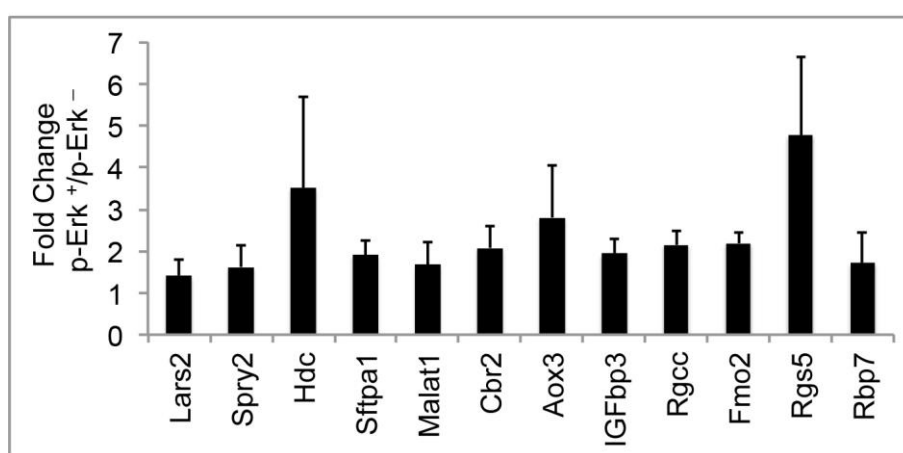


Figure 4-7 Real Time PCR validation from frozen samples.

12 genes that were found upregulated in the p-Erk positive samples were validated by Real Time PCR. For all genes expression went in the same direction as in the sequencing data. N=7

4.2.5 RNA-Seq from FFPE material

The workflow for FFPE samples is similar to the one for frozen samples (figure 5). Initially, the tissue gets fixed in Zn-Formalin over-night, dehydrated and embedded in paraffin. The paraffin embedded tissue can be stored for a long time until needed. Then sections are made and stained for p-Erk, which serve as a template for adjacent CV stained sections. RNA was isolated and libraries were prepared following a protocol that is optimized for degraded RNA samples (see and Methods section 2.12.3). 8 libraries from 4 mice (1 p-Erk positive sample and 1 p-Erk negative sample per mouse) were sequenced and data were analysed in collaboration with Ann Hedley.

More than 500 genes were differentially regulated with a fold change >2 and $p < 0.05$. Enrichment analysis showed that Cytoskeleton remodelling, Wnt and transforming growth factor (TGF) signalling were among the most significantly upregulated pathways from p-Erk negative to p-Erk positive samples (Figure 4-8)

p-Erk associated pathway analysis - FFPE tissues $FC > 1.5$, $p < 0.05$

Enrichment analysis report							
Enrichment by Pathway Maps							p-Erk neg to pos
#	Maps	Total	pValue	Min FDR	p-value	FDR	In Data
1	CFTR folding and maturation (normal and CF)	24	6.677E-09	5.442E-06	6.677E-09	5.442E-06	11
2	Cytoskeleton remodeling_TGF_WNT and cytoskeletal remo	111	2.632E-08	7.379E-06	2.632E-08	7.379E-06	22
3	Cytoskeleton remodeling_Cytoskeleton remodeling	102	2.716E-08	7.379E-06	2.716E-08	7.379E-06	21
4	Development_Thromboxane A2 signaling pathway	49	7.675E-08	1.564E-05	7.675E-08	1.564E-05	14
5	Development_TGF-beta receptor signaling	50	1.017E-07	1.658E-05	1.017E-07	1.658E-05	14
6	Immune response_HMGB1/RAGE signaling pathway	53	2.267E-07	3.080E-05	2.267E-07	3.080E-05	14
7	Regulation of CFTR activity (normal and CF)	62	2.947E-07	3.431E-05	2.947E-07	3.431E-05	15
8	Development_EGFR signaling pathway	71	3.395E-07	3.459E-05	3.395E-07	3.459E-05	16
9	Development_Non-genomic action of Retinoic acid in cell d	56	4.760E-07	4.310E-05	4.760E-07	4.310E-05	14
10	Transcription_CREB pathway	49	5.827E-07	4.749E-05	5.827E-07	4.749E-05	13

Wnt pathway genes that are upregulated from p-Erk neg to p-Erk pos			ErbB family ligands that are upregulated from p-Erk neg to p-Erk pos		
Symbol	FC	FDR	Symbol	FC	FDR
Sox9	15.79	7.48E-04	Ereg	24.82	2.78E-13
Porcn	3.59	4.85E-03	Areg	4.25	4.98E-11
Wnt7a	3.08	2.71E-01	Tgfa	2.69	4.80E-03
Tcf7l1	2.38	5.44E-04	Hbegf	2.31	1.99E-02
Fzd7	1.92	2.48E-03			
Fzd4	1.92	2.33E-01			

Figure 4-8 Comparative gene expression analysis between p-Erk negative and positive tumour regions from R26DM.lsl-MYC/MYC;KRasG12D mice in FFPE samples.

4 pErk negative and 4 p-Erk positive samples from 4 mice were prepared for RNA-seq following the protocol for degraded RNA samples. FC for p-Erk positive/p-Erk negative was calculated individually for samples from each mouse and statistical analysis was done with data from all 8 samples. Pathway analysis was done for genes upregulated in p-Erk positive samples with $FC > 1.5$ and $p < 0.05$

Moreover, pathways associated with cystic fibrosis transmembrane conductance regulator (CFTR) activity, folding and maturation, cAMP response element-binding protein (CREB) pathway and immune response pathways were found upregulated. ErbB family ligands, as part of the epidermal growth factor receptor (EGFR) signalling pathway had high fold changes: Epiregulin (*Ereg*), which is upregulated by more than 20 fold, Amphiregulin (*Areg*), heparin-binding EGF-like growth factor (*HB-EGF*) and *TGF- α* , all showed significantly increased expression in the p-Erk

positive dataset. Also the Wnt pathway is highly upregulated in the p-Erk positive dataset. *Porcupine*, which is important for posttranslational modification and secretion of Wnt proteins, is significantly enriched more than 3-fold and SRY-box containing protein 9 (*Sox9*), which is a Wnt pathway target is more than 15-fold enriched. Also, several Wnt protein members, and Frizzled (*Fzd*) proteins, which are G protein coupled receptors that bind Wnt ligands are enriched (not all of them are significantly upregulated). As a first validation that the Wnt pathway is indeed associated with tumour progression, adjacent p-Erk stained sections were stained for Sox9 (Figure 4-9). There was a very good overlap between p-Erk positive and Sox9 positive regions.

I could not find a significant number of overlapping genes between the frozen and the FFPE dataset. The fact that the FFPE sample set generated much more significantly regulated genes than the frozen sample set suggests that the distinction between p-Erk-positive and negative regions was inadequate in the frozen samples.

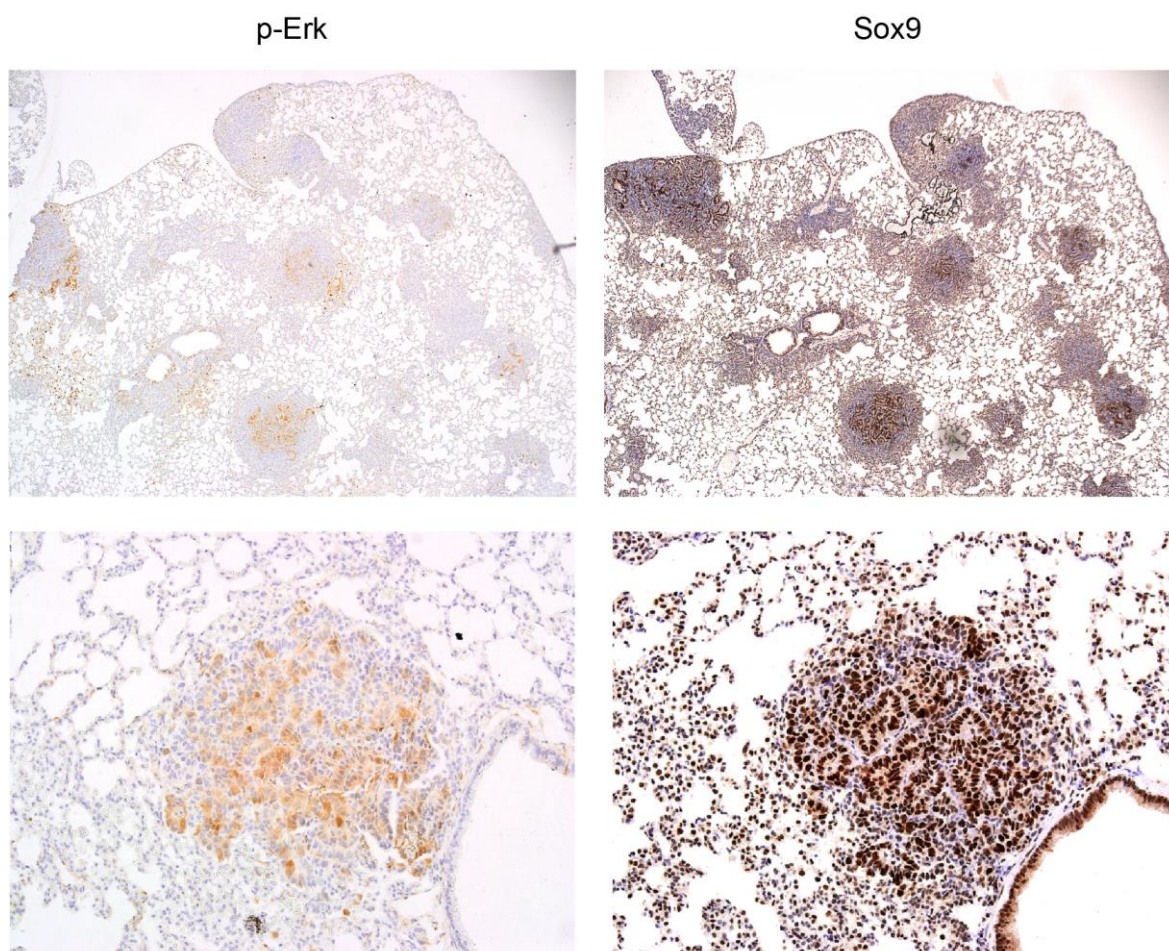


Figure 4-9 Sox9 correlates with p-Erk expression in lung tumours from R26^{DM}.Isl-MYC/MYC ;KRas^{G12D} mice.

Adjacent sections were stained with Sox9 and p-Erk, showing a high overlap between p-Erk and Sox9 signal.

Real time validation was not possible with cDNA generated from FFPE samples, as CT values from the Beta 2 microtubulin (*B2m*) house keeping gene, that usually has CT values ~18, were ~10 cycles higher and most genes that are expressed at a lower level were not even detectable. The next chapter will focus on the validation of the importance of Wnt and EGFR signalling for tumour progression and also on the validation of individual genes.

4.2.6 Comparison of Gene expression between tumours from *KRas*^{G12D} and *R26*^{DM.Isi-MYC/MYC};*KRas*^{G12D} mice

I showed in chapter 3 that low levels of *Myc*, driven by the Rosa26 promoter accelerate *KRas*^{G12D} driven tumourigenesis. *Myc* did not only increase tumour burden by leading to more and bigger tumours, but also accelerated tumour progression. Jackson et al. showed, that *KRas*^{G12D} mice display hyperplasia and small adenomas 6 weeks after allele induction, whereas I found progression to adenocarcinoma in *R26*^{DM.Isi-MYC/MYC};*KRas*^{G12D} mice at the same time point (Jackson et al., 2001). I therefore wanted to compare gene expression from *KRas*^{G12D} and *R26*^{DM.Isi-MYC/MYC} tumours to find out the role of *MYC* overexpression in *KRas*^{G12D} driven tumourigenesis.

As lesions from *KRas*^{G12D} mice are were very small 6 weeks after allele induction it would have been very difficult to capture enough material. I therefore decided to use tumour material from *KRas*^{G12D} lungs 9 weeks after induction, as tumours had a decent size.

I prepared frozen samples from 5 *KRas*^{G12D} mice and prepared libraries along with 6 previously sequenced frozen samples from 3 *R26*^{DM.Isi-MYC/MYC};*KRas*^{G12D} mice. I compared *KRas*^{G12D} gene expression with the p-Erk negative and p-Erk positive gene expression profiles from *R26*^{DM.Isi-MYC/MYC};*KRas*^{G12D} mice. 287 genes were upregulated in *KRas*^{G12D} samples compared to p-Erk negative *R26*^{DM.Isi-MYC/MYC};*KRas*^{G12D} samples, and 180 genes were downregulated (FC >2, p<0.05). 214 genes were found upregulated in *KRas*^{G12D} samples compared to p-Erk positive *R26*^{DM.Isi-MYC/MYC};*KRas*^{G12D} samples and 210 genes were downregulated.

Interestingly, many genes that were significantly upregulated during the transition from p-Erk negative to positive in the *R26*^{DM.Isi-MYC/MYC};*KRas*^{G12D} FFPE samples were also upregulated in the *KRas*^{G12D} samples, compared to either p-Erk negative

(46 genes) or p-Erk positive (22 genes) $R26^{DM.Isi-MYC/MYC};KRas^{G12D}$ samples (FC>2, p<0.05). Most genes that were not significantly regulated between $R26^{DM.Isi-MYC/MYC};KRas^{G12D}$ and $KRas^{G12D}$ samples, still went in the same direction as genes from p-Erk negative to p-Erk positive $R26^{DM.Isi-MYC/MYC};KRas^{G12D}$ samples (Figure 4-10).

Gene expression analysis between $R26^{DM.Isi-MYC/MYC};KRas^{G12D}$ and $KRas^{G12D}$ lung tumours

Symbol	FC p-Erk neg to pos	FDR p-Erk neg to pos	FC p-Erk neg to Kras	FDR p-Erk neg to Kras	FC p-Erk pos to Kras	FDR p-Erk pos to Kras
St8sia6	29.98	9.42E-20	12.94	3.50E-15	4.01	3.97E-05
Ereg	24.82	2.78E-13	5.64	4.94E-04	2.13	4.37E-01
Scgb1a1	23.27	1.23E-02	3.34	2.83E-02	22.53	5.86E-13
Gkn2	18.47	2.75E-03	90.04	7.16E-07	-5.01	6.44E-04
Sox9	15.79	7.48E-04	12.24	2.88E-03	2.84	6.16E-01
E330017A01Rik	14.16	1.45E-02	19.06	7.06E-01	5.72	8.98E-01
Dlk1	10.46	2.33E-26	6.09	1.54E-05	2.09	4.49E-01
B4galt6	9.46	1.24E-03	4.43	2.35E-02	1.74	9.24E-01
Basp1	9.03	1.31E-04	1.89	1.00E+00	1.78	9.39E-01
Scgb3a2	8.45	2.76E-02	-1.03	1.00E+00	12.84	1.11E-11
Clu	8.13	1.00E-11	1.56	6.86E-01	1.36	9.20E-01
Itih2	7.58	5.59E-07	16.17	2.06E-04	2.18	8.20E-01
Zfp618	7.37	8.49E-04	5.39	2.44E-02	1.59	1.00E+00
Scara3	7.11	1.03E-03	1.54	1.00E+00	1.56	1.00E+00
Apln	6.79	2.75E-03	4.92	4.65E-04	3.12	4.42E-02
Itga2	6.79	2.47E-11	1.51	1.00E+00	-1.47	9.39E-01
Parm1	6.54	1.71E-04	4.35	1.19E-03	1.25	1.00E+00
Ptpn	6.50	1.66E-03	2.52	9.19E-01	-2.30	8.22E-01
Hecw1	6.49	2.25E-04	-1.02	1.00E+00	-1.72	9.33E-01
Tdo2	6.48	1.08E-02	1.19	1.00E+00	5.27	8.80E-01
Nudt14	6.34	2.50E-02	-1.12	1.00E+00	-1.09	1.00E+00
Samd5	6.22	8.29E-04	2.48	9.24E-01	2.08	9.53E-01
Krt79	6.16	1.11E-04	-2.98	2.65E-01	-3.19	1.32E-01
Cldn4	6.11	1.16E-02	-2.09	8.52E-01	-3.06	2.26E-01
Cd24a	5.94	1.40E-15	3.52	4.88E-05	2.42	9.72E-03
Slc38a1	5.68	1.17E-11	1.71	8.22E-01	1.75	6.87E-01
Procr	5.62	1.35E-04	2.50	5.25E-02	1.46	8.84E-01
Iqgap2	5.30	3.59E-04	2.55	2.56E-01	1.95	6.88E-01
Slc35f1	5.05	6.50E-03	13.11	2.36E-03	3.13	4.45E-01

Figure 4-10 Comparative gene expression analysis between $R26^{DM.Isi-MYC/MYC};KRas^{G12D}$ and $KRas^{G12D}$ lung tumours.

5 $KRas^{G12D}$ samples (9 weeks after allele induction) and 6 previously sequenced $R26^{DM.Isi-MYC/MYC};KRas^{G12D}$ samples (3 p-Erk negative, 3 p-Erk positive samples, 6 weeks after allele induction) were prepared for RNA-seq. Shown are upregulated genes from the FFPE sample set (figure 8) and corresponding genes expression changes from p-Erk negative and positive $R26^{DM.Isi-MYC/MYC};KRas^{G12D}$ samples to $KRas^{G12D}$ samples. A high proportion of genes that was upregulated in p-Erk positive $R26^{DM.Isi-MYC/MYC};KRas^{G12D}$ tumour regions was also upregulated in $KRas^{G12D}$ tumours (compared to $R26^{DM.Isi-MYC/MYC};KRas^{G12D}$ tumours).

This is surprising, as I expected $KRas^{G12D}$ tumours to be more benign than $R26^{DM.Isi-MYC/MYC};KRas^{G12D}$ tumours. Instead, many genes associated with tumour progression were found to be higher expressed in $KRas^{G12D}$ samples than in $R26^{DM.Isi-MYC/MYC};KRas^{G12D}$ samples. This suggests that even though Myc accelerates tumour progression, $KRas^{G12D}$ tumours 9 weeks after allele induction

might be more advanced than *R26^{DM.lsl-MYC/MYC};KRas^{G12D}* tumours 6 weeks after allele induction.

By histological examination of 2 paraffin embedded *KRas^{G12D}* lungs 9 weeks post induction, I could identify aggressive looking tumour regions with enlarged, pleomorphic nuclei. This should be confirmed by more extensive histological examination, for instance by staining frozen *KRas^{G12D}* lungs with Sox9, which expression was 12 fold higher in the *KRas^{G12D}* samples than in p-Erk negative *R26^{DM.lsl-MYC/MYC};KRas^{G12D}* samples.

4.3 Discussion

The aim of this chapter was to identify lung tumour progression genes in the *R26^{DM.lsl-MYC/MYC};KRas^{G12D}* model. This undertaking was associated with solving several technical problems but also led to new insights.

In the control experiment with *KRas^{G12D};Tp53^{null} Myc-ER* transfected cell lines, gene expression was analysed and compared using two different protocols. This experiment revealed that gene expression analysis even from very limited material is highly reliable. This finding is very valuable, as gene expression analysis from limited tissue material is often necessary. For instance, the importance of tumour heterogeneity is more and more emerging and analysis of different parts of the tumour (which might be very small) can reveal important information.

Another important finding is that gene expression analysis from FFPE tissue material using RNA-sequencing is possible. Most histological tissue samples are preserved by formalin fixation. FFPE tissues retain a very good morphology and many antibodies are made for IHC on FFPE samples. This means that the same samples, which are morphologically well studied and characterized, can also be used for gene expression analysis instead of having to use separate frozen material. Until recently, RNA-sequencing could only be performed on RNA with high integrity. During library preparation for RNA-sequencing, intact RNA is first transcribed into cDNA, which is then sheared to produce smaller fragments. With this new technology it is however possible to generate cDNA from degraded RNA, which then saves the shearing step. Hence, the end product that gets sequenced is very similar and explains why the generated data are reliable.

Interestingly, the gene expression analysis suggests, that lung tumours from *KRas^{G12D}* mice are more advanced than the ones from *R26^{DM.lsl-MYC/MYC};KRas^{G12D}* mice. Aim of the experiment was to identify genes that are related to Myc overexpression. As lesions were too small in *KRas^{G12D}* lungs 6 weeks after allele induction, I had to use lungs 9 weeks after allele induction. For a cleaner analysis, it would however been better to compare gene expression between *KRas^{G12D}* and *R26^{DM.lsl-MYC/MYC};KRas^{G12D}* lungs from the same time-point. It would have been possible for instance to use material from both mouse models 9 weeks after allele induction.

Feldser et al. identified in a *KRas^{G12D}/Tp53^{null}* model 42 upregulated genes in adenocarcinomas compared to adenomas (FC>1.75, p<0.05) (Feldser et al., 2010). I found only 6 of these genes are upregulated in the p-Erk positive *R26^{DM.lsl-MYC/MYC}/KRas^{G12D}* dataset (FFPE data). This study used microarrays to determine changes in gene expression. Microarrays are less sensitive than gene expression analysis by RNA-sequencing. Microarrays can only detect changes in gene transcript expression, whereas RNA-sequencing allows the determination of the absolute number of individual transcripts. This might be the reason why only a relatively small number of genes were found to be significantly regulated in this study.

Interestingly, Sox9 was one of the few overlapping genes. I could also confirm by IHC that Sox9 signal overlaps with p-Erk signal in *KRas^{G12D};Tp53^{F1/F1}* lung tumours (not shown), suggesting that Sox9 as a Wnt target might play a general role in tumour progression in *KRas^{G12D}* mutant lung cancer.

The Wnt signalling pathway is frequently upregulated in NSCLC (Stewart, 2014) and is associated with poor prognosis (Ettinger et al., 2013). Wnt pathway has also been found upregulated specifically in KRas mutant lung cancer models (Lee et al., 2009). Moreover, Wnt pathway activation has been shown to accelerate tumourigenesis in KRas mutant mice (Pacheco-Pinedo et al., 2011).

The upregulation of ErbB-ligands in the p-Erk positive dataset is surprising, as *KRas* mutant cells are thought to be independent from upstream signals. Therefore, *KRAS* mutant lung cancers are resistant to EGFR inhibitors (Pao et al., 2005). Some ErbB ligands are however able to bind and activate multiple ErbB family members. *Ereg*

for instance, which was found 24-fold upregulated in the p-Erk positive dataset is a pan-ErbB ligand that can bind and activate all functional homo- and heterodimers. Therefore, inhibition of all ErbB family members might be more efficient than EGFR inhibition alone.

The next chapter will focus on further validation of Wnt, and ErbB pathway, and also on the validation of individual genes.

5 Validation of p-Erk associated genes

5.1 Introduction

In Chapter 4 gene expression between p-Erk negative and p-Erk positive tumour regions from *R26^{DM}.Isl-MYC/MYC;KRas^{G12D}* mice was compared. p-Erk was used as a progression marker to identify potential tumour progression genes. Roughly 500 genes were found to be upregulated in the p-Erk positive tumour regions from *R26^{DM}.Isl-MYC/MYC;KRas^{G12D}* mice. This chapter will focus on the validation of the data.

ErbB and Wnt signalling stand out as two major pathways that were enriched in p-Erk positive dataset. Individual pathway members, such as Epiregulin (*Ereg*) and Amphiregulin (*Areg*) in the case of ErbB, and Porcupine (*Porcn*) and SRY-box containing gene 9 (*Sox9*) in the case of Wnt, were among the highest upregulated genes.

5.1.1 ErbB signalling in cancer

ErbB receptors activate pathways involved in proliferation, migration, survival and metabolism and therefore play an important role in cancer (Citri & Yarden, 2006). ErbB receptor signalling can be deregulated by various mechanisms. The receptors themselves can be either amplified or mutated. EGFR is amplified in a wide range of cancers and somatic mutations in the tyrosine kinase domain occur in NSCLC (Shigematsu & Gazdar, 2006). ErbB2 amplification can be found in breast, ovary, salivary and gastric cancers and in a small percentage of NSCLC (Hynes and Stern, 1994). ErbB3 mutations occur in 11% of colorectal cancers (Jaiswal et al., 2013). Another mechanism of ErbB signalling deregulation is a surplus of ligands, which can lead to constitutive receptor activation. EGF ligands are produced as precursors, which are cleaved and processed by proteases such as a disintegrin and metalloprotease (ADAM) family and matrix metalloproteinases (MMPs) (Salomon et al., 1995, Daub et al., 1996).

One major downstream pathway is PI3K/Akt pathway, which appears to be deregulated in many cancers. In tumours this pathway can become constitutively activated by activating PI3K mutations or by deactivating mutations in PTEN, a negative PI3K regulator (Eng, 2003, Samuels et al., 2004). In ErbB2⁺ breast cancers the PI3K/Akt pathway becomes activated via ErbB3. ErbB3 is the preferred binding

partner of ErbB2 and is among the 4 ErbB receptors the main PI3K activator (Engelman et al., 2005).

Another major ErbB downstream pathway is the MAPK pathway. Activating EGFR mutations lead to MAPK activation. Alternatively, the MAPK can be deregulated by downstream mutant KRAs. In lung and colon cancer EGFR and KRas mutations are therefore mutually exclusive (Cancer Genome Atlas Research, 2014). In pancreatic ductal adenocarcinoma (PDAC) however, it has been shown that EGFR signalling plays an important role in KRas mutant cancer (Navas et al., 2012).

5.1.1.1 ErbB signalling in lung cancer

Epidermal growth factor receptor (EGFR) is mutated or amplified in ~17% of lung ADC (Cancer Genome Atlas Research, 2014). EGFR mutations are mutually exclusive with KRas mutations and KRas mutant lung cancers are resistant to EGFR inhibition (Pao et al., 2005). The pan-ErbB ligand Ereg is however highly expressed in KRas mutant NSCLC. In KRas mutant NSCLC lines, Ereg expression was shown to positively correlate with KRas copy number. Moreover, Ereg levels were shown to be higher in human KRas mutant lung ADC samples than in KRas wild-type samples. High Ereg expression levels have been also associated with shorter survival (Sunaga et al., 2013).

ErbB2 is mutated or amplified in ~5% of lung ADC, ErbB3 in 2.5% and ErbB4 in ~9% (Cancer Genome Atlas Research, 2014). ErbB3 is a preferred binding partner of EGFR and is thereby often deregulated in EGFR mutant lung cancer. High activity of the ErbB3 downstream pathway PI3K/Akt correlates with sensitivity to the EGFR inhibitor gefitinib (Engelman et al., 2005). Also ErbB2 plays an important role in EGFR mutant lung cancer. ErbB2 is an important EGFR binding partner and ErbB2 amplification is associated with positive gefitinib treatment outcome in EGFR mutant lung cancer (Cappuzzo et al., 2005).

5.1.1.2 ErbB signalling description

ErbB receptors

The ErbB receptors have four family members, the epidermal growth factor receptor (EGFR, also called ErbB1 or Her1), ErbB2 (also called Her2), ErbB3 (also called

Her3) and ErbB4 (Her4). They belong to the receptor tyrosine kinase family even though ErbB3 has no kinase activity. ErbB3 can however be phosphorylated by heterodimerization to any of the other ErbB family members. ErbB proteins function through dimerization by forming homo- or heterodimers upon ligand binding (Figure 5-1).

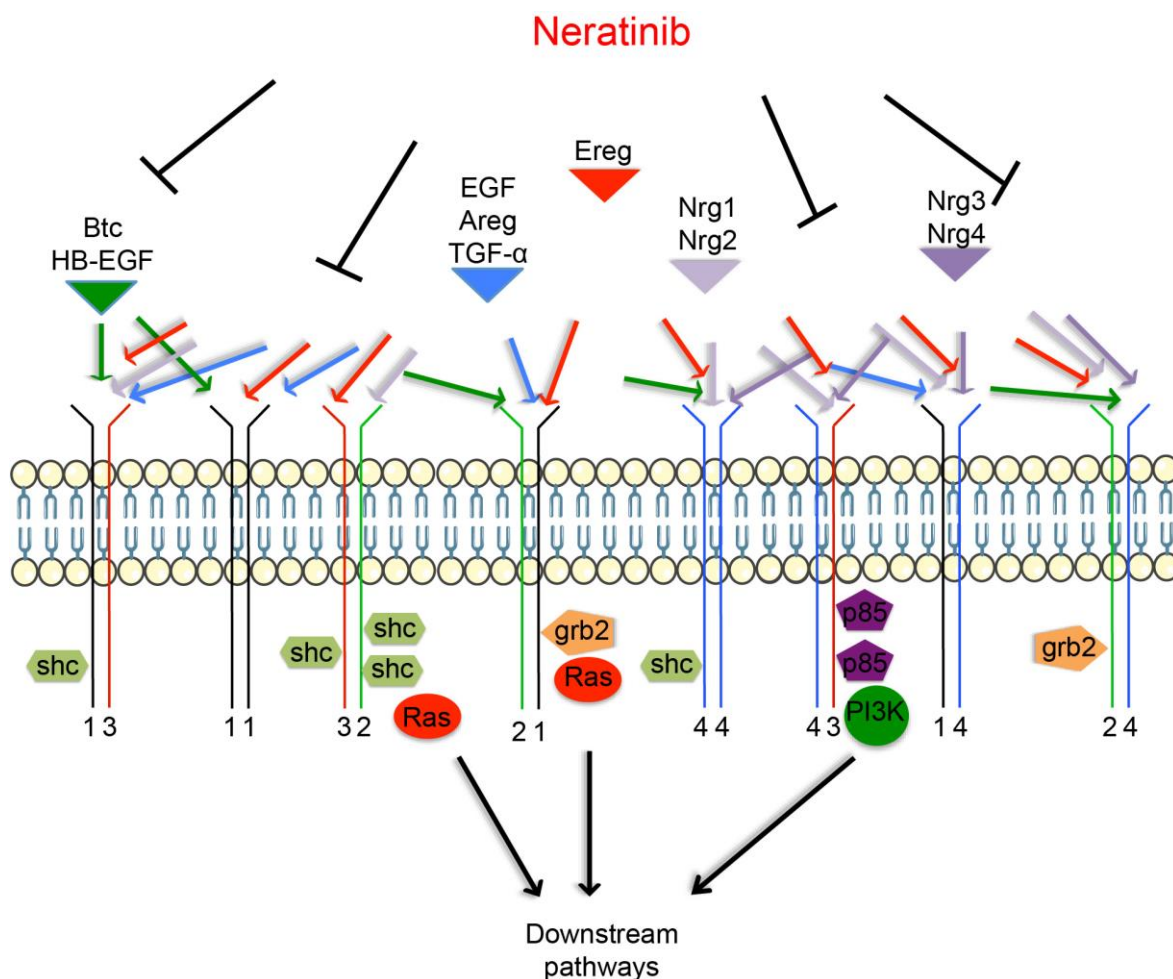


Figure 5-1 ErbB signalling.

The ErbB signalling pathways becomes activated upon ligand binding. Ligands fall into three groups: EGF, Areg, TGF- α (blue) bind EGFR (ErbB1). Btc and HB-EGF bind EGFR (ErbB1) and ErbB4 (green). Ereg belongs to this group as well, but has a broader binding spectrum and can bind to all receptor combinations (red). Nrg1 and Nrg2 (light purple) bind ErbB3 and ErbB4, Nrg3 and Nrg4 (dark purple) bind only ErbB4. Phosphorylated receptor tyrosine residues serve as docking sites for adaptor proteins, that then lead to effector activation. PTB (Shc) and SH2 (Grb2) domain containing proteins are adaptor proteins for Ras effectors, PI3K contains a p85 domain in the regulatory subunit. Neratinib inhibits kinase activity of ErbB1, ErbB2 and ErbB4.

All homo- and heterodimer combinations are functional except ErbB2 homodimers, as ErbB2 is unable to bind ligands (Klapper et al., 1999) and ErbB3 homodimers, as ErbB3 is lacking kinase activity (Guy et al., 1994). Therefore ErbB2 and ErbB3 require a heterodimeric partner. ErbB2 is the preferred heterodimeric partner for the other three ErbB receptors (Graus-Porta et al., 1997) and is able to increase the potency of its partner protein. It is able to enhance tyrosine phosphorylation capacity

of EGFR upon epidermal growth factor (EGF) binding (Graus-Porta et al., 1995) and of ErbB3 and ErbB4 upon NRG binding (Beerli et al., 1995). Moreover, ErbB2 increases the ligand affinity of its binding partners (Karunagaran et al., 1996; Sliwkowski et al., 1994). Also, ErbB2 heterodimers have a higher recycling rate and undergo less endocytosis than other ErbB dimers, which leads to more sustained signalling (Lenferink et al., 1998; Worthylake et al., 1999).

ErbB Ligands

ErbB receptor ligands can be classified into three groups. The first group, which consists of EGF, Areg (Shoyab et al., 1988) and transforming growth factor- α (TGF- α) (Massague, 1990), binds specifically to EGFR. The second group, consisting of Betacullin (Btc) (Sasada et al., 1993), Heparin-binding EGF (HB-EGF) (Higashiyama et al., 1992) and Ereg (Toyoda et al., 1995) has a strong affinity for ErbB1 and ErbB4. Neuregulins (NRG) make up the third group of ligands. NRG1 and NRG2 bind to ErbB3 and ErbB4 (Carraway et al., 1997; Riese et al., 1995), whereas NRG3 and NRG4 bind only ErbB4 (Harari et al., 1999; Zhang et al., 1997).

Epiregulin

Ereg is a ligand with a very broad specificity. Besides binding to EGFR and ErbB4 homodimers, it preferentially binds to ErbB heterodimers and is able to bind and activate all functional heterodimers (Shelly et al., 1998). It has a much lower binding affinity to individual receptors than ligands that specifically bind to a certain receptor (Toyoda et al., 1995). As mentioned earlier ErbB2 can increase the binding affinity of certain ligands to their receptors and in the case of Ereg it does so by increasing its binding affinity to ErbB4 (Riese et al., 1998). In some instances Ereg's broad specificity makes it even a more potent mitogenic activator than EGF or TGF- α and is a potent activator of Mitogen-Activated Protein Kinase (MAPK) signalling (Draper et al., 2003). In agreement with this Ereg is highly expressed in many cancer cell lines (Toyoda et al., 1997) and has been described as a marker of advanced NSCLC (Zhang et al., 2008).

ErbB Receptor signalling

Auto-phosphorylated tyrosine receptors serve as docking stations for adaptor proteins that then transfer the signal. All four ErbB receptors contain recognition

sites for Src Homology 2 (SH2) and Phosphotyrosine-binding (PTB) domains, which allow binding of proteins such as Src, Growth factor receptor-bound protein 2 (Grb2) and Src homology 2 containing transforming protein 1 (Shc) (Batzer et al., 1994; Stover et al., 1995). Grb2 and Shc are both adaptor proteins for Guanine nucleotide Exchange Factors (GEFs) such as Son of sevenless (Sos), which are involved in Ras activation. Thereby all four ErbB proteins are linked to the MAPK pathway. ErbB3 is the main phosphatidylinositol-4,5-bisphosphate 3-kinase (Pi3k) activator, as it contains multiple binding sites for the p85 regulatory subunit of Pi3k (Prigent and Gullick, 1994). EGFR can also bind Stat proteins through their SH2 domains and thereby activate Stat signalling (Silvennoinen et al., 1993).

Different ErbB ligands are expressed at distinct stages during development and differ in their tissue specific expression. By regulating ErbB receptor expression the cell is able to modulate its response to the ligands. The ligands and the receptor expression profile determine the signalling downstream of the receptors and give the cell room to fine-tune the response to external stimuli.

5.1.2 The Wnt pathway in cancer

The connection between Wnt signaling and cancer was initiated by the discovery that mammary tumours that occur in mice that have been infected with the murine mammary tumour virus were frequently caused by activation of Wnt1 (Mester et al., 1987). APC is as part of the β -catenin destruction complex a negative regulator of Wnt signalling and is the most frequently mutated tumour suppressor gene in human cancers. Most sporadic colorectal cancers carry APC mutations, which leads to increased β -catenin protein stability (Polakis, 2007). WTX is also part of the β -catenin destruction complex and is associated with Wilm's tumour formation (Huff 2011). In GSK3 β , another part of the destruction complex, in frame splice deletions that affect the kinase domain occur in mylogenous leukemia (Abrahamsson et al., 2009). Also β -catenin itself can be mutated, which prevents its destruction by kinases (Polakis, 2007). The Wnt coreceptor LRP5 is found to be aberrantly spliced in parathyroid and breast cancers (Bjorklund et al., 2009). Wnt signalling can also be epigenetically activated in cancer. Many Wnt inhibitor genes such as NDK2, Axin2 and sFRP5 are frequently occupied by EZH2. EZH2 is a methyl transferase that leaves repressive H3K23me3 chromatin marks and is part of the polycomb repressor complex 2 (PRC2) (Rodriguez & Paredes, 2011).

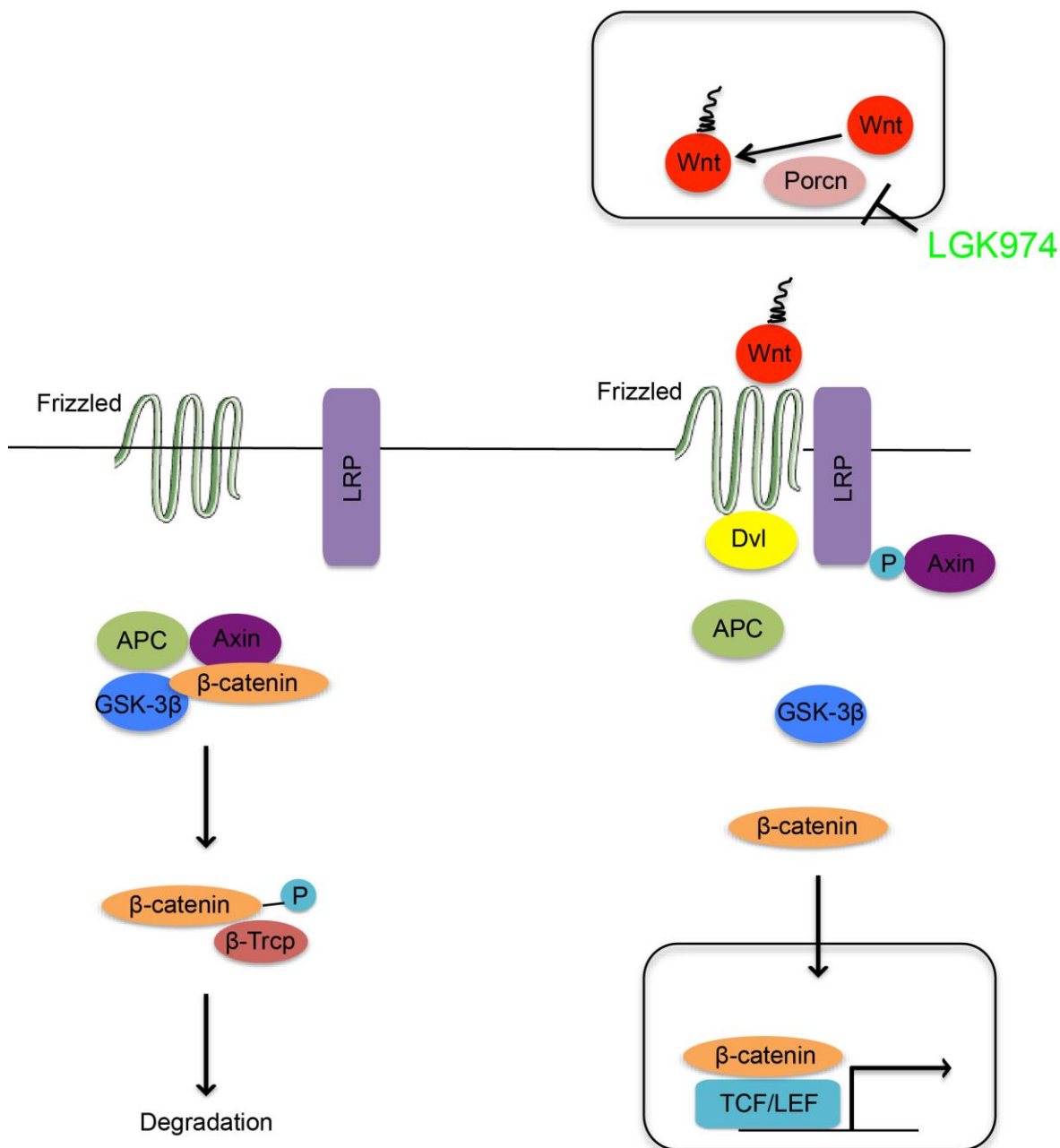


Figure 5-2 Wnt signalling pathway.

In absence of Wnt ligands, APC, Axin and GSK-3 β form a complex and β -catenin is phosphorylated and thereby marked for proteosomal degradation by β -TRCP. Upon ligand binding, activation of Dvl leads to dissociation of the Axin/APC/GSK-3 β complex and β -catenin is free to translocate to the nucleus and activate target genes. LGK974 inhibits Porcn, which acetylates Wnt proteins.

5.1.2.1 Wnt pathway in lung cancer

The Wnt pathway is often highly active in human NSCLC (Stewart, 2014). To be specific many Wnt ligands, such as *WNT-1* (Nakashima et al., 2008), *WNT-2* (You et al., 2004), *WNT-3* (Nakashima et al., 2012) and *WNT-5a* (Huang et al., 2005) are often overexpressed in NSCLC. Moreover, the WNT receptor Frizzled homolog 8 (*FZD8*) is commonly overexpressed (Wang et al., 2012). Several Dishevelled homolog (*DVL*) proteins, such as *DVL-1*, *DVL-2* and *DVL-3* are also overexpressed

in NSCLC (Wei et al., 2008) and so is *PORCN*, which is crucial for post-translational modification and secretion of WNT proteins (Chen et al., 2008). Overexpression of Wnt pathway members is also associated with poor prognosis, which has been specifically shown for *DVL-1* and *DVL-3* (Zhao et al., 2010) and for *WNT-1* (Nakashima et al., 2008), *WNT-3* (Nakashima et al., 2012) and *WNT-5a* (Huang et al., 2005).

The Wnt pathway has also been shown to be upregulated in a *KRas* mutant lung cancer mouse model (Lee et al., 2009) and pathway activation was shown to accelerate *KRas* driven tumourigenesis (Pacheco-Pinedo et al., 2011).

5.1.2.2 Pathway description

When the Wnt signalling pathway is inactive, which is the case when no Wnt ligand is bound to the frizzled receptor, pro-proliferation proteins such as β -catenin are bound and phosphorylated by the regulatory Axin/APC/GSK-3 β complex (Lee et al., 2003) (Figure 5-2). Phosphorylated β -catenin is a target for proteosomal degradation through β TrCP/Skp pathway (Price, 2006).

Upon Wnt binding to Frizzled LRP is in direct contact with the receptor and activates dishevelled. Activated dishevelled inhibits GSK-3 β , which prevents GSK-3 β from phosphorylating β -catenin. β -catenin is then free to translocate to the nucleus and can bind to LEF/TCF transcription factors and thereby activate transcription of its target genes. Wnt signalling plays a crucial role during development and is involved in several physiological processes such as cell proliferation and migration, which explains its importance in cancer. Wnt targets include for instance Myc (He et al., 1998), Cyclin D1 (Tetsu and McCormick, 1999), c-jun (Mann et al., 1999) and Sox9 (Blache et al., 2004).

In order to validate the importance of the pathways for tumour progression I needed inhibitors that broadly inhibit the respective pathway, but are at the same time specific and do not inhibit other pathways.

For Wnt pathway inhibition I chose the porcupine inhibitor LGK974 (Figure 5-2). There are 19 different Wnt ligands that can activate the pathway. Inhibiting them or knocking them down individually would be challenging. The palmitoyl transferase Porcn acetylates Wnt proteins, which is important for Wnt secretion and activity

(Galli et al., 2007; Herr and Basler, 2012). *Porcn* was more than 3-fold upregulated in the p-Erk positive dataset (Chapter 4). LGK974 binds and inhibits Porcupine and thereby inhibits the whole Wnt pathway (Liu et al., 2013).

For ErbB signalling I chose Neratinib, which is a pan-EGFR inhibitor and has been shown to inhibit all four ErbB family members (Canonici et al., 2013) (Figure 5-1). Neratinib binds to Cysteine residues in the ATP binding pocket, which is conserved in ErbB1, 2 and 4 and is thereby specific in inhibiting ErbB family members (Wissner and Mansour, 2008). *KRAS* mutant cancers possess an inherent resistance to the EGFR inhibitors Erlotinib or Gefitinib (Pao et al., 2005). However, the in the p-Erk positive samples upregulated ErbB ligands do not only bind EGFR. HB-EGF-like growth factor and Ereg have high affinity to ErbB1 and ErbB4 (Paria et al., 1999) and Ereg has a broad affinity to all receptors, as described above. Upregulation of pan-ErbB ligands such as *HB-EGF* and *Ereg* in the p-Erk positive regions suggests that simultaneous activation of downstream pathways through all family members is necessary for tumour progression. Therefore blocking all 4 ErbB family members will probably be much more effective than blocking EGFR alone.

In this chapter I first investigated the role of ErbB signalling and Wnt pathway *in vitro*. For this purpose I tested *KRAS* mutant human adenocarcinoma cell lines for sensitivity to the inhibitors. The cell lines have mutation for *KRAS* in common, but each one presents otherwise an individual set of mutations in various tumour suppressor- and oncogenes. Response rates from this heterogenous panel of lung cancer cell lines will give valuable information about how broad the dependence on the two pathways in *KRAS* mutant cell lines is.

The next step was to validate our individual candidate genes. Long term goal is to explore their importance *in vivo* in an shRNA screen, using the *R26^{DM}.Isl-MYC/MYC;KRAs^{G12D}* model. shRNAs against genes that were found upregulated in the p-Erk positive regions will be cloned in cis with Cre recombinase into lentiviral vectors so that any cell that recombines the conditional alleles will express the shRNA as well. As the capacity to screen *in vivo* is limited, I reasoned that analysis of diverse human NSCLC lines with only *KRAS* mutation in common would reveal which genes are worth to be explored *in vivo*. For this purpose an *in vitro* siRNA screen was performed.

5.2 Results

5.2.1 *In vitro* pathway validation

In order to find concentrations that affect cell viability, a dilution series with LGK974 and Neratinib in a panel of *KRAS* mutant lung adenocarcinoma cell lines was performed. Cells were seeded at low confluency (20-40%) and confluency was monitored over time using long term Incucyte video-microscopy (Figure 5-3 and Figure 5-4).

LGK974 dilution series

For LGK974, I used 1 μ M as a reference concentration, as this concentration has been shown to efficiently inhibit Wnt signalling *in vitro* (Jiang et al., 2013) and concentrations either side of this reference from 100nM to 25 μ M were thus tested. The titration revealed that 10 μ M LGK974 suppressed cell propagation over time compared to untreated or DMSO control in most tested *KRAS* mutant cell lines (Figure 5-3). An increase to 25 μ M reduced the cell number further in some cell lines.

Lower concentrations had no consistent effects. Therefore 10 μ M seems to be an appropriate concentration and was used for all further cell culture experiments.

The *KRAS*^{G12C} mutant cell line H23 and the *EGFR*^{L858R} mutant cell line H3255 seem to be largely resistant to Porcupine inhibition, as even an increase to 25 μ M had no effect on cell confluency.

It has to be noted that the seeding confluency was higher for these two cell lines (~60%), which might also explain why the cells were less sensitive to the inhibitor. Each experiment was carried out three times but it was difficult to find the optimal seeding density for the H23 and H3255 cell lines. When seeded at lower density the cells grow very slowly and are of low contrast and are therefore difficult to image.

Neratinib dilution series

Neratinib has been shown to have a very broad concentration range at which it is efficient depending on the cell line and ErbB mutation status (Rabindran et al., 2004) and was therefore tested at concentrations ranging from 10nM to 1 μ M (Figure 5-4). H358 and H441 show a modest response to the inhibitor at 50nM, which is further

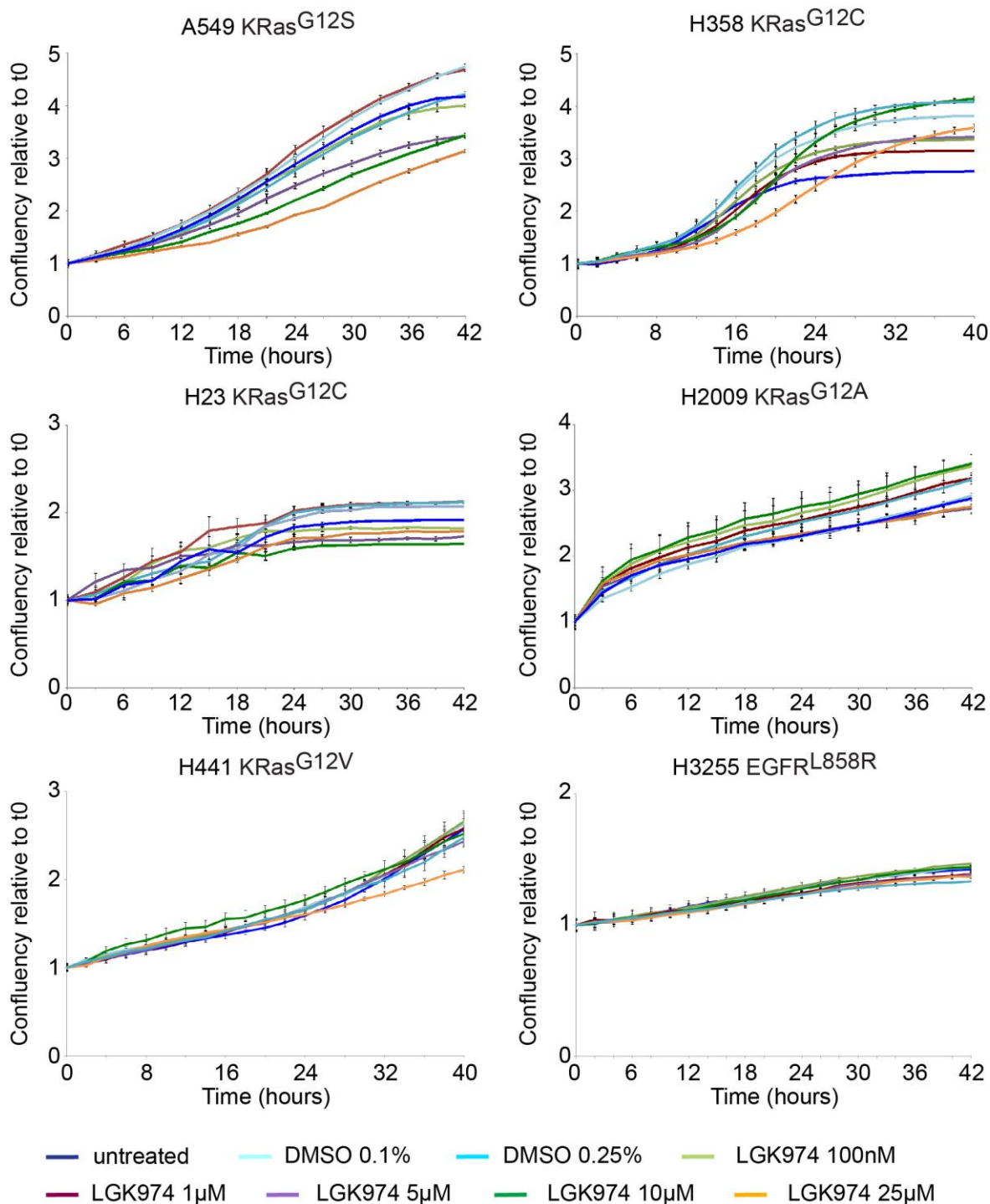


Figure 5-3 LGK974 Dilution series.

Indicated cell lines were seeded in the evening and treated with different concentrations of LGK974 the next morning. Confluency was monitored with Incucyte over time. For 25µM LGK974 the DMSO concentration had to be increased to 0.25%. A549 and H2009 cells are LGK974 sensitive.

increased by higher concentrations in a dose dependent manner. Below 50nM no effect was observed in any of the tested cell lines. Other cell lines, such as A549 and H2009 showed a clear response from 250nM. H23 seems to be resistant to ERBB inhibition and the *EGFR* mutant cell line H3255 shows a modest response with concentrations starting from 500nM, but again these two cell lines were seeded at a higher confluency. As first migration and invasion experiments showed that

most cell lines respond to 100nM Neratinib, this dose was used for all further cell culture experiments.

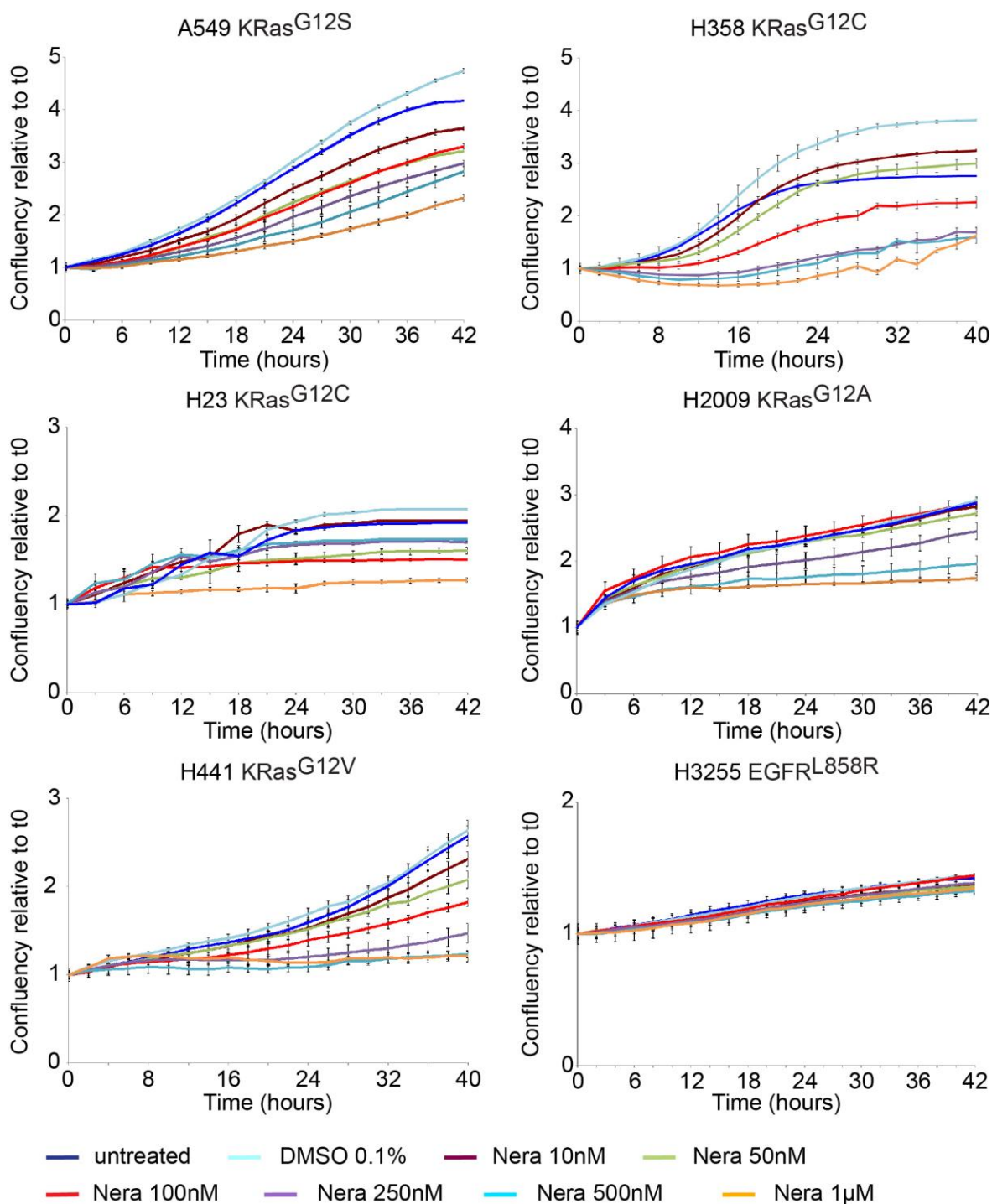


Figure 5-4 Neratinib dilution series.

Indicated cell lines were seeded in the evening and treated with different concentrations of Neratinib the next morning. Confluency was monitored with Incucyte over time. A549, H358, H2009 and H441 cells are Neratinib sensitive.

Effects on cell migration

I then tested the effect of LGK974 and Neratinib on motility of human *KRAS* mutant lung cancer cell lines by performing a migration scratch assay. In this setup cells

are seeded at 100% confluency and then a scratch is made through the confluent monolayer. The cells then close the wound by migration, which was monitored over time with long-term time-lapse Incucyte video-microscopy, which calculates the wound density relative to the width of the initial scratch wound (RWD).

I noticed that some cell lines were sensitive to only one of the two inhibitors and that the response was then not further increased by the combination of the inhibitors. Some cell lines however were sensitive to both inhibitors and the response was increased by their use in combination.

H460 and A427 (Figure 5-5) were sensitive to LGK974, which is very clear from the migration graphs of both cell lines and can also be seen in the H460 confluency graph. In the A427 the combination reduced confluency modestly, this cell line seems to be more susceptible to inhibition of migration.

H358 and H441 (Figure 5-6) proved to be Neratinib sensitive. Neratinib on its own strongly inhibited migration and reduced cell confluency. The combination of the two inhibitors slightly increased the effects on migration and confluency, but this might be a DMSO effect, as the DMSO concentration is doubled in the combined treated cells. In the H441, LGK974 has no effect on cell confluency, but Neratinib does and the combination does not increase this effect much further. LGK974 has a modest effect on cell motility, whereas Neratinib initially inhibited migration strongly and the cells then caught up towards the end of the run. Combined treated cells on the other hand hardly migrated over time.

The cell lines A549 and H2009 are sensitive to both inhibitors (Figure 5-7). Either inhibitor on its own slightly inhibits migration, which is further increased by the combination. The same is true for confluency in the A549 cells in the H2009 no clear effect of the inhibitors on cell confluency can be seen. Growth inhibition might be stronger in these cells when seeded at lower density.

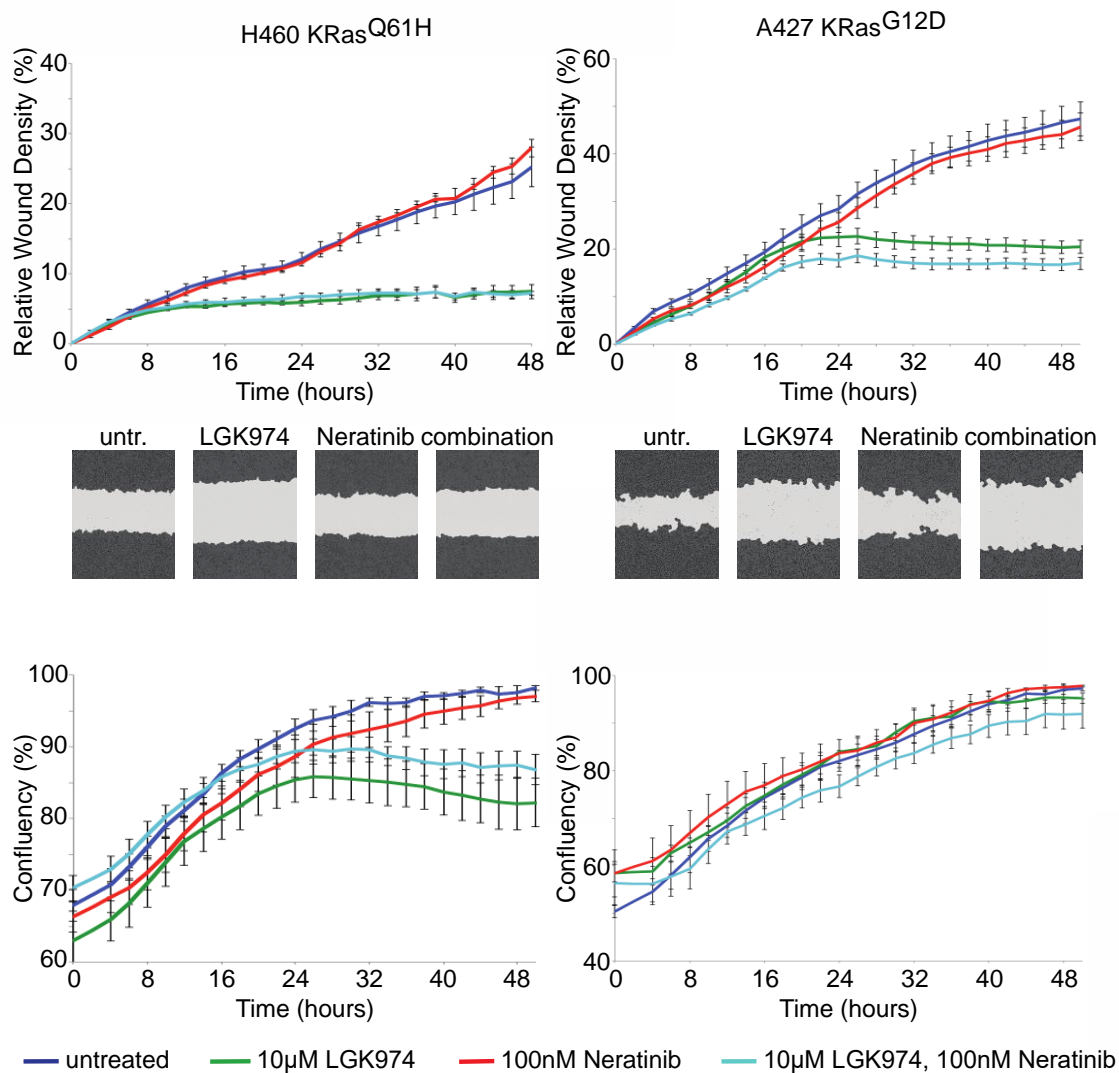


Figure 5-5 Effect of LGK974 and Neratinib on Migration and Confluency of KRas mutant lung cancer cell lines – LGK974 sensitive cell lines.

Indicated cell lines were seeded in the evening and treated with the inhibitors the next morning. For migration assay, a scratch was made through a confluent cell monolayer. Wound closure and confluency was monitored with Incucyte over time. Pictures were taken at the end of the run. LGK974 treatment clearly inhibited cell migration and propagation in the H460 cells and cell migration in the A427 cells. Neratinib treatment had no effect.

The ErbB inhibitor Neratinib and the Wnt inhibitor LGK974 inhibit migration and cell growth, measured by cell confluency, in most tested *KRAS* mutant lung cancer cell lines, showing the importance of the two pathways.

Murine cancer cell lines

A murine cell line derived from *R26^{DM.lsl-MYC/WT};KRas^{G12D}* tumours was generated and tested for responsiveness to the inhibitors. As the EGFR and Wnt pathways were increased in the more aggressive (p-Erk positive) tumour regions of these mice, responsiveness to ErbB and Wnt inhibitors would confirm the importance of the pathways in this genetic setting. A *KRAS^{G12D};Tp53^{null}* cell line that is also derived

from murine lung tumours was also tested. In addition to the migration assay an invasion assay was also performed. For invasion assays the setup is similar to migration assays, but the scratch is over-layered with matrigel: invasion into matrigel is thus required for wound closure.

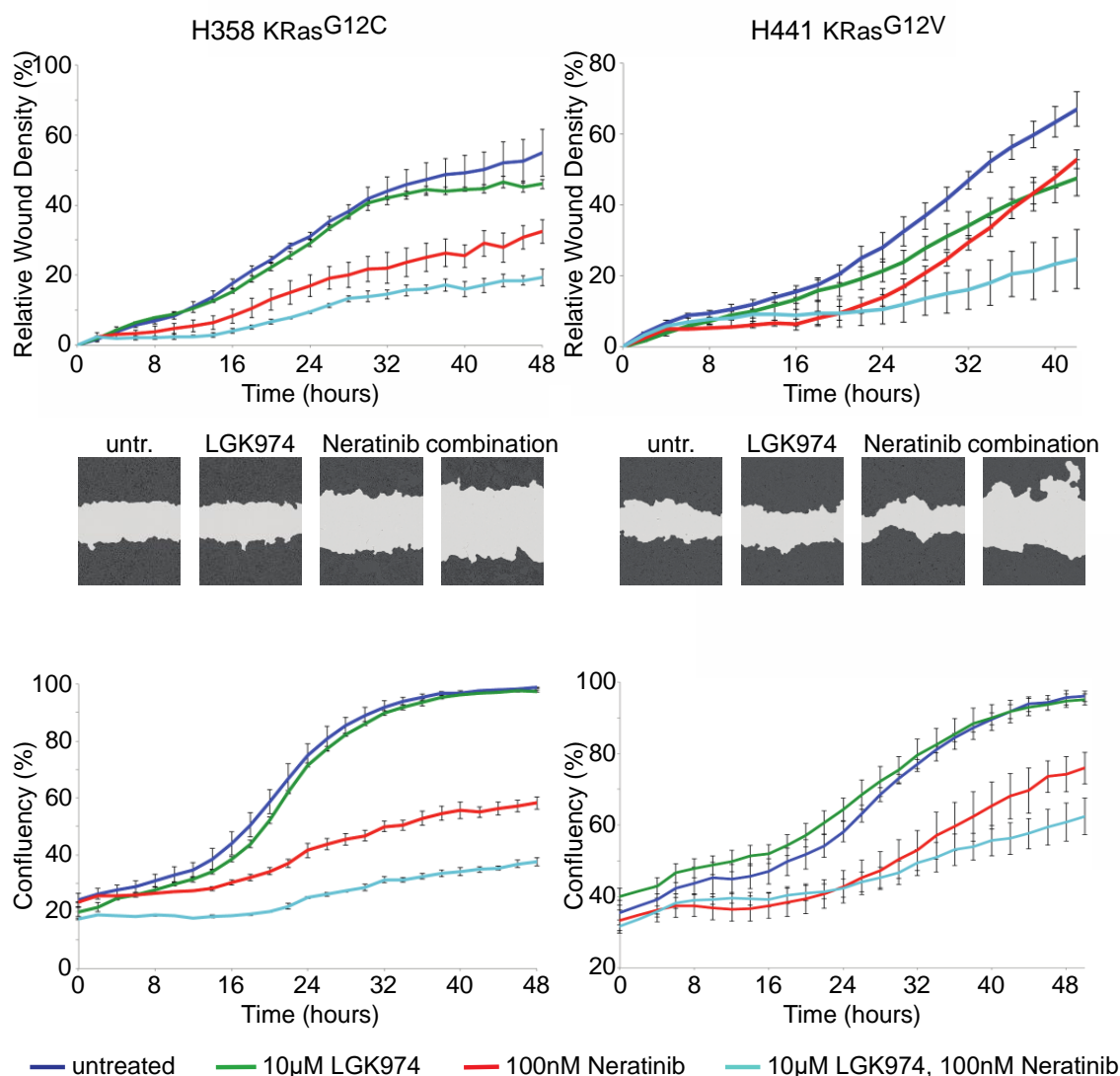


Figure 5-6 Effect of LGK974 and Neratinib on Migration and Confluency of KRas mutant lung cancer cell lines – Neratinib sensitive cell lines.

Indicated cell lines were seeded in the evening and treated with the inhibitors the next morning. For migration assay, a scratch was made through a confluent cell monolayer. Wound closure and confluency was monitored with Incucyte over time. Pictures were taken at the end of the run. Neratinib treatment clearly inhibited cell migration and propagation in the H358 and H441 cells. LGK974 treatment had no effect on H358 cells and mildly inhibited cell migration in the H441 cells.

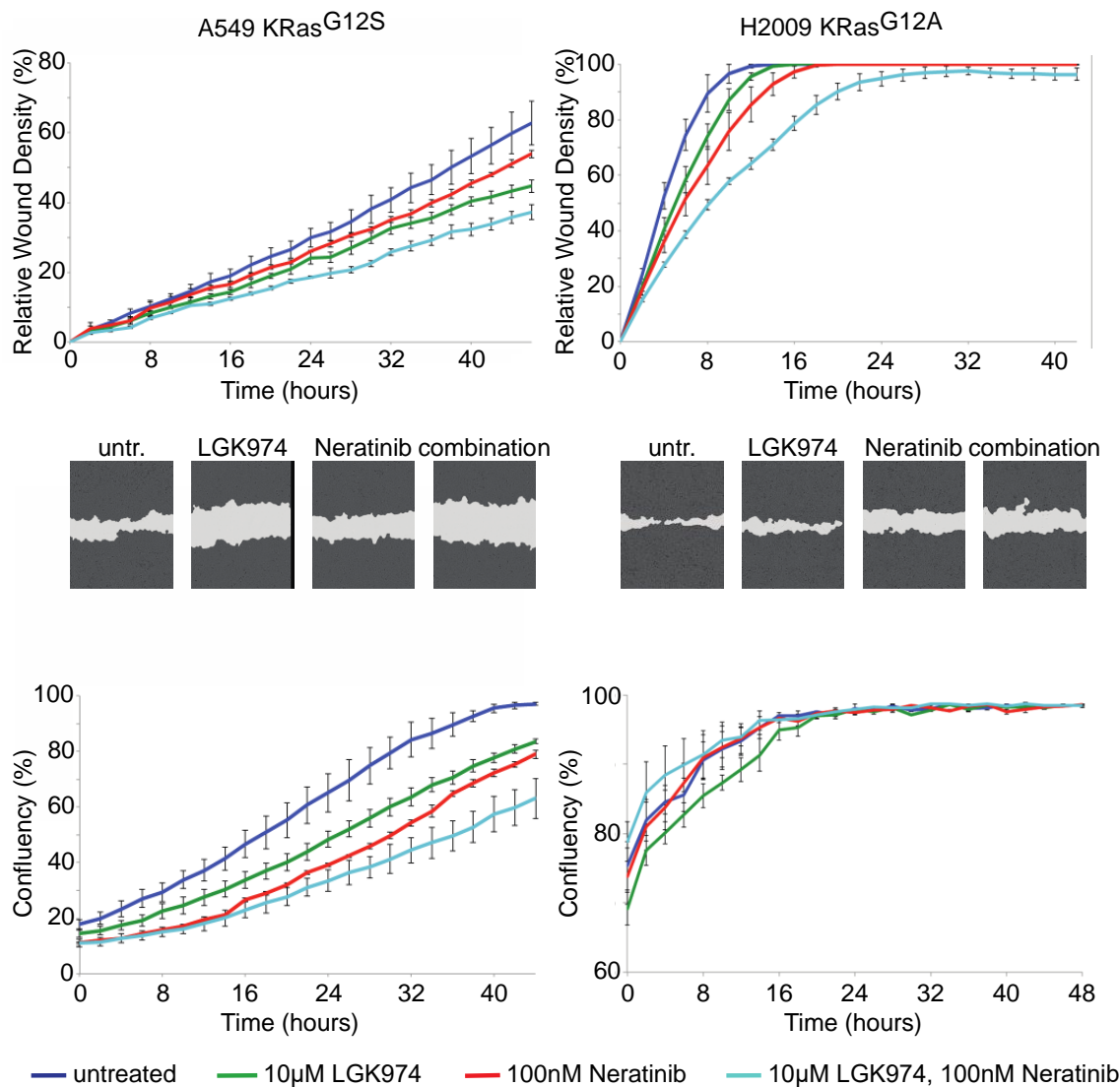


Figure 5-7 Effect of LGK974 and Neratinib on Migration and Confluency of KRas mutant lung cancer cell lines – Dual sensitive cell lines.

Indicated cell lines were seeded in the evening and treated with the inhibitors the next morning. For migration assay, a scratch was made through a confluent cell monolayer. Wound closure and confluency was monitored with Incucyte over time. Pictures were taken at the end of the run and after 10h for A549 and H2009, respectively. Neratinib and LGK974 treatment (individually and in combination) inhibited cell migration and propagation in the A549 cells and cells migration in the H2009 cells.

Either inhibitor alone did not reliably inhibit invasion, but they did inhibit invasion when used in combination (Figure 5-8). Migration analysis gave a similar result with the combination of both inhibitors having the strongest effect on migration. Both, Wnt and ErbB inhibition suppressed cell propagation, but the effect was more pronounced when both pathways were inhibited. In the *R26^{DM.lsl-MYC/WT};KRas^{G12D}* cell line proliferation seems to be blocked completely, but it has to be mentioned that these cells are of low contrast, which makes the Incucyte analysis difficult. These data confirm the importance of the two pathways in the genetic setting in which they were originally discovered.

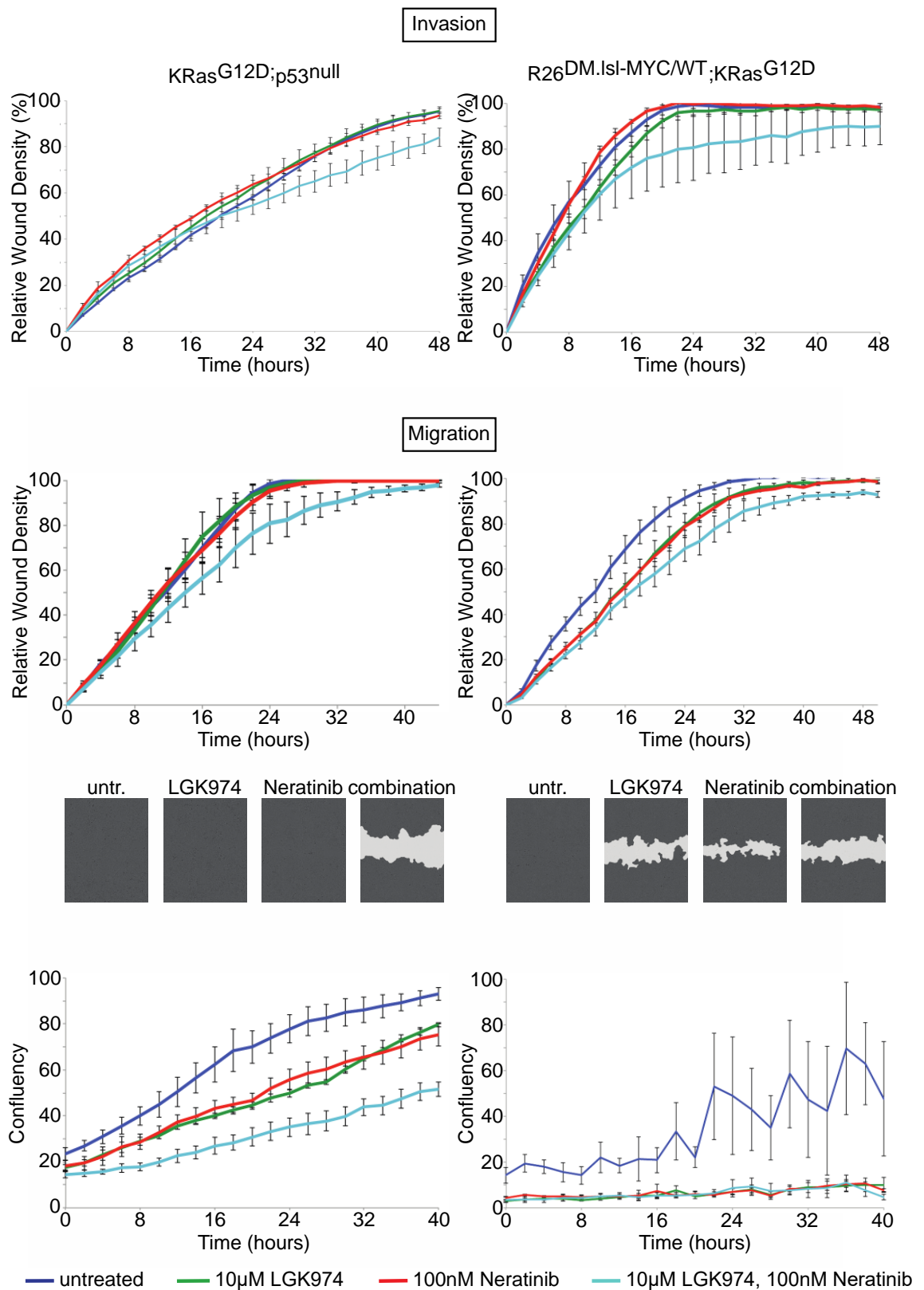


Figure 5-8 Effect of LGK974 and Neratinib on invasion, migration and propagation of KRas mutant mouse cell lines.
 Indicated cell lines were seeded in the evening and treated with the inhibitors the next morning. For migration and invasion assay, a scratch was made through a confluent cell monolayer, in the invasion assay the scratch was layered with matrigel. Wound closure and confluency was monitored with Incucyte over time. Pictures were taken after 20h and 24h for KRas^{G12D};p53^{null} and R26^{DM.Isl-Myc/WT};KRas^{G12D}, respectively. Both cell lines are sensitive to LGK974 and Neratinib.

The fact that the *KRas*^{G12D};*Tp53*^{null} murine cell line and most *KRAS* mutant human lung cancer cell lines are also sensitive to the inhibitors suggests that ErbB and Wnt signalling might be of general importance for *KRAS* mutant lung cancer cell lines.

5.2.2 *In vivo* pathway validation

In order to determine the importance of ErbB signalling and Wnt pathway in *KRAS* mutant lung cancer cell lines *in vivo* *R26*^{DM.lsl-MYC/MYC};*KRas*^{G12D} mice were treated with the inhibitors. In xenograft mouse models using *Her-2* mutant cell lines Neratinib was shown to inhibit tumour growth substantially at a dose of 40mg/kg/day and tumour growth was further decreased with a dose of 80mg/kg/day. Therefore, a dose of 40mg/kg/day was initially chosen.

A dose of 10mg/kg/day LGK974 has been shown to be well tolerated and to significantly inhibit pancreatic tumour growth *in vivo* (Jiang et al., 2013) and was therefore chosen.

Treatment was started 4 weeks post allele induction by Adeno-Cre, as tumour size and burden at this time point is already comparable to the well characterized time point of 6 weeks post induction. Mice were treated for 2 weeks and the lungs were histologically compared to vehicle treated mice. Neither treatment with either inhibitor alone nor the combination of both had any effect on overall tumour burden (Figure 5-9). Ki67 staining revealed that all treatment schemes resulted in tumours that were proliferating at a comparable level as vehicle controls or untreated tumours 4 weeks post Adeno-Cre infection (Figure 5-10). Also TUNEL staining showed that there is no significant increase in apoptosis as the number of TUNEL positive cells of all treatments was comparable to vehicle treated controls or untreated tumours 4 weeks post Adeno-Cre infection. From p-Erk and adjacent Ki67 stainings we know that tumour progression does not correlate with a higher proliferation rate. As the two pathways are associated with tumour progression in this model it is therefore to be expected that Wnt and ErbB pathway inhibition affect tumour progression rather than tumour growth. Examination of lungs taken 4 weeks post induction revealed that p-Erk is already detectable at this time point (Figure 5-11). However, after 2 weeks of treatment with either inhibitor or the combination p-Erk positive tumours could still be found. Possibly, Wnt and ErbB pathway

inhibition are not able to reverse tumour progression once it happened, but may still be able to prevent tumour progression.

Treatment of R26^{DM.lsl-MYC/MYC};KRas^{G12D} mice with LGK974 and Neratinib
- starting 4 weeks post allele induction

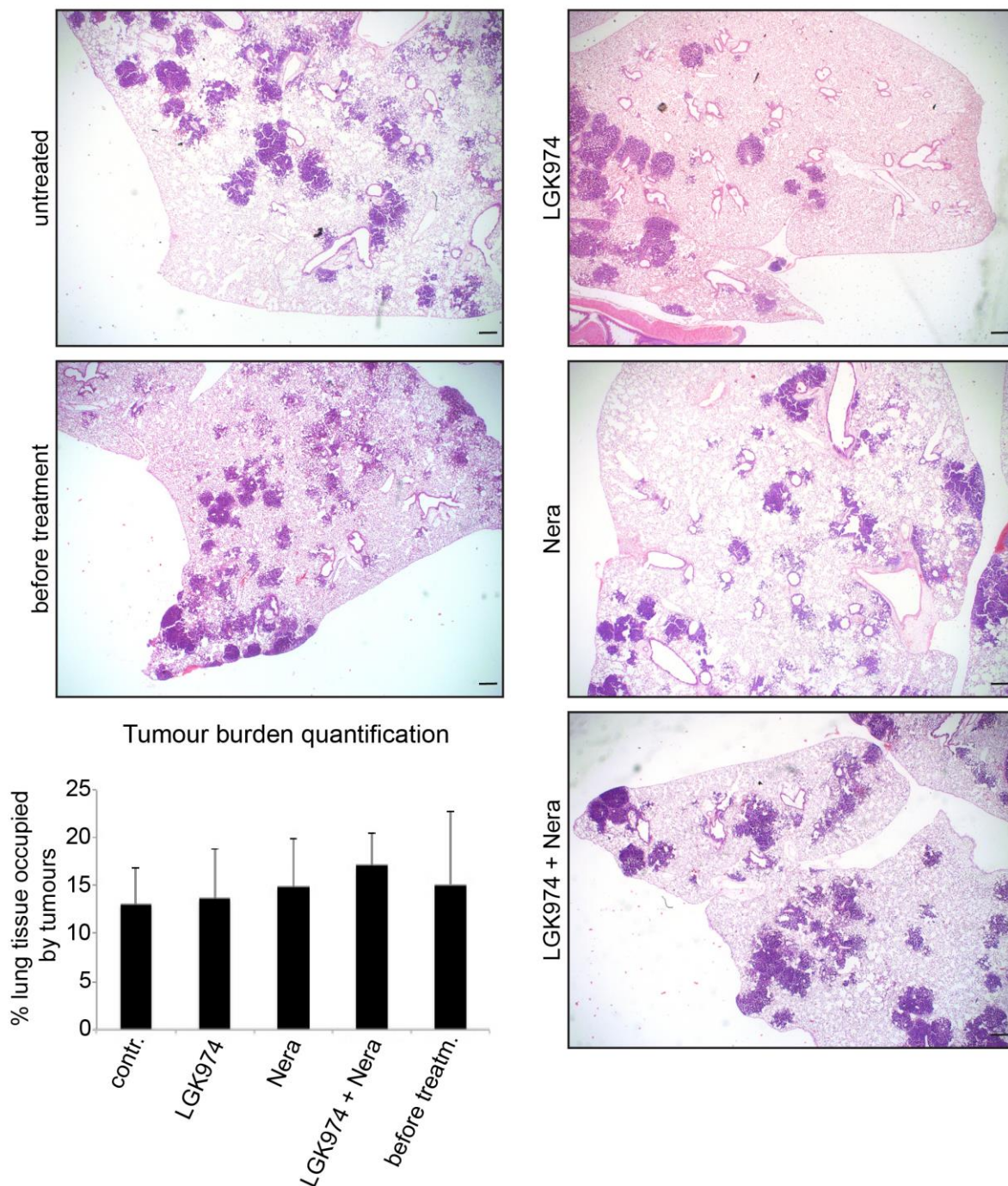


Figure 5-9 Tumour burden after LGK974 and Neratinib treatment starting 4 weeks post allele induction.

The panels show representative overview pictures from untreated R26^{DM.lsl-Myc/Myc};KRas^{G12D} control mice (n=10) 6 weeks post allele induction (1*10⁷ PFU), mice that were treated for 2 weeks with LGK974 (10mg/kg/day) (n=5), Neratinib (40mg/kg/day) (n=5) or the combination (n=3) starting 4 weeks post allele induction and untreated mice (n=2) 4 weeks post allele induction. Treatments had no effect on tumour burden. Scale bars: 300µm.

Analysis of R26^{DM.lsl-MYC/MYC};KRas^{G12D} lung tumours after LGK974 and Neratinib treatment - starting 4 weeks post allele induction

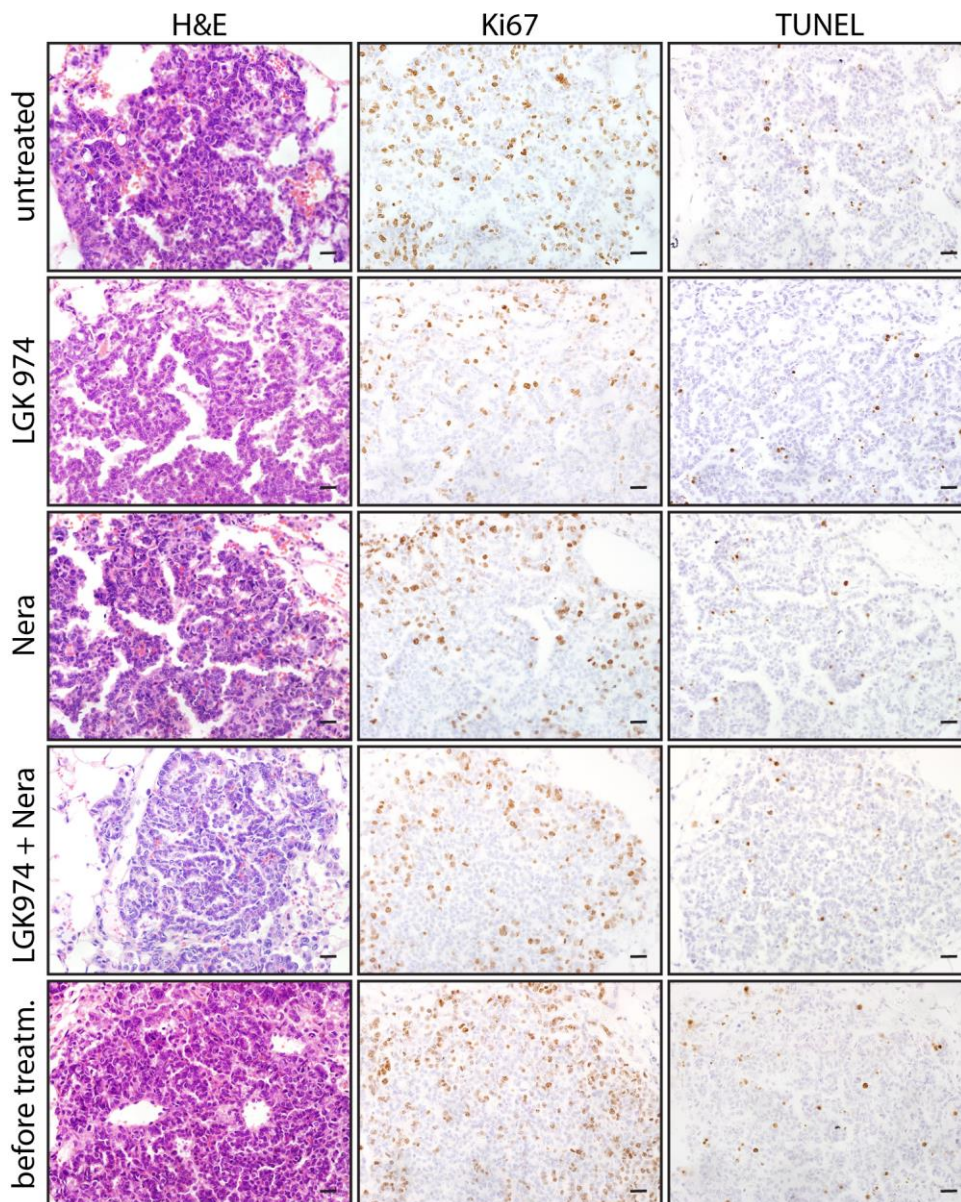


Figure 5-10 Proliferation and apoptosis after LGK974 and Neratinib treatment starting 4 weeks post allele induction.

Panels show Ki67 and TUNEL stainings of lung tumours and H&E staining from untreated R26^{DM.lsl-Myc/Myc};KRas^{G12D} control mice (n=10) 6 weeks post allele induction (1×10^7 PFU), mice that were treated for 2 weeks with LGK974 (10mg/kg/day) (n=5), Neratinib (40mg/kg/day) (n=5) or the combination (n=3) starting 4 weeks post allele induction and untreated mice (n=2) 4 weeks post allele induction. Treatments had no effect on number of Ki67 or TUNEL positive cells. Scale bars: 20µm.

We therefore decided to start the treatment earlier, at a time point at which tumours are significantly smaller and p-Erk signal cannot be detected. Importantly, the Neratinib dose was increased to 80mg/kg/day, given the failure of 40mg/kg/day to suppress p-Erk expression. 2 weeks after Adeno-Cre infection hardly any tumours can be found and the few detected ones are multiple times smaller than the ones

present at the 6 or 4 weeks time-point. Also, no p-Erk positive tumours could be found in this cohort.

Tumour Progression in R26^{DM.lsl-MYC/MYC};KRas^{G12D} lung tumours after LGK974 and Neratinib treatment - starting 4 weeks post allele induction

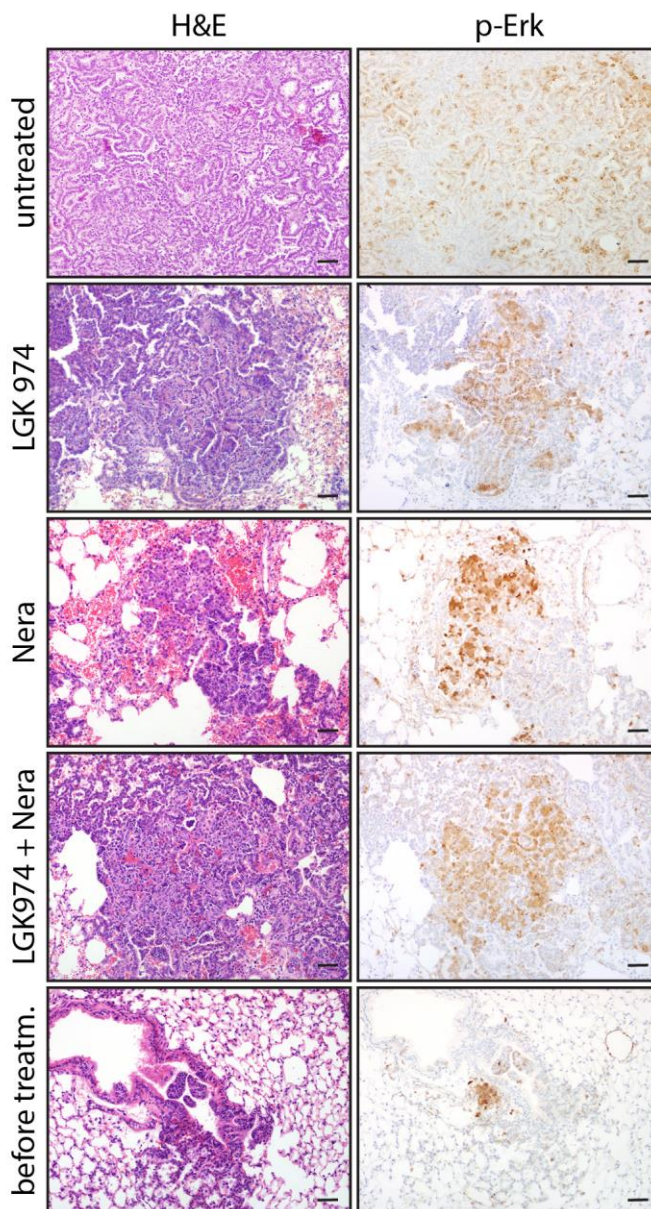


Figure 5-11 Tumour progression after LGK974 and Neratinib treatment starting 4 weeks post allele induction.

Panels show images of p-Erk positive lung tumours and adjacent H&E staining from untreated R26^{DM.lsl-Myc/Myc};KRas^{G12D} control mice (n=10) 6 weeks post allele induction (1*10⁷ PFU), mice that were treated for 2 weeks with LGK974 (n=5), Neratinib (n=5) or the combination (n=3) starting 4 weeks post allele induction and untreated mice (n=2) 4 weeks post allele induction. p-Erk signal was still detectable after treatment. Scale bars: 50µm.

Preliminary data, which have to be confirmed by increasing the number of mice, showed that treatment with Neratinib or combined treatment of Neratinib and LGK974 for 4 weeks starting 2 weeks after Adeno-Cre infection resulted in a dramatic decrease in tumour burden, compared to vehicle control that was

Treatment of R26^{DM.Isl-MYC/MYC};KRas^{G12D} mice with LGK974 and Neratinib
 - starting 2 weeks post allele induction

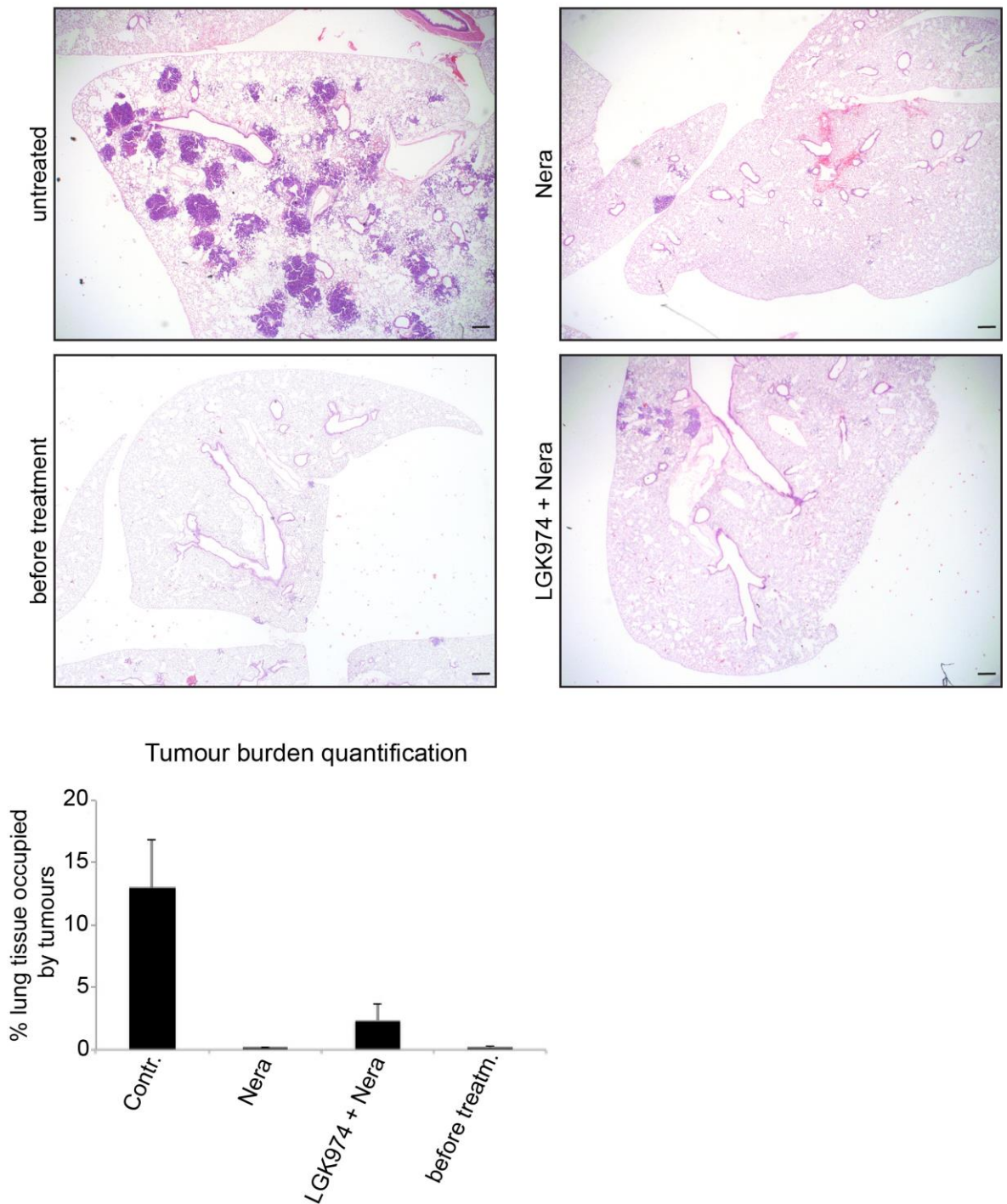


Figure 5-12 Tumour burden after LGK974 and Neratinib treatment starting 2 weeks post allele induction

The panels show representative overview pictures from untreated R26^{DM.Isl-Myc/Myc};KRas^{G12D} control mice (n=10) 6 weeks post allele induction (1×10^7 PFU), mice that were treated for 4 weeks with Neratinib (80mg/kg/day) (n=3) or LGK974 (10mg/kg/day) and Neratinib (80mg/kg/day) (n=2) starting 2 weeks post allele induction and untreated mice (n=3) 2 weeks post allele induction. Tumour burden was clearly reduced after treatment. Scale bars: 300µm.

comparable to the tumour burden at the 2 weeks time point (Figure 5-12). The experiment could not be carried out with a higher number of mice because the Adeno-Cre infection has to be done with mice of the same age. As the litter size is

usually not big enough for this kind of experiment, it needs to be repeated. These preliminary data suggest that Neratinib and LGK974 can interfere with tumour emergence and progression, but are not able to regress established tumours or tumour progression. Further treatments will show if Neratinib and LGK974 can indeed inhibit tumour emergence.

5.2.3 *In vitro* siRNA screen

In order to validate individual genes that I found to be upregulated in the p-Erk positive tumour regions, I performed a siRNA screen in collaboration with Kay Hewitt from the siRNA screening facility at our institute and Emma Shanks, who helped with the data analysis. The genes were selected by sorting the genes that were significantly upregulated (FDR < 0.05) in the p-Erk positive regions by fold change. Genes that have been reported to be amplified (according to cBioportal) and/or overexpressed (according to Oncomine) in human lung cancer were selected. From this selection the 51 genes with the highest fold change were chosen for the *in vitro* siRNA screen (Table 5-1). We chose to perform a deconvoluted screen, meaning that for each gene 4 siRNAs were tested separately. Deconvolution has the advantage to obtain more information about individual siRNAs than by pooling. In a pool siRNAs that do not considerably knockdown the gene of interest might dilute the effect of the siRNAs that do knockdown the respective gene. On the other hand deconvolution creates challenges in the data analysis that I will explain as I go through the data.

Targeting cell viability and cell mobility are promising therapeutic approaches. Therefore both features were included in the screen. In order to simplify the screening process, cell viability was assessed based on nuclei count relative to the non-targeting control (NTC) 72h post transfection. I am aware that the term “loss of viability” is not perfectly accurate, as lack of proliferation and cell death can both contribute to a reduction in cell number, but will be further used in this chapter.

Viability Screen

In order to assess the importance of these genes in a human setting, *KRAS* mutant human lung adenocarcinoma cell lines were tested. 3 cell lines were included in the cell viability screen, A549, H2009 and H460.

Symbol	FC	FDR	Amplified in human NSCLC (cbioportal)	Overexpressed in human NSCLC (Oncomine)
Ereg	24.82	2.78E-13	Y	Y
Sox9	15.79	7.48E-04	Y	Y
Dlk1	10.46	2.33E-26	Y SCC	N
B4galt6	9.46	1.24E-03	Y SCC	weak
Basp1	9.03	1.31E-04	Y > 10%	Y
Itga2	6.79	2.47E-11	N	Y
Cldn4	6.11	1.16E-02	Y	Y
Cd24a	5.94	1.40E-15	No data	Y
Slc38a1	5.68	1.17E-11	Y (rare)	Y
Arntl2	4.54	4.90E-02	Y > 6%	Y
Dsc2	4.43	4.51E-02	Y > 6%	Y
S100a6	4.00	1.51E-07	Y > 18%	Y
Itgb4	3.92	2.29E-02	Y	Y
Atp13a4	3.92	3.03E-14	Y >25% SCC	Y
Kif23	3.76	8.81E-07	Y (rare)	Y
Porcn	3.59	4.85E-03	N	weak
Krt8	3.57	1.87E-05	Y	Y
Vcam1	3.57	3.59E-02	Y (rare)	Y
Krt18	3.50	1.80E-11	Y	Y
Lamc2	3.48	2.56E-09	Y > 10%	Y
Tnfrsf12a	3.42	1.47E-02	Y	Y
Tspan8	3.41	5.23E-06	Y > 6%	Y
Atp6v1g3	3.40	2.80E-03	Y > 6%	Y
Ecm1	3.25	7.13E-03	Y > 18%	Y
S100a14	3.18	6.52E-04	Y > 18%	weak
Lgals3bp	3.16	2.09E-07	Y	Y
Nt5e	3.04	1.20E-05	Gains and losses	Y
Lad1	3.01	2.92E-05	Y > 6%	Y
Igfbp5	2.99	1.36E-05	Y (rare)	Y
Pdia4	2.98	3.16E-05	Y	Y
Cd38	2.97	3.82E-02	Y	Y
Krt19	2.96	2.06E-06	Y (rare)	Y
Slc2a1	2.95	1.11E-02	Y	Y
Myrf	2.92	1.26E-02	N	Y
Plekha6	2.91	3.34E-05	Y > 6%	Y
Ndrg1	2.84	7.71E-03	Y > 10%	Y
Rabgap1l	2.83	3.95E-05	Y > 10%	weak
Phlda1	2.82	7.01E-04	Gains and losses	Y
Gapdh	2.80	1.08E-02	Gains and losses	Y
Fabp5	2.79	6.15E-03	Y	weak
Cmas	2.75	4.21E-02	Y	Y
Golm1	2.75	3.84E-05	N	Y
Ptges	2.73	5.26E-03	Y	Y
Stk39	2.71	2.21E-06	Y	Y
Fam3c	2.65	6.40E-09	Y	Y
Pgk1	2.61	1.23E-03	Y	Y
Cacnb3	2.59	3.70E-02	Gains and losses	Y
Tnfrsf21	2.57	1.58E-03	Y	Y
Fmo1	2.57	7.51E-03	Y > 10%	Y
S100a11	2.53	1.21E-04	Y >20%	weak
Ceacam1	2.50	1.08E-05	Y	Y

Table 5-1 Genes that were included in the siRNA screen

Genes that were found significantly (FDR<0.05) upregulated in the p-Erk positive R26^{DM}.Isl⁻ MYC/MYC;KRas^{G12D} tumour regions were sorted by fold change. Genes that have been reported to be amplified (cBioportal) and/or overexpressed (Oncomine) were selected. From this selection the 51 genes with the highest Fold Change were included in the screen.

Looking at the individual siRNAs targeting the same gene it can be seen that the loss of viability is highly variable for most genes (Table 5-2). This might be due to differences in knockdown efficiency or to off-target effects.

In order to make use of the additional information obtained by deconvoluting the siRNAs, I looked at the siRNAs that caused a loss of viability that was bigger than the average loss (Figure 5-13). For each cell line, the average loss of viability from all 51 genes and all 4 siRNAs for each gene was calculated. In the analysis I did not only consider how many siRNAs against a certain gene caused loss of viability, but also how consistent that was across multiple cell lines. Genes that play a role in cell viability for a variety of cell lines with different sets of mutations are the most interesting targets for therapy. Therefore only siRNAs that resulted in a loss of viability bigger than the mean loss in 2 or more of the tested cell lines were included in the analysis.

Figure 5-13 shows the loss of viability for each individual cell line. The graph in Figure 5-14 contains data from all 3 cell lines. In order to rank the genes by their effect on viability, a scoring system was used. siRNAs that caused more than average loss of viability in 2 cell lines, were scored as 1, the ones that did the same in all 3 cell lines were scored as 2. For each gene the score was calculated by summing up the scores of the siRNAs that caused more than average loss of viability. For the graph genes were first sorted by mean loss of viability and then by their score (Table 5-2). The gene with the highest score (7) is flavin containing monooxygenase 1 (*FMO1*), 3 siRNAs caused more than average loss of viability in all 3 cell lines and the 4th one in 2 cell lines. The effect on cell viability is about 50%. Kinesin family member 23 (*KIF23*) has a score of 6 and knockdown results in loss of viability of more than 70%. As the effect of *FMO1* and *KIF23* knockdown was very strong and consistent across the cell lines, it would be interesting to see if this is specific for *KRAS* mutant cancer cell lines and also if the knockdown of *KIF23* affects normal cells.

siRNA Viability screen in KRas mutant NSCLC cell lines

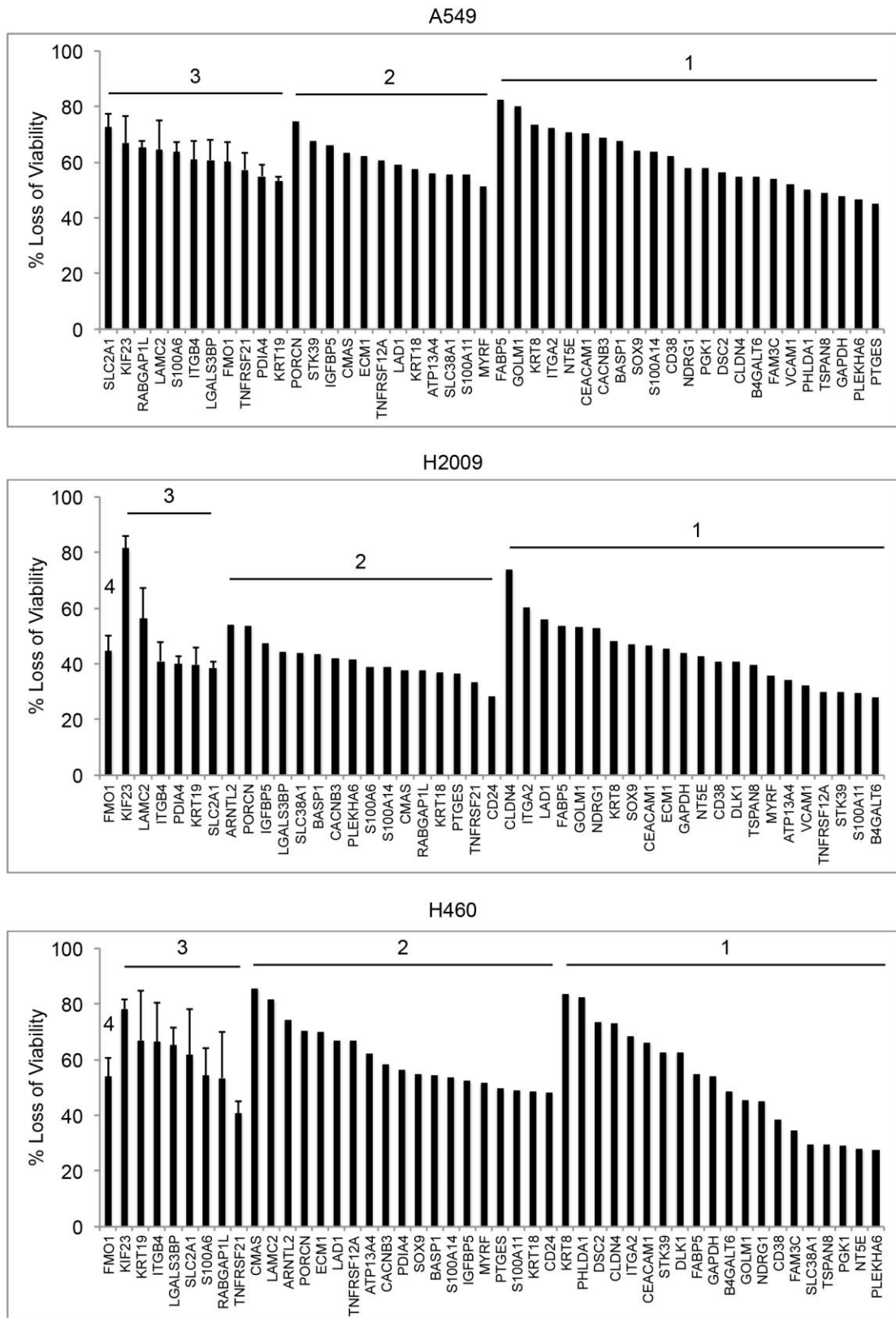


Figure 5-13 Viability screen human KRas mutant lung cancer cell lines.

4 individual siRNAs for each gene knockdown were used. siRNAs that resulted in loss of viability > mean loss in at least two of the three tested cell lines were included in the graph. Genes were sorted by number of siRNAs they are represented by (indicated by numbers 1-4 in the graph) and by loss of viability. Mean loss of viability for the individual cell lines: A549: 42.3%, H2009: 26.0% and H460: 27.7%. Error bars represent Standard Error.

Gene Symbol	A549			
	Sequence 1 - MEDIAN	Sequence 2 - MEDIAN	Sequence 3 - MEDIAN	Sequence 4 - MEDIAN
ARNTL2	51.10	30.30	31.23	16.54
ATP13A4	53.80	-21.15	58.35	37.38
ATP6V1G3	13.75	12.94	25.05	25.14
B4GALT6	43.99	54.82	56.91	55.97
BASP1	34.97	15.85	67.77	18.48
CACNB3	68.97	29.82	42.03	34.39
CD24	38.20	33.83	36.08	41.57
CD38	59.96	-10.02	62.12	28.34
CEACAM1	49.40	21.93	64.71	70.43
CLDN4	42.93	36.45	54.85	41.43
CMAS	69.34	58.30	33.33	57.03
DLK1	59.09	41.59	37.56	22.80
DSC2	45.29	22.65	56.19	36.00
ECM1	56.01	58.01	43.23	68.26
EREG	33.51	54.89	34.76	-10.94
FABP5	-22.05	42.49	82.57	41.43
FAM3C	48.32	54.12	14.52	26.87
FMO1	41.06	48.66	58.32	73.33
GAPDH	47.80	48.12	40.25	25.49
GOLM1	-42.16	-18.02	80.24	42.52
IGFBP5	71.48	60.67	44.80	34.01
ITGA2	19.09	72.34	58.71	33.76
ITGB4	47.78	39.42	68.32	66.76
KIF23	58.64	86.47	55.76	-31.39
KRT18	30.77	59.34	65.94	49.47
KRT19	26.39	55.28	54.42	50.14
KRT8	73.46	38.19	41.90	6.95
LAD1	33.52	30.28	70.58	47.52
LAMC2	78.63	67.04	48.02	22.49
LGALS3BP	59.74	48.62	74.08	49.36
MYRF	48.02	37.54	54.56	52.68
NDRG1	14.89	1.94	58.10	7.85
NT5E	70.62	18.36	36.28	11.80
PDIA4	54.32	47.95	62.69	55.54
PGK1	39.95	57.99	29.29	20.17
PHLDA1	-0.91	20.72	22.49	49.97
PLEKHA6	21.65	36.56	46.60	-2.26
PORCN	58.06	47.70	91.51	20.79
PTGES	25.06	45.07	22.88	23.30
RABGAP1L	27.49	61.24	64.66	69.73
S100A11	51.42	59.47	43.94	50.60
S100A14	33.64	-5.58	22.16	63.92
S100A6	57.58	69.84	38.23	63.60
SLC2A1	82.23	68.66	52.30	67.24
SLC38A1	28.31	53.22	9.13	57.85
SOX9	8.93	33.53	64.01	14.38
STK39	62.50	72.68	45.07	29.78
TNFRSF12A	60.10	60.91	34.61	50.93
TNFRSF21	43.63	54.87	68.77	48.19
TSPAN8	14.76	32.30	21.98	48.90
VCAM1	26.34	52.23	36.10	30.72

Gene Symbol	H2009			
	Sequence 1 - MEDIAN	Sequence 2 - MEDIAN	Sequence 3 - MEDIAN	Sequence 4 - MEDIAN
ARNTL2	22.89	65.31	42.81	11.78
ATP13A4	34.36	-5.54	18.17	40.20
ATP6V1G3	15.93	7.51	13.00	-1.21
B4GALT6	10.18	27.98	19.44	19.86
BASP1	39.55	38.02	47.40	19.90
CACNB3	45.09	8.33	38.80	20.29
CD24	17.21	28.02	15.68	28.82
CD38	7.81	-7.67	40.84	11.91
CEACAM1	3.88	11.46	19.38	46.53
CLDN4	18.01	35.27	73.79	24.38
CMAS	36.58	22.36	25.11	38.72
DLK1	22.28	40.68	15.22	20.51
DSC2	9.65	12.62	9.60	24.90
ECM1	45.30	32.94	11.62	24.35
EREG	21.23	0.22	6.63	-4.72
FABP5	-4.56	22.48	53.73	14.82
FAM3C	13.44	24.00	9.33	8.59
FMO1	39.46	37.97	40.07	61.22
GAPDH	43.71	25.87	8.56	21.24
GOLM1	18.69	-1.61	53.13	19.08
IGFBP5	55.00	40.03	19.62	18.12
ITGA2	5.83	60.29	4.18	-1.86
ITGB4	27.52	37.23	46.84	48.56
KIF23	73.20	83.26	88.04	-12.50
KRT18	9.61	17.41	47.56	26.14
KRT19	15.53	37.38	51.16	30.54
KRT8	48.20	30.33	17.72	-6.98
LAD1	12.22	-0.83	56.06	15.47
LAMC2	61.89	71.82	35.00	31.88
LGALS3BP	49.03	39.88	24.78	26.99
MYRF	25.76	33.34	35.83	2.33
NDRG1	22.79	6.70	52.85	11.88
NT5E	42.82	20.57	43.86	13.83
PDIA4	34.97	42.85	42.41	0.42
PGK1	15.77	9.09	15.47	15.21
PHLDA1	20.29	15.71	0.81	23.49
PLEKHA6	24.60	57.08	26.01	7.73
PORCN	59.87	12.62	47.71	4.72
PTGES	25.56	38.76	34.05	7.45
RABGAP1L	28.91	21.80	34.96	40.01
S100A11	13.18	29.66	0.12	2.56
S100A14	46.72	21.33	12.65	30.68
S100A6	25.28	47.49	32.36	30.18
SLC2A1	36.87	43.26	22.39	35.53
SLC38A1	10.44	45.96	7.94	41.68
SOX9	5.18	47.17	29.21	34.52
STK39	15.22	29.89	18.75	24.03
TNFRSF12A	19.61	29.92	-6.57	14.27
TNFRSF21	11.50	31.82	34.76	18.63
TSPAN8	6.80	-1.50	27.06	39.51
VCAM1	25.49	32.14	-2.63	13.40

Gene Symbol	H460			
	Sequence 1 - MEDIAN	Sequence 2 - MEDIAN	Sequence 3 - MEDIAN	Sequence 4 - MEDIAN
ARNTL2	2.17	74.04	74.79	16.25
ATP13A4	89.28	-25.36	35.06	-3.21
ATP6V1G3	13.86	-3.07	-30.34	30.82
B4GALT6	-10.94	48.71	16.65	-1.65
BASP1	43.08	15.08	65.82	19.71
CACNB3	44.43	22.87	72.51	60.27
CD24	17.08	41.61	-8.11	54.70
CD38	21.67	-48.71	38.61	1.75
CEACAM1	9.93	-9.53	21.89	66.15
CLDN4	12.37	18.22	72.96	54.07
CMAS	90.71	-2.41	16.89	80.73
DLK1	7.94	62.66	7.92	37.73
DSC2	8.82	12.07	73.49	54.92
ECM1	83.92	21.64	3.51	56.00
EREG	17.45	16.88	66.94	-39.29
FABP5	-39.22	3.75	54.80	57.03
FAM3C	12.24	34.42	-26.86	-23.58
FMO1	66.98	48.01	62.57	38.43
GAPDH	54.03	-5.27	0.19	-16.24
GOLM1	37.52	-35.77	45.48	-10.40
IGFBP5	57.19	47.95	-6.39	0.54
ITGA2	-25.13	68.55	4.37	-5.96
ITGB4	55.26	14.56	94.03	50.21
KIF23	72.92	77.24	84.54	-47.00
KRT18	-27.40	27.66	60.17	37.30
KRT19	-8.60	84.72	31.43	84.62
KRT8	83.72	27.37	71.18	-8.31
LAD1	21.17	-5.58	86.63	47.32
LAMC2	94.71	68.25	23.29	5.92
LGALS3BP	72.65	70.70	52.04	9.95
MYRF	70.03	6.63	33.16	19.68
NDRG1	7.29	-15.56	45.05	8.80
NT5E	27.82	37.04	17.04	-1.51
PDIA4	17.82	59.30	53.40	7.07
PGK1	4.80	29.09	5.89	-2.54
PHLDA1	34.52	43.62	-28.95	82.29
PLEKHA6	22.72	27.70	25.61	32.06
PORCN	57.48	-12.58	83.25	-22.07
PTGES	-0.44	66.41	32.72	-16.37
RABGAP1L	24.72	28.59	46.27	85.26
S100A11	30.23	67.84	-7.72	6.29
S100A14	57.03	-1.83	-10.37	50.40
S100A6	43.42	73.77	-8.69	45.59
SLC2A1	78.13	77.84	26.39	28.91
SLC38A1	35.35	29.34	-19.10	16.14
SOX9	-8.80	37.02	72.85	17.27
STK39	62.71	17.76	-7.55	6.72
TNFRSF12A	42.20	91.49	1.75	-8.65
TNFRSF21	3.11	32.24	44.14	46.06
TSPAN8	-46.47	-12.09	-1.20	29.33
VCAM1	-48.48	26.90	-22.97	-16.83

Gene Symbol	Sequence 1	Sequence 2	Sequence 3	Sequence 4	Score
ARNTL2	0	1	1	0	2
ATP13A4	2	0	1	0	3
ATP6V1G3	0	0	0	0	0
B4GALT6	0	2	0	0	2
BASP1	1	0	2	0	3
CACNB3	2	0	1	0	3
CD24	0	1	0	1	2
CD38	0	0	2	0	2
CEACAM1	0	0	0	2	2
CLDN4	0	0	2	0	2
CMAS	2	0	0	2	4
DLK1	0	1	0	0	1
DSC2	0	0	1	0	1
ECM1	2	0	0	1	3
EREG	0	0	0	0	0
FABP5	0	0	2	0	2
FAM3C	0	1	0	0	1
FMO1	1	2	2	2	7
GAPDH	2	0	0	0	2
GOLM1	0	0	2	0	2
IGFBP5	2	2	0	0	4
ITGA2	0	2	0	0	2
ITGB4	2	0	2	2	6
KIF23	2	2	2	0	6
KRT18	0	0	2	2	4
KRT19	0	2	2	2	6
KRT8	2	0	0	0	2
LAD1	0	0	2	0	2
LAMC2	2	2	1	0	5
LGALS3BP	2	2	1	0	5
MYRF	1	0	2	0	3
NDRG1	0	0	2	0	2
NT5E	2	0	0	0	2
PDIA4	1	2	2	0	5
PGK1	0	1	0	0	1
PHLDA1	0	0	0	1	1
PLEKHA6	0	1	1	0	2
PORCN	2	0	2	0	4
PTGES	0	2	1	0	3
RABGAP1L	0	1	2	2	5
S100A11	1	2	0	0	3
S100A14	1	0	0	2	3
S100A6	1	2	0	2	5
SLC2A1	2	2	0	2	6
SLC38A1	0	2	0	1	3
SOX9	0	1	1	0	2
STK39	1	1	0	0	2
TNFRSF12A	1	2	0	0	3
TNFRSF21	0	2	2	1	5
TSPAN8	0	0	0	2	2
VCAM1	0	1	0	0	1

Table 5-2 Viability data of the KRas mutant human lung Adenocarcinoma cell lines A549, H2009 and H460.

Loss of Viability was calculated based on the cell number relative to non-targeting control (NTC) 72h after transfection. Individual values of each siRNA are shown, Loss of Viability > mean Loss of Viability are highlighted in yellow if Loss of Viability was only > mean Loss of Viability in the shown cell line, highlighted in green if Loss of Viability > mean Loss of Viability in 1 further cell line (assigned a score of a) and highlighted in red if Loss of Viability > mean Loss of Viability in all three cell lines (assigned a score of 2). Scores of individual siRNAs were summed up for each gene.

Solute carrier family 2, member 1 (*SLC2A1*), integrin beta 4 (*ITGB4*) and keratin 19 (*KRT19*) have a score of 6 and knockdown has a robust effect on cell viability with an average loss of more than 50% for all 3 genes. Laminin gamma 2 (*LAMC2*) and *PORCN* knockdown affect cell viability with about 65% with still good scores of 5 and 4, respectively.

Summarized viability screen of 3 KRas mutant NSCLC cell lines

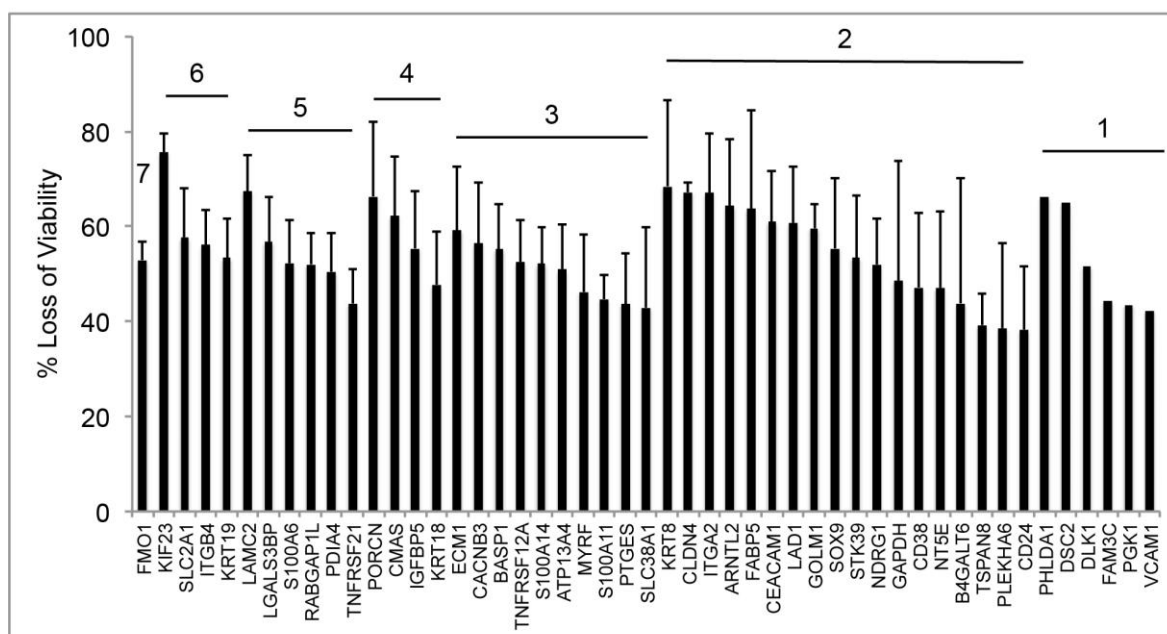


Figure 5-14 Summarized Viability of human KRas mutant lung cancer cell lines.

4 individual siRNAs for each gene knockdown were used. siRNAs that resulted in loss of viability > mean loss in at least two of the three tested cell lines were included in the graph. Numbers represent a score: siRNAs that caused loss of viability > mean loss in all three cell lines received a score of 2, in two cell lines received a score of 1. Scores of individual siRNAs were summed up for each gene. Genes were sorted by score and by loss of viability. Knockdown of FMO1, KIF23, SLC2A1, ITGB4, KRT19, LAMC2 and PORCN caused the highest loss of viability with a good consistency among the cell lines. Mean loss of viability for the individual cell lines: A549: 42.3%, H2009: 26.0% and H460: 27.7%. Error bars represent Standard Error.

Keratin 8 (*KRT8*), claudin4 (*CLDN4*), integrin alpha 2 (*ITGA2*), pleckstrin homology domain containing, family A member 6 (*PHLDA1*) and desmocollin 2 (*DSC2*) have with about 65% average loss of viability a strong effect, however it is less consistent in terms of number of siRNAs and consistency across the cell lines, therefore the knockdown needs to be confirmed for these 5 genes.

To summarize the effect of knockdown of the 51 selected genes, *FMO1*, *KIF23*, *SLC2A1*, *ITGB4*, *KRT19*, *LAMC2* and *PORCN* cause the highest loss of viability in *KRAS* mutant human lung Adenocarcinoma cell lines with a good consistency among all tested cell lines. *KRT8*, *CLDN4*, *ITGA2*, *PHLDA1* and *DSC2* might be relevant for cell viability of these cells, but the knockdown has to be confirmed.

Migration screen

As readout for migration 48h after transfection a scratch was made through a confluent monolayer of cells. Using long-term time lapse Incucyte video-microscopy, wound closure was monitored over time and the wound width relative to the initial scratch was calculated. The experimental setup is based on the effect of contact inhibition that blocks cell proliferation once cells are confluent (McClatchey and Yap, 2012). Over-confluency is problematic as well, as the pin of the wound maker then tends to pull out cells next to the wound and cells adjacent to the scratch might be uplifted. It is therefore crucial that the scratch is made through a cell monolayer that is 100% confluent. If cells are less confluent, wound closure might occur as a result of cell proliferation.

The migration screen was performed with 2 cell lines that migrate efficiently: A549 and H2009. H460 could not be screened for migration, as they hardly migrate at all.

Analysing the migration screen data was a challenge as many siRNAs had a strong effect on cell viability. Cells that are less viable as a result of cell death or lack of cell proliferation might be less motile and migrate less. Moreover, less viable cells are likely to be less confluent at the time of the scratch (cell number was optimized for NTC), which can influence the result of the migration assay. As a transfection control we used “Allstars for cell death”, a mixture of siRNAs that targets key regulators of cell viability and kills most transfected cells. Allstars transfected wells which contained hardly any cells always gave very random relative wound density (RWD) values, confirming that cells with a big loss of viability give unreliable results.

Nevertheless I first had a look at the overall results including all siRNAs. In the migration assay viability based on nuclei count was again determined at the end of the experiment. The results were different from the viability screen with a much lower average loss of viability. This is probably because the cells are seeded and transfected at a much higher density for the migration assay. This is likely to

decrease the transfection efficiency (even though transfection efficiency was high enough to kill the Allstars transfected cells) and moreover, more confluent cells might need stronger effects to lose viability.

Loss of Viability and migration in siRNA screen

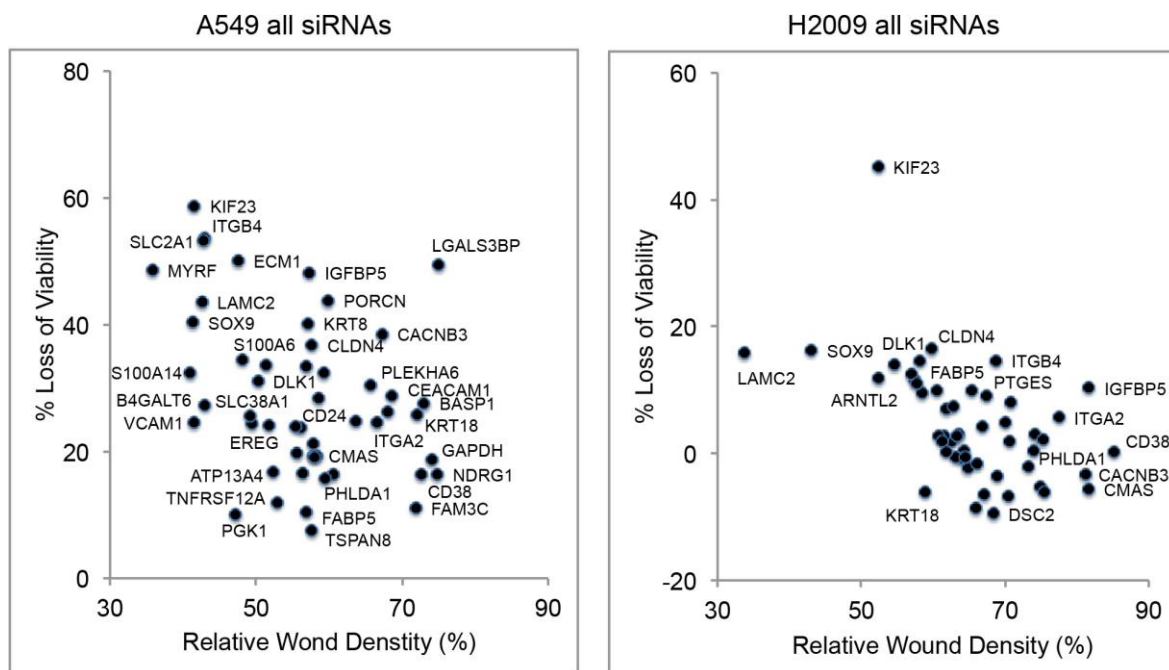


Figure 5-15 Migration screen human KRAs mutant lung cancer cell lines.

4 individual siRNAs for each gene knockdown were used. All siRNAs were included in the graph. Mean Loss of Viability was plotted against mean Relative Wound density for each gene. In the A549 cells knockdown of MYRF, KIF23, ITGB4, SLC2A1, LAMC2, SOX9, S100A14, B4GALT6 and VCAM1 had the strongest effect on RWD. In the H2009 cells knockdown of KIF23, DLK1, ARNTL2, Sox9 and LAMC2 had the strongest effect on RWD.

In Figure 5-15 viability is plotted against relative wound density (RWD) for both cell lines individually. In the A549 cell line myelin regulatory factor (*MYRF*), *KIF23*, *ITGB4*, *SLC2A1*, *LAMC2*, *SOX9*, S100 calcium binding protein A4 (*S100A4*), UDP-Gal:betaGlcNAc beta 1,4-galactosyltransferase, polypeptide 6 (*B4GALT6*) and vascular cell adhesion molecule 1 (*VCAM1*) siRNAs have the strongest effect on RWD. Several of them had also a high score in the viability screen and *MYRF* siRNAs reduced viability with an average of almost 50%. Knockdown of *S100A14*, *B4GALT6* and *VCAM* cause only moderate loss of viability, so knockdown of these 3 genes seem to inhibit migration without considerably affecting viability. Then on the other hand there is lectin, galactoside-binding, soluble, 3 binding protein (*LGALS3BP*), whose knockdown causes a big loss of viability, but according to the RWD value they seem to migrate fine.

Migration screen without siRNAs that cause >30% loss of viability

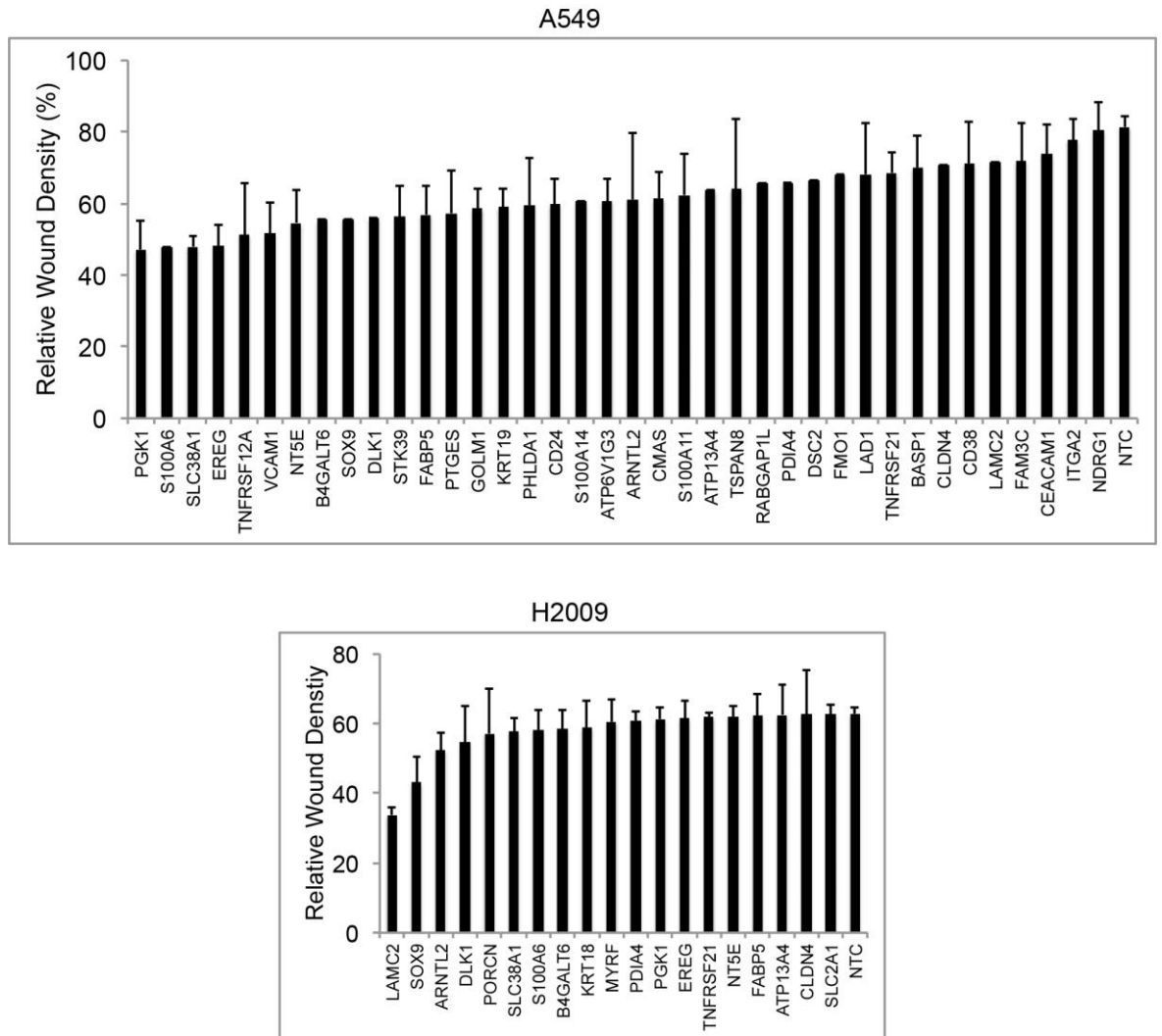


Figure 5-16 Migration without Loss of Viability > 30%.

4 individual siRNAs for each gene knockdown were used. siRNAs that caused Loss of Viability > 30% were excluded from the graph. Mean Loss of Viability > non-targeting control (NTC) is shown. A549: MYRF, KIF23, ITGB4 and SLC2A1 disappeared from the graph because low RWD was due to high loss of viability. RWD values for SOX9, B4GALT6 and VCAM remained low. H2009: KIF23 was removed due to high loss of viability, RWD of DLK1, ARNTL2, SOX9 and LAMC2 did not change. N>=2, Error bars represent Standard Error and are shown for n>=3.

In the H2009 cell line *KIF23*, delta-like 1 homolog (*DLK1*), aryl hydrocarbon receptor nuclear translocator-like 2 (*ARNTL2*), *SOX9* and *LAMC2* siRNAs reduce the RWD considerably. In the migration screen loss of viability was low for the vast majority of siRNAs and *KIF23* is the only one with a high average loss of viability of more than 40%. Therefore the low RWD of the other 4 genes appears to be solely due to migration inhibition.

Combined migration graph

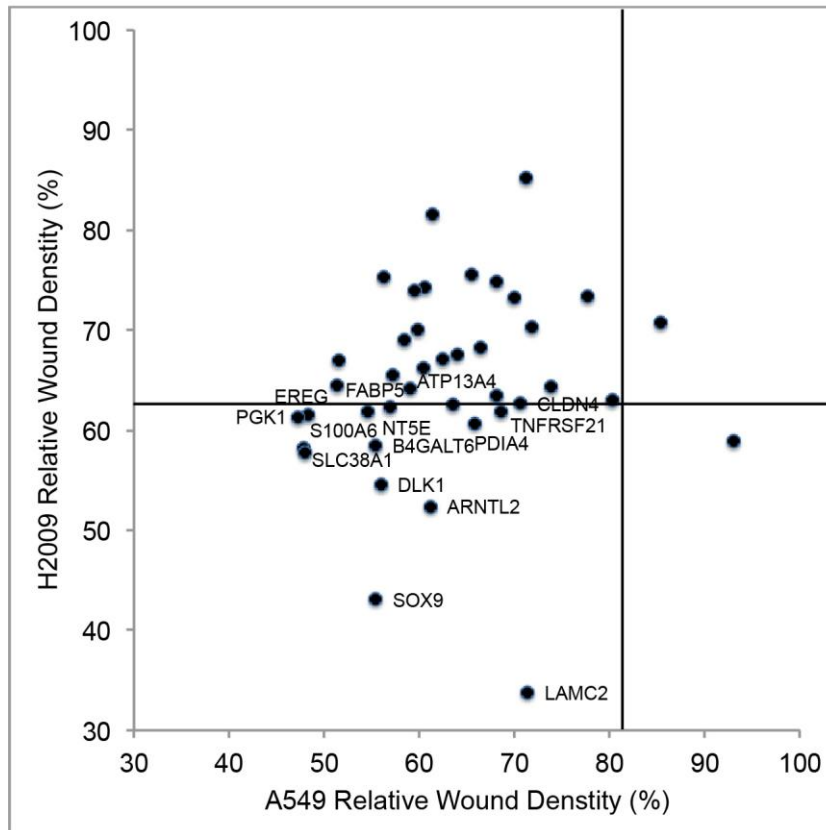


Figure 5-17 Combined migration graph.

4 individual siRNAs for each gene knockdown were used. Relative wound density from all genes are shown. siRNAs that caused more than 30% loss of viability were excluded from the graph. Lines indicate respective Relative Wound Density of non-targeting control. Knockdown of SOX9, DLK1 and ARNTL2 had the strongest effects in both cell lines. N>=2.

In order to account for an influence of viability loss on RWD data, I excluded all siRNAs that caused more than 30% of viability and only included genes that were then still represented by 2 or more siRNAs. 30% is an arbitrarily chosen number, assuming that a loss of viability up to 30% does not have too dramatic effects on the migration assay. The upper panel in Figure 5-16 shows for A549 the RWDs that are lower than the NTC. *MYRF*, *KIF23*, *ITGB4* and *SLC2A1* disappeared because only the siRNAs that caused high loss of viability gave rise to low RWD numbers. *LAMC2* and S100 calcium binding protein A14 (*S100A14*) RWD values are still below NTC, but much higher than before removing the siRNAs that cause high loss of viability. *SOX9*, *B4GALT6* and *VCAM* siRNAs still give rise to low RWD numbers below 60%, which is much lower than NTC (~80%). Possibly, the siRNAs that cause loss of viability result in a stronger knockdown than the ones that only inhibit migration, but this speculation needs to be confirmed by testing the knockdown of the individual siRNAs. Besides these 3 genes knockdown of phosphoglycerate kinase 1 (*PGK1*), S100 calcium binding protein A6 (*S100A6*), solute carrier family

38, member 1 (*SLC38A1*), *EREG* and tumor necrosis factor receptor superfamily, member 12a (*TNFRSF12A*) cause the strongest reduction in RWD.

The lower panel in Figure 5-16 shows for H2009 the RWDs that are lower than the NTC. This was the case for a relatively small number of genes many siRNAs resulted in a RWD higher than NTC. It might have been better to run the assay for longer. According to previous experiments the H2009 migrated very quickly, this is why the assay was stopped after 20h. But by then the NTC wound was only about 60% closed. A better wound closure probably would have given a better separation of the individual genes. As only *KIF23* was removed from the analysis, the values for *DLK1*, *ARNTL2*, *SOX9* and *LAMC2* did not change.

Looking at the combined RWD graph for both cell lines, *SOX9*, *DLK1* and *ARNTL2* siRNAs reduced RWD considerably in both cell lines (Figure 5-17). Knockdown needs to be confirmed to exclude the possibility of a non-target effect.

5.3 Discussion

Treatment of *KRas* mutant cancer with EGFR inhibitors is controversial, as mutations, which lead to constitutive KRas signalling are thought to make the cell independent from upstream signalling. Moreover, treatment of *KRAS* mutant lung cancer with EGFR inhibitor has proven to have no benefit for the patients (Pao et al., 2005). However, we observed that in a subset of *R26^{DM}.Isl-MYC/MYC;KRas^{G12D}* driven tumours p-Erk positive regions are emerging, suggesting that KRas downstream signalling is higher in these subpopulations. The RNA sequencing data revealed that high levels of ErbB family ligands are associated with p-Erk positivity in these tumours. As these ligands do not only bind EGFR but also to the three other ErbB family members and heterodimers, all 4 ErbB family members might contribute to further activation of the MAPK pathway (Figure 5-18).

Treatment with the pan-ErbB inhibitor Neratinib confirmed that most tested *KRAS* mutant cell lines are sensitive to pan-ErbB inhibition. It would be interesting to investigate which additional mutations favour or disfavour treatment outcome. In the siRNA screen knockdown of *EREG* had no strong effect on viability in the human cell lines. *EREG* knockdown does inhibit migration in the A549, but not in H2009. It is possible, that by inhibiting *EREG* alone cells are not greatly affected, as they

might be able to compensate its loss by upregulating other pan-ErbB ligands. This would explain why Neratinib treatment had a stronger effect on viability and migration in the tested cell lines.

In vivo preliminary data suggest that Neratinib treatment interferes with tumour formation in the $R26^{DM.lsl-MYC/MYC};KRas^{G12D}$ model. The number of treated mice will be increased to confirm this and as an additional control experiment, mice are currently being treated with the EGFR inhibitor Erlotinib, to investigate if pan-ErbB inhibition is indeed more effective than EGFR inhibition alone. This experiment is currently ongoing.

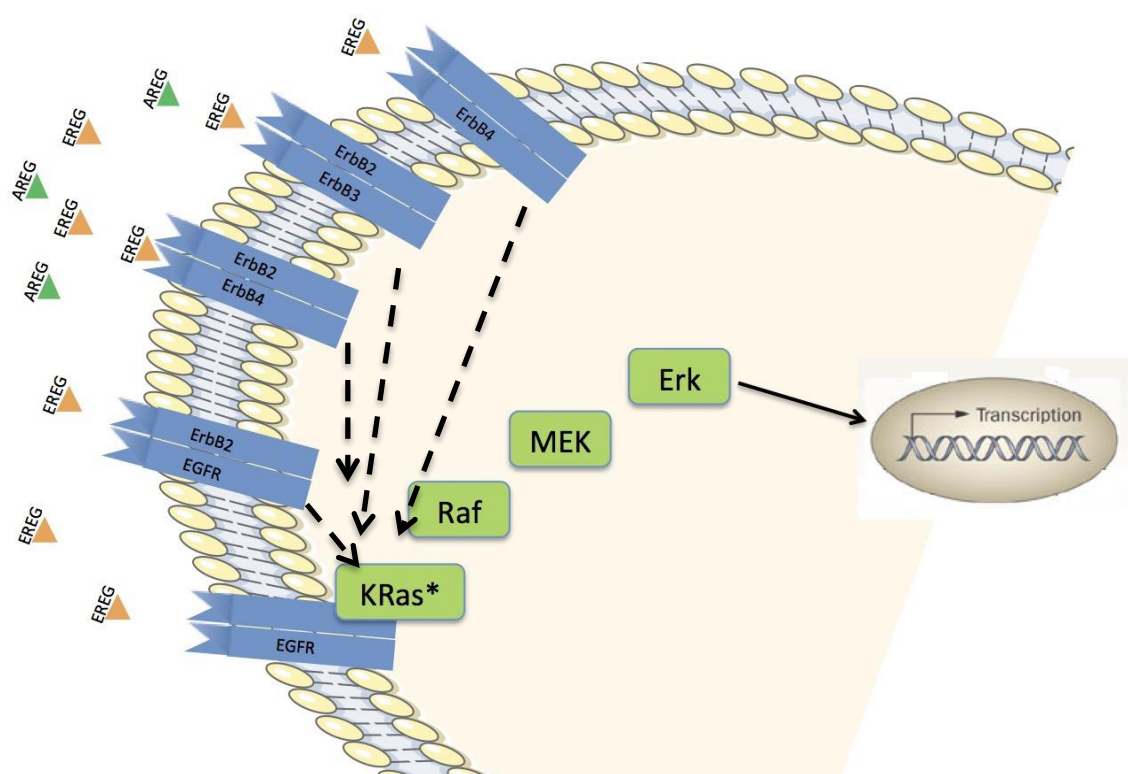


Figure 5-18 Model of how pan ErbB family ligands contribute to MAPK signalling. Ereg can bind and activate EGFR and ErbB4 homodimers and to all heterodimers of the 4 ErbB family members. Increased signalling through all ErbB family members would explain why part of the KRas mutant tumours present increased p-Erk signal.

Inhibition of Wnt signalling *in vitro* proved to inhibit migration and cell confluency in multiple *KRAS* mutant cell lines. *PORCN* siRNA knockdown decreased viability in all three human cell lines, prominently in the A549. *SOX9* knockdown had only a weak effect on cell viability, but strongly inhibited migration in the A549 and H2009. The importance of Wnt signalling for lung cancer has been shown recently in a *BRaf* driven mouse model (Juan et al., 2014). Treatment with LGK974 prevented tumour formation, which was rescued by sustained *Myc* or stabilized β -*catenin* expression.

The *Braf* and *KRas* models differ, as *KRas* activates MAPK and PI3K signalling and *Braf* activates only MAPK signalling. *Braf* mutant lung tumours become senescent and stop proliferating soon after tumour formation, whereas *KRas* mutant lung tumours do not become senescent. Moreover in the *Braf* model *Myc* overexpression helps the tumour to overcome senescence. The observation that inhibition of tumour formation by Porcupine inhibition is rescued by downstream actors *Myc* and β -catenin, might explain why Porcupine inhibition had no effect on proliferation or p-Erk positivity in the $R26^{DM.lsl-MYC/MYC};KRas^{G12D}$ model. Deregulated *Myc* expression might make the tumour independent from upstream inhibition. On the other hand, I showed that $R26^{DM.lsl-MYC/WT};KRas^{G12D}$ cells are sensitive to Porcupine inhibition *in vitro*. Treatment outcomes *in vivo* can be very different from *in vitro*, as the organism adds many additional factors, such as immune system and tumour environment.

Therefore even though both pathways are associated with tumour progression in our model, Porcupine inhibition might not increase the effect of ErbB inhibition alone. Instead, inhibition of *Myc* downstream effectors might be more efficient.

In order to show that the two inhibitors indeed inhibit the respective pathways, it would be good to show a cellular response on protein level. *Sox9* and *Myc* are both Wnt targets, therefore they are expected to decrease after LGK974 treatment. In the LGK974 resistant cell lines H358 and H441 Wnt targets might not go down because the cells found a way to circumvent pathway inhibition. Moreover protein levels of Wnt targets after higher LGK974 concentrations could be determined, as the H358 and H441 cell lines might be sensitive to higher LGK974 concentrations, which is also suggested by the drug titration (Figure 5-3). Also it would be good to determine *in vivo* by IHC if the levels of the Wnt targets *Sox9* and *Myc* decrease upon LGK974 treatment.

In order to show evidence of inhibition of ErbB signalling, the levels of phosphorylated ErbB receptors could be determined. Phosphorylation of EGFR at Tyr1068 for instance activates EGFR and the downstream MAPK pathway (Rojas et al., 1996). Downstream of the ErbB receptors, phosphorylation of members of the MAPK pathway, such as Erk1/2 phosphorylation at Tyr202/Tyr204 could be measured. Moreover, determining Epiregulin levels would be important, as oncogenic *KRas* has been shown to induce Epiregulin expression (Sunaga et al., 2013). Epiregulin itself on the other hand binds to ErbB family members and

contributes in this way to MAPK signalling. Therefore downregulation of Epiregulin by ErbB inhibition would confirm its role as an oncogenic MAPK signalling target. A good cell line to start with would be H358, as it has been shown to have high Epiregulin levels and Epiregulin levels have been shown to go down upon knockdown of mutant *KRas* (Sunaga et al., 2013). In the Neratinib resistant cell lines H460 and A427 however, MAPK signalling might not be inhibited, which could explain resistance to Neratinib, if this is the case. *In vivo*, Neratinib treatment of *R26^{DM, Isl1-MYC/MYC; KRas^{G12D}}* for two weeks starting 4 weeks after allele induction could not suppress p-Erk positivity. In order to test if the inhibitor is at least able to inhibit phosphorylation of the ErbB receptors, tumours could be stained by IHC using phospho-specific antibodies.

In addition to the ErbB and Wnt pathways, I validated several individual p-Erk associated genes that showed effects in our *in vitro* analyses. I then examined the literature in order to find out if their role in viability and or migration has been reported before or if there is a functional explanation.

Kif23 is a member of the kinesin-like protein family. Kinesins are involved in organelle transport along the microtubule and chromosome movement during cell division (Hornick et al., 2010; Neef et al., 2006). It has been shown that Kif23 downregulation reduces proliferation of glioma cells (Takahashi et al., 2012), confirming its role in cell division. Moreover, *KIF23* mutations are associated with a disease called congenital dyserythropoietic anemia type III, arising from defects in erythropoiesis probably due to proliferative defects in erythrocyte precursor cells (Liljeholm et al., 2013). The crucial role in cell proliferation would explain the dramatic decrease in cell number caused by *KIF23* knockdown. In the sequencing data, the p-Erk negative samples had an average *Kif23* transcript read count of >200, suggesting that the gene is essential in proliferating cells. Before considering KIF as a potential therapeutic target it will be important to test its knockdown in normal, untransformed cells.

Three isoforms of FMOs exist. Fmo1 is primarily expressed in fetal liver and Fmo2 in adult liver. FMOs are involved in N-oxidation of trimethylamines, a reaction that stabilizes proteins and has been shown to protect proteins from Urea denaturing effects (Ganguly, 2015).

Slc2a1 is also called glucose transporter protein type 1 (Glut1). It is located in the plasma membrane and facilitates glucose import into the cell (Olson and Pessin, 1996). Cancer cells are highly dependent on glucose and an increased glycolytic metabolism is associated with cancer progression (Pertega-Gomes et al., 2015; Vander Heiden et al., 2009; Ward and Thompson, 2012). The effect on cell viability by knocking down this transporter highlights the dependence on glucose metabolism.

Itbg4 is a receptor for laminins and high expression is associated with cancer invasion and migration (Masugi et al., 2015; Yang et al., 2013).

Krt19 belongs to the keratin family and is a type I cytokeratin, which are acidic and usually form heterodimers with basic dimers. The small Keratin 19 is an exception, as it does not dimerize (Moll et al., 1982). Keratins are important for epithelial structure and Keratin 19 serves as an epithelial cell marker.

Dlk1 is an EGF repeat containing transmembrane protein that gets cleaved by tumour necrosis factor alpha converting enzyme (TACE), which generates a soluble form of Dlk1 (Wang and Sul, 2006). Dlk1 is expressed in preadipocytes and inhibits adipocyte differentiation (Smas et al., 1997). It was shown in MEFs that inhibition of adipocyte differentiation is due to MEK/ERK activation (Kim et al., 2007). Interestingly MEK/ERK pathway activation through Dlk1 upregulates Sox9 (Wang and Sul, 2009). Sox9 is a Wnt target, which is involved in chondrogenesis and osteogenesis. The fact that Dlk1 and Sox9 were both among the top hits in the migration screen supports each other's role in cell migration. Sox9 is a Wnt target, whereas Porcn is crucial for Wnt secretion and thereby much further upstream than Sox9. Interestingly Porcn was in our setting more important for cell viability than migration. But as mentioned before these two characteristics influence each other and cannot be clearly separated, at least not in the used experimental setup.

Arntl2 is a basic helix-loop-helix transcription factor and is likely to play a role in circadian clock regulation (Hogenesch et al., 2000).

Laminins are extracellular glycoproteins and make up the major noncollagenous component of basement membranes (Malinda and Kleinman, 1996). They are composed of alpha, beta and gamma chains. Different alpha, beta and gamma

chains are combined to form heterotrimeric isoforms. Lamc2 is found in lung, skin and kidney epithelial cells. It was recently shown in a xenograft model that Lamc2 enhances the metastatic potential of A549 cells (Moon et al., 2015).

The genes that were shortlisted in the viability and migration screen give clues about which genes may play a role in tumour progression. Thereby the screen helped to narrow down the list of genes for *in vivo* investigation. However genes that did not score high in our screen might still be important for tumour progression in a different experimental setting or in different cell lines. Therefore *in vivo* investigation is clearly needed to confirm the importance of these genes in tumour progression.

I was able to generate a cell line from $R26^{DM.lsl-MYC/WT};KRas^{G12D}$ tumours. As an internal validation, it would have been useful to also screen this cell line. Validation of the p-Erk upregulated genes in the same genetic background as the tumours that the data were derived from would confirm that the p-Erk positive tumour cells depend on high expression of these genes. I hypothesize that the cells that survived and were able to propagate in culture are at least partly derived from p-Erk positive tumours. P-Erk could be detected in protein lysates from these cells, confirming that the cells are at least partially p-Erk positive (not shown).

We actually attempted to screen the $R26^{DM.lsl-MYC/WT};KRas^{G12D}$ tumour derived 567T3 cell line. However, the average loss of viability upon siRNA treatment was very low in the 567T3 cells compared to the loss of viability in the human cell lines. 567T3 cells proved difficult to transfect, therefore it is possible that the knockdown was not as efficient as it could have been with a higher transfection rate. The poor transfection rate did not generate any useful data. However, I think the fact that a significant number of genes seem to be important for viability and migration of even genetically unrelated (apart from the *KRas* mutation) human lung cancer cell lines, suggests that these gene have a role in tumour progression of *KRas* mutant cancer.

6 Final discussion and future directions

6.1 The role of moderately deregulated MYC expression in the lung

I showed that low levels of deregulated *MYC* expression, driven by the Rosa26 promoter give rise to proliferation in the bronchioles within a few days, but did not lead to tumours, even in the long-term (Figure 3-4, Table 3-1 & Table 3-2). *MYC* expression did not lead to apoptosis and loss of functional *Tp53* had no effect on short-term proliferation nor did it facilitate tumour formation (figure 3-6). This suggests that p53 was not engaged and hence presence or absence of p53 did not make any difference.

The same *MYC* levels that were alone not able to initiate tumour formation did however accelerate *KRas* driven tumourigenesis (Figure 3-8). Also, I showed that mutant *KRas* stabilized *MYC* protein 4 days after allele induction (Figure 3-7) (Sears et al., 2000). So far *Myc* and *KRas* have been thought to complement each other by abrogating each other's tumour suppressive functions: *Myc* can overcome *KRas* induced senescence and *KRas* can suppress *Myc* induced apoptosis. As *MYC* does not induce apoptosis in *R26^{DM.lsl-MYC/MYC}* lungs and *KRas^{G12D}* tumours are not senescent, this cooperative mechanism can be excluded. This shows that even *Myc* and *KRas* that are expressed below the tumour suppressive engaging threshold can cooperate in lung tumourigenesis. Moreover, this demonstrates the importance of *Myc* in *KRas* driven tumourigenesis. It had been shown before that *Myc* is essential for *KRas* driven tumourigenesis, even in established *KRas* mutant tumours. Expression of the dominant-negative *Myc* interacting protein *Omomyc* led to regression and eradication of established mutant *KRas* lung tumours (Soucek et al., 2008; Soucek et al., 2013). *MYC* is amplified or mutated in 2-3% of *KRAS* mutant lung ADC (Cancer Genome Atlas Research, 2014; Gao et al., 2013). Moreover *MGA*, whose loss of function leads to increased *MYC* activity, is also mutated in 2-3% of *KRAS* mutant lung ADC and is mutational exclusive with *MYC* amplification. The Wnt pathway, which is frequently hyperactivated in *KRas* mutant lung cancer presents another possibility to induce *Myc* transcription. I now showed that *MYC* overexpression accelerates mutant *KRas* driven lung tumourigenesis. This all suggests that *Myc* levels limit *KRas* driven tumourigenesis and that tumours find multiple ways to functionally increase *Myc*.

6.2 Pharmacological inhibition of p-Erk associated pathways

I showed that deregulated *MYC* expression accelerates *KRas*^{G12D} driven lung tumourigenesis. This acceleration did not only increase tumour size and burden, but also promoted tumour progression. Tumour progression is associated with a change in cell morphology and correlates with Erk phosphorylation. Erk was used as a progression marker in the *R26*^{DM.Isi-MYC/MYC};*KRas*^{G12D} model and gene expression between p-Erk negative and p-Erk positive tumour regions was compared. Pathway analysis revealed that the Wnt pathway and ErbB signalling were strongly enriched in the p-Erk positive dataset. We therefore pharmacologically inhibited the Wnt and ErbB signalling pathways in a panel of *KRAS* mutant human lung ADC cell lines and *in vivo* in the *R26*^{DM.Isi-MYC/MYC};*KRas*^{G12D} model.

6.3 Targeting the Wnt pathway

In human NSCLC, many Wnt pathway members are frequently overexpressed: *WNT1* (Nakashima et al., 2008), *WNT2* (You et al., 2004), *WNT3* (Nakashima et al., 2012) and *WNT11* (Bartis et al., 2013), *LRP6* (Li et al., 2004) *DSH1*, *DSH2* and *DSH3* (Uematsu et al., 2003; Wei et al., 2008; Zhao et al., 2010). Pathway inhibitors such as *WNT7a* (Winn et al., 2005) and *WIF1* (Mazieres et al., 2004) however are frequently silenced. Overexpression of WNT pathway members is also associated with poor prognosis, which has been specifically shown for *DVL-1* and *DVL-3* (Zhao et al., 2010), and for *WNT-1* (Nakashima et al., 2008), *WNT-3* (Nakashima et al., 2012) and *WNT-5a* (Huang et al., 2005). Moreover it has been shown that the canonical Wnt pathway mediates lung metastasis through LEF1 (Nguyen et al., 2009). Conversely, high β -CATENIN levels are associated with good prognosis, which is likely due to its function in cell adhesion (Hommura et al., 2002; Kren et al., 2003).

Despite activation of the canonical Wnt pathway involving β -catenin stabilization, Wnt ligands can also activate so called “non-canonical Wnt pathways” (Gordon and Nusse, 2006). The two best-described non-canonical Wnt pathways are the cell polarity pathway and the Wnt/Ca⁺⁺ flux pathway (Wang and Malbon, 2003). The GTPases Rho and Rac are important players of the cell polarity pathway and are involved in cell migration (Schlessinger et al., 2009). In the dataset generated from

R26^{DM.Isl-MYC/MYC};KRas^{G12D} tumours Porcupine was strongly enriched in the p-Erk positive samples. As Porcupine mediates post-translational modification and secretion of all Wnt ligands, which can signal through canonical and non-canonical Wnt pathways, both pathway types may be involved in tumour progression in this model. The strong upregulation of Sox9, a canonical Wnt pathway target, suggests however an important role of the canonical Wnt pathway.

Given the frequency of Wnt deregulation in human lung cancer the Wnt pathway is thought to be a promising target for therapeutic intervention. Until recently the lack of Wnt inhibitors has limited the study of the potential benefits of therapeutic Wnt intervention. A new inhibitor, the anti-Fzd antibody OMP-18R5, binds and blocks Fzd1, Fzd2, Fzd5, Fzd7 and Fzd8 (Gurney et al., 2012). All 5 receptors are known to be involved in canonical Wnt signalling. OMP-18R5 was shown to inhibit tumour growth in xenograft models, using cells from minimally passaged human tumours. OMP-18R5 inhibited tumour growth in 7 of 8 xenografts using human NSCLC cells (Gurney et al., 2012). No information about the mutations in these cells was given. The lack of markers that can predict response to Wnt inhibition is a general problem (Jiang et al., 2013).

With regard to *KRas* mutant lung cancer, Wnt pathway has been shown to be upregulated in a *KRas* mutant mouse model (Lee et al., 2009). Oncogenic *Braf*, *KRas* and *Mek1* mutations have been shown to induce Lrp6 phosphorylation. Upon Wnt binding Lrp6 binds Frizzled receptors and activates Dishevelled. This demonstrates one possibility how MAPK signalling can upregulate the Wnt pathway (Lemieux et al., 2014). *KRas* however can also activate the Wnt pathway further downstream through Pi3k, which inhibits Gsk-3 β and thereby leads to stabilization of β -catenin (Cross et al., 1995). The Wnt pathway has also been shown to accelerate *KRas* driven tumourigenesis, suggesting cooperation between *KRas* downstream signalling and Wnt pathway. (Pacheco-Pinedo et al., 2011).

Another Wnt inhibitor is LGK974, which I used in my work to inhibit the Wnt pathway. LGK974 inhibits Porcupine and Porcupine itself was more than 3-fold upregulated in the p-Erk positive dataset, generated from *R26^{DM.Isl-MYC/MYC};KRas^{G12D}* tumours, suggesting a functional role in tumour progression. Also *Sox9* and *CyclinD1*, both targets of the Wnt pathway were more than 15-fold and 2-fold enriched in the p-Erk positive dataset, respectively. I showed in a panel of *KRAS* mutant NSCLC cell lines,

that LGK974 inhibits cell propagation and migration (Figure 5-3 – Figure 5-7). Also, knockdown of Porcupine had a strong effect on cell viability in the A549 cell line (Figure 5-15). *In vivo* however, in the $R26^{DM.IsI-MYC/MYC};KRas^{G12D}$ model, LGK974 treatment did not decrease overall tumour burden and proliferation rate and did not suppress Erk phosphorylation (Figure 5-9 – Figure 5-11).

In a mutant *Braf* driven lung cancer mouse model, LGK974 was shown to drastically decrease tumour burden (Juan et al., 2014). Noticeably, the treatment was started 2 weeks after allele induction, whereas I started the treatment 4 weeks after allele induction in the $R26^{DM.IsI-MYC/MYC};KRas^{G12D}$ model. Hence, earlier treatment start might also be more successful in our model. More importantly, it was shown in the *Braf* model that sustained β -catenin or *Myc* (driven by the Rosa26 promoter) expression could completely rescue the LGK974 effect on tumour burden. *Myc* upregulation through loss of APC has been shown to be ~4 fold (Sansom et al., 2004). I showed in MEFs, that *Myc* transcripts driven by the Rosa26 promoter are not even 2-fold induced. This suggests that the Wnt phenotype is mainly attributed to *Myc* upregulation and that even slightly elevated *Myc* levels are striking. This might however also explain why LGK974 failed to reduce tumour burden in the $R26^{DM.IsI-MYC/MYC};KRas^{G12D}$ model. *Myc* is driven by the Rosa26 promoter in our model, which is not known to be regulated by Wnt signalling. Therefore it is to be expected that deregulated expression of a key Wnt target gene interferes with upstream inhibition. In the $R26^{DM.IsI-MYC/MYC};KRas^{G12D}$ model two important downstream Wnt players are induced: Gsk-3 β through Pi3k signalling and *MYC* through overexpression. Noticeably, *MYC* is overexpressed artificially in our system, which is different from *MYC* overexpression in human cancer. Hence, when *Myc* is overexpressed and driven by endogenous, Wnt responsive promoters, Wnt inhibition might be much more efficient.

Interestingly, endogenous *Myc* transcripts were not enriched in the p-Erk positive dataset and protein levels also did not correlate with p-Erk positivity, as I showed by IHC. Moreover, *Sox9* was strongly enriched in the p-Erk positive dataset. These two facts suggest, that the $R26^{DM.IsI-MYC/MYC};KRas^{G12D}$ model is different from the *Braf* model and that *Myc* might be a less important Wnt target in our model.

I hypothesize, that Wnt inhibition further downstream e.g. through TCF/LEF transcriptional inhibition would be more successful in the $R26^{DM.lsl-MYC/MYC};KRas^{G12D}$ model.

6.4 Targeting ErbB signalling

14% of lung ADCs are mutant for *EGFR* (*ErbB1*) (Cancer Genome Atlas Research, 2014). *EGFR* mutant lung cancers are sensitive to EGFR inhibition through Erlotinib and Gefitinib (Khozin et al., 2014; Maemondo et al., 2010). *KRAS* mutations are however mutually exclusive with *EGFR* mutations and *KRAS* mutant lung cancers are resistant to EGFR inhibition (Pao et al., 2005).

Inhibition of KRas mediated signalling through inhibition of upstream signals is difficult for two reasons: 1) KRas can be activated by the large family of receptor tyrosine kinases (RTKs) and blocking every single one of them would be challenging. 2) mutant KRas has a decreased GTPase activity, which leads to constitutive signalling and makes KRas largely independent from activation through upstream signals.

I observed in the $R26^{DM.lsl-MYC/MYC};KRas^{G12D}$ model that allele induction gives rise to tumours that are largely p-Erk negative and increased Erk phosphorylation, which is detectable by IHC, is a sporadic event that likely depends on additional, MAPK signalling upregulating incidents. Moreover, the pan-EGFR ligand *Ereg* together with other ErbB ligands (*Areg*, *TGF- α* and *HB-EGF*) were manifold enriched in the p-Erk positive samples, suggesting that upstream signalling can contribute to increased KRas activity and downstream signalling.

In vitro, treatment with the pan-ErbB inhibitor Neratinib reduced cell propagation and suppressed migration in a panel of *KRAS* mutant lung ADC cell lines. *In vivo* however, Neratinib did not decrease overall tumour burden nor did it suppress Erk-phosphorylation (Figure 5-9 - Figure 5-11). This might have several reasons: 1) Neratinib did not effectively inhibit all 4 ErbB family members. To answer this question, a decrease in phosphorylation of the individual ErbB proteins needs to be confirmed. 2) Inhibition of upstream signals through ErbB might not efficiently inhibit mutant *KRAS*. As mutant KRas is able to signal independently without activation through upstream signals, it is not expected that abrogation of upstream signals

would completely inhibit KRas. The upregulation of ErbB family ligands in the p-Erk positive regions suggests that upstream signals can still increase KRas activity. As a consequence, inhibition of upstream signals should result in decreased KRas activity. On the other hand roughly 500 genes were upregulated in the p-Erk positive samples and only a subset of them is involved in ErbB/MAPK signalling. These genes might be able to compensate for ErbB-inhibition. Combined treatment with the Wnt inhibitor LGK974 provided however no benefit. 3) Other RTKs might compensate for ErbB suppression. KRas cannot only be activated through ErbB family members, but also through other RTKs, such as fibroblast growth factor receptors (FGFR), vascular endothelial growth factor receptors (VEGFR) and RET receptors. These receptors might get activated upon ErbB inhibition and be able to compensate. 4) pan-ErbB inhibition can prevent tumour progression but not reverse it. Once MAPK signalling is active it can be further increased through positive feedback loops. Phosphorylated Erk can for instance activate Raf by inhibiting the Raf kinase inhibitor protein (RKIP) (Shin et al., 2009). This suggests that once a certain level of MAPK signalling is reached, it is able to maintain itself and substantial intervention is required to interrupt this feedback mechanism.

I started treatment of *R26^{DM.lsl-MYC/MYC};KRas^{G12D}* mice with Neratinib 4 weeks after allele induction. At this time point p-Erk signal is already detectable in some tumours. Therefore an earlier treatment start before the occurrence of detectable Erk phosphorylation might be more successful. Preliminary data with treatments starting 2 weeks post induction suggest that this is indeed the case and that Neratinib treatment interferes with tumour emergence and progression.

6.5 Validation of individual p-Erk associated genes

Roughly 500 genes were found to be upregulated in the p-Erk positive dataset. In order to validate their importance in *KRas* mutant lung cancer, an *in vitro* screen with 3 *KRas* mutant human lung ADC cell lines (A549, H2009 and H460) was performed. 51 genes that were most highly and significantly ($p < 0.05$) regulated and that had been reported to be amplified (cBioportal) and/or overexpressed (Oncomine) in human lung cancer were selected for the screen.

Data analysis revealed, that most of the tested genes play a role in viability of all 3 cell lines. Knockdown of *FMO1*, *KIF23*, *SLC2A1*, *ITGB4*, *KRT19*, *LAMC2* and

PORCN reduced viability most consistently across all cell lines. *SOX9*, *DLK1* and *ARNTL2* were most important for cell migration in the A549 and H2009 cell lines.

I sought to further investigate the role of these genes in human lung cancer. An online Kaplan Meyer analysis tool (Gyorffy et al., 2013) was used to investigate how expression levels of these genes correlate with overall survival (OS) and responsiveness to chemo- and radiotherapy of human lung cancer patients. High expression of 33 of the 51 tested genes was associated with significantly ($p < 0.05$) altered OS in lung cancer patients ($n = 1926$) and 25 of them were associated with decreased OS. Histological analysis of subgroups revealed that 27 genes were associated with decreased OS in lung ADC ($n = 719$), but only 3 genes were associated with decreased OS in SCC ($n = 525$). This supports the classification of the *R26^{DM}.Isl-MYC/MYC;KRas^{G12D}* tumours as representative for human ADC.

In the Adenocarcinoma subgroup, 17 genes had a significant hazard ratio (HR) above 1.5. The strongest reduction in OS was associated with high expression of *GAPDH* (HR = 3.34), and with high expression of *SLC2A1* (*GLUT1*; HR = 2.55). Other indicators of poor OS include S100 proteins *A11* (HR = 2.32) and *A6* (HR = 1.96), and structural proteins *KRT8* (HR = 2.09) and *KRT18* (HR = 1.99).

High expression of 5 genes was associated with poor response to chemotherapy ($n = 176$): *SLC2A1* (HR=1.96), *S100A11* (HR=1.89), *FABP5* (HR=1.69), *GAPDH* (HR=1.68) and *ARNTL2* (HR=1.67) and two of them were also associated with poor response to radiotherapy ($n = 70$): *ARNTL2* and *FABP5*. High expression of 4 more genes was associated with poor response to radiotherapy: *S100A14* (HR=1.93), *PHLDA1* (HR=1.93), *CD24* (HR=1.91) and *EREG* (HR=1.89).

These data suggest, that a considerable number of genes that were found to be upregulated in p-Erk positive lung tumour regions of *R26^{DM}.Isl-MYC/MYC;KRas^{G12D}* mice play an important role in human NSCLC.

6.6 Serum markers for early disease detection

In the dataset generated from *R26^{DM}.Isl-MYC/MYC;KRas^{G12D}* tumours among the highest significantly upregulated genes in the p-Erk positive samples were several genes that encode for secreted proteins. The highest enriched one was *Ereg* (~24-

fold), followed by *Areg* (~4-fold), *Bmp-4* (~4-fold), *HB-Egf* (~2.5-fold) and *TGF- α* (~2.5-fold). During tumourigenesis tumour cells produce and secrete an increased amount of signalling molecules, which may be valuable for early diagnosis (Buckhaults et al., 2001; Sporn and Roberts, 1985; Welsh et al., 2001). In cancers other than lung cancer proteins that are found in the blood serum are used for diagnosis. For instance Alpha-fetoprotein (AFP), Prostate-specific antigen (PSA) and cancer antigen 125 (CA-125) are used for liver, prostate and ovarian cancer diagnosis, respectively.

For lung cancer several markers have been found to be elevated in lung cancer patients: Carcinoembryonic antigen (CEA) (Okada et al., 2004), Plasma kallikrein (KLKB1) (Heo et al., 2007), Haptoglobin β chain (HP β) (Kang et al., 2011) and Complement component 9 (C9) (Narayanasamy et al., 2011). No markers for diagnosis are however in clinical use so far. Most markers were identified in already diagnosed lung cancer patients; therefore they might not be detectable in early disease. The above mentioned genes that encode for secreted proteins were found to be elevated in the p-Erk positive *R26^{DM.IsI-MYC/MYC};KRas^{G12D}* tumour regions. These advanced, p-Erk positive regions are very sporadic at the investigated time point and just start to emerge. Therefore the data represent markers of early disease progression and might be useful for early diagnosis. In order to investigate the potential use of these secreted proteins as early markers, the comparison of Ereg levels in the blood between *R26^{DM.IsI-MYC/MYC};KRas^{G12D}* mice 6 weeks after allele induction and uninduced mice, is planned. If we can confirm that Ereg serum levels are significantly elevated in tumour bearing mice it would be informative to extend the analysis to other (*KRas* mutant) lung cancer mouse models. Ereg might be a good candidate, as its expression levels were manifold enriched in the p-Erk positive samples. If tumour emergence and early progression is indeed associated with drastic increase in Ereg levels, the difference to serum from cancer-free patients should be clear and hopefully result in low false-positive rates. It is however more likely that a combination of markers will be used for diagnostic purposes, rather than one marker alone.

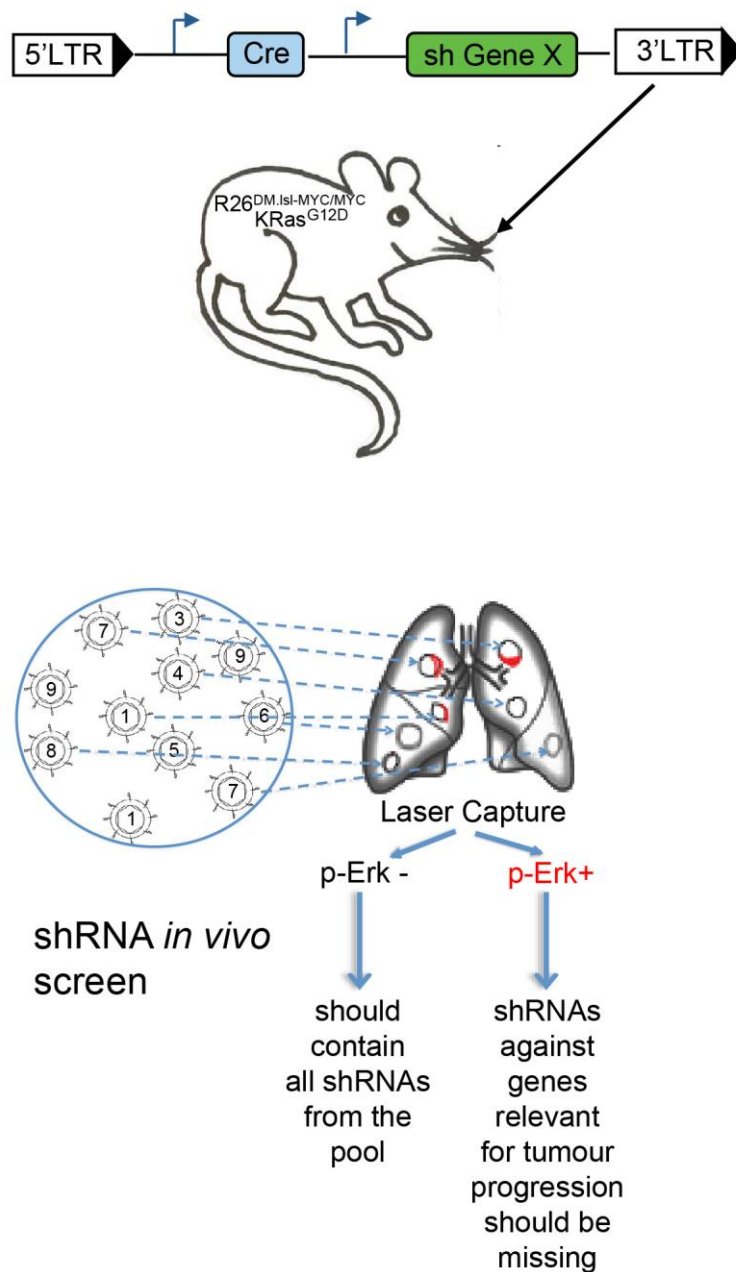


Figure 6-1 In vivo shRNA screen.

shRNAs against potential tumour progression genes are cloned in cis with Cre recombinase into lentiviral vectors and pool containing vectors with different shRNAs is used to infect *R26^{DM, Isl-1}-MYC/MYC; KRas^{G12D}* mice by intranasal delivery. Cells that are infected and recombine the alleles also express the shRNA. At the end of the experiment, p-Erk negative and p-Erk positive regions are laser captured, separately pooled and screened for the presence of the shRNAs. P-Erk negative samples should contain all shRNAs from the pool, in the p-Erk positive samples shRNAs against genes required for tumour progression should be missing.

The ability to reliably detect serum markers in a simple blood test would be a non-invasive, cost-effective method to increase early diagnosis of lung cancer.

6.7 Future directions

In the *in vitro* siRNA screen 3 *KRas* mutant human lung ADC cell lines were screened for 51 genes that were found to be enriched in p-Erk positive tumour

regions from *R26^{DM.lsl-MYC/MYC};KRas^{G12D}* mice. The screen was performed to narrow down the list of genes to be tested in an *in vivo* shRNA screen. Knockdown of *SOX9*, *DLK1* and *ARNTL2* considerably reduced migration in the H2009 and A549 cell lines. *FMO1*, *KIF23*, *SLC2A1*, *ITGB4*, *KRT19*, *LAMC2* and *PORCN* were most important for viability of all 3 tested cell lines (A549, H2009, H460). In order to validate their role in tumour progression *in vivo*, shRNAs will be cloned in cis with Cre recombinase into lentiviral vectors and a pool, containing vectors with different shRNAs will be used to infect *R26^{DM.lsl-MYC/MYC};KRas^{G12D}* mice by intranasal delivery (Figure 6-1). Any cell that recombines the alleles will also express the shRNA. At the end of the experiment (6 weeks after allele induction or later) p-Erk negative and p-Erk positive tumour regions will be laser captured, separately pooled and screened for the presence of the shRNAs. The p-Erk negative samples should contain all shRNAs from the pool, unless the respective gene is required for tumour initiation. In the p-Erk positive samples, shRNAs against genes that are essential for tumour progression should be missing. A follow-up experiment with inducible shRNAs could then be performed to test the effect of knockdown of these genes on established tumours.

Bibliography

Abrahamsson, A. E., Geron, I., Gotlib, J., Dao, K. H., Barroga, C. F., Newton, I. G., Giles, F. J., Durocher, J., Creusot, R. S., Karimi, M., *et al.* (2009). Glycogen synthase kinase 3b missplicing contributes to leukemia stem cell generation. *Proc Natl Acad Sci* 106: 3925–3929.

Adams, J. M., Harris, A. W., Pinkert, C. A., Corcoran, L. M., Alexander, W. S., Cory, S., Palmiter, R. D., and Brinster, R. L. (1985). The c-myc oncogene driven by immunoglobulin enhancers induces lymphoid malignancy in transgenic mice. *Nature* 318, 533-538.

Allen, T. D., Zhu, C. Q., Jones, K. D., Yanagawa, N., Tsao, M. S., and Bishop, J. M. (2011). Interaction between MYC and MCL1 in the genesis and outcome of non-small-cell lung cancer. *Cancer Res* 71, 2212-2221.

Bartis, D., Csongei, V., Weich, A., Kiss, E., Barko, S., Kovacs, T., Avdicevic, M., D'Souza, V. K., Rapp, J., Kvell, K., *et al.* (2013). Down-regulation of canonical and up-regulation of non-canonical Wnt signalling in the carcinogenic process of squamous cell lung carcinoma. *PLoS One* 8, e57393.

Batzer, A. G., Rotin, D., Urena, J. M., Skolnik, E. Y., and Schlessinger, J. (1994). Hierarchy of binding sites for Grb2 and Shc on the epidermal growth factor receptor. *Mol Cell Biol* 14, 5192-5201.

Beerli, R. R., Graus-Porta, D., Woods-Cook, K., Chen, X., Yarden, Y., and Hynes, N. E. (1995). Neu differentiation factor activation of ErbB-3 and ErbB-4 is cell specific and displays a differential requirement for ErbB-2. *Mol Cell Biol* 15, 6496-6505.

Berndt, N., Hamilton, A. D., and Sebt, S. M. (2011). Targeting protein prenylation for cancer therapy. *Nat Rev Cancer* 11, 775-791.

Bjorklund, P., Svedlund, J., Olsson, A. K., Akerstrom, G., and Westin, G. (2009). The internally truncated LRP5 receptor presents a therapeutic target in breast cancer. *PLoS ONE* 4, 4243.

Blache, P., van de Wetering, M., Duluc, I., Domon, C., Berta, P., Freund, J. N., Clevers, H., and Jay, P. (2004). SOX9 is an intestine crypt transcription factor, is regulated by the Wnt pathway, and represses the CDX2 and MUC2 genes. *J Cell Biol* 166, 37-47.

Blackwell, T. K., Kretzner, L., Blackwood, E. M., Eisenman, R. N., and Weintraub, H. (1990). Sequence-specific DNA binding by the c-Myc protein. *Science* 250, 1149-1151.

Blackwood, E. M., and Eisenman, R. N. (1991). Max: a helix-loop-helix zipper protein that forms a sequence-specific DNA-binding complex with Myc. *Science* 251, 1211-1217.

Blasco, R. B., Francos, S., Santamaria, D., Canamero, M., Dubus, P., Charron, J., Baccarini, M., and Barbacid, M. (2011). c-Raf, but not B-Raf is essential for development of K-Ras oncogene-driven non-small cell lung carcinoma. *Cancer Cell* 19, 652-663.

Bouchard, C., Dittrich, O., Kiermaier, A., Dohmann, K., Menkel, A., Eilers, M., and Luscher, B. (2001). Regulation of cyclin D2 gene expression by the Myc/Max/Mad network: Myc-dependent TRRAP recruitment and histone acetylation at the cyclin D2 promoter. *Genes Dev* 15, 2042-2047.

Buckhaults, P., Rago, C., St Croix, B., Romans, K. E., Saha, S., Zhang, L., Vogelstein, B., and Kinzler, K. W. (2001). Secreted and cell surface genes expressed in benign and malignant colorectal tumors. *Cancer Res* 61, 6996-7001.

Cancer Genome Atlas Research, N. (2012). Comprehensive genomic characterization of squamous cell lung cancers. *Nature* 489, 519-525.

Cancer Genome Atlas Research, N. (2014). Comprehensive molecular profiling of lung adenocarcinoma. *Nature* 511, 543-550.

Canonici, A., Gijzen, M., Mullooly, M., Bennett, R., Bouguern, N., Pedersen, K., O'Brien, N. A., Roxanis, I., Li, J. L., Bridge, E., *et al.* (2013). Neratinib overcomes trastuzumab resistance in HER2 amplified breast cancer. *Oncotarget* 4, 1592-1605.

Carraway, K. L., 3rd, Weber, J. L., Unger, M. J., Ledesma, J., Yu, N., Gassmann, M., and Lai, C. (1997). Neuregulin-2, a new ligand of ErbB3/ErbB4-receptor tyrosine kinases. *Nature* 387, 512-516.

Chardin, P., and Tavitian, A. (1986). The *ral* gene: a new *ras* related gene isolated by the use of a synthetic probe. *EMBO J* 5, 2203-2208.

Chen, Z., Cheng, K., Walton, Z., Wang, Y., Ebi, H., Shimamura, T., Liu, Y., Tupper, T., Ouyang, J., Li, J., *et al.* (2012). A murine lung cancer co-clinical trial identifies genetic modifiers of therapeutic response. *Nature* 483, 613-617.

Chen, Z., Fillmore, C. M., Hammerman, P. S., Kim, C. F., and Wong, K. K. (2014). Non-small-cell lung cancers: a heterogeneous set of diseases. *Nat Rev Cancer* 14, 535-546.

Chen, Z., Li, J., Li, Q. S., Fan, J. Q., Dong, X. M., Xu, J. P., Wang, X. M., Yang, G. W., Yan, P., Wen, G. Z., *et al.* (2008). Suppression of PPN/MG61 attenuates Wnt/beta-catenin signaling pathway and induces apoptosis in human lung cancer. *Oncogene* 27, 3483-3488.

Ching, T., Huang, S. and Garmire, L. X. (2014). Power analysis and sample size estimation for RNA-Seq differential expression. *RNA* 20, 1684-1696.

Citri, A., Yarden, Y. (2006). EGF-ERBB signaling: towards the systems level. *Nat Rev Mol Cell Biol* 7, 505-516.

Cleveland, J. L., Huleihel, M., Bressler, P., Siebenlist, U., Akiyama, L., Eisenman, R. N., and Rapp, U. R. (1988). Negative regulation of *c-myc* transcription involves *myc* family proteins. *Oncogene Res* 3, 357-375.

Cross, D. A., Alessi, D. R., Cohen, P., Andjelkovich, M., and Hemmings, B. A. (1995). Inhibition of glycogen synthase kinase-3 by insulin mediated by protein kinase B. *Nature* 378, 785-789.

D'Cruz, C. M., Gunther, E. J., Boxer, R. B., Hartman, J. L., Sintasath, L., Moody, S. E., Cox, J. D., Ha, S. I., Belka, G. K., Golant, A., *et al.* (2001). *c-MYC* induces

mammary tumorigenesis by means of a preferred pathway involving spontaneous Kras2 mutations. *Nat Med* 7, 235-239.

Dang, C. V. (1999). c-Myc target genes involved in cell growth, apoptosis, and metabolism. *Mol Cell Biol* 19, 1-11.

Dankort, D., Filenova, E., Collado, M., Serrano, M., Jones, K., and McMahon, M. (2007). A new mouse model to explore the initiation, progression, and therapy of BRAFV600E-induced lung tumors. *Genes Dev* 21, 379-384.

Datta, S. R., Dudek, H., Tao, X., Masters, S., Fu, H., Gotoh, Y., and Greenberg, M. E. (1997). Akt phosphorylation of BAD couples survival signals to the cell-intrinsic death machinery. *Cell* 91, 231-241.

Daub, H., Weiss, F. U., Wallasch, C., and Ullrich, A. (1996). Role of transactivation of EGF receptor in signalling by G-protein-coupled receptors. *Nature* 379, 557-560.

DeMayo, F. J., Finegold, M. J., Hansen, T. N., Stanley, L. A., Smith, B., and Bullock, D. W. (1991). Expression of SV40 T antigen under control of rabbit uteroglobin promoter in transgenic mice. *Am J Physiol* 261, L70-76.

Dhillon, A. S., Hagan, S., Rath, O., and Kolch, W. (2007). MAP kinase signalling pathways in cancer. *Oncogene* 26, 3279-3290.

Donehower, L. A., Harvey, M., Slagle, B. L., McArthur, M. J., Montgomery, C. A., Jr., Butel, J. S., and Bradley, A. (1992). Mice deficient for p53 are developmentally normal but susceptible to spontaneous tumours. *Nature* 356, 215-221.

Draper, B. K., Komurasaki, T., Davidson, M. K., and Nanney, L. B. (2003). Epiregulin is more potent than EGF or TGFalpha in promoting in vitro wound closure due to enhanced ERK/MAPK activation. *J Cell Biochem* 89, 1126-1137.

Drilon, A., Wang, L., Hasanovic, A., Suehara, Y., Lipson, D., Stephens, P., Ross, J., Miller, V., Ginsberg, M., Zakowski, M. F., *et al.* (2013). Response to Cabozantinib in patients with RET fusion-positive lung adenocarcinomas. *Cancer Discov* 3, 630-635.

DuPage, M., Dooley, A. L., and Jacks, T. (2009). Conditional mouse lung cancer models using adenoviral or lentiviral delivery of Cre recombinase. *Nat Protoc* 4, 1064-1072.

Egan, S. E., Giddings, B. W., Brooks, M. W., Buday, L., Sizeland, A. M., and Weinberg, R. A. (1993). Association of Sos Ras exchange protein with Grb2 is implicated in tyrosine kinase signal transduction and transformation. *Nature* 363, 45-51.

Ehrhardt, A., Bartels, T., Geick, A., Klocke, R., Paul, D., and Halter, R. (2001). Development of pulmonary bronchiolo-alveolar adenocarcinomas in transgenic mice overexpressing murine c-myc and epidermal growth factor in alveolar type II pneumocytes. *Br J Cancer* 84, 813-818.

Elson, A., Deng, C., Campos-Torres, J., Donehower, L. A., and Leder, P. (1995). The MMTV/c-myc transgene and p53 null alleles collaborate to induce T-cell lymphomas, but not mammary carcinomas in transgenic mice. *Oncogene* 11, 181-190.

Eng, C. (2003). *PTEN*: one gene, many syndromes. *Hum Mutat* 22, 183-198.

Engelman, J. A., Chen, L., Tan, X., Crosby, K., Guimaraes, A. R., Upadhyay, R., Maira, M., McNamara, K., Perera, S. A., Song, Y., *et al.* (2008). Effective use of PI3K and MEK inhibitors to treat mutant Kras G12D and PIK3CA H1047R murine lung cancers. *Nat Med* 14, 1351-1356.

Engelman, J. A., Janne, P. A., Mermel, C., Pearlberg, J., Mukohara, T., Fleet, C., Cichowski, K., Johnson, B. E., and Cantley, L. C. (2005). ErbB-3 mediates phosphoinositide 3-kinase activity in gefitinib-sensitive non-small cell lung cancer cell lines. *Proc Natl Acad Sci* 102, 3788-3793.

Esteban, L. M., Vicario-Abejon, C., Fernandez-Salguero, P., Fernandez-Medarde, A., Swaminathan, N., Yienger, K., Lopez, E., Malumbres, M., McKay, R., Ward, J. M., *et al.* (2001). Targeted genomic disruption of H-ras and N-ras, individually or in combination, reveals the dispensability of both loci for mouse growth and development. *Mol Cell Biol* 21, 1444-1452.

Ettinger, D. S., Akerley, W., Borghaei, H., Chang, A. C., Cheney, R. T., Chirieac, L. R., D'Amico, T. A., Demmy, T. L., Govindan, R., Grannis, F. W., Jr., *et al.* (2013). Non-small cell lung cancer, version 2.2013. *J Natl Compr Canc Netw* 11, 645-653; quiz 653.

Evan, G. I., Wyllie, A. H., Gilbert, C. S., Littlewood, T. D., Land, H., Brooks, M., Waters, C. M., Penn, L. Z., and Hancock, D. C. (1992). Induction of apoptosis in fibroblasts by c-myc protein. *Cell* 69, 119-128.

Feldser, D. M., Kostova, K. K., Winslow, M. M., Taylor, S. E., Cashman, C., Whittaker, C. A., Sanchez-Rivera, F. J., Resnick, R., Bronson, R., Hemann, M. T., and Jacks, T. (2010). Stage-specific sensitivity to p53 restoration during lung cancer progression. *Nature* 468, 572-575.

Fernandez, P. C., Frank, S. R., Wang, L., Schroeder, M., Liu, S., Greene, J., Cocito, A., and Amati, B. (2003). Genomic targets of the human c-Myc protein. *Genes Dev* 17, 1115-1129.

Filmus, J., Robles, A. I., Shi, W., Wong, M. J., Colombo, L. L., and Conti, C. J. (1994). Induction of cyclin D1 overexpression by activated ras. *Oncogene* 9, 3627-3633.

Fisher, G. H., Wellen, S. L., Klimstra, D., Lenczowski, J. M., Tichelaar, J. W., Lizak, M. J., Whitsett, J. A., Koretsky, A., and Varmus, H. E. (2001). Induction and apoptotic regression of lung adenocarcinomas by regulation of a K-Ras transgene in the presence and absence of tumor suppressor genes. *Genes Dev* 15, 3249-3262.

Furth, P. A., St Onge, L., Boger, H., Gruss, P., Gossen, M., Kistner, A., Bujard, H., and Hennighausen, L. (1994). Temporal control of gene expression in transgenic mice by a tetracycline-responsive promoter. *Proc Natl Acad Sci U S A* 91, 9302-9306.

Galli, L. M., Barnes, T. L., Secret, S. S., Kadowaki, T., and Burrus, L. W. (2007). Porcupine-mediated lipid-modification regulates the activity and distribution of Wnt proteins in the chick neural tube. *Development* 134, 3339-3348.

Ganguly, P., Hajari, T., Shea, J.-E., and van der Vegt, N. F. A. (2015). Mutual Exclusion of Urea and Trimethylamine N-Oxide from Amino Acids in Mixed Solvent Environment. *The Journal of Physical Chemistry Letters* 6, 581-585.

Gao, J., Aksoy, B. A., Dogrusoz, U., Dresdner, G., Gross, B., Sumer, S. O., Sun, Y., Jacobsen, A., Sinha, R., Larsson, E., *et al.* (2013). Integrative analysis of complex cancer genomics and clinical profiles using the cBioPortal. *Sci Signal* 6, p11.

Geick, A., Redecker, P., Ehrhardt, A., Klocke, R., Paul, D., and Halter, R. (2001). Uteroglobin promoter-targeted c-MYC expression in transgenic mice cause hyperplasia of Clara cells and malignant transformation of T-lymphoblasts and tubular epithelial cells. *Transgenic Res* 10, 501-511.

Giangreco, A., Reynolds, S. D., and Stripp, B. R. (2002). Terminal bronchioles harbor a unique airway stem cell population that localizes to the bronchoalveolar duct junction. *Am J Pathol* 161, 173-182.

Glasser, S. W., Korfhagen, T. R., Wert, S. E., Bruno, M. D., McWilliams, K. M., Vorbroker, D. K., and Whitsett, J. A. (1991). Genetic element from human surfactant protein SP-C gene confers bronchiolar-alveolar cell specificity in transgenic mice. *Am J Physiol* 261, L349-356.

Gordon, M. D., and Nusse, R. (2006). Wnt signaling: multiple pathways, multiple receptors, and multiple transcription factors. *J Biol Chem* 281, 22429-22433.

Graus-Porta, D., Beerli, R. R., Daly, J. M., and Hynes, N. E. (1997). ErbB-2, the preferred heterodimerization partner of all ErbB receptors, is a mediator of lateral signaling. *EMBO J* 16, 1647-1655.

Graus-Porta, D., Beerli, R. R., and Hynes, N. E. (1995). Single-chain antibody-mediated intracellular retention of ErbB-2 impairs Neu differentiation factor and epidermal growth factor signaling. *Mol Cell Biol* 15, 1182-1191.

Guerra, C., Mijimolle, N., Dhawahir, A., Dubus, P., Barradas, M., Serrano, M., Campuzano, V., and Barbacid, M. (2003). Tumor induction by an endogenous K-ras oncogene is highly dependent on cellular context. *Cancer Cell* 4, 111-120.

Gurney, A., Axelrod, F., Bond, C. J., Cain, J., Chartier, C., Donigan, L., Fischer, M., Chaudhari, A., Ji, M., Kapoun, A. M., *et al.* (2012). Wnt pathway inhibition via the targeting of Frizzled receptors results in decreased growth and tumorigenicity of human tumors. *Proc Natl Acad Sci U S A* 109, 11717-11722.

Guy, P. M., Platko, J. V., Cantley, L. C., Cerione, R. A., and Carraway, K. L., 3rd (1994). Insect cell-expressed p180erbB3 possesses an impaired tyrosine kinase activity. *Proc Natl Acad Sci U S A* 91, 8132-8136.

Gyorffy, B., Surowiak, P., Budczies, J., and Lanczky, A. (2013). Online survival analysis software to assess the prognostic value of biomarkers using transcriptomic data in non-small-cell lung cancer. *PLoS One* 8, e82241.

Hanahan, D., and Weinberg, R. A. (2011). Hallmarks of cancer: the next generation. *Cell* 144, 646-674.

Harari, D., Tzahar, E., Romano, J., Shelly, M., Pierce, J. H., Andrews, G. C., and Yarden, Y. (1999). Neuregulin-4: a novel growth factor that acts through the ErbB-4 receptor tyrosine kinase. *Oncogene* 18, 2681-2689.

He, T. C., Sparks, A. B., Rago, C., Hermeking, H., Zawel, L., da Costa, L. T., Morin, P. J., Vogelstein, B., and Kinzler, K. W. (1998). Identification of c-MYC as a target of the APC pathway. *Science* 281, 1509-1512.

Henschke, C. I., Yip, R., Yankelevitz, D. F., Smith, J. P., and International Early Lung Cancer Action Program, I. (2013). Definition of a positive test result in computed tomography screening for lung cancer: a cohort study. *Ann Intern Med* 158, 246-252.

Heo, S. H., Lee, S. J., Ryoo, H. M., Park, J. Y., and Cho, J. Y. (2007). Identification of putative serum glycoprotein biomarkers for human lung adenocarcinoma by multilectin affinity chromatography and LC-MS/MS. *Proteomics* 7, 4292-4302.

Hermeking, H., Rago, C., Schuhmacher, M., Li, Q., Barrett, J. F., Obaya, A. J., O'Connell, B. C., Mateyak, M. K., Tam, W., Kohlhuber, F., *et al.* (2000). Identification of CDK4 as a target of c-MYC. *Proc Natl Acad Sci U S A* 97, 2229-2234.

Herr, P., and Basler, K. (2012). Porcupine-mediated lipidation is required for Wnt recognition by Wls. *Dev Biol* 361, 392-402.

Higashiyama, S., Lau, K., Besner, G. E., Abraham, J. A., and Klagsbrun, M. (1992). Structure of heparin-binding EGF-like growth factor. Multiple forms, primary structure, and glycosylation of the mature protein. *J Biol Chem* 267, 6205-6212.

Ho, V. M., Schaffer, B. E., Karnezis, A. N., Park, K. S., and Sage, J. (2009). The retinoblastoma gene Rb and its family member p130 suppress lung adenocarcinoma induced by oncogenic K-Ras. *Oncogene* 28, 1393-1399.

Hofer, F., Fields, S., Schneider, C., and Martin, G. S. (1994). Activated Ras interacts with the Ral guanine nucleotide dissociation stimulator. *Proc Natl Acad Sci U S A* 91, 11089-11093.

Hogenesch, J. B., Gu, Y. Z., Moran, S. M., Shimomura, K., Radcliffe, L. A., Takahashi, J. S., and Bradfield, C. A. (2000). The basic helix-loop-helix-PAS protein MOP9 is a brain-specific heterodimeric partner of circadian and hypoxia factors. *J Neurosci* 20, RC83.

Hommura, F., Furuuchi, K., Yamazaki, K., Ogura, S., Kinoshita, I., Shimizu, M., Moriuchi, T., Katoh, H., Nishimura, M., and Dosaka-Akita, H. (2002). Increased expression of beta-catenin predicts better prognosis in nonsmall cell lung carcinomas. *Cancer* 94, 752-758.

Horeweg, N., van der Aalst, C. M., Vliegenthart, R., Zhao, Y., Xie, X., Scholten, E. T., Mali, W., Thunnissen, E., Weenink, C., Groen, H. J., *et al.* (2013). Volumetric computed tomography screening for lung cancer: three rounds of the NELSON trial. *Eur Respir J* 42, 1659-1667.

Hornick, J. E., Karanjeet, K., Collins, E. S., and Hinchcliffe, E. H. (2010). Kinesins to the core: The role of microtubule-based motor proteins in building the mitotic spindle midzone. *Semin Cell Dev Biol* 21, 290-299.

Huang, C. L., Liu, D., Nakano, J., Ishikawa, S., Kontani, K., Yokomise, H., and Ueno, M. (2005). Wnt5a expression is associated with the tumor proliferation and the

stromal vascular endothelial growth factor--an expression in non-small-cell lung cancer. *J Clin Oncol* 23, 8765-8773.

Huff, W. (2011). Wilms' tumours: About tumour suppressor genes, an oncogene and a chameleon gene. *Nat Rev Cancer* 11, 111-121.

Humphrey, L. L., Deffebach, M., Pappas, M., Baumann, C., Artis, K., Mitchell, J. P., Zakher, B., Fu, R., and Slatore, C. G. (2013). Screening for lung cancer with low-dose computed tomography: a systematic review to update the US Preventive services task force recommendation. *Ann Intern Med* 159, 411-420.

Hundley, J. E., Koester, S. K., Troyer, D. A., Hilsenbeck, S. G., Barrington, R. E., and Windle, J. J. (1997). Differential regulation of cell cycle characteristics and apoptosis in MMTV-myc and MMTV-ras mouse mammary tumors. *Cancer Res* 57, 600-603.

Hurlin, P. J., Steingrimsson, E., Copeland, N. G., Jenkins, N. A., and Eisenman, R. N. (1999). Mga, a dual-specificity transcription factor that interacts with Max and contains a T-domain DNA-binding motif. *EMBO J* 18, 7019-7028.

Hydbring, P., Bahram, F., Su, Y., Tronnersjo, S., Hogstrand, K., von der Lehr, N., Sharifi, H. R., Lilischkis, R., Hein, N., Wu, S., *et al.* (2010). Phosphorylation by Cdk2 is required for Myc to repress Ras-induced senescence in cotransformation. *Proc Natl Acad Sci U S A* 107, 58-63.

Hynes, N. E., Stern, D. F. (1994). The biology of erbB-2/neu/HER-2 and its role in cancer. *Biochim. Biophys. Acta* 1198, 165-184.

Inoki, K., Li, Y., Zhu, T., Wu, J., and Guan, K. L. (2002). TSC2 is phosphorylated and inhibited by Akt and suppresses mTOR signalling. *Nat Cell Biol* 4, 648-657.

International Early Lung Cancer Action Program, I., Henschke, C. I., Yankelevitz, D. F., Libby, D. M., Pasmantier, M. W., Smith, J. P., and Miettinen, O. S. (2006). Survival of patients with stage I lung cancer detected on CT screening. *N Engl J Med* 355, 1763-1771.

Iwanaga, K., Yang, Y., Raso, M. G., Ma, L., Hanna, A. E., Thilaganathan, N., Moghaddam, S., Evans, C. M., Li, H., Cai, W. W., *et al.* (2008). Pten inactivation accelerates oncogenic K-ras-initiated tumorigenesis in a mouse model of lung cancer. *Cancer Res* 68, 1119-1127.

Jacks, T., Fazeli, A., Schmitt, E. M., Bronson, R. T., Goodell, M. A., and Weinberg, R. A. (1992). Effects of an Rb mutation in the mouse. *Nature* 359, 295-300.

Jackson, E. L., Olive, K. P., Tuveson, D. A., Bronson, R., Crowley, D., Brown, M., and Jacks, T. (2005). The differential effects of mutant p53 alleles on advanced murine lung cancer. *Cancer Res* 65, 10280-10288.

Jackson, E. L., Willis, N., Mercer, K., Bronson, R. T., Crowley, D., Montoya, R., Jacks, T., and Tuveson, D. A. (2001). Analysis of lung tumor initiation and progression using conditional expression of oncogenic K-ras. *Genes Dev* 15, 3243-3248.

Jager, R., Herzer, U., Schenkel, J., and Weiher, H. (1997). Overexpression of Bcl-2 inhibits alveolar cell apoptosis during involution and accelerates c-myc-induced tumorigenesis of the mammary gland in transgenic mice. *Oncogene* 15, 1787-1795.

Jaiswal, B. S., Kljavin, N. M., Stawiski, E. W., Chan, E., Parikh, C., Durinck, S. (2013). Oncogenic ErBB3 mutations in human cancers. *Cancer Cell* 23, 603-617.

Janne, P. A., Shaw, A. T., Pereira, J. R., Jeannin, G., Vansteenkiste, J., Barrios, C., Franke, F. A., Grinsted, L., Zazulina, V., Smith, P., *et al.* (2013). Selumetinib plus docetaxel for KRAS-mutant advanced non-small-cell lung cancer: a randomised, multicentre, placebo-controlled, phase 2 study. *Lancet Oncol* 14, 38-47.

Ji, H., Ramsey, M. R., Hayes, D. N., Fan, C., McNamara, K., Kozlowski, P., Torrice, C., Wu, M. C., Shimamura, T., Perera, S. A., *et al.* (2007). LKB1 modulates lung cancer differentiation and metastasis. *Nature* 448, 807-810.

Jiang, X., Hao, H. X., Gowney, J. D., Woolfenden, S., Bottiglio, C., Ng, N., Lu, B., Hsieh, M. H., Bagdasarian, L., Meyer, R., *et al.* (2013). Inactivating mutations of RNF43 confer Wnt dependency in pancreatic ductal adenocarcinoma. *Proc Natl Acad Sci U S A* 110, 12649-12654.

Johnson, L., Mercer, K., Greenbaum, D., Bronson, R. T., Crowley, D., Tuveson, D. A., and Jacks, T. (2001). Somatic activation of the K-ras oncogene causes early onset lung cancer in mice. *Nature* 410, 1111-1116.

Jonkers, J., Meuwissen, R., van der Gulden, H., Peterse, H., van der Valk, M., and Berns, A. (2001). Synergistic tumor suppressor activity of BRCA2 and p53 in a conditional mouse model for breast cancer. *Nat Genet* 29, 418-425.

Juan, J., Muraguchi, T., Iezza, G., Sears, R. C., and McMahon, M. (2014). Diminished WNT → beta-catenin → c-MYC signaling is a barrier for malignant progression of BRAFV600E-induced lung tumors. *Genes Dev* 28, 561-575.

Junttila, M. R., Karnezis, A. N., Garcia, D., Madriles, F., Kortlever, R. M., Rostker, F., Brown Swigart, L., Pham, D. M., Seo, Y., Evan, G. I., and Martins, C. P. (2010). Selective activation of p53-mediated tumour suppression in high-grade tumours. *Nature* 468, 567-571.

Kang, S. M., Sung, H. J., Ahn, J. M., Park, J. Y., Lee, S. Y., Park, C. S., and Cho, J. Y. (2011). The Haptoglobin beta chain as a supportive biomarker for human lung cancers. *Mol Biosyst* 7, 1167-1175.

Karunagaran, D., Tzahar, E., Beerli, R. R., Chen, X., Graus-Porta, D., Ratzkin, B. J., Seger, R., Hynes, N. E., and Yarden, Y. (1996). ErbB-2 is a common auxiliary subunit of NDF and EGF receptors: implications for breast cancer. *EMBO J* 15, 254-264.

Katayama, R., Shaw, A. T., Khan, T. M., Mino-Kenudson, M., Solomon, B. J., Halmos, B., Jessop, N. A., Wain, J. C., Yeo, A. T., Benes, C., *et al.* (2012). Mechanisms of acquired crizotinib resistance in ALK-rearranged lung Cancers. *Sci Transl Med* 4, 120ra117.

Kauffmann-Zeh, A., Rodriguez-Viciana, P., Ulrich, E., Gilbert, C., Coffey, P., Downward, J., and Evan, G. (1997). Suppression of c-Myc-induced apoptosis by Ras signalling through PI(3)K and PKB. *Nature* 385, 544-548.

Khozin, S., Blumenthal, G. M., Jiang, X., He, K., Boyd, K., Murgo, A., Justice, R., Keegan, P., and Pazdur, R. (2014). U.S. Food and Drug Administration approval

summary: Erlotinib for the first-line treatment of metastatic non-small cell lung cancer with epidermal growth factor receptor exon 19 deletions or exon 21 (L858R) substitution mutations. *Oncologist* 19, 774-779.

Kim, C. F., Jackson, E. L., Woolfenden, A. E., Lawrence, S., Babar, I., Vogel, S., Crowley, D., Bronson, R. T., and Jacks, T. (2005). Identification of bronchioalveolar stem cells in normal lung and lung cancer. *Cell* 121, 823-835.

Kim, K. A., Kim, J. H., Wang, Y., and Sul, H. S. (2007). Pref-1 (preadipocyte factor 1) activates the MEK/extracellular signal-regulated kinase pathway to inhibit adipocyte differentiation. *Mol Cell Biol* 27, 2294-2308.

Kinzler, K. W., and Vogelstein, B. (1996). Lessons from hereditary colorectal cancer. *Cell* 87, 159-170.

Klapper, L. N., Glathe, S., Vaisman, N., Hynes, N. E., Andrews, G. C., Sela, M., and Yarden, Y. (1999). The ErbB-2/HER2 oncoprotein of human carcinomas may function solely as a shared coreceptor for multiple stroma-derived growth factors. *Proc Natl Acad Sci U S A* 96, 4995-5000.

Kobayashi, S., Boggon, T. J., Dayaram, T., Janne, P. A., Kocher, O., Meyerson, M., Johnson, B. E., Eck, M. J., Tenen, D. G., and Halmos, B. (2005). EGFR mutation and resistance of non-small-cell lung cancer to gefitinib. *N Engl J Med* 352, 786-792.

Koera, K., Nakamura, K., Nakao, K., Miyoshi, J., Toyoshima, K., Hatta, T., Otani, H., Aiba, A., and Katsuki, M. (1997). K-ras is essential for the development of the mouse embryo. *Oncogene* 15, 1151-1159.

Kren, L., Hermanova, M., Goncharuk, V. N., Kaur, P., Ross, J. S., Pavlovsky, Z., and Dvorak, K. (2003). Downregulation of plasma membrane expression/cytoplasmic accumulation of beta-catenin predicts shortened survival in non-small cell lung cancer. A clinicopathologic study of 100 cases. *Cesk Patol* 39, 17-20.

Kumar, M. S., Hancock, D. C., Molina-Arcas, M., Steckel, M., East, P., Diefenbacher, M., Armenteros-Monterroso, E., Lassailly, F., Matthews, N., Nye, E.,

et al. (2012). The GATA2 transcriptional network is requisite for RAS oncogene-driven non-small cell lung cancer. *Cell* 149, 642-655.

Land, H., Chen, A. C., Morgenstern, J. P., Parada, L. F., and Weinberg, R. A. (1986). Behavior of *myc* and *ras* oncogenes in transformation of rat embryo fibroblasts. *Mol Cell Biol* 6, 1917-1925.

Lazarov, M., Green, C. L., Zhang, J. Y., Kubo, Y., Dajee, M., and Khavari, P. A. (2003). Escaping G1 restraints on neoplasia--Cdk4 regulation by Ras and NF-kappa B. *Cell Cycle* 2, 79-80.

Lee, C. L., Moding, E. J., Huang, X., Li, Y., Woodlief, L. Z., Rodrigues, R. C., Ma, Y., and Kirsch, D. G. (2012). Generation of primary tumors with Flp recombinase in FRT-flanked p53 mice. *Dis Model Mech* 5, 397-402.

Lee, E., Salic, A., Kruger, R., Heinrich, R., and Kirschner, M. W. (2003). The roles of APC and Axin derived from experimental and theoretical analysis of the Wnt pathway. *PLoS Biol* 1, E10.

Lee, S., Kang, J., Cho, M., Seo, E., Choi, H., Kim, E., Kim, J., Kim, H., Kang, G. Y., Kim, K. P., *et al.* (2009). Profiling of transcripts and proteins modulated by K-ras oncogene in the lung tissues of K-ras transgenic mice by omics approaches. *Int J Oncol* 34, 161-172.

Lemieux, E., Cagnol, S., Beaudry, K., Carrier, J., and Rivard, N. (2014). Oncogenic KRAS signalling promotes the Wnt/beta-catenin pathway through LRP6 in colorectal cancer. *Oncogene*.

Lenferink, A. E., Pinkas-Kramarski, R., van de Poll, M. L., van Vugt, M. J., Klapper, L. N., Tzahar, E., Waterman, H., Sela, M., van Zoelen, E. J., and Yarden, Y. (1998). Differential endocytic routing of homo- and hetero-dimeric ErbB tyrosine kinases confers signaling superiority to receptor heterodimers. *EMBO J* 17, 3385-3397.

Li, D., Shimamura, T., Ji, H., Chen, L., Haringsma, H. J., McNamara, K., Liang, M. C., Perera, S. A., Zaghlul, S., Borgman, C. L., *et al.* (2007). Bronchial and peripheral murine lung carcinomas induced by T790M-L858R mutant EGFR respond to HKI-272 and rapamycin combination therapy. *Cancer Cell* 12, 81-93.

Li, Y., Lu, W., He, X., Schwartz, A. L., and Bu, G. (2004). LRP6 expression promotes cancer cell proliferation and tumorigenesis by altering beta-catenin subcellular distribution. *Oncogene* 23, 9129-9135.

Liljeholm, M., Irvine, A. F., Vikberg, A. L., Norberg, A., Month, S., Sandstrom, H., Wahlin, A., Mishima, M., and Golovleva, I. (2013). Congenital dyserythropoietic anemia type III (CDA III) is caused by a mutation in kinesin family member, KIF23. *Blood* 121, 4791-4799.

Lim, K. H., O'Hayer, K., Adam, S. J., Kendall, S. D., Campbell, P. M., Der, C. J., and Counter, C. M. (2006). Divergent roles for RalA and RalB in malignant growth of human pancreatic carcinoma cells. *Curr Biol* 16, 2385-2394.

Lin, A. W., Barradas, M., Stone, J. C., van Aelst, L., Serrano, M., and Lowe, S. W. (1998). Premature senescence involving p53 and p16 is activated in response to constitutive MEK/MAPK mitogenic signaling. *Genes Dev* 12, 3008-3019.

Linnoila, R. I., Mulshine, J. L., Steinberg, S. M., and Gazdar, A. F. (1992). Expression of surfactant-associated protein in non-small-cell lung cancer: a discriminant between biologic subsets. *J Natl Cancer Inst Monogr*, 61-66.

Liu, J., Pan, S., Hsieh, M. H., Ng, N., Sun, F., Wang, T., Kasibhatla, S., Schuller, A. G., Li, A. G., Cheng, D., *et al.* (2013). Targeting Wnt-driven cancer through the inhibition of Porcupine by LGK974. *Proc Natl Acad Sci U S A* 110, 20224-20229.

Maemondo, M., Inoue, A., Kobayashi, K., Sugawara, S., Oizumi, S., Isobe, H., Gemma, A., Harada, M., Yoshizawa, H., Kinoshita, I., *et al.* (2010). Gefitinib or chemotherapy for non-small-cell lung cancer with mutated EGFR. *N Engl J Med* 362, 2380-2388.

Malinda, K. M., and Kleinman, H. K. (1996). The laminins. *Int J Biochem Cell Biol* 28, 957-959.

Mann, B., Gelos, M., Siedow, A., Hanski, M. L., Gratchev, A., Ilyas, M., Bodmer, W. F., Moyer, M. P., Riecken, E. O., Buhr, H. J., and Hanski, C. (1999). Target genes of beta-catenin-T cell-factor/lymphoid-enhancer-factor signaling in human colorectal carcinomas. *Proc Natl Acad Sci U S A* 96, 1603-1608.

Mason, R. J., Kalina, M., Nielsen, L. D., Malkinson, A. M., and Shannon, J. M. (2000). Surfactant protein C expression in urethane-induced murine pulmonary tumors. *Am J Pathol* 156, 175-182.

Massague, J. (1990). Transforming growth factor- α . A model for membrane-anchored growth factors. *J Biol Chem* 265, 21393-21396.

Masugi, Y., Yamazaki, K., Emoto, K., Effendi, K., Tsujikawa, H., Kitago, M., Itano, O., Kitagawa, Y., and Sakamoto, M. (2015). Upregulation of integrin beta4 promotes epithelial-mesenchymal transition and is a novel prognostic marker in pancreatic ductal adenocarcinoma. *Lab Invest* 95, 308-319.

Mazieres, J., He, B., You, L., Xu, Z., Lee, A. Y., Mikami, I., Reguart, N., Rosell, R., McCormick, F., and Jablons, D. M. (2004). Wnt inhibitory factor-1 is silenced by promoter hypermethylation in human lung cancer. *Cancer Res* 64, 4717-4720.

McClatchey, A. I., and Yap, A. S. (2012). Contact inhibition (of proliferation) redux. *Curr Opin Cell Biol* 24, 685-694.

McGrath, J. P., Capon, D. J., Goeddel, D. V., and Levinson, A. D. (1984). Comparative biochemical properties of normal and activated human ras p21 protein. *Nature* 310, 644-649.

Moll, R., Franke, W. W., Schiller, D. L., Geiger, B., and Krepler, R. (1982). The catalog of human cytokeratins: patterns of expression in normal epithelia, tumors and cultured cells. *Cell* 31, 11-24.

Moon, Y. W., Rao, G., Kim, J. J., Shim, H. S., Park, K. S., An, S. S., Kim, B., Steeg, P. S., Sarfaraz, S., Changwoo Lee, L., *et al.* (2015). LAMC2 enhances the metastatic potential of lung adenocarcinoma. *Cell Death Differ* 22, 1341-1352.

Morton, J. P., and Sansom, O. J. (2013). MYC-y mice: from tumour initiation to therapeutic targeting of endogenous MYC. *Mol Oncol* 7, 248-258.

Murphy, D. J., Junttila, M. R., Pouyet, L., Karnezis, A., Shchors, K., Bui, D. A., Brown-Swigart, L., Johnson, L., and Evan, G. I. (2008). Distinct thresholds govern Myc's biological output in vivo. *Cancer Cell* 14, 447-457.

Muthalagu, N., Junntila, M. R., Wiese, K. E., Wolf, E., Morton, J., Bauer, B., Evan, G. I., Eilers, M., and Murphy, D. J. (2014). BIM is the primary mediator of MYC-induced apoptosis in multiple solid tissues. *Cell Rep* 8, 1347-1353.

Nakashima, N., Liu, D., Huang, C. L., Ueno, M., Zhang, X., and Yokomise, H. (2012). Wnt3 gene expression promotes tumor progression in non-small cell lung cancer. *Lung Cancer* 76, 228-234.

Nakashima, T., Liu, D., Nakano, J., Ishikawa, S., Yokomise, H., Ueno, M., Kadota, K., and Huang, C. L. (2008). Wnt1 overexpression associated with tumor proliferation and a poor prognosis in non-small cell lung cancer patients. *Oncol Rep* 19, 203-209.

Narayanasamy, A., Ahn, J. M., Sung, H. J., Kong, D. H., Ha, K. S., Lee, S. Y., and Cho, J. Y. (2011). Fucosylated glycoproteomic approach to identify a complement component 9 associated with squamous cell lung cancer (SQLC). *J Proteomics* 74, 2948-2958.

National Lung Screening Trial Research, T., Aberle, D. R., Adams, A. M., Berg, C. D., Black, W. C., Clapp, J. D., Fagerstrom, R. M., Gareen, I. F., Gatsonis, C., Marcus, P. M., and Sicks, J. D. (2011). Reduced lung-cancer mortality with low-dose computed tomographic screening. *N Engl J Med* 365, 395-409.

Nau, M. M., Brooks, B. J., Battey, J., Sausville, E., Gazdar, A. F., Kirsch, I. R., McBride, O. W., Bertness, V., Hollis, G. F., and Minna, J. D. (1985). L-myc, a new myc-related gene amplified and expressed in human small cell lung cancer. *Nature* 318, 69-73.

Neef, R., Klein, U. R., Kopajtich, R., and Barr, F. A. (2006). Cooperation between mitotic kinesins controls the late stages of cytokinesis. *Curr Biol* 16, 301-307.

Nguyen, D. X., Chiang, A. C., Zhang, X. H., Kim, J. Y., Kris, M. G., Ladanyi, M., Gerald, W. L., and Massague, J. (2009). WNT/TCF signaling through LEF1 and HOXB9 mediates lung adenocarcinoma metastasis. *Cell* 138, 51-62.

Nikitin, A. Y., Alcaraz, A., Anver, M. R., Bronson, R. T., Cardiff, R. D., Dixon, D., Fraire, A. E., Gabrielson, E. W., Gunning, W. T., Haines, D. C., *et al.* (2004).

Classification of proliferative pulmonary lesions of the mouse: recommendations of the mouse models of human cancers consortium. *Cancer Res* 64, 2307-2316.

Okada, M., Nishio, W., Sakamoto, T., Uchino, K., Yuki, T., Nakagawa, A., and Tsubota, N. (2004). Prognostic significance of perioperative serum carcinoembryonic antigen in non-small cell lung cancer: analysis of 1,000 consecutive resections for clinical stage I disease. *Ann Thorac Surg* 78, 216-221.

Olson, A. L., and Pessin, J. E. (1996). Structure, function, and regulation of the mammalian facilitative glucose transporter gene family. *Annu Rev Nutr* 16, 235-256.

Ott, C. J., Kopp, N., Bird, L., Paranal, R. M., Qi, J., Bowman, T., Rodig, S. J., Kung, A. L., Bradner, J. E., and Weinstock, D. M. (2012). BET bromodomain inhibition targets both c-Myc and IL7R in high-risk acute lymphoblastic leukemia. *Blood* 120, 2843-2852.

Oxford, G., Owens, C. R., Titus, B. J., Foreman, T. L., Herlevsen, M. C., Smith, S. C., and Theodorescu, D. (2005). RalA and RalB: antagonistic relatives in cancer cell migration. *Cancer Res* 65, 7111-7120.

Pacheco-Pinedo, E. C., Durham, A. C., Stewart, K. M., Goss, A. M., Lu, M. M., Demayo, F. J., and Morrissey, E. E. (2011). Wnt/beta-catenin signaling accelerates mouse lung tumorigenesis by imposing an embryonic distal progenitor phenotype on lung epithelium. *J Clin Invest* 121, 1935-1945.

Pao, W., Wang, T. Y., Riely, G. J., Miller, V. A., Pan, Q., Ladanyi, M., Zakowski, M. F., Heelan, R. T., Kris, M. G., and Varmus, H. E. (2005). KRAS mutations and primary resistance of lung adenocarcinomas to gefitinib or erlotinib. *PLoS Med* 2, e17.

Paria, B. C., Elenius, K., Klagsbrun, M., and Dey, S. K. (1999). Heparin-binding EGF-like growth factor interacts with mouse blastocysts independently of ErbB1: a possible role for heparan sulfate proteoglycans and ErbB4 in blastocyst implantation. *Development* 126, 1997-2005.

Pelengaris, S., Khan, M., and Evan, G. I. (2002). Suppression of Myc-induced apoptosis in beta cells exposes multiple oncogenic properties of Myc and triggers carcinogenic progression. *Cell* 109, 321-334.

Penn, L. J., Brooks, M. W., Laufer, E. M., and Land, H. (1990). Negative autoregulation of c-myc transcription. *EMBO J* 9, 1113-1121.

Perera, S. A., Li, D., Shimamura, T., Raso, M. G., Ji, H., Chen, L., Borgman, C. L., Zaghlul, S., Brandstetter, K. A., Kubo, S., *et al.* (2009). HER2YVMA drives rapid development of adenosquamous lung tumors in mice that are sensitive to BIBW2992 and rapamycin combination therapy. *Proc Natl Acad Sci U S A* 106, 474-479.

Pertega-Gomes, N., Felisbino, S., Massie, C. E., Vizcaino, J. R., Coelho, R., Sandi, C., Simoes-Sousa, S., Jurmeister, S., Ramos-Montoya, A., Asim, M., *et al.* (2015). A glycolytic phenotype is associated with prostate cancer progression and aggressiveness: a role for monocarboxylate transporters as metabolic targets for therapy. *J Pathol* 236, 517-530.

Peukert, K., Staller, P., Schneider, A., Carmichael, G., Hanel, F., and Eilers, M. (1997). An alternative pathway for gene regulation by Myc. *EMBO J* 16, 5672-5686.

Philipp, A., Schneider, A., Vasrik, I., Finke, K., Xiong, Y., Beach, D., Alitalo, K., and Eilers, M. (1994). Repression of cyclin D1: a novel function of MYC. *Mol Cell Biol* 14, 4032-4043.

Pignon, J. P., Tribodet, H., Scagliotti, G. V., Douillard, J. Y., Shepherd, F. A., Stephens, R. J., Dunant, A., Torri, V., Rosell, R., Seymour, L., *et al.* (2008). Lung adjuvant cisplatin evaluation: a pooled analysis by the LACE Collaborative Group. *J Clin Oncol* 26, 3552-3559.

Polakis, P. (2007). The many ways of wnt in cancer. *Curr Opin Genet Dev* 17, 45-51.

Price, M. A. (2006). CKI, there's more than one: casein kinase I family members in Wnt and Hedgehog signaling. *Genes Dev* 20, 399-410.

Prigent, S. A., and Gullick, W. J. (1994). Identification of c-erbB-3 binding sites for phosphatidylinositol 3'-kinase and SHC using an EGF receptor/c-erbB-3 chimera. *EMBO J* 13, 2831-2841.

Puyol, M., Martin, A., Dubus, P., Mulero, F., Pizcueta, P., Khan, G., Guerra, C., Santamaria, D., and Barbacid, M. (2010). A synthetic lethal interaction between K-Ras oncogenes and Cdk4 unveils a therapeutic strategy for non-small cell lung carcinoma. *Cancer Cell* 18, 63-73.

Rabindran, S. K., Discafani, C. M., Rosfjord, E. C., Baxter, M., Floyd, M. B., Golas, J., Hallett, W. A., Johnson, B. D., Nilakantan, R., Overbeek, E., *et al.* (2004). Antitumor activity of HKI-272, an orally active, irreversible inhibitor of the HER-2 tyrosine kinase. *Cancer Res* 64, 3958-3965.

Rekhtman, N., Ang, D. C., Sima, C. S., Travis, W. D., and Moreira, A. L. (2011). Immunohistochemical algorithm for differentiation of lung adenocarcinoma and squamous cell carcinoma based on large series of whole-tissue sections with validation in small specimens. *Mod Pathol* 24, 1348-1359.

Riese, D. J., 2nd, Komurasaki, T., Plowman, G. D., and Stern, D. F. (1998). Activation of ErbB4 by the bifunctional epidermal growth factor family hormone epiregulin is regulated by ErbB2. *J Biol Chem* 273, 11288-11294.

Riese, D. J., 2nd, van Raaij, T. M., Plowman, G. D., Andrews, G. C., and Stern, D. F. (1995). The cellular response to neuregulins is governed by complex interactions of the erbB receptor family. *Mol Cell Biol* 15, 5770-5776.

Rodriguez-Paredes, M., and Esteller, M. (2011). Cancer epigenetics reaches mainstream oncology. *Nat Med* 17: 330–339.

Rojas, M., Yao, S., and Lin, Y. Z. (1996). Controlling epidermal growth factor (EGF)-stimulated Ras activation in intact cells by a cell-permeable peptide mimicking phosphorylated EGF receptor. *J Biol Chem* 271, 27456-27461.

Salomon, D. S., Brandt, R., Ciardiello, F., and Normanno, N. (1995). *Crit Rev Oncol Hematol* 19, 183-232.

Samuels, Y., Wang, Z., Bardelli, A., Silliman, N., Ptak, J., Szabo S., Yan, H., Gazdar, A., Powell, S. M., Riggins, G. J., Willson, J. K., Markowitz, S., Kinzler, K. W., Vogelstein, B., and Velculescu V. E. (2004). High frequency of mutations of the PI3KCA gene in human cancers. *Science* 304, 554

Sansom, O. J., Meniel, V. S., Muncan, V., Phesse, T. J., Wilkins, J. A., Reed, K. R., Vass, J. K., Athineos, D., Clevers, H., and Clarke, A. R. (2007). Myc deletion rescues Apc deficiency in the small intestine. *Nature* 446, 676-679.

Sansom, O. J., Reed, K. R., Hayes, A. J., Ireland, H., Brinkmann, H., Newton, I. P., Battle, E., Simon-Assmann, P., Clevers, H., Nathke, I. S., *et al.* (2004). Loss of Apc in vivo immediately perturbs Wnt signaling, differentiation, and migration. *Genes Dev* 18, 1385-1390.

Sarkisian, C. J., Keister, B. A., Stairs, D. B., Boxer, R. B., Moody, S. E., and Chodosh, L. A. (2007). Dose-dependent oncogene-induced senescence in vivo and its evasion during mammary tumorigenesis. *Nat Cell Biol* 9, 493-505.

Sasada, R., Ono, Y., Taniyama, Y., Shing, Y., Folkman, J., and Igarashi, K. (1993). Cloning and expression of cDNA encoding human betacellulin, a new member of the EGF family. *Biochem Biophys Res Commun* 190, 1173-1179.

Scheffzek, K., Ahmadian, M. R., Kabsch, W., Wiesmuller, L., Lautwein, A., Schmitz, F., and Wittinghofer, A. (1997). The Ras-RasGAP complex: structural basis for GTPase activation and its loss in oncogenic Ras mutants. *Science* 277, 333-338.

Schlessinger, K., Hall, A., and Tolwinski, N. (2009). Wnt signaling pathways meet Rho GTPases. *Genes Dev* 23, 265-277.

Schmitt, C. A., McCurrach, M. E., de Stanchina, E., Wallace-Brodeur, R. R., and Lowe, S. W. (1999). INK4a/ARF mutations accelerate lymphomagenesis and promote chemoresistance by disabling p53. *Genes Dev* 13, 2670-2677.

Sears, R., Nuckolls, F., Haura, E., Taya, Y., Tamai, K., and Nevins, J. R. (2000). Multiple Ras-dependent phosphorylation pathways regulate Myc protein stability. *Genes Dev* 14, 2501-2514.

Serrano, M., Lin, A. W., McCurrach, M. E., Beach, D., and Lowe, S. W. (1997). Oncogenic ras provokes premature cell senescence associated with accumulation of p53 and p16INK4a. *Cell* 88, 593-602.

Shaw, A. T., Kim, D. W., Nakagawa, K., Seto, T., Crino, L., Ahn, M. J., De Pas, T., Besse, B., Solomon, B. J., Blackhall, F., *et al.* (2013). Crizotinib versus chemotherapy in advanced ALK-positive lung cancer. *N Engl J Med* 368, 2385-2394.

Shaw, A. T., Ou, S. H., Bang, Y. J., Camidge, D. R., Solomon, B. J., Salgia, R., Riely, G. J., Varella-Garcia, M., Shapiro, G. I., Costa, D. B., *et al.* (2014). Crizotinib in ROS1-rearranged non-small-cell lung cancer. *N Engl J Med* 371, 1963-1971.

Shelly, M., Pinkas-Kramarski, R., Guarino, B. C., Waterman, H., Wang, L. M., Lyass, L., Alimandi, M., Kuo, A., Bacus, S. S., Pierce, J. H., *et al.* (1998). Epiregulin is a potent pan-ErbB ligand that preferentially activates heterodimeric receptor complexes. *J Biol Chem* 273, 10496-10505.

Shigematsu, H., Gazdar, A. F. (2006). Somatic mutations of epidermal growth factor receptor signaling pathways in lung cancers. *Int J Cancer* 118, 257-262.

Shimamura, T., Chen, Z., Soucheray, M., Carretero, J., Kikuchi, E., Tchaicha, J. H., Gao, Y., Cheng, K. A., Cohoon, T. J., Qi, J., *et al.* (2013). Efficacy of BET bromodomain inhibition in Kras-mutant non-small cell lung cancer. *Clin Cancer Res* 19, 6183-6192.

Shin, S. Y., Rath, O., Choo, S. M., Fee, F., McFerran, B., Kolch, W., and Cho, K. H. (2009). Positive- and negative-feedback regulations coordinate the dynamic behavior of the Ras-Raf-MEK-ERK signal transduction pathway. *J Cell Sci* 122, 425-435.

Shoyab, M., McDonald, V. L., Bradley, J. G., and Todaro, G. J. (1988). Amphiregulin: a bifunctional growth-modulating glycoprotein produced by the phorbol 12-myristate 13-acetate-treated human breast adenocarcinoma cell line MCF-7. *Proc Natl Acad Sci U S A* 85, 6528-6532.

Silvennoinen, O., Schindler, C., Schlessinger, J., and Levy, D. E. (1993). Ras-independent growth factor signaling by transcription factor tyrosine phosphorylation. *Science* 261, 1736-1739.

Sinn, E., Muller, W., Pattengale, P., Tepler, I., Wallace, R., and Leder, P. (1987). Coexpression of MMTV/v-Ha-ras and MMTV/c-myc genes in transgenic mice: synergistic action of oncogenes in vivo. *Cell* 49, 465-475.

Sjolander, A., Yamamoto, K., Huber, B. E., and Lapetina, E. G. (1991). Association of p21ras with phosphatidylinositol 3-kinase. *Proc Natl Acad Sci U S A* 88, 7908-7912.

Slamon, D. J., Boone, T. C., Seeger, R. C., Keith, D. E., Chazin, V., Lee, H. C., and Souza, L. M. (1986). Identification and characterization of the protein encoded by the human N-myc oncogene. *Science* 232, 768-772.

Slebos, R. J., Kibbelaar, R. E., Dalesio, O., Kooistra, A., Stam, J., Meijer, C. J., Wagenaar, S. S., Vanderschueren, R. G., van Zandwijk, N., Mooi, W. J., and et al. (1990). K-ras oncogene activation as a prognostic marker in adenocarcinoma of the lung. *N Engl J Med* 323, 561-565.

Sliwkowski, M. X., Schaefer, G., Akita, R. W., Lofgren, J. A., Fitzpatrick, V. D., Nuijens, A., Fendly, B. M., Cerione, R. A., Vandlen, R. L., and Carraway, K. L., 3rd (1994). Coexpression of erbB2 and erbB3 proteins reconstitutes a high affinity receptor for heregulin. *J Biol Chem* 269, 14661-14665.

Smas, C. M., Chen, L., and Sul, H. S. (1997). Cleavage of membrane-associated pref-1 generates a soluble inhibitor of adipocyte differentiation. *Mol Cell Biol* 17, 977-988.

Soda, M., Takada, S., Takeuchi, K., Choi, Y. L., Enomoto, M., Ueno, T., Haruta, H., Hamada, T., Yamashita, Y., Ishikawa, Y., *et al.* (2008). A mouse model for EML4-ALK-positive lung cancer. *Proc Natl Acad Sci U S A* 105, 19893-19897.

Soucek, L., Whitfield, J., Martins, C. P., Finch, A. J., Murphy, D. J., Sodir, N. M., Karnezis, A. N., Swigart, L. B., Nasi, S., and Evan, G. I. (2008). Modelling Myc inhibition as a cancer therapy. *Nature* 455, 679-683.

Soucek, L., Whitfield, J. R., Sodir, N. M., Masso-Valles, D., Serrano, E., Karnezis, A. N., Swigart, L. B., and Evan, G. I. (2013). Inhibition of Myc family proteins eradicates KRas-driven lung cancer in mice. *Genes Dev* 27, 504-513.

Spira, A., Beane, J. E., Shah, V., Steiling, K., Liu, G., Schembri, F., Gilman, S., Dumas, Y. M., Calner, P., Sebastiani, P., *et al.* (2007). Airway epithelial gene expression in the diagnostic evaluation of smokers with suspect lung cancer. *Nat Med* 13, 361-366.

Sporn, M. B., and Roberts, A. B. (1985). Autocrine growth factors and cancer. *Nature* 313, 745-747.

Stewart, D. J. (2014). Wnt signaling pathway in non-small cell lung cancer. *J Natl Cancer Inst* 106, djt356.

Stewart, T. A., Pattengale, P. K., and Leder, P. (1984). Spontaneous mammary adenocarcinomas in transgenic mice that carry and express MTV/myc fusion genes. *Cell* 38, 627-637.

Stover, D. R., Becker, M., Liebetanz, J., and Lydon, N. B. (1995). Src phosphorylation of the epidermal growth factor receptor at novel sites mediates receptor interaction with Src and P85 alpha. *J Biol Chem* 270, 15591-15597.

Strasser, A., Harris, A. W., Bath, M. L., and Cory, S. (1990). Novel primitive lymphoid tumours induced in transgenic mice by cooperation between myc and bcl-2. *Nature* 348, 331-333.

Stripp, B. R., Sawaya, P. L., Luse, D. S., Wikenheiser, K. A., Wert, S. E., Huffman, J. A., Lattier, D. L., Singh, G., Katyal, S. L., and Whitsett, J. A. (1992). cis-acting elements that confer lung epithelial cell expression of the CC10 gene. *J Biol Chem* 267, 14703-14712.

Sunaga, N., Kaira, K., Imai, H., Shimizu, K., Nakano, T., Shames, D. S., Girard, L., Soh, J., Sato, M., Iwasaki, Y., *et al.* (2013). Oncogenic KRAS-induced epiregulin overexpression contributes to aggressive phenotype and is a promising therapeutic target in non-small-cell lung cancer. *Oncogene* 32, 4034-4042.

Sutherland, K. D., Proost, N., Brouns, I., Adriaensen, D., Song, J. Y., and Berns, A. (2011). Cell of origin of small cell lung cancer: inactivation of Trp53 and Rb1 in distinct cell types of adult mouse lung. *Cancer Cell* 19, 754-764.

Takahashi, S., Fusaki, N., Ohta, S., Iwahori, Y., Iizuka, Y., Inagawa, K., Kawakami, Y., Yoshida, K., and Toda, M. (2012). Downregulation of KIF23 suppresses glioma proliferation. *J Neurooncol* 106, 519-529.

Tetsu, O., and McCormick, F. (1999). Beta-catenin regulates expression of cyclin D1 in colon carcinoma cells. *Nature* 398, 422-426.

Toyoda, H., Komurasaki, T., Uchida, D., and Morimoto, S. (1997). Distribution of mRNA for human epiregulin, a differentially expressed member of the epidermal growth factor family. *Biochem J* 326 (Pt 1), 69-75.

Toyoda, H., Komurasaki, T., Uchida, D., Takayama, Y., Isobe, T., Okuyama, T., and Hanada, K. (1995). Epiregulin. A novel epidermal growth factor with mitogenic activity for rat primary hepatocytes. *J Biol Chem* 270, 7495-7500.

Tuveson, D. A., Shaw, A. T., Willis, N. A., Silver, D. P., Jackson, E. L., Chang, S., Mercer, K. L., Grochow, R., Hock, H., Crowley, D., *et al.* (2004). Endogenous oncogenic K-ras(G12D) stimulates proliferation and widespread neoplastic and developmental defects. *Cancer Cell* 5, 375-387.

Uematsu, K., He, B., You, L., Xu, Z., McCormick, F., and Jablons, D. M. (2003). Activation of the Wnt pathway in non small cell lung cancer: evidence of dishevelled overexpression. *Oncogene* 22, 7218-7221.

Umanoff, H., Edelman, W., Pellicer, A., and Kucherlapati, R. (1995). The murine N-ras gene is not essential for growth and development. *Proc Natl Acad Sci U S A* 92, 1709-1713.

Vander Heiden, M. G., Cantley, L. C., and Thompson, C. B. (2009). Understanding the Warburg effect: the metabolic requirements of cell proliferation. *Science* 324, 1029-1033.

Vennstrom, B., Sheiness, D., Zabielski, J., and Bishop, J. M. (1982). Isolation and characterization of c-myc, a cellular homolog of the oncogene (v-myc) of avian myelocytomatosis virus strain 29. *J Virol* 42, 773-779.

Vogel, U. S., Dixon, R. A., Schaber, M. D., Diehl, R. E., Marshall, M. S., Scolnick, E. M., Sigal, I. S., and Gibbs, J. B. (1988). Cloning of bovine GAP and its interaction with oncogenic ras p21. *Nature* 335, 90-93.

Vogelstein, B., Fearon, E. R., Hamilton, S. R., Kern, S. E., Preisinger, A. C., Leppert, M., Nakamura, Y., White, R., Smits, A. M., and Bos, J. L. (1988). Genetic alterations during colorectal-tumor development. *N Engl J Med* 319, 525-532.

Vojtek, A. B., Hollenberg, S. M., and Cooper, J. A. (1993). Mammalian Ras interacts directly with the serine/threonine kinase Raf. *Cell* 74, 205-214.

Wang, H. Q., Xu, M. L., Ma, J., Zhang, Y., and Xie, C. H. (2012). Frizzled-8 as a putative therapeutic target in human lung cancer. *Biochem Biophys Res Commun* 417, 62-66.

Wang, H. Y., and Malbon, C. C. (2003). Wnt signaling, Ca²⁺, and cyclic GMP: visualizing Frizzled functions. *Science* 300, 1529-1530.

Wang, X., Cunningham, M., Zhang, X., Tokarz, S., Laraway, B., Troxell, M., and Sears, R. C. (2011). Phosphorylation regulates c-Myc's oncogenic activity in the mammary gland. *Cancer Res* 71, 925-936.

Wang, Y., and Sul, H. S. (2006). Ectodomain shedding of preadipocyte factor 1 (Pref-1) by tumor necrosis factor alpha converting enzyme (TACE) and inhibition of adipocyte differentiation. *Mol Cell Biol* 26, 5421-5435.

Wang, Y., and Sul, H. S. (2009). Pref-1 regulates mesenchymal cell commitment and differentiation through Sox9. *Cell Metab* 9, 287-302.

Ward, P. S., and Thompson, C. B. (2012). Metabolic reprogramming: a cancer hallmark even warburg did not anticipate. *Cancer Cell* 21, 297-308.

Wei, Q., Zhao, Y., Yang, Z. Q., Dong, Q. Z., Dong, X. J., Han, Y., Zhao, C., and Wang, E. H. (2008). Dishevelled family proteins are expressed in non-small cell lung cancer and function differentially on tumor progression. *Lung Cancer* 62, 181-192.

Welsh, J. B., Zarrinkar, P. P., Sapinoso, L. M., Kern, S. G., Behling, C. A., Monk, B. J., Lockhart, D. J., Burger, R. A., and Hampton, G. M. (2001). Analysis of gene expression profiles in normal and neoplastic ovarian tissue samples identifies candidate molecular markers of epithelial ovarian cancer. *Proc Natl Acad Sci U S A* 98, 1176-1181.

Whyte, D. B., Kirschmeier, P., Hockenberry, T. N., Nunez-Oliva, I., James, L., Catino, J. J., Bishop, W. R., and Pai, J. K. (1997). K- and N-Ras are geranylgeranylated in cells treated with farnesyl protein transferase inhibitors. *J Biol Chem* 272, 14459-14464.

Wikenheiser, K. A., Clark, J. C., Linnoila, R. I., Stahlman, M. T., and Whitsett, J. A. (1992). Simian virus 40 large T antigen directed by transcriptional elements of the human surfactant protein C gene produces pulmonary adenocarcinomas in transgenic mice. *Cancer Res* 52, 5342-5352.

Winn, R. A., Marek, L., Han, S. Y., Rodriguez, K., Rodriguez, N., Hammond, M., Van Scoyk, M., Acosta, H., Mirus, J., Barry, N., *et al.* (2005). Restoration of Wnt-7a expression reverses non-small cell lung cancer cellular transformation through frizzled-9-mediated growth inhibition and promotion of cell differentiation. *J Biol Chem* 280, 19625-19634.

Wissner, A., and Mansour, T. S. (2008). The development of HKI-272 and related compounds for the treatment of cancer. *Arch Pharm (Weinheim)* 341, 465-477.

Wolfman, A., and Macara, I. G. (1990). A cytosolic protein catalyzes the release of GDP from p21ras. *Science* 248, 67-69.

Worthylake, R., Opresko, L. K., and Wiley, H. S. (1999). ErbB-2 amplification inhibits down-regulation and induces constitutive activation of both ErbB-2 and epidermal growth factor receptors. *J Biol Chem* 274, 8865-8874.

Xu, C., Fillmore, C. M., Koyama, S., Wu, H., Zhao, Y., Chen, Z., Herter-Sprie, G. S., Akbay, E. A., Tchaicha, J. H., Altabef, A., *et al.* (2014). Loss of Lkb1 and Pten leads to lung squamous cell carcinoma with elevated PD-L1 expression. *Cancer Cell* 25, 590-604.

Xu, X., Rock, J. R., Lu, Y., Futtner, C., Schwab, B., Guinney, J., Hogan, B. L., and Onaitis, M. W. (2012). Evidence for type II cells as cells of origin of K-Ras-induced distal lung adenocarcinoma. *Proc Natl Acad Sci U S A* 109, 4910-4915.

Xue, W., Meylan, E., Oliver, T. G., Feldser, D. M., Winslow, M. M., Bronson, R., and Jacks, T. (2011). Response and resistance to NF-kappaB inhibitors in mouse models of lung adenocarcinoma. *Cancer Discov* 1, 236-247.

Yang, Z. Y., Jiang, H., Qu, Y., Wei, M., Yan, M., Zhu, Z. G., Liu, B. Y., Chen, G. Q., Wu, Y. L., and Gu, Q. L. (2013). Metalloproteinase-1 regulates invasion and migration of gastric cancer cells partially through integrin beta4. *Carcinogenesis* 34, 2851-2860.

You, L., He, B., Xu, Z., Uematsu, K., Mazieres, J., Mikami, I., Reguart, N., Moody, T. W., Kitajewski, J., McCormick, F., and Jablons, D. M. (2004). Inhibition of Wnt-2-mediated signaling induces programmed cell death in non-small-cell lung cancer cells. *Oncogene* 23, 6170-6174.

Young, N. P., and Jacks, T. (2010). Tissue-specific p19Arf regulation dictates the response to oncogenic K-ras. *Proc Natl Acad Sci U S A* 107, 10184-10189.

Zarogoulidis, K., Zarogoulidis, P., Darwiche, K., Boutsikou E., Machairiotis N., Tsakiridis, K., Katsikogiannis, N., Kougioumtzi, I., Karapantzos, I., Huang, H., and Dionysios, S. (2013). Treatment of non-small cell lung cancer (NSCLC). *J Thorac Dis.* 5, 389-396.

Zhang, D., Sliwkowski, M. X., Mark, M., Frantz, G., Akita, R., Sun, Y., Hillan, K., Crowley, C., Brush, J., and Godowski, P. J. (1997). Neuregulin-3 (NRG3): a novel neural tissue-enriched protein that binds and activates ErbB4. *Proc Natl Acad Sci U S A* 94, 9562-9567.

Zhang, J., Iwanaga, K., Choi, K. C., Wislez, M., Raso, M. G., Wei, W., Wistuba, II, and Kurie, J. M. (2008). Intratumoral epiregulin is a marker of advanced disease in non-small cell lung cancer patients and confers invasive properties on EGFR-mutant cells. *Cancer Prev Res (Phila)* 1, 201-207.

Zhang, X. F., Settleman, J., Kyriakis, J. M., Takeuchi-Suzuki, E., Elledge, S. J., Marshall, M. S., Bruder, J. T., Rapp, U. R., and Avruch, J. (1993). Normal and oncogenic p21ras proteins bind to the amino-terminal regulatory domain of c-Raf-1. *Nature* 364, 308-313.

Zhao, Y., Yang, Z. Q., Wang, Y., Miao, Y., Liu, Y., Dai, S. D., Han, Y., and Wang, E. H. (2010). Dishevelled-1 and dishevelled-3 affect cell invasion mainly through canonical and noncanonical Wnt pathway, respectively, and associate with poor prognosis in nonsmall cell lung cancer. *Mol Carcinog* 49, 760-770.

Zindy, F., Eischen, C. M., Randle, D. H., Kamijo, T., Cleveland, J. L., Sherr, C. J., and Roussel, M. F. (1998). Myc signaling via the ARF tumor suppressor regulates p53-dependent apoptosis and immortalization. *Genes Dev* 12, 2424-2433.

Zindy, F., Williams, R. T., Baudino, T. A., Rehg, J. E., Skapek, S. X., Cleveland, J. L., Roussel, M. F., and Sherr, C. J. (2003). Arf tumor suppressor promoter monitors latent oncogenic signals in vivo. *Proc Natl Acad Sci U S A* 100, 15930-15935.